

DOCTORADO EN BIOMEDICINA Y FARMACIA



VNIVERSITAT
DE VALÈNCIA

**MUC1 BIOACTIVATION CONTRIBUTES TO
LUNG FIBROSIS**

TESIS DOCTORAL

Presentada por:

BEATRIZ BALLESTER LLOBELL

Dirigida por:

DR. JULIO CORTIJO GIMENO

DR. JAVIER MILARA PAYÁ

VALENCIA, 2019



Dr. JULIO CORTIJO GIMENO, Professor of Pharmacology Department, Universidad de Valencia, and **Dr. JAVIER MILARA PAYÁ**, Hospital pharmacist of Pharmacy Unit, Hospital General Universitario de Valencia

Certify:

That the work embodied in the accompanying thesis entitled “**MUC1 BIOACTIVATION CONTRIBUTES TO LUNG FIBROSIS**” has been carried out entirely under my direct supervision and guidance and that the candidate has fulfilled the requirements of the regulations laid down for PhD examination

And as evidence thereof, I hereby issue this certificate.

In Valencia, March 2019

Dr. Julio Cortijo Gimeno

Dr. Javier Milara Payá

ACKNOWLEDGMENTS

La presente tesis doctoral, más allá de ciencia, investigación y muchas horas de trabajo, lleva algo mucho más importante detrás, las vivencias compartidas con muchas personas que con su apoyo y cariño incondicional han hecho posible que este trabajo saliera adelante y no se quedara a mitad camino. Por ello, quisiera intentar tratar de expresarles mi más sincero agradecimiento a todas esas personas, aunque unas palabras no sean suficientes para plasmar dicho agradecimiento.

En primer lugar, agradecer al Dr. Julio Cortijo por abrirme las puertas de su laboratorio cuando llegué como una alumna entusiasmada por conseguir alguna beca de investigación. Al final lo conseguí y siempre podré estar agradecida de haber podido crecer tanto a nivel personal como profesional gracias a su experiencia y confianza depositada en mí. Sus consejos siempre han acabado dejando huella en mí. Al Dr. Javier Milara, aquel profesor jovencito y gracioso de prácticas que conocí cuando estudiaba la carrera y con el cual me reencontré estudiando el máster. Ante mi entusiasmo por dedicarme a la investigación me convenció que este era un buen grupo para iniciar mi carrera investigadora y así empezó todo. Sin duda, su pasión por la investigación, su conocimiento inabarcable y su capacidad de esfuerzo y superación son mi claro ejemplo a seguir, sin olvidar sus consejos y su incondicional apoyo a nivel tanto personal como profesional mostrado durante todos estos años, haciendo posible que los días malos dejaran siempre de ser tan malos y los problemas dejaran de ser problemas. Sin duda, una pieza clave en este largo recorrido.

A mis mucho más que compañer@s del trabajo, amig@s, del departamento de farmacología de la Universidad de Valencia, por todas las horas de risas, agobios, estreses e ilusiones compartidas. Son muchas las personas con las que he podido compartir mi tiempo en el laboratorio durante toda esta trayectoria y sin duda todas ellas han de una manera u otra contribuido a esta tesis doctoral. Muchas gracias a Pili, Adela, Patri, Sonia.G, Lucy, Gracia, Teresa Peiró y Anselm, ese primer equipo Cortijo con el que me encontré e hizo que ir a trabajar fuera siempre algo ameno y divertido. Quisiera destacar a Adela, por su clave papel como mami del laboratorio cuidando a sus pollitos, y a Anselm, porque él ha sido mi referencia a seguir desde que pise el laboratorio, porque él me ha enseñado mucho de lo que sé, porque él ha sufrido y escuchado mis agobios como el que más y porque él ha tenido mucha paciencia y nunca se ha enfadado ante cualquier despiste o error de su estudiante de TFM.

A Teresita, esa veterinaria que llegó al laboratorio un día para revolucionarlo cada vez que lo pisaba, porque lo que empezó conmigo enseñándole a hacer un Western Blot o una inmunohistoquímica, continuó por una ayuda y una paciencia desinteresada ante mis dificultades con el mundo de la veterinaria y acabó en horas y horas inevitables de conversación

y en una gran amistad aún a la distancia. Gracias por ser esa hermana mayor que nunca he tenido y estar SIEMPRE ahí. Nunca olvidaré nuestra temporada de jaimitadas junto con Lucy.

Al segundo equipo Cortijo con el que he compartido mi tiempo estos años, Martín, Xavi Lluch, Pilar, Sonia.C, Cristina, Paula e Inés, porque ellos son los que me han hecho reír y amenizado las horas en el laboratorio, porque ellos más que nadie conocen mi yo en situación de estrés y mi continua necesidad vital de ser productiva en cada segundo del día, pero son también ellos los que han conseguido que de vez en cuando desordenara un poco mi vida y disfrutara con ellos y nuestras infinitas aventuras. Todos ellos creo que saben que tienen una importancia especial para mí, por ser ellos los que han sufrido y compartido mi día a día en esta última turbulenta etapa del recorrido, siendo ellos los responsables de que fuera capaz, a pesar de todo, de levantarme cada día e ir a trabajar, y no solo eso, sino que han sido capaces de a pesar de todo sacarme SIEMPRE una sonrisa, aunque fuera entre medio de lágrimas, y darme fuerzas para que nunca me rindiera y llegara a este ansiado final. Después de estos años y de todo lo vivido, sabemos que esto solo ha sido el comienzo de un gran recorrido y que siempre seréis el mejor team con el que se puede trabajar. A Sonia.C, porque casi casi has vivido conmigo este recorrido de principio a fin. Siempre dispuesta a darme ese abrazo que tanto necesitaba, a escuchar esas inquietudes que tanto me preocupaban, a compartir esos dramas que tanto me afectaban y a celebrar conmigo toda buena noticia. A Pilar, esa gran curiosa y gran trabajadora alumna de prácticas a la que un buen día le deleitaba yo contándole mis experimentos de tesis. Ahora ya te has hecho mayor y eres tú la que deleitas a otros contando tus experimentos y a mí viéndote hacerlo, pero más aun viendo cómo eres capaz de detectar mis días buenos y mis días malos, de hacerme razonar de una manera diferente al resto y de transmitirme siempre una fuerza y seguridad en mí increíble con tus palabras. Gracias por enseñarme TANTO y ayudarme a crecer TANTO como persona. A Inés, porque nunca hubiéramos imaginado esto cuando solo éramos unas simples conocidas en el cole. Llegaste al laboratorio pisando fuerte con esa sonrisa y alegría que contagias, y con esas interesantes preguntas que sólo a ti se te ocurren, por eso siempre quise que fueras parte del equipo. Gracias por compartir conmigo absolutamente TODO, por darme apoyo y escucharme siempre en esos momentos de estrés y nervios, por tener SIEMPRE tiempo para dedicarme en esos momentos clave de mi vida, por cuidarme tanto, por vivir conmigo mis grandes inquietudes y por alegrarte por las buenas noticias incluso más que yo. A Cris, ese gran fichaje Cortijo de pies graciosos y con una inigualable disposición para ayudar a todos siempre. Llegaste en el momento clave para mí y a pesar de ser prácticamente desconocidas, rápidamente pasaste a ser un pilar esencial para mí en mi día a día en el laboratorio. Gracias por hacerme reír tanto, por estar dispuesta SIEMPRE a ayudarme, por

conseguir que sea algo menos productiva y más divertida en algunos momentos, por sorprenderme cuando menos me lo esperaba con esos detalles que tú sabías que me iban a alegrar e incluso a hacer llorar de emoción y por saber decirme palabras tan bonitas y sinceras que incluso han llegado a emocionarme. Tienes el récord de tiempo en convertirte en alguien importante en mi vida a tal nivel. A Paula, mi pupila, por formar conmigo esa secta que nos define, siempre dispuesta a aprender de mí, pero siempre capaz de enseñarme cosas nuevas. Gran parte de los experimentos que aquí aparecen son gracias a ti. Muchas gracias por estar dispuesta a ser mi sombra en el laboratorio cuando mi cabeza más lo necesitaba, por vigilar siempre que no hubieran despistes por mi parte e incluso por estar dispuesto a reemplazarme siempre que ha sido necesario. Has sido la mejor pupila que podría haber tenido.

También agradecer el tiempo compartido y la ayuda de todos aquellos que compartieron conmigo el tiempo en la fundación de investigación del Hospital General Universitario de Valencia, Amparo, Eloisa, Sandra, Silvia, Eva, Marais, Sisco, Héctor, Franklin y Alejandro, porque ellos contribuyeron a que los largos días en la fundación fueran menos largos, además de estar siempre dispuestos a ayudarme y aconsejarme y especialmente a Alejandro por compartir conmigo nuestras inquietudes comunes. A Ester, porque sin duda su paso por la fundación de investigación no pudo dejar indiferente a nadie, incluido a mí. Claro ejemplo de fuerza y superación personal. Tus “gatitos” dejaron huella en mí. A Joan, porque hay muchos más momentos especiales y años detrás del breve tiempo compartido en la fundación, pero los abrazos de aquellos tiempos no me dejaron indiferente a la hora de enfrentarme a los numerosos westerns que aparecen en esta tesis.

A mis compañer@s los biotecnólogos, porque con vosotros es con los que realmente empecé todo esto, los que habéis hecho que quisiera estudiar biotecnología una y otra vez solo que por repetir miles de los momentos vividos juntos, y los que me entienden más que nadie cuando hablo de mis experimentos, de mi incertidumbre de futuro y de en definitiva qué implica realizar una tesis doctoral. A Carles, por aparecer siempre en los momentos más clave de mi vida para arrancarme la mayor de mis sonrisas y darme uno de esos abrazos tan necesarios que te recargan de energía para seguir adelante. GRACIAS por cuidarme tanto. A Luci, pura definición de amiga incondicional. Porque aún a la distancia siempre has sido ese gran apoyo que NUNCA me ha fallado y que hace que te defina como especial y única en mi vida, siempre dispuesta a contagiarme su positividad y hacerme ver el lado bueno de todo. Al resto de miembros de pueblo llano, María, Majo y Jenni, porque compartir mi día a día con vosotras en la carrera hizo que los principios de todo esto fueran mucho más sencillos. A mi compañera de máster Alba, porque los primeros pasos en este camino los compartí intensamente contigo y luego, aunque

a la distancia, siempre has aparecido cuando lo he necesitado para darme uno de esos discursos clave que tanta falta me hacían para sacar fuerzas y seguir adelante.

A mis amigos Héctor y Clara, porque sin entender mucho de qué iban esos experimentos frikis o porque me gustaba tanto este mundillo, me habéis escuchado y habéis hecho por entenderme como los que más, me habéis mostrado SIEMPRE vuestro apoyo, habéis compartido, sufrido y celebrado conmigo tanto las buenas como las malas noticias y me habéis acompañado durante este camino y mucho más siempre sacándome la mejor de mis sonrisas.

A mi hermano Mario y a mi madre, por hacer grandes esfuerzos por ser capaces de entender este mundo de la investigación, por sentirnos orgullosos de mi trabajo, por confiar en mí y hacerme creer siempre que soy capaz de lo que me proponga, por ser siempre una referencia a seguir, por estar en mi día a día aguantando tanto los buenos como los malos momentos, y lo más importante, por ahora más que nunca estar fuertemente unidos.

Y por último, pero al más importante, a ti papá, porque aunque me has soltado la mano justo en el final de este camino, me has acompañado de la mano de una manera especial y única durante la mayor parte del recorrido y aunque ahora esa manera de acompañarme, físicamente no pueda ser la misma, sigue siendo tanto especial como única, porque indudablemente sé que eras el que menos me la querías soltar y que tú más que nadie deseabas con todas tus fuerzas estar en este día, mi día, día en el que tu pequeña llega a ese objetivo tan perseguido y que nadie ha vivido más de cerca que tú. Gracias por aún desde el desconocimiento esforzarte siempre por comprender todo este mundillo, por sentirte infinitamente orgulloso de mí, por intentar aconsejarme lo mejor posible y por darme una energía y apoyo incondicional para no rendirme nunca a pesar de los obstáculos. Sé que allá donde estés serás el que más orgulloso se sentirá de mí ahora mismo y que aunque no hayas entendido nada serás él que aplaude con más fuerza al finalizar y yo sonreiré al pensar que parte de esos aplausos son tuyos. Te prometo que continuaré luchando como siempre te prometí y como tú me enseñaste que debía hacer. Sin duda, te mereces más que nadie la plaza de INVITADO ESPECIAL en este día.

"Investigar es ver lo que todo el mundo ha visto, y pensar lo que
nadie más ha pensado"

Albert Szent-Györgyi

A tí, papá

ABSTRACT

Background

Idiopathic pulmonary fibrosis (IPF) is a specific form of chronic, progressive fibrosing interstitial pneumonia of unknown cause. Recently, it has been proposed that IPF results from repeated episodes of injury to alveolar epithelial cells, which may be associated with a release of profibrotic mediators (such as transforming growth factor β 1 (TGF β 1)) fostering uncontrolled fibroblast activation, cell transformations into mesenchymal like myofibroblasts and an overwhelming matrix accumulation in the lung interstitium, which destroys normal alveolar architecture and disrupts gas exchange. The median survival time from IPF diagnosis is 2–4 years and to date, despite extensive research on IPF, no pharmacologic therapies have definitively been shown to meaningfully improve IPF life expectancy. Mucin 1 (MUC1) is a transmembrane mucin whose overexpression in carcinomas potentiates intracellular signalling by MUC1 cytoplasmic tail (MUC1-CT) phosphorylation, bioactivation and interaction with several proteins implicated in different cellular processes linked to IPF disease. MUC1 extracellular domain contains the KL6 epitope domain, which serves as biomarker in IPF. However, there is no evidence on the role of MUC1 intracellular bioactivation in the development of pulmonary fibrosis.

Objective

To characterize MUC1 intracellular bioactivation in IPF.

Methods and Results

The expression of MUC1 cytoplasmic tail (CT) and its phosphorylated forms at Thr⁴¹ and Tyr⁴⁶ were analysed by western blot and immunohistochemistry in healthy and IPF lung tissue. Lung fibroblasts and alveolar type II epithelial cells were stimulated with TGF β 1 or the pro-fibrotic factor galectin 3 to evaluate the role of MUC1 on the epithelial and fibroblast to mesenchymal transition, proliferation and senescence *in vitro*. A model of bleomycin-induced lung fibrosis was used in MUC1-Knockout (KO) and Wild type mice. The expression of MUC1-CT and its phosphorylated forms at Thr⁴¹ and Tyr⁴⁶ were increased in lung tissue from IPF patients and bleomycin-induced fibrotic mice. TGF β 1 increased MUC1-CT Thr⁴¹ and Tyr⁴⁶ phosphorylations, thus increasing the expression of the active pro-fibrotic factor β -catenin to form a nuclear complex of phospho-Smad3/MUC1-CT and MUC1-CT/ β -catenin. The nuclear complex activated alveolar epithelial type II and fibroblast to myofibroblast transitions as well as cell senescence and fibroblast proliferation. The antifibrotic pirfenidone as well as the inhibition of MUC1-CT nuclear translocation reduced cellular transformations, senescence and proliferation *in vitro*. The pro-fibrotic galectin 3 directly activated MUC1-CT and served as a

bridge between TGF β receptors and MUC1-C domain, indicating a TGF β 1 dependent and independent bioactivation of MUC1-CT. Lung fibrosis development was attenuated in MUC1-KO bleomycin-induced lung fibrosis mice.

Conclusions

MUC1-CT bioactivation is enhanced in IPF and may lead to future strategies as a druggable target for IPF.

INDEX

| | |
|--|-----------|
| INTRODUCTION | 27 |
| CHAPTER 1: IDIOPATHIC PULMONARY FIBROSIS | 29 |
| 1.1 DIFFUSE PARENCHYMAL LUNG DISEASES (DPLDs). DEFINITION AND CLASSIFICATION | 31 |
| 1.2 IDIOPATHIC PULMONARY FIBROSIS | 33 |
| 1.2.1 DEFINITION | 33 |
| 1.2.2 EPIDEMIOLOGY | 35 |
| 1.2.3 CLINICAL PRESENTATION | 35 |
| 1.2.4 POTENTIAL RISK FACTORS | 37 |
| 1.2.5 PATHOBIOLOGIC FEATURES | 40 |
| 1.2.6 CLINICAL TREATMENT | 43 |
| 1.2.6.1 PHARMACOLOGIC MANAGEMENT | 44 |
| 1.2.6.1.1 Failed clinical trials | 44 |
| 1.2.6.1.2 Approved pharmacological therapies | 45 |
| 1.2.6.1.3 Current main clinical trials | 47 |
| 1.2.6.2 NON PHARMACOLOGIC MANAGEMENT | 57 |
| 1.2.7 DIAGNOSIS | 58 |
| 1.2.8 IPF ANIMAL MODELS | 59 |
| CHAPTER 2: TRANSFORMING GROWTH FACTOR β | 63 |
| 2.1 ACTIVATION | 65 |
| 2.2 BIOLOGICAL ACTIONS | 65 |
| 2.3 SIGNALLING | 66 |
| 2.3.1 SMAD-DEPENDENT CANONICAL PATHWAY | 66 |
| 2.3.2 SMAD INDEPENDENT OR NON-CANONICAL PATHWAY | 68 |
| CHAPTER 3: MUCINS | 71 |
| 3.1 GENERAL FEATURES | 73 |
| 3.2 SECRETED MUCINS | 75 |

| | |
|--|------------|
| 3.2.1 SECRETED GEL-FORMING MUCINS | 75 |
| 3.2.2 SECRETED NON-GEL-FORMING MUCINS | 77 |
| 3.3 TRANSMEMBRANE MUCINS | 78 |
| 3.3.1 MUC4 | 79 |
| 3.3.2 MUC16 | 80 |
| 3.3.3 MUC1 | 81 |
| 3.3.3.1 STRUCTURE AND LOCATION | 81 |
| 3.3.3.2 SIGNALLING | 84 |
| 3.3.3.2.1 Barrier function, mucosal maintenance and interactions with mucosal pathogens | 84 |
| 3.3.3.2.2 Regulation of inflammatory responses | 85 |
| 3.3.3.2.3 Contribution to carcinogenesis and metastasis | 86 |
| HYPOTHESIS AND OBJECTIVES | 91 |
| CHAPTER 4: HYPOTHESIS | 93 |
| CHAPTER 5: OBJECTIVES | 97 |
| MATERIAL AND METHODS | 101 |
| CHAPTER 6: MATERIALS | 103 |
| 6.1 REAGENTS | 105 |
| 6.2 PATIENTS | 110 |
| 6.3 EXPERIMENTATION ANIMALS | 111 |
| CHAPTER 7: METHODS | 113 |
| 7.1 CELL CULTURE | 115 |
| 7.1.1 ISOLATION AND CULTURE OF PRIMARY ALVEOLAR TYPE II CELLS | 115 |
| 7.1.2 ISOLATION AND CULTURE OF PRIMARY LUNG FIBROBLASTS | 117 |
| 7.1.3 CULTURE OF IMMORTALIZED CELL LINES | 118 |
| 7.1.4 SMALL INTERFERING RNA - MEDIATED GENE SILENCING | 119 |
| 7.1.5 IN VITRO STIMULATION | 120 |

| | |
|---|-----|
| 7.1.6 SMAD BINDING ELEMENT ASSAY | 120 |
| 7.1.7 PROLIFERATION ASSAY | 122 |
| 7.1.8 CELL SENESENCE | 122 |
| 7.1.9 CELL IMMUNOFLUORESCENCE | 123 |
| 7.2. FIBROSIS ANIMAL MODEL | 125 |
| 7.2.1 PROTOCOL | 125 |
| 7.2.2 LUNG FUNCTION | 127 |
| 7.2.3 MOLECULAR IMAGE | 127 |
| 7.2.3.1 MICRO-CT-PET ANALYSIS | 127 |
| 7.2.3.2 MICRO-CT-SPECT ANALYSIS | 129 |
| 7.2.4 SAMPLE COLLECTION | 130 |
| 7.2.5 BRONCHOALVEOLAR LAVAGE FLUID | 130 |
| 7.2.5.1 TOTAL AND DIFFERENTIAL CELL COUNT | 130 |
| 7.2.5.2 ENZYME-LINKED IMMUNOSORBENT ASSAY (ELISA) | 130 |
| 7.3 HISTOLOGY | 132 |
| 7.3.1 TISSUE FIXATION AND DEHYDRATATION | 132 |
| 7.3.2 IMMUNOHISTOCHEMICAL ANALYSIS | 132 |
| 7.3.3 MASSON'S TRICHROME STAINING | 135 |
| 7.3.4 COIMMUNOFLUORESCENCE ASSAY | 136 |
| 7.4 GENE EXPRESSION ANALYSIS | 136 |
| 7.4.1 RNA EXTRACTION AND QUANTIFICATION | 136 |
| 7.4.2 REVERSE TRANSCRIPTION REACTION | 137 |
| 7.4.3 REAL TIME PCR | 138 |
| 7.5 PROTEIN EXPRESSION ANALYSIS | 140 |
| 7.5.1 WESTERN BLOTTING ANALYSIS | 140 |
| 7.5.2 IMMUNOPRECIPITATION | 143 |
| 7.6 STATISTICAL ANALYSIS | 144 |

| | |
|--|------------|
| RESULTS | 145 |
| CHAPTER 8: MUC1-CT EXPRESSION AND ACTIVATION IN IPF PATIENTS | 147 |
| 8.1. MUC1-CT EXPRESSION IS INCREASED AND ACTIVATED IN THE LUNG OF IPF PATIENTS | 149 |
| 8.2 TGF β 1 PHOSPHORYLATES MUC1-CT | 152 |
| CHAPTER 9: TGFβ1 AND MUC1-CT CROSSTALK IN IPF | 155 |
| 9.1 TGF β 1 COLLABORATES WITH MUC1-CT TO INDUCE ALVEOLAR TYPE II EPITHELIAL TO MESENCHYMAL AND FIBROBLAST TO MYOFIBROBLAST TRANSITIONS | 157 |
| 9.2 TGF β 1 PATHWAY ACTIVATION PROMOTES A P-SMAD3/MUC1-CT/ACT-B-CATENIN NUCLEAR PROTEIN COMPLEX FORMATION AND SMAD BINDING ELEMENT ACTIVATION | 161 |
| 9.3 MUC1-CT AND β -CATENIN ACTIVATION ARE DEPENDENT OF SMAD3 PHOSPHORYLATION | 166 |
| 9.4 MUC1 MEDIATES CELL SENESCENCE AND PROLIFERATION INDUCED BY TGF β 1 IN ATII CELLS AND LUNG FIBROBLASTS | 167 |
| 9.5 GALECTIN 3 ACTIVATES MUC1-CT VIA DEPENDENT AND INDEPENDENTLY OF THE TGF β RECEPTORS | 169 |
| 9.6 MUC1-CT CQC MOTIF INHIBITION REDUCES TGF1-INDUCED MUC1-CT NUCLEAR TRANSLOCATION, ALVEOLAR TYPE II TO MESENCHYMAL TRANSITION, FIBROBLAST TO MYOFIBROBLAST TRANSITION, ALVEOLAR TYPE II AND FIBROBLAST SENESCENCE AND FIBROBLAST PROLIFERATION | 171 |
| CHAPTER 10: MUC1-KO MOUSE MODEL OF BLEOMYCIN-INDUCED PULMONARY FIBROSIS | 175 |
| 10.1 SURVIVAL AND LUNG FUNCTION ARE IMPROVED IN A MUC1-KO BLEOMYCIN-INDUCED PULMONARY FIBROSIS MOUSE MODEL | 177 |
| 10.2 LUNG FIBROSIS IS INHIBITED IN A MUC1-KO BLEOMYCIN-INDUCED PULMONARY FIBROSIS MOUSE MODEL | 178 |
| 10.3 PULMONARY ARTERY REMODELLING AND LUNG METABOLIC ACTIVITY ARE ATTENUATED IN A MUC1-KO BLEOMYCIN-INDUCED PULMONARY FIBROSIS MOUSE MODEL | 179 |
| 10.4 TISSUE REMODELLING IS INHIBITED IN A MUC1-KO BLEOMYCIN-INDUCED PULMONARY FIBROSIS MOUSE MODEL | 181 |

| | |
|--|------------|
| 10.5 P-SMAD3/MUC1-CT/B-CATENIN NUCLEAR PROTEIN COMPLEX IS PROMOTED IN A BLEOMYCIN – INDUCED PULMONARY FIBROSIS MOUSE MODEL | 188 |
| DISCUSSION AND CONCLUSIONS | 191 |
| CHAPTER 11: DISCUSSION | 193 |
| 11.1 MUC1-CT EXPRESSION, LOCATION AND BIOACTIVATION IN IPF | 195 |
| 11.2 TGF β 1 AND MUC1–CT CROSSTALK IN THE IPF CONTEXT | 197 |
| 11.3 PHARMACOLOGICAL APPROACHES | 199 |
| CHAPTER 12: CONCLUSIONS | 205 |
| BIBLIOGRAPHY | 209 |
| ABBREVIATIONS INDEX | 235 |
| ANNEXES | 243 |
| ANNEX 1: ETHICS COMMITTEE APPROVAL AND WRITTEN INFORMED CONSENT MODEL FROM PATIENTS | 245 |
| ANNEX 2: ETHICS COMMITTEE APPROVAL FOR EXPERIMENTATION ANIMAL PROCEDURE | 249 |

INTRODUCTION

CHAPTER 1

IDIOPATHIC PULMONARY FIBROSIS

IDIOPATHIC PULMONARY FIBROSIS

1.1 DIFFUSE PARENCHYMAL LUNG DISEASES. DEFINITION AND CLASSIFICATION

Diffuse parenchymal lung diseases (DPLDs) or interstitial lung diseases (ILDs) are two imprecise clinical terms used to encompass the large and heterogeneous group of disorders (**Table 1**) characterized by cellular proliferation, interstitial inflammation, fibrosis, or a combination of such findings within the alveolar wall. These disorders are not due to infection or cancer [1]. The interstitium includes the space between the epithelial and endothelial basement membranes from the alveolar wall. However, these disorders frequently affect not only the interstitium, but also the airspaces, peripheral airways and vessels along with their respective epithelial and endothelial linings [2].

The group of DPLDs comprise a wide spectrum of diverse diseases. However, typically, all of them present with increasing breathlessness, lung crackles, and a widespread shadowing on the chest radiograph, associated with substantial morbidity and mortality [2]. Some ILDs are acute, whereas others are chronic, progressive and irreversible [3].

DPLDs range from disorders of known cause (collagen vascular disease, environmental or drug related) to disorders of unknown cause. The latter include idiopathic interstitial pneumonias (IIPs), granulomatous lung disorders (e.g., sarcoidosis) and a further group comprising several rare forms of DPLD with distinctive and well-defined clinicopathologic features, including lymphangioleiomyomatosis, pulmonary Langerhans' cell histiocytosis/histiocytosis X (HX) and eosinophilic pneumonia [2] (**Table 1**).

Interstitial fibrosis is the predominant phenotype in most cases of DPLDs. The majority of patients with interstitial fibrosis ultimately receive a diagnosis of chronic hypersensitivity pneumonitis (due to mold or bird exposure); pulmonary sarcoidosis; an underlying autoimmune disease; or if no cause is identified, IIP [1]. IIPs are classified as major IIPs (idiopathic pulmonary fibrosis (IPF), Idiopathic nonspecific interstitial pneumonia, respiratory bronchiolitis–interstitial lung disease, desquamative interstitial pneumonia, cryptogenic organizing pneumonia and acute interstitial pneumonia), rare IIPs (idiopathic lymphoid interstitial pneumonia and idiopathic pleuroparenchymal fibroelastosis) and unclassifiable cases because of an inadequate clinical, radiologic, or pathologic data or major discordance between clinical, radiologic, and pathologic findings [4].

Table 1. Diffuse parenchymal lung diseases (DPLDs) classification [2, 4].

| DPLD of known cause or association | DPLD of unknown cause | | |
|------------------------------------|------------------------------|---|---|
| | Granulomatous lung disorders | Idiopathic interstitial pneumonias (IIPs) | Other forms |
| Collagen vascular disease | Sarcoidosis | Major IIPs: <ul style="list-style-type: none"> • Idiopathic pulmonary fibrosis • Idiopathic non-specific interstitial pneumonia. • Respiratory bronchiolitis-interstitial lung disease. • Desquamative interstitial pneumonia • Cryptogenic organizing pneumonia • Acute interstitial pneumonia | Lymphangioleiomyomatosis |
| Drugs | | Rare IIPs: <ul style="list-style-type: none"> • Idiopathic lymphoid interstitial pneumonia • Idiopathic pleuroparenchymal fibroelastosis | Pulmonary Langerhans cell histiocytosis |
| Environmental factors | | Unclassifiable IIPs | Eosinophilic pneumonia |

1.2 IDIOPATHIC PULMONARY FIBROSIS

1.2.1 DEFINITION

The most common IIP is IPF [1]. It is defined as an specific form of chronic, progressive fibrosing interstitial pneumonia of unknown cause, occurring primarily in older adults, limited to the lungs and associated with the histopathologic and/or radiologic pattern of Usual interstitial pneumonia (UIP) [5]. Although disease course is variable and somewhat unpredictable, the median survival time from diagnosis is 2–4 years [6].

UIP pattern is characterized on high-resolution computed tomography (HRCT) by the presence of reticular opacities, often associated with traction bronchiectasis, and by the structure of honeycombing (**Figure 1**). The latter is manifested as clustered cystic airspaces, typically of comparable diameters on the order of 3–10 mm but occasionally as large as 2.5 cm. This pattern is usually subpleural and is characterized by well-defined walls. Ground glass opacities are also common, but usually less extensive than the reticulation. The distribution of UIP on HRCT is characteristically basal and peripheral, though often patchy. On histopathologic terms, this pattern is characterized by a heterogeneous appearance in which areas of fibrosis with scarring and honeycomb change alternate with areas of less affected or normal parenchyma (**Figure 2**). The fibrotic zones are composed mainly of dense collagen, although subepithelial fibroblast foci are also a consistent finding. Honeycomb change areas are composed of cystic fibrotic air spaces that are frequently lined by bronchiolar epithelium and filled with mucus and inflammatory cells. Smooth muscle metaplasia in the interstitium is commonly seen in both areas. Finally, inflammation is also characteristic in histopathologic UIP pattern, though it is usually mild. It consists of a patchy interstitial infiltrate of lymphocytes and plasma cells associated with hyperplasia of alveolar type II (ATII) cells and bronchiolar epithelium [5].

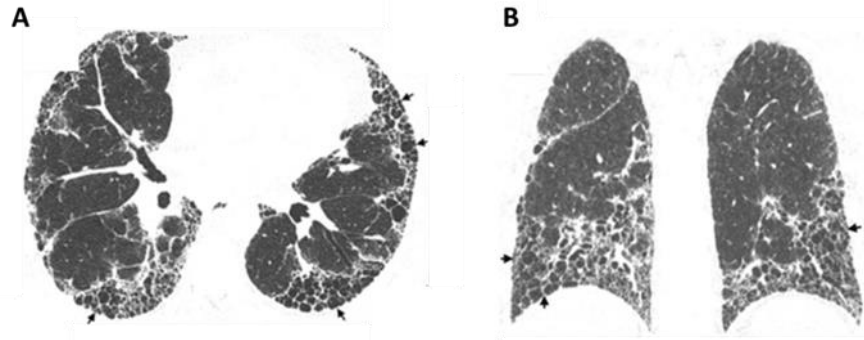


Figure 1. High-resolution computed tomography (HRCT) images demonstrating usual interstitial pneumonia (UIP) pattern. Axial (A) and coronal (B) HRCT images show basal and peripheral predominant patchy reticular abnormality with multiple layers of honeycombing (arrows). Adapted image from Raghu G, et al. [5].

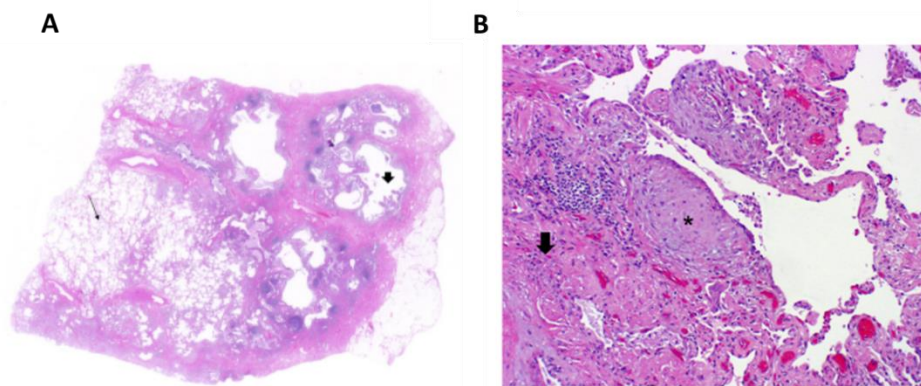


Figure 2. Surgical lung biopsy specimens demonstrating Usual Interstitial Pneumonia (UIP) pattern. (A) Histopathological image showing a patchy pattern alternating honeycomb spaces (thick arrow) with preserved lung tissue regions (thin arrow). (B) Histopathological image showing a fibroblast foci (asterisk) adjacent to the regions of more chronic fibrosis (thick arrow). Adapted image from Raghu G, et al. [5].

1.2.2 EPIDEMIOLOGY

IPF occurs worldwide. Nevertheless, the estimates of incidence and prevalence are difficult to establish because they vary depending on the definition used, the study design, time periods and the underlying population characteristics (such as age, gender, geographic location, etc.). To date, there are numerous published reviews that examine incidence and prevalence data from certain countries, but the different methodologies of case determination and different classification systems have prevented valid comparison between studies [7].

In general, studies agree that the condition is more common in men and in older people (median age at diagnosis is about 65 years) and, the prevalence of the disease appears to be increasing over time. However, it is unclear whether this increase reflects increased recognition because of the evolution of diagnostic methods, greater physician awareness around the disease or an aging population [1, 7].

From the different published studies, incidence ranges from 0.2 per 100 000 per year to 93.7 per 100 000 per year, with a tighter range of 3–9 per 100 000 per year based on conservative estimates from Europe and North America and fewer than 4 cases per 100 000 per year in South America and East Asia [7]. In Europe, the British Thoracic Society has estimated that the prevalence is around 50 per 100 000, with the highest rates in Northern Ireland, North West England, Scotland and Wales [8]. In the United States, the prevalence of IPF has been reported to range from 10 to 60 cases per 100 000 [1].

1.2.3 CLINICAL PRESENTATION

Clinicians should consider IPF in the differential diagnosis for adults presenting with unexplained exertional dyspnea, chronic dry cough, or velcro-like crackles on examination (**Table 2**). Moreover, spirometric results typically identify a reduced forced vital capacity (FVC), a reduced total lung capacity, and a reduction in diffusing capacity for carbon monoxide (DL_{CO}). However, FVC values and lung volumes can be normal during the early stages of IPF or when emphysema is also present. Lastly, in IPF, chest radiography often shows bilateral reticulation predominant in the lower lung zones [1].

Pulmonary and extrapulmonary comorbid conditions are also increasingly being recognized as important in patients with IPF [3]. In fact, one single-centre study demonstrated that 11.4% of IPF patients had no comorbidities; 57.7% had 1-3 comorbidities and 30.5% had 4-7 comorbidities [9]. Comorbidities of interest include both respiratory (chronic obstructive

pulmonary disease (COPD), pulmonary hypertension (PH), obstructive sleep apnoea, lung cancer and pulmonary embolism), as well as, non-respiratory (gastroesophageal reflux (GER), cardiovascular and metabolic comorbidities). Regarding the prevalence of each comorbidity, a systematic literature review including relevant observational studies from January 1990 to January 2015 estimated that prevalence of PH was 3–86% of patients, 6–91% for obstructive sleep apnoea, 3–48% for lung cancer, 6–67% for COPD, 3–68% for ischaemic heart disease and 0–94% for GER. It was also observed that mortality was highest among patients with IPF and lung cancer [10].

Table 2. Clinical presentation of Idiopathic Pulmonary Fibrosis [1]

| |
|--|
| History |
| <ul style="list-style-type: none"> • Chronic exertional dyspnea* • Chronic cough without purulence • Fatigue |
| Physical examination |
| <ul style="list-style-type: none"> • Bilateral Velcro-like crackles* • Clubbing • Acrocyanosis |
| Physiological findings |
| <ul style="list-style-type: none"> • Low DLco* • Resting hypoxemia or exertional desaturation • Normal or low FVC |
| Chest radiograph |
| <ul style="list-style-type: none"> • Nonspecific changes or bilateral basal reticular abnormalities |

* This finding is nearly universal in IPF. Other findings are often absent in the early stages of the disease.

FVC=forced vital capacity; DLco= diffusing capacity for carbon monoxide.

1.2.4 POTENTIAL RISK FACTORS

Although IPF is a disease of unknown etiology, a number of potential risk factors have been suggested:

- **Cigarette smoking:** Smoking is strongly associated with IPF, particularly for individuals with a smoking history of more than 20 pack-years [5].
- **Environmental exposures:** A significantly increased risk has been observed after exposure to metal dusts (brass, lead, and steel) and wood dust (pine). Farming, raising birds, hair dressing, stone cutting/polishing, and exposure to livestock and to vegetable dust/animal dust have also been associated with IPF [5]. It has been found recently, that interstitial lung abnormalities are associated with long-term average exposure to the air pollutants oxides of nitrogen, nitrogen dioxide and fine particulates [11].
- **Microbial agents:** Several studies have suggested a possible role for chronic infection with Epstein-Barr virus, cytomegalovirus, adenovirus, hepatitis C virus, human herpesvirus 7 (HHV-7), and HHV-8 as a persistent antigenic stimulus in IPF [12].
- **Gastroesophageal reflux (GER):** IPF patients have a high prevalence of abnormal esophageal acid exposure [13]. Based on descriptive studies in humans and experimental models in animals, it has been hypothesized that GER may lead to IPF progression due to chronic microaspirations (i.e., tracheobronchial aspirations of small amounts of gastric secretions) [14-16]. It has been observed that the reported use of GER medications is associated with decreased radiologic fibrosis and is an independent predictor of longer survival time in patients with IPF [17].
- **Obstructive sleep apnea (OSA):** moderate to severe OSA is associated with subclinical ILD and with evidence of alveolar epithelial injury and extracellular matrix (ECM) remodelling, an association that is strongest among normal-weight individuals [18].
- **Older age:** age is the strongest demographic risk factor for IPF, suggesting that ‘accelerated’ lung aging is a driving force for its development. Indeed, almost all of the cellular and molecular hallmarks of aging are exaggerated or occur prematurely in IPF [3].
- **Male sex.**
- **Genetic factors:** it is thought that several genetic factors might contribute to the development of IPF. The most convincing evidence for genetic predisposition to IPF comes from a familial clustering —i.e., cases affecting two or more members of the same biological family- of the disease (familial interstitial pneumonia (FIP)). FIP accounts for at least 5–10% of all cases of IPF. In addition, changes in gene sequence and variants in novel loci have been found to account for about a third of the risk of sporadic IPF development [19, 20].

Familial Interstitial Pneumonia

Genetic mutations that contribute to FIP have been identified in only 30% of families with this condition. These mutations are found in genes with known biological roles in alveolar epithelial cells (AECs). Approximately 5% of patients with FIP have mutations in genes encoding surfactant proteins, mainly pulmonary surfactant-associated protein C (SFTPC) and, less frequently, SFTPA2. Both proteins are manufactured and secreted by ATII cells and these mutations provoke either toxicity and possible cell death, or cell activation and epithelial–mesenchymal transition (EMT) in these cells, which leads to a fibrotic response [19]. Several different mutations in telomerase components (catalytic component (TERT), and RNA component (TERC)) and genes associated with telomere biology have been reported in the ~25% of FIP cases that result in abnormally short telomeres [19]. The mutated genes associated with telomere biology are: Poly (A)-specific Ribonuclease Deadenylation Nuclease (*PARN*), Regulator of Telomere Elongation Helicase 1 (*RTEL1*), dyskerin (*DKC1*), telomere-binding protein *TINF2* and nuclear assembly factor 1 (*NAF1*) [21-24]. Importantly, telomere attrition has been found in leukocytes and ATII cells from patients with FIP. Critically short telomeres activate a DNA damage response, which provokes cellular senescence or apoptosis [19].

Sporadic IPF

Two recent genome-wide association studies (GWAS) have identified several specific gene variants that significantly increase the risk of developing IPF. These genes are involved in epithelial cell–cell adhesion and integrity, the innate immune response, host defence and DNA repair [19].

The highest genetic risk factor for sporadic IPF is a common variant in the promoter region of mucin 5B gene (*MUC5B*), which encodes the major mucin macromolecule in airway mucus [25, 26] required for mucociliary clearance, maintaining immune homeostasis in the lungs, and controlling infections in the airway and middle ear [27]. A GWAS found that 38% of subjects with IPF and 9% of controls had a minor allele of the single nucleotide polymorphism (SNP) rs35705950 located 3-kb upstream of the *MUC5B* transcription start site. In addition to it, expression of this lung mucin has been found to be 14.1 times higher in subjects with IPF than those without IPF. The SNP rs35705950 was also associated with a 37.4-times upregulation in *MUC5B* expression in the lung in unaffected subjects. However, this genetic variant caused no significant difference in *MUC5B* expression in IPF patients. Therefore, this SNP is strongly associated with *MUC5B* overexpression in the lungs of

unaffected subjects and with the development of IPF. Moreover, it has been observed that MUC5B is expressed in IPF lesions. Interestingly, the minor risk allele rs35705950 is also associated with 34% subjects with FIP [28].

Several variants of genes that participate in epithelial functions were also found to increase the risk of IPF, including *DSP*, which encodes desmoplakin, an obligate component of desmosomes, which are especially important for maintaining the integrity of tissues that experience mechanical stress, such as the peripheral portions of lungs; *DPP9*, which encodes dipeptidyl peptidase 9, a protein that influences cell–ECM interactions, proliferation and apoptosis; and *AKAP13*, which encodes a Rho guanine nucleotide exchange factor regulating activation of RhoA, that is known to interact with a central fibrogenic pathway [19, 29].

25–30% of patients with sporadic IPF have substantially shorter telomeres in both leukocytes and ATII cells [19]. Then, several common variants that influence telomere length have been also associated with sporadic IPF. These variants are found in *TERT*, in genomic regions near *TERC* and in *OBFC1* (oligonucleotide-binding fold containing 1), which encodes a subunit of an alpha accessory factor that stimulates DNA polymerase- α -primase activity [30, 31]. Moreover, a recent case–control exome sequencing study identified variants in *RTEL1* and *PARN* as significant contributors to sporadic IPF [32].

Finally, regarding host defence, in addition to MUC5B, variants in ATPase, class VI, type 11A (*ATP11A*) and toll-interacting protein (*TOLLIP*) have been associated with sporadic IPF. The *ATP11A* gene encodes an ATP-binding cassette (ABC) transporter [33] and *TOLLIP* is an inhibitor of the transforming growth factor (TGF) β pathway [3] and also a protein in the toll-like receptor (TLR) pathway, which inhibits responses to microbes [1, 19]

- **Epigenetic factors:** regulation of gene expression by epigenetic influences has been recently suggested as an important mechanism of IPF. In fact, a study on epigenetic changes in IPF lung revealed that the levels of 18 microRNAs (miRNAs), including let-7d, were decreased in IPF lungs [3]. In the same way, a genome-wide methylation analysis identified numerous differentially methylated genes associated with the regulation of apoptosis and biosynthetic cellular processes in IPF lungs [34, 35]. Furthermore, IPF fibroblasts express less cyclooxygenase-2, and synthesize less prostaglandin E2, a potent downregulator of fibroblast activation, as a consequence of epigenetic abnormalities of histone acetylation [36].

1.2.5 PATHOBIOLOGIC FEATURES

The underlying cause of IPF was initially proposed to be chronic inflammation [37, 38]. However, in the last few years, advances in our understanding of its pathogenetic process have resulted in a shift from chronic inflammation to a multifactorial and heterogeneous process at different stages of evolution, with foci of proliferative fibroblasts, myofibroblast formation, abnormal lung epithelial cells, and an overwhelming matrix accumulation in the lung interstitium, which destroys normal alveolar architecture and disrupts gas exchange [39].

The alveolar epithelium comprises two main cell types: the alveolar type I (ATI) and ATII cells. The type I cells are involved in the process of gas exchange between the alveoli and blood and the type II cells synthesise, store and release pulmonary surfactant to optimise conditions for gas exchange. In IPF, loss of ATI and endothelial cells is produced and consequently, loss of integrity of the alveolar–capillary barrier basement membrane (BM) is produced, triggering the destruction of the alveolar structures and fusion of their BMs. ATII cells impaired renewal capacity and hyperplastic proliferation of them to cover the damaged BM are identified in IPF tissue [40-46]. Moreover, ATII cells demonstrate genomic instability; shortened telomeres; epigenetic changes; deregulated nutrient sensing; oxidative injury (as a result of reactive oxygen species (ROS) production); proteostatic deregulation and endoplasmic reticulum (ER) stress; mitochondrial dysfunction and altered intercellular communication [1, 47-49]. These processes drive them to release potent fibrogenic growth factors (such as TGF β 1, platelet-derived growth factor (PDGF) and connective-tissue growth factor (CTGF)), tumour necrosis factor α (TNF α), endothelin-1 (ET-1), osteopontin, angiotensinogen, several matrix metalloproteinases (including MMP1, MMP7 and MMP19) and a number of chemokines (including C-C motif chemokine ligand 2 (CCL2; also known as monocyte chemoattractant protein 1), stromal cell-derived factor 1 (also known as CXC motif chemokine 12, CXCL12) and interleukin (IL)-13) that perpetuate the cycle of injury, failed repair, and fibrosis [3]. Consequently, an aberrant epithelial mesenchymal cross-talk is triggered and it drives the recruitment and activation of highly synthetic and contractile myofibroblasts [50]. ATII cells also inhibit angiogenesis and promote the activation of coagulation signalling pathways that are involved in wound healing [51, 52].

IPF is also characterised by an excess of myofibroblasts that are persistently activated in fibrotic lungs [53]. The activated myofibroblasts are stellate- or spindle-shaped, and are characterised by secretion of ECM components (a characteristic shared with fibroblasts), such as collagen type I, and by the formation of contractile apparatus (a characteristic shared with airway smooth muscle cells), such as α -smooth muscle actin (α -SMA) microfilaments [54]. Other

phenotypic changes in IPF myofibroblasts include resistance to apoptosis, uncontrolled proliferation and invasive phenotypes [55, 56]. These features translate into an excessive accumulation of ECM components in the lung interstitium — predominantly fibrillar collagens, fibronectin, tenascin and proteoglycans [57]. Myofibroblasts in IPF lungs have heterogeneous phenotypes [58], possibly due to multiple origins of fibroblasts under IPF conditions (**Figure 3**). It has been suggested that myofibroblasts have at least four possible origins: resident lung fibroblasts, which differentiate directly under the influence of tissue injury to proliferate and express constituents of the ECM and α -SMA fibres (fibroblast-mesenchymal transition (FMT)) [59], epithelial cells [60, 61], fibrocytes [44, 62], and endothelial cells [63, 64]. Pleural mesothelial cells (PMCs) and lung pericytes transitioning to mesenchymal cells are also plausible candidates [65-69].

- **Epithelial–mesenchymal transition:** this process is characterized by the downregulation of epithelial markers, such as the tight junction proteins zonula occludens-1 (ZO-1) and E-cadherin, and the upregulation of mesenchymal markers, such as fibronectin, type I collagen, α -SMA, and vimentin [70]. Subsequently, epithelial cells lose their polarity and tight junctions and become more mobile [71].
- **Fibrocyte–mesenchymal transition:** mesenchymal cells can be also derived from bone marrow-derived progenitor circulating cells (fibrocytes), which locate and extravasate into tissue injury sites and differentiate into myofibroblasts [44, 72]. They constitutively express markers of stromal cells (collagen I and III and fibronectin) and hematopoietic cells (CD45, major histocompatibility complex II, and CD34) [44, 73, 74] and can express α -SMA in response to TGF β and ET-1 when they transform into myofibroblasts [75-77].
- **Endothelial–mesenchymal transition (EndMT):** similar to the EMT, during the EndMT, endothelial cells lose typical markers such as CD31 and vascular endothelial cadherin and gain mesenchymal markers such as fibroblast-specific protein 1 (FSP-1), α -SMA, vimentin, and collagen type I [64, 78].
- **Pericytes-mesenchymal transition:** Lung pericytes are mesenchymal-derived cells [79], localized within the BM of the alveolar–capillary barrier or perivascular linings, which share a common BM with endothelial cells [80, 81]. Currently, little is known about lung pericytes or their contribution to lung injury, but several studies have suggested that the transformation of pericytes to myofibroblasts may be crucial to pathogenic features of lung injury, including vascular leak and fibrogenesis [66, 82].

- **Pleural mesothelial cells – mesenchymal transition:** The pleura is a metabolically active monolayer of PMCs that closely approximates the lung parenchyma. IPF begins in the subpleural region and extends centrally, resulting in a progressive decline in lung function [67]. The close proximity of PMCs to the underlying lung ideally positions them to respond to cytokines, chemokines, and growth factors released during parenchymal stress, injury, infection, or inflammation. Furthermore, PMCs appear to extravasate into the lung parenchyma [69].

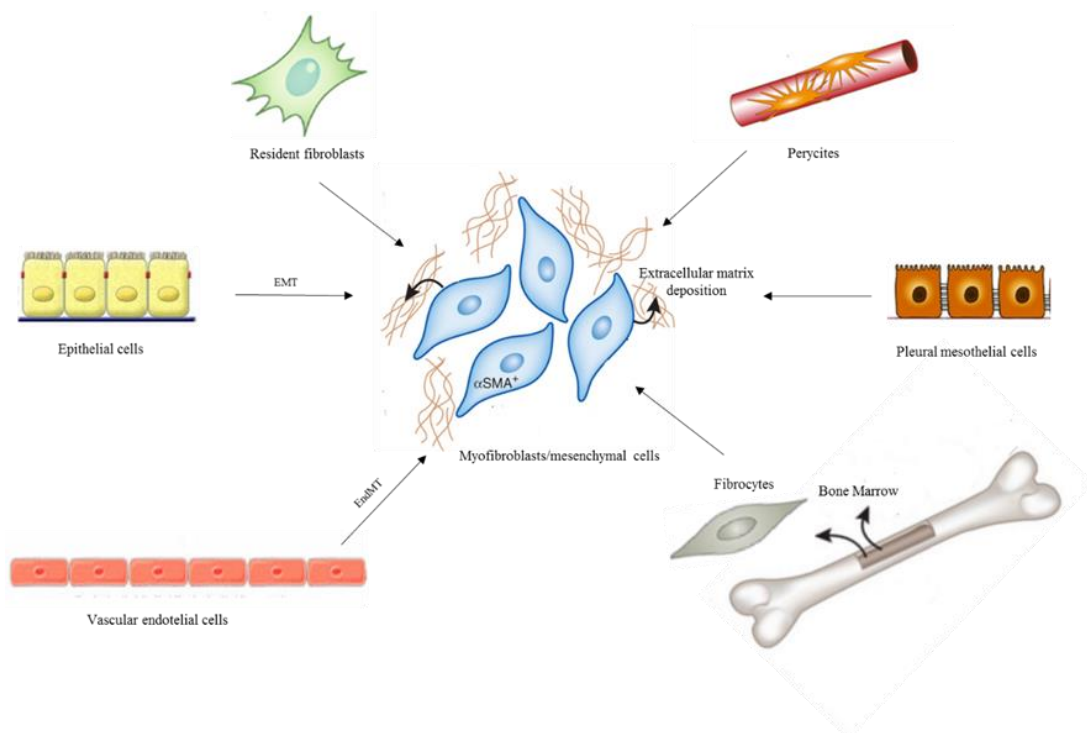


Figure 3. Origins of myofibroblasts in idiopathic pulmonary fibrosis (IPF). *Myofibroblast in IPF may be derived from lung resident fibroblasts (fibroblast-mesenchymal transition (FMT)), epithelial cells (epithelial-mesenchymal transition (EMT)), vascular endothelial cells (endothelial-mesenchymal transition (EndMT)), bone marrow fibrocytes, pleural mesothelial cells and perycites.*

Abnormal behaviour of AECs and fibroblasts is also associated with recapitulation of developmental pathways. For example, alveolar epithelium and fibroblasts from lungs affected by IPF overexpress members of the Wnt/ β -catenin pathway [83-85]. This pathway involves the binding of Wnt proteins (cysteine-rich secreted co-proteins) to frizzled cell-surface receptors and low-density lipoprotein co-receptors, which inhibits glycogen synthase kinase-3 β (GSK-3 β)

and the consequent hypophosphorylation of β -catenin, which is translocated into the nucleus [86], where it has been shown to induce myfibroblast activation, EMT, and collagen synthesis in *in vitro* studies [87]. Other examples are: the Sonic hedgehog (Shh) pathway, that becomes aberrantly activated in IPF, mainly in epithelial cells lining honeycomb cysts [88, 89] or the Notch signalling pathway, which is reactivated in AECs [65].

Finally, cell-type analyses in the lungs of both human IPF and bleomycin-injured mice have demonstrated that fibroblasts and epithelial cells acquire senescent identities [90]. Senescence of both types of cells appears to be a central phenotype that promotes lung fibrosis through the increased production of a complex senescence associated secretory phenotype (SASP) based on growth factors, cytokines, chemokines and matrix metalloproteinases, as well as, acquired apoptosis resistance [49]. The specific composition of SASP in lung strongly depends on the cell type, the senescence-inducing stimuli and the diversity of the microenvironment. In the case of IPF, the consequences of epithelial cell senescence might be: i) Non re-epithelialisation due to their inability to divide and, ii) FMT due to their profibrotic secretory profile [91]. Moreover, it's assumed that senescent epithelial cells are deleterious because it has been observed that by depleting senescent epithelial cells with senolytic compounds, alveolar SASP was reduced, which had potent antifibrotic effects and partly restored the normal epithelial cell phenotype [92]. Regarding fibroblasts, as a pharmacologic approach, a recent study has shown that deletion of senescent fibroblasts by suicide gene or senolytic strategies reduces pulmonary production of the characteristic SASP from senescent fibroblasts contributing to the fibrotic process [90].

1.2.6 CLINICAL TREATMENT

Despite extensive research on IPF, its pathophysiology is not still fully understood and, treatment options for this disease remain limited [93]. In 2011, the American Thoracic Society (ATS), European Respiratory Society (ERS), Japanese Respiratory Society and the Latin American Thoracic Association published joint guidelines for evidence based management of IPF [5]. Provision of 'best supportive therapy' is one of the principle approaches to management of IPF and is recommended despite variable strength in supporting evidence. Another category of treatment includes the use of pharmacologic agents with therapeutic intent, often at an investigational state in the context of controlled clinical trials.

1.2.6.1 PHARMACOLOGIC MANAGEMENT

1.2.6.1.1. Failed clinical trials

The focus of IPF treatment in previous decades was to use anti-inflammatory/immunomodulatory drugs in combination with antioxidants. In fact, in IFIGENIA study, N-acetyl L-cystein (NAC) added to azathioprine/prednisone resulted in a slower declines in FVC and DL_{CO} than the conventional two-drug therapy (prednisone and azathioprine) used previously to treat IPF [94]. However, any therapeutic usefulness of “anti-inflammatory/immunomodulatory” treatment in IPF was severely questioned by the unfavorable outcome of the IPF-Net consortium PANTHER trial where the treatment arm with prednisolone/azathioprine and NAC had to be prematurely terminated due to an increase in mortality (8 with the triple treatment versus 1 with placebo; p<0.01), hospitalizations and serious adverse events [95]. Following it, NAC monotherapy results were also negative [96], although a subgroup of IPF patients with the rs3750920 (*TOLLIP*) TT genotype showed a favourable response [97].

Advances in our understanding of the pathogenesis of IPF resulted in more preclinical and clinical trials focused on drugs with antiproliferative and antifibrotic effects. In this context, numerous failed drugs were tested in IPF patients. Firstly, interferon (IFN)- γ was initially investigated because of its immunomodulatory, antifibrotic, and antiproliferative effects. However, in a large phase III multicenter trial (INSPIRE), INF- γ combined with prednisone did not improve the duration of pulmonary function, progression-free survival, or quality of life [98]. Secondly, though effective in PH, ET-1 receptor antagonists failed in IPF clinical trials. ET-1 is an active vasoconstrictor peptide with pro-inflammatory and profibrotic properties. As ET-1 receptor antagonist, bosentan, was tested in two large phase III blinded, randomized trials (BUILD-1 and BUILD-3), and no difference in time of IPF progression or death was observed between the bosentan and placebo groups [99]. Similarly, two other ET-1 receptor antagonists, macitentan and ambrisentan, were tested in two phase II, randomized, double-blind, placebo-controlled studies (ARTEMIS-IPF and MUSIC respectively), and neither study showed benefits in the IPF patients. Furthermore, ambrisentan increased the risk of respiratory hospitalization (13% versus 9%) [100, 101].

Other examples for failures in IPF were the soluble TNFR2:IgG1 Fc chimeric TNF α capturing protein etanercept [102], which didn't improve the primary endpoints (changes in FVC, DL_{CO}, and alveolar–arterial gradient at rest) in patients with IPF [103]; the mammalian Target of Rapamycin (mTOR) kinase inhibitor everolimus, which is a derivative of rapamycin that

blocks the cell cycle at the G1–S phase, but it caused a more rapid disease progression compared to a placebo in a 3-year, placebo-controlled, double-blind, randomized trial [104] and the PDGF receptor (PDGFR)/cAbl/cKit inhibitor imatinib mesylate, which failed to improve survival or lung function in IPF patients compared to a placebo in a well-designed, multicentre, randomized, placebo-controlled trial [105].

Anticoagulants have also been suggested as anti-IPF drugs based on human and animal studies [106]. In this regard, to test the efficacy of the anticoagulant warfarin, a double-blind, placebo-controlled, randomized trial was designed. In this study, warfarin increased mortality in IPF patients compared to the placebo group [107].

Finally, it was thought that the parenchymal distortion in severe IPF caused abnormalities in the pulmonary vasculature including impaired nitric oxide (NO) production, pulmonary vasoconstriction and remodelling, potentially contributing to impaired gas exchange and PH. In this context, in the STEP-IPF trial, investigators treated patients with severe IPF ($DL_{CO} < 35\%$) with the phosphodiesterase (PDE) 5 inhibitor Sildenafil, which enhances signalling through the NO pathway and promotes pulmonary arterial vasodilation (in well ventilated lung areas). While Sildenafil did not meet the primary outcome measure of improved 6-min walk distance (6MWD) compared to placebo in the overall study population, there were small but statistically significant improvements in secondary measures, including improved DL_{CO} , arterial oxygenation, dyspnea symptoms and quality of life compared to placebo [108]. However, sildenafil significantly improved 6MWD (by 99.3m) in the subgroup of patients with IPF and right sided ventricular systolic dysfunction that was associated with an improvement in quality of life. Then, sildenafil may have acted in this group by addressing PH [109]. Therefore, sildenafil is not routinely recommended for IPF treatment because there is insufficient evidence of its beneficial effects in IPF.

1.2.6.1.2. Approved pharmacological therapies

Although numerous clinical trials have failed, two new therapies for IPF have been recently approved, pirfenidone and nintedanib, marking the beginning of IPF as a treatable disease.

Pirfenidone

In line with the antioxidant treatments tested in IPF, pirfenidone was initially considered as an antioxidant therapy since it demonstrated O_2^- scavenging activity [110, 111]. In fact, oral NAC has been used in conjunction with pirfenidone to treat IPF, but it has not substantially altered the tolerability profile of pirfenidone and is unlikely to be beneficial in IPF [112]. Beyond its antioxidant activity, pirfenidone is a pleiotropic molecule that inhibits $TGF\beta$, collagen

synthesis and fibroblast proliferation, and also mediates tissue repair [113-116]. In addition, it has been recently published that pirfenidone induces anti-fibrotic effects in systemic sclerosis-associated ILD by interfering the Shh signalling pathway [117]. In spite of these findings, pirfenidone molecular target is still not well defined.

Initially, two phase III trials in Japan with 275 patients found that pirfenidone increased progression-free survival, a decreased rate of FVC decline, and decreased acute exacerbations of IPF at week 52 [118, 119]. These results led to the regulatory approval of pirfenidone as a treatment of IPF in Japan in 2008. To confirm these findings, two large parallel, multi-national, randomized, placebo-controlled, multicentre trials of pirfenidone versus a placebo, were conducted in 110 centres in Europe, Australia, and North America (CAPACITY I and II) [120]. The results from these studies were inconsistent, but in spite of this, pirfenidone was approved in Europe in 2011 and Canada in 2012. However, due to inconsistencies in the CAPACITY study, it was not approved until 2014 in the United States because the Food and Drug Administration (FDA) required more data. This additional study, the Assessment of Pirfenidone to Confirm Efficacy and Safety in IPF (ASCEND), was conducted in New Zealand, North, Central, and South America, and Australia. Similar to previous studies, treatment with pirfenidone was found to be generally safe, with no unacceptable side effect profile, and the number of adverse events and deaths were reduced in the pirfenidone group compared to placebo group [121]. Recently, an increased 3-years survival rate of 73% has been observed in a real-life IPF cohort (without including the restrictions of a clinical trial) compared to previously used medications [122].

Nintedanib

Nintedanib, formerly known as BIBF 1120, was approved by the FDA in 2014 and in the EU, Canada, Japan, Switzerland and other countries in 2015. Nintedanib is a tyrosine kinase inhibitor that blocks tyrosine kinase signalling by inhibiting the activation of vascular endothelial growth factor (VEGF), fibroblast growth factor (FGF), and PDGF receptors. Firstly, in a mouse model, nintedanib notably improved IPF in a preventative and therapeutic model [123]. Following it, the TOMORROW trial, a double-blind, randomized, placebo-controlled phase II trial, suggested that nintedanib reduced the rate of FVC decline by 68% compared to a placebo after 12 months, with preservation of health-related quality of life. In addition to it, nintedanib reduced the occurrence of acute exacerbation versus the placebo, which was considered to be more than promising [124]. Following this trial, two identical phase III trials (INPULSIS-1 and INPULSIS-2) were conducted to evaluate the safety and efficacy of nintedanib treatment in patients with IPF. The INPULSIS studies were double-blind, randomized, parallel-group, placebo-controlled, multicentre trials conducted at 205 sites in 24 countries in Europe, America, Asia,

and Australia. In both trials, after 52 weeks of treatment, nintedanib significantly reduced the rate of decline in FVC and it was frequently associated with diarrhea, which led to discontinuation of the study medication in less than 5% of patients [125]. In a recent study, it has been shown that the rate of decline in FVC and the treatment effect of nintedanib are the same in patients with preserved lung volume (FVC >90% predicted) as in patients with greater impairment in FVC, supporting the value of early treatment of IPF [126].

1.2.6.1.3. Current main clinical trials

Despite the approval of pirfenidone and nintedanib, there is still no therapy that definitively improves quality of life or survival of IPF patients. Therefore, numerous targeted therapies outlined briefly below are being tested in numerous clinical trials (**Table 3**).

Zileuton

A randomized phase II clinical trial (clinicaltrials.gov identifier NCT00262405) comparing zileuton (inhibitor of 5-lipoxygenase (5-LO)) with azathioprine/prednisone has been completed in IPF patients, but yet no results have been posted after study completion in May 2007. Leukotrienes, lipid mediators of inflammation derived from the 5-LO pathway of arachidonic metabolism, are elevated in IPF patients and they have been shown to induce matrix protein synthesis in addition to promoting fibroblast migration and proliferation [127, 128].

QAX576 and lebrikizumab

QAX576 and lebrikizumab are both anti-IL-13 drugs. A non-randomized phase II trial (clinicaltrials.gov identifier: NCT00532233) and a double-blind, randomized, placebo-controlled phase II trial (clinicaltrials.gov identifier: NCT01266135) with QAX576 have been terminated but the anticipated publications are not available. Lebrikizumab, has been tested in a multicentre, randomized, placebo-controlled, double-blind phase II study (clinicaltrials.gov identifier: NCT01872689) and it has been shown that in spite of being well tolerated, lebrikizumab monotherapy is not associated with a benefit on lung function or mortality over 52 weeks of treatment in patients with IPF [129]. Then, a phase II, randomized, multicentre, double-blind, placebo-controlled, parallel-group trial to evaluate the efficacy and safety of lebrikizumab as combination therapy with background pirfenidone in patients with IPF has been designed. It has not been reported a treatment benefit relating to FVC change over 52 weeks, but a suggestion of benefit on mortality and acute exacerbations have been observed [130].

Carlumab (CNTO888)

A placebo-controlled, randomized phase II trial (clinicaltrials.gov identifier: NCT00786201) has been conducted for CNTO-888 (carlumab), a monoclonal antibody against human CCL2. No unexpected serious adverse events have been noted and, although dosing was stopped prematurely, it is unlikely that carlumab provides benefit to IPF patients [131].

Fresolimumab (GC1008)

A pioneering phase I, open-label, single-dose (escalating) study has evaluated whether fresolimumab (GC1008), a human monoclonal antibody that neutralizes TGF β 1, is safe for treating patients with IPF. This study (clinicaltrials.gov identifier: NCT00125385) has been completed, but the results have not been published yet. Nevertheless, it has been published that fresolimumab reverses markers of skin fibrosis [132].

BG00011 (STX-100) and GSK3008348

Since targeting TGF β 1 may alter physiological homeostasis and lead to undesirable side effects, its activation cascade might be a more attractive IPF therapeutic target. In this aim, a phase I study (clinicaltrials.gov identifier: NCT02612051) have been designed to examine a single nebulized dose of GSK3008348 (an integrin $\alpha\beta$ 6 antagonist). The humanized monoclonal antibody anti- $\alpha\beta$ 6 integrin BG0011 (also known as STX-100) has been investigated in escalating doses in a phase II study (clinicaltrials.gov identifier: NCT01371305). Both studies have been completed but, only the results from GSK3008348 phase I clinical trial have been published, supporting further development of it as a novel inhaled treatment option for IPF [133].

Pamrevlumab (FG-3019)

A randomized phase II trial (clinicaltrials.gov identifier: NCT01262001) to evaluate pamrevlumab (FG-3019), an anti-CTGF antibody, has been completed. In spite of the requirement of a larger follow up study to confirm the results, in comparison to placebo, IPF patients treated with pamrevlumab showed less lung fibrosis progression measured by Quantitative High Resolution Computed Tomography [134]

Losartan

Angiotensin II (ANGII) is a vasoconstrictor that is overexpressed in the lungs of IPF patients [135]. It has been shown that ANGII acts *in vitro* as a proapoptotic factor in AECs, induces human lung fibroblast proliferation and induces lung procollagen production via the angiotensin type 1 (AT1) receptor [136-138]. Losartan, an AT1 receptor antagonist, has been investigated in a non - applicable phase clinical trial (clinicaltrials.gov identifier: NCT00879879).

This study has been finished, but not all of the results have been published. Nevertheless, the only report on this study has described a stable or improved FVC response and a low toxicity profile [139].

BMS-986020

Lysophosphatidic acid (LPA) is a profibrotic mediator with proinflammatory activity regulated through a family of at least five G-protein-coupled receptors, designated LPA1–5 [140]. BMS-986020 (formerly AM152), a specific LPA1 antagonist, was shown to be safe and well-tolerated by IPF patients in a phase I clinical study. Then, a phase II study (clinicaltrials.gov identifier: NCT01766817) was also completed, slowing the rate of FVC decline, but elevating hepatic enzymes [141].

Tetrathiomolybdate and minocycline hydrochloride

A phase I/II trial (clinicaltrials.gov identifier: NCT00189176) has been completed to evaluate tetrathiomolybdate, an agent with angiostatic properties. It has been shown to attenuate fibrosis, with a concomitant reduction in angiogenesis in a bleomycin model of pulmonary fibrosis [142, 143]. Furthermore, minocycline hydrochloride, a semisynthetic derivative of tetracycline with antiangiogenic properties, has also been tested in a phase III clinical study (clinicaltrials.gov identifier: NCT00203697). Results from both studies are awaited.

TD139

Inhaled TD139, a novel inhibitor of galectin 3, a β -galactoside-binding animal lectin highly expressed in IPF patients [144], has been tested in a phase I/II placebo-controlled clinical trial (clinicaltrials.gov identifier: NCT02257177). This study has been completed and the results indicate that TD139 is both safe and well tolerated [145].

GSK-2126458

The phosphoinositide 3-kinase (PI3K)/protein kinase B (AKT)/mTOR-dependent pathway is deregulated in fibroproliferative diseases such as pulmonary fibrosis [146]. Regarding it, a dose-escalation/dose-finding, placebo-controlled, randomized, double-blind phase I study (clinicaltrials.gov identifier: NCT01725139) has recently been completed to assess GSK-2126458, a highly selective pyridyl sulfonamide inhibitor of class I isozymes of PI3K and mTOR in subjects with IPF. The results of this study demonstrate an acceptable safety profile of GSK-2126458 in patients with IPF at exposures for which target engagement has been demonstrated [147].

Nandrolone decanoate

A phase I/II open-label study (clinicaltrials.gov identifier: NCT02055456) with nandrolone decanoate, an anabolic androgenic steroid to induce *TERT* gene expression, in diseases characterized by abnormal telomere shortening, including IPF, is currently in an unknown recruitment status [19].

IW001

It has been observed that 40–60% of IPF patients may display an autoimmune response against type V collagen (Col (V)) [148], a minor collagen found primarily within the fibrils of the major lung collagen, type I. Oral immunotherapy with Col (V) (IW001) has been tested in an open label, phase I, multicentre study (clinicaltrials.gov identifier: NCT01199887). This study has been finished and IW001 appears to be safe and well-tolerated, and may have a beneficial impact on disease progression based on trends in FVC stabilisation [148].

PRM-151

The endogenous blood plasma protein pentraxin (PTX-2), has been shown to accumulate at sites of fibrosis in animal models [149]. Moreover, PTX-2 inhibits differentiation of monocytes into pro-inflammatory and pro-fibrotic macrophages and fibrocytes, while promoting their differentiation into regulatory macrophages [150]. This in turn promotes epithelial healing and resolution of inflammation and scarring. A phase II, randomized, double-blind, placebo controlled, pilot study (clinicaltrials.gov identifier: NCT02550873), designed to evaluate the efficacy and safety of PRM-151 (recombinant human PTX-2) administration is currently active. Preliminary results show that PRM-151 is well tolerated at all dose levels, with no serious adverse reactions. Moreover, FVC and 6MWD tests show trends towards improvement in the PRM-151 dose groups. However, efficacy and safety of PRM-151 in IPF will be investigated in a dedicated future trial [151].

Octreotide

Octreotide is a somatostatin (growth hormone inhibiting hormone) analog with a long half-life *in vivo*. Somatostatin receptors and octreotide uptake are increased in the IPF lungs. A phase I/II clinical study (clinicaltrials.gov identifier: NCT00463983) with IPF patients receiving an intramuscular injection of slow release octreotide has been designed. It has been observed that it is well tolerated and provide a proof of concept that octreotide treatment slows down the progression of lung fibrosis. Nevertheless, these results need to be confirmed by a larger placebo-controlled study [152].

KD025

Actin filament assembly and actomyosin contraction are directed by the Rho-associated coiled-coil forming protein kinase (ROCK) family of serine/threonine kinases [153]. Currently, a phase II clinical study (clinicaltrials.gov identifier: NCT02688647) is ongoing to evaluate the safety, tolerability, and activity of KD025, ROCK2 inhibitor, compared to standard of care in male and postmenopausal/surgically sterilized female subjects with IPF. Preliminary results have shown that KD025 reduced patients' decline in FVC at week 24 by 73 percent, compared with patients receiving supportive care [154].

Tipelukast (MN-001)

Tipelukast is a leukotriene receptor antagonist, PDE inhibitor (mainly 3 and 4), and 5-LO inhibitor. It also down-regulates genes that promote fibrosis (such as collagen type 1), and genes responsible for promoting inflammation (like C-C chemokine receptor type 2 (CCR2) and monocyte chemoattractant protein 1 (MCP-1)). Currently, a phase II randomized, placebo-controlled, double-blind study (clinicaltrials.gov identifier: NCT02503657) with MN-001 in moderate to severe IPF patients is ongoing.

GLPG1690

Autotaxin (ATX) is a secreted lysophospholipase D largely responsible for extracellular LPA production. In pulmonary fibrosis, ATX levels rise in the bronchoalveolar lavage fluid (BALF) and stimulate LPA production [155]. Recently, a multicentre randomized, double-blind, parallel group, placebo-controlled, phase II study (clinicaltrials.gov identifier: NCT02738801) with GLPG1690, a selective ATX inhibitor, has been completed. It has been well-tolerated, with most side effects being mild to moderate and, results particularly for FVC, are encouraging and support further clinical assessment of GLPG1690 as a treatment for IPF [156].

Sirolimus

Sirolimus is a rapamycin analogous and mTOR inhibitor. Currently, a non - applicable phase, short-term pilot study (clinicaltrials.gov identifier NCT01462006) is ongoing. As compared with placebo, short treatment with sirolimus resulted in reduction of circulating fibrocyte concentrations in IPF patients, and was associated with an acceptable safety profile. Future studies to assess the effect of long-term sirolimus treatment on the natural history of IPF are warranted [157].

PBI-4050

Recent studies have determined that PBI-4050 acts as an agonist for GPR40 and as an antagonist for GPR84, both of them free fatty acid receptors. It has been shown that inhibits fibrosis in a number of models of tissue fibrosis [158] and reduces the production of TGF β 1, CTGF and IL-6 [19]. Recently, a phase II, open-label, single-arm study (clinicaltrials.gov identifier NCT02538536) with PBI-4050 has been completed, and FVC results are encouraging for PBI-4050 alone and in combination with nintedanib, despite limitations in sample size and study design [159].

Rituximab

Rituximab is a chimeric anti-CD20 monoclonal antibody that works by destroying B cells, which produce autoantibodies. It's approved by the FDA for the treatment of autoimmune diseases such as rheumatoid arthritis. Currently, a double-blinded, phase II trial (clinicaltrials.gov identifier NCT01969409) in IPF patients has been designed to determine if rituximab reduces the autoantibody levels that might be contributing to the lung damage in IPF. This study is currently active and the results are not posted yet. However, a positive response to rituximab with few complications of treatment has been observed in connective tissue disease related ILD [160].

CC-90001

Preclinical evidence suggests that Jun N-Terminal Kinase (JNK) enzyme function is required for key steps in the pulmonary fibrotic process [161]. In this regard, a phase II, multicentre, multinational, randomized, double-blind, placebo-controlled study (clinicaltrials.gov identifier NCT03142191) of two treatment doses of CC-90001, a second generation JNK inhibitor, in subjects with IPF, is currently recruiting patients.

Vismodegib plus pirfenidone

Vismodegib is a Shh pathway inhibitor [19] which has been tested in a single arm, multicentre, open-label, phase Ib study (clinicaltrials.gov identifier NCT02648048) to be evaluated in combination with pirfenidone in participants with IPF. This study has been completed but the results have not been posted yet.

Pirfenidone plus nintedanib

Due to the lack of comparative trials of pirfenidone and nintedanib in the same population of IPF patients or effective predictive markers of response to therapy, the choice of the treatment is left to the physicians' judgment and patients' preference [162]. Interestingly, two phase IV studies (clinicaltrials.gov identifiers: NCT02598193 and NCT02579603) to evaluate

the tolerability and safety of a combination treatment of nintedanib and pirfenidone in participants with IPF have been completed recently. This combination was well tolerated by the majority of patients with IPF, and associated with similar types of treatment-emergent adverse events and discontinuation rates expected with either treatment alone. Results of these trials encourage further study to determine efficacy and safety of pirfenidone and nintedanib taken as combination treatment versus monotherapy in patients with IPF [163].

Mesenchymal stem cell therapy

The use of mesenchymal stem cells (MSCs) has been proposed as a potential therapeutic for IPF because of their role in tissue repair and wound healing combined with their immunomodulatory properties and immuno-privileged status [19]. Then, several phase I clinical trials (clinicaltrials.gov identifiers: NCT01385644, NCT01919827 and NCT02013700) focused on the use of MSCs as IPF therapy have been completed. The results published until this moment have reported no complications or toxic effects. However, there are no significant changes in pulmonary function or 6 MWD [19].

Table 3. Selected novel drug candidates for idiopathic pulmonary fibrosis.

| Therapy | Development status | Mechanism of action | Clinical trials.gov ID |
|---------------------------------|---------------------------------|---|-----------------------------|
| Pirfenidone | Approved | - TGF β inhibitor - Shh pathway inhibitor - Antioxidant | |
| Nintedanib | Approved | Inhibitor of VEGFR, PDGFR and FGFR | |
| Pirfenidone + Nintedanib | Phase IV (completed) | | NCT02598193 NCT02579603 |
| Zileuton | Phase II (completed) | 5-LO inhibitor | NCT00262405 |
| QAX576 | Phase II (completed/terminated) | Anti-IL-13 | NCT00532233/ NCT01266135 |

| | | | |
|--------------------------------------|---|---|-------------|
| Lebrikizumab | Phase II (completed) | Anti-IL-13 | NCT01872689 |
| Carlumab (CNTO-888) | Phase II (completed) | Anti-CCL2 | NCT00786201 |
| Fresolimumab (GC1008) | Phase I (completed) | TGF β neutralizing antibody | NCT00125385 |
| BG00011 (STX-100) | Phase II (completed) | Anti- $\alpha\beta$ 6 integrin | NCT01371305 |
| GSK3008348 | Phase I (completed) | $\alpha\beta$ 6 antagonist | NCT02612051 |
| Pamrevlumab (FG-3019) | Phase II (completed) | Anti-CTGF | NCT01262001 |
| Losartan | Non - applicable phase (completed) | AT1 receptor antagonist | NCT00879879 |
| BMS-986020 | Phase II (completed) | LPA receptor 1 antagonist | NCT01766817 |
| Tetrathiomolybdate | Phase I/II (completed) | Angiostatic agent | NCT00189176 |
| Minocycline hydrochloride | Phase III (unknown recruitment status) | Antiangiogenic agent | NCT00203697 |
| TD139 | Phase I/II (completed) | Galectin 3 inhibitor | NCT02257177 |
| GSK-2126458 | Phase I (completed) | PI3K class I isozymes inhibitor/ mTOR inhibitor | NCT01725139 |
| Nandrolone decanoate | Phase I/II (unknown recruitment status) | <i>TERT</i> gene expression induction | NCT02055456 |
| IW001 | Phase I (completed) | Oral immunotherapy with Col V | NCT01199887 |

| | | | |
|------------------------------------|--|---|---|
| PRM-151 | Phase II (Active, not recruiting) | Recombinant human PTX-2 | NCT02550873 |
| Ocreotide | Phase I/II (completed) | Somatostatin analog | NCT00463983 |
| KD025 | Phase II (recruiting participants) | ROCK2 inhibitor | NCT02688647 |
| Tipelukast (MN-001) | Phase II (recruiting participants) | - Leukotriene receptor antagonist. - PDEs inhibitor. - 5-LO inhibitor | NCT02503657 |
| GLPG1690 | Phase II (completed) | Autotaxin inhibitor | NCT02738801 |
| Sirolimus | Non - applicable Phase (active, not recruiting participants) | mTOR inhibitor | NCT01462006 |
| PBI 4050 | Phase II (completed) | GPR40 agonist/ GPR84 antagonist | NCT02538536 |
| Rituximab | Phase II (active, not recruiting participants) | Anti-CD20 | NCT01969409 |
| CC-90001 | Phase II (recruiting participants) | JNK inhibitor | NCT03142191 |
| Vismodegib plus pirfenidone | Phase Ib (completed) | Shh pathway inhibitor + Pirfenidone | NCT02648048 |
| MSCs therapy | Phase I (completed) | - Tissue repair - Wound healing - Immunomodulatory properties | NCT01385644/ NCT01919827/ NCT02013700 |

TGFβ: transforming growth factor β; Shh: sonic hedgehog; VEGFR: vascular endothelial growth factor receptor; PDGFR: platelet derived growth factor receptor; FGFR: fibroblast growth factor receptor; 5-LO: 5-lipoxygenase; IL-13: interleukin 13; CCL2: chemokine ligand 2; CTGF: connective tissue growth factor; AT1: angiotensin type I; LPA: lysophosphatidic acid; PI3K: phosphatidylinositol 3-kinase; mTOR: mammalian target of rapamycin; Col V: collagen type V; PTX-2: pentraxin; ROCK2: Rho associated coiled-coil containing protein kinase 2; PDE: phosphodiesterase; JNK: Jun N-Terminal Kinase; MSCs: mesenchymal stem cells.

Current main clinical trials focused on symptoms or comorbidities

In addition to all the clinical trials mentioned above, several ongoing or recently completed clinical trials have been designed to alter IPF symptoms or comorbidities, which may improve pulmonary function and quality of life.

IPF-associated cough

A pilot phase II study (clinicaltrials.gov identifier: NCT01442779) of low dose oral IFN- α has been completed and it has been observed that it improves the IPF-associated cough. A phase III, double blinded, randomized, placebo controlled, crossover trial (clinicaltrials.gov identifier: NCT00600028) to test the efficacy of thalidomide in suppressing the chronic cough of IPF has been also completed and, it has been shown to improve cough and respiratory quality of life in patients with IPF [164]. Lastly, currently, a non-applicable phase clinical study (clinicaltrials.gov identifier: NCT02173145) of azithromycin is recruiting patients. The investigators hypothesize that immunomodulatory treatment reduces cough frequency and might improve lung function.

IPF-associated dyspnea

A phase III clinical trial (clinicaltrials.gov identifier: NCT03018756) is currently ongoing to evaluate the effects of inhaled opiate therapy (fentanyl citrate) on dyspnea, which is a severe symptom that is closely linked to poor perceived quality of life in IPF patients [19].

IPF-associated pulmonary hypertension

A phase II open label, dose escalation study (clinicaltrials.gov identifier: NCT01265888) to find the minimally and maximum effective dose of inhaled NO in patients with PH secondary to IPF has been completed. Previously, it was demonstrated continued benefits of inhaled NO for improvement of arterial oxygenation, pulmonary arterial pressure and exercise tolerance in a patient with end-stage IPF and PH [165]. A phase II/III clinical study (clinicaltrials.gov identifier: NCT00981747) of sildenafil plus losartan to target vascular reactivity in IPF patients have been also conducted, but it has been terminated because of withdrawn funding. In addition to it, a phase II study (clinicaltrials.gov identifier: NCT00694850) of BAY63-2521, stimulator of soluble guanylate cyclase, is ongoing to evaluate if it is safe and can help to improve the well-being symptoms and outcome of PH associated with lung fibrosis. Finally, a phase II/III multicentre, randomized, double-blinded, placebo-controlled trial (clinicaltrials.gov identifier: NCT02630316) of treprostinil, analog of prostacyclin, is also currently ongoing to evaluate the safety and efficacy of inhaled treprostinil in subjects with PH associated with ILD, including combined pulmonary fibrosis and emphysema.

IPF-associated gastroesophageal reflux

Currently, a phase II study (clinicaltrials.gov identifier: NCT01982968) is ongoing to test the hypothesis that treatment with laparoscopic anti-reflux surgery in subjects with IPF and abnormal GER, may slow the decline of FVC over 48 weeks. Otherwise, a randomized, double-blind, placebo-controlled pilot trial (clinicaltrials.gov identifier: NCT02085018) of omeprazole in IPF has been recently completed to test whether the stomach acidity "switched off" by omeprazole does reduce GER and consequently cough in patients with IPF. Omeprazole was shown to be well tolerated and adverse event profiles were similar to placebo group, although there was a small excess of lower respiratory tract infection and a small fall in forced expiratory volume and FVC associated with omeprazole [166].

Antimicrobial therapy

A phase III clinical study (clinicaltrials.gov identifier: NCT02759120) of antimicrobial therapy (co-trimoxazole or doxycycline) is currently recruiting patients to assess the influence of this antimicrobial therapy in clinical outcomes such as respiratory hospitalization and all-cause mortality.

1.2.6.2. NON PHARMACOLOGIC MANAGEMENT

Non pharmacologic management strategies help patients with IPF to live healthier and with more normal lives. Smoking cessation should be a priority for patients who are actively using tobacco products. Moreover, influenza, pneumococca, and other age-appropriate vaccines should be administered [1]. Other options are:

- **Supplemental oxygen:** clinical practice guidelines strongly recommend supplemental oxygen for patients with IPF. Oxygen administration reduces exertional dyspnea and improves exercise tolerance [1]. A non-applicable phase clinical trial (clinicaltrials.gov identifier: NCT02551068) to determine if patients with IPF taking nintedanib will have improved exercise endurance, breathlessness and quality of life if breathing 60% oxygen compared to standard of care during an 8 week exercise training program, is currently recruiting patients.
- **Pulmonary rehabilitation:** exercise limitation, exercised-induced hypoxia and PH are common in patients with IPF. To solve this problem, pulmonary rehabilitation is a comprehensive intervention to improve the physical and psychological condition of the patient and also promote the long-term adherence to health-enhancing behaviours [3]. This intervention involves: aerobic conditioning, strength and flexibility training, educational lectures, nutritional interventions, and psychosocial support [5].

- **Lung transplantation:** given the progressive and incurable nature of IPF, lung transplantation is commonly considered for patients with moderate to severe disease. The ideal timing for referral and listing for lung transplantation remains challenging owing to the wide variability in clinical course and life expectancy as well as the rapid and often catastrophic clinical deterioration associated with acute exacerbations [3]. Only 66% of transplant recipients with IPF survive for more than 3 years after transplantation and only 53% survive for more than 5 years [1].

1.2.7 DIAGNOSIS

When the history and physical examination of a patient suggest ILD, clinicians should exclude an identifiable cause of it, such as domestic and occupational exposures, connective tissue disease and drug toxicity. It's also looked for signs and symptoms of autoimmune conditions. However, the presence of autoantibodies is not sufficient to rule out IPF and input from a rheumatologist should be sought. After that, if no cause can be identified, IPF should be included in the differential diagnosis, particularly for patients who are more than 50 years of age [1, 3]. The current diagnostic approach for IPF depends on identification of the UIP pattern on HRCT [1, 3]. However, if HRCT features do not enable a confident diagnosis of the UIP pattern, guidelines indicate that surgical lung biopsy is needed to achieve a conclusive diagnosis. As for any other surgical procedure, surgical lung biopsy has a risk of mortality and major complications and it should be considered only when the histopathological pattern is expected to meaningfully alter treatment decisions and outcome prediction [3]. Finally, if a histologic UIP pattern is found in the absence of a known cause, IPF can often be confidently diagnosed. Nevertheless, face-to-face multidisciplinary discussions involving clinicians, radiologists, and pathologists are recommended as a key feature of the diagnostic pathway [1, 3] (**Figure 4**).

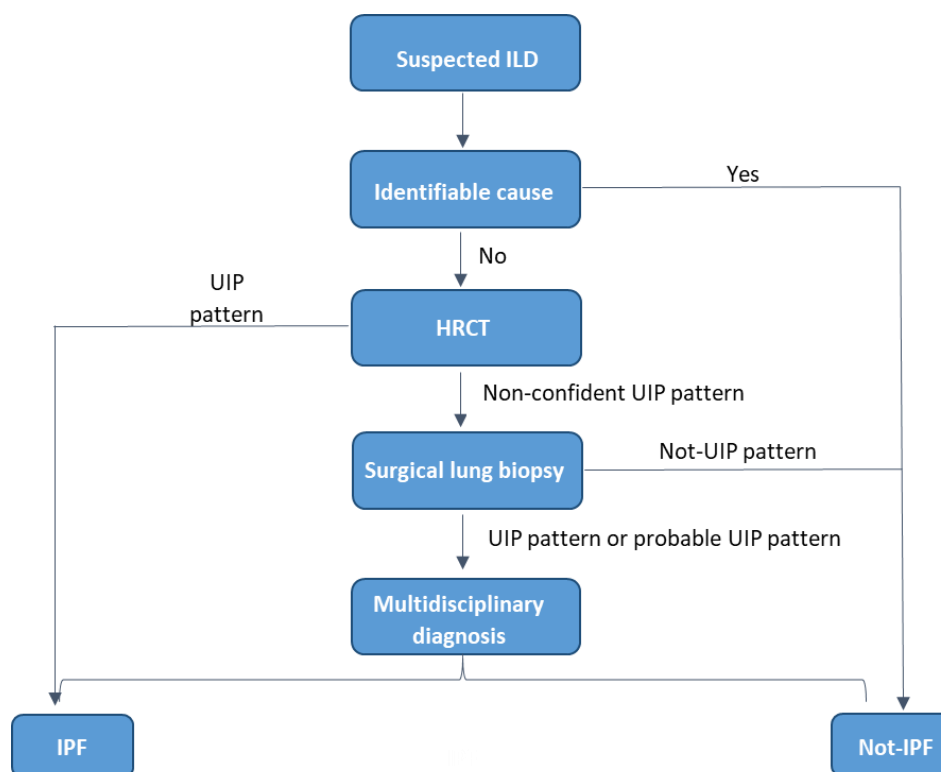


Figure 4. Suggested approach for the diagnosis of idiopathic pulmonary fibrosis (IPF). *If the history and physical examination of a patient suggest interstitial lung disease (ILD), clinicians should exclude other ILDs that are not IPF. High-resolution computed tomography (HRCT) is particularly useful to identify the pattern of usual interstitial pneumonia (UIP), which establishes a diagnosis of IPF. Surgical lung biopsy is currently recommended in patients with a non-confident UIP pattern on HRCT. Nevertheless, multidisciplinary diagnosis is highly recommended as a key feature of the diagnostic pathway if an UIP pattern or probable UIP pattern are identified on surgical lung biopsies. Adapted image from Martinez FJ, et al. [3].*

1.2.8 IPF ANIMAL MODELS

Given the challenges associated with performing clinical trials in patients with IPF, it is imperative that preclinical data packages be robust in their analyses and interpretations to have the best chance of selecting promising drug candidates to advance to clinical trials. Animal models don't fully recapitulate physiologic findings of IPF or histopathologic pattern of UIP. However, they do enable mechanistic investigations relevant to fibrogenesis [167].

Currently, bearing in mind that alternative animal models may not offer better discrimination for pharmacological assessment, mice are considered the first line animal model for preclinical testing with rats used subsequently if a second species is required, or practical

considerations make mice unsuitable. In spite of the advanced age in IPF, given the significant practical hurdles associated with generation of aged mice (e.g., time and cost), there isn't currently compelling reason to recommend either standard or prioritized use of aged mice for pharmacological testing, unless there is a particular age-related target that warrants such investigations. Finally, IPF is more common in men than women. Then, the ATS recommends firstly the use of male animals and secondly, the use of female mice to confirm key findings [167].

The most accurate analysis for lung fibrosis in IPF models involves several endpoints, including combinations of histologic assessment of fibrotic distribution by Masson's trichrome staining, and other optional parameters, such as measures of gene expression generally by quantitative polymerase chain reaction (PCR), lung function assessment by non-invasive methods (whole-body plethysmography) or invasive methods (Buxco-force pulmonary maneuvers and FlexiVent) and imaging by X-ray computed tomography (CT) or single-photon emission CT (SPECT) [167].

IPF animal models can roughly be divided into those that have a strong inflammatory component and models of less inflammatory injury. Use of bleomycin, radiation, silica aerosolization, asbestos, fluorescein, and many cytokine overexpression systems lead to fibrogenesis after a robust inflammatory response, whereas transgenic delivery of TGF β , TGF α , TNF α or IL-1 β by adenovirus and lentivirus vectors, targeted depletion of epithelial cells, and models of IPF fibroblasts delivered to immunodeficient mice are less dependent on inflammation [167, 168].

The model of bleomycin-induced lung fibrosis represents the cheapest, easiest, fastest, most reproducible, and thus most extensively used animal model of IPF. Bleomycin is a chemotherapeutic antibiotic that has been identified as a pro-fibrotic agent when lymphoma patients developed pulmonary fibrosis after intravenous administration of bleomycin. So far, bleomycin has been delivered by multiple methods including intratracheal (IT), intraperitoneal, subcutaneous, intravenous, and inhalational. However, IT is the most commonly route of administration. It is believed that IT administration better recapitulates the human phenotype that is limited to the lungs. Regarding to the dosing regimens used, in mouse studies, weight-based dosing is most common, beginning at 1.25 U/kg and up to a maximum of 4 U/kg. Finally, C57BL/6J strain is the predominant one used, as this particular strain is highly susceptible to lung injury following IT bleomycin administration [169].

The bleomycin model is characterized by periods of acute lung injury and inflammation (days 0–7), fibroproliferation (days 3–14), and established fibrosis (generally days 14–28) that generally resolves over a variable time period [167]. During the first week (days 0-7), following a single bleomycin IT instillation, the response is primarily characterized by lung inflammation [170]. During the following days (days 7 to 21), alveolar and interstitial fibrosis become progressively more prominent with partial to complete effacement of the alveoli. These pathologic lung tissue changes, like increased levels of (protein and lipid) pro-fibrotic mediators and consequent increased matrix deposition, explain the rapid loss of ventilation at day 7 due to the presence of inflammatory cells and fluid in the alveolar space, followed by a more pronounced decrease of ventilation at day 14 due to interstitial fibrosis [170].

CHAPTER 2

TRANSFORMING GROWTH FACTOR β

TRANSFORMING GROWTH FACTOR β

The vertebrate genome contains more than 30 pleiotropic ligands that belong to the TGF β superfamily, which consists of TGF β s, activins, inhibins, bone morphogenetic proteins (BMPs), antiMüllerian hormone and growth and differentiation factors. Specifically, three highly homologous isoforms of TGF β exist in humans: TGF β 1, TGF β 2 and TGF β 3, being TGF β 1 the most important isoform in IPF [171].

2.1 ACTIVATION

Each TGF β ligand is synthesized as a precursor, which forms a homodimer that interacts with its latency-associated peptide (LAP) and a latent TGF β -binding protein (LTBP), forming a larger complex called the large latent complex (LLC), which interacts with ECM. In this complex, TGF β is unable to bind to TGF β receptors. The TGF β activation process involves the release of the LLC from the ECM, followed by further proteolysis of LAP-LTBP to release active TGF β to its receptors. MMP2, MMP9, thrombospondin 1 and pH changes in the local environment are known to activate latent TGF β and free active TGF β for binding to its receptors at the cell membrane. α v β 6 integrin can also activate TGF β by interacting with the amino acid sequence arginine–glycine–aspartic (RGD) located near the C-terminus of TGF β ligand and inducing the release of mature TGF β from LLC [171-173]. It has been observed that expression of α v β 6 is significantly upregulated in IPF lung tissue and localised to damaged epithelial sites [133].

2.2 BIOLOGICAL ACTIONS

TGF β is involved in a wide range of biological processes both during embryogenesis and in adult tissue homeostasis. These cellular processes include: growth inhibition through its antiproliferative action in epithelial, endothelial, haematopoietic and immune cells; pro-apoptotic actions through transcription activation of cyclin-dependent kinase inhibitor 1A and 2A; cell migration and invasion; EMT and EndMT induction; synthesis of ECM proteins like collagen by fibroblasts; inhibition of ECM degradation by antiproteinase induction or metalloprotease downregulation; and immune-suppression through T cell proliferation suppression and B cell apoptosis induction. However, although normally dynamically regulated and involved in maintenance of tissue homeostasis, TGF β s are often chronically over-expressed in disease states, including cancer, fibrosis and inflammation, and this excessive production of

TGF β drives disease progression by modulating cell growth, migration or phenotype [171, 174, 175].

2.3 SIGNALLING

TGF β signals by binding to and activating serine/threonine kinase type I and type II receptors (TGF β receptor type I (T β RI) and TGF β receptor type II (T β RII)), inducing heteromeric complex formation. Following TGF β binding, type I receptors become phosphorylated by the type II receptors. Consequently, the activation of the T β RI leads to the propagation of signalling by at least two independent routes: the SMAD-dependent canonical pathway and the SMAD-independent or non-canonical pathways [87, 171].

2.3.1 SMAD-DEPENDENT CANONICAL PATHWAY

In the Smad-dependent pathway, activation of T β RI leads to phosphorylation of the Smad proteins. There are eight distinct Smad proteins, constituting three functional classes: the receptor-regulated Smad (R-Smad), the co-mediator Smad (co-Smad), and the inhibitory Smad (I-Smad). R-Smads (Smad1, 2, 3, 5, and 8) are directly phosphorylated and activated by the type I receptor kinases. Smad2 and Smad3 are substrates of T β RI, whereas type I receptors for BMPs utilize Smad1, Smad5 and Smad8. Upon phosphorylation by the receptor, R-Smads together with co-Smad (Smad 4) translocate to the nucleus. Once in the nucleus, the R-Smad-co-Smad complex preferentially associates with the genomic Smad-binding element (SBE) in a sequence specific manner. However, it generally occurs in concert with other DNA-binding transcription factors that bind to distinct sequences adjacent to the SBE. Then, all together regulate transcriptional responses. For instance, TGF β induces the expression of profibrotic molecules such as collagen, CTGF and α -SMA. In addition, it induces the EMT and leads to tissue fibrosis. R-Smads can also modulate miRNA biogenesis by facilitating the processing of primary miRNA into precursor miRNA in the nucleus. Otherwise, the I-Smads (Smad6 and Smad7) negatively regulate TGF β signalling by mediating the degradation of the T β RI, inhibiting phosphorylation of R-Smads by the T β RI kinase or inhibiting the formation of the R-Smad-co-Smad complex [171, 176] (**Figure 5**).

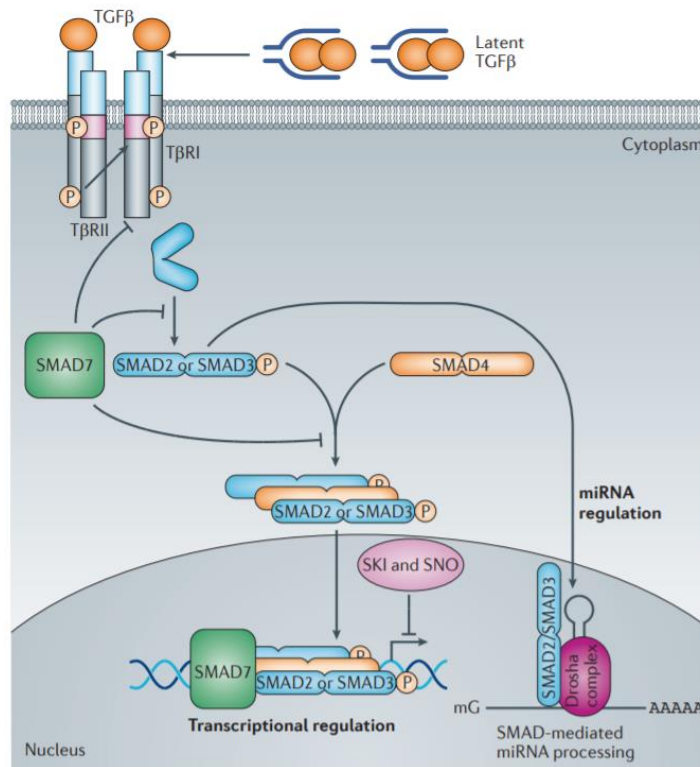


Figure 5. Schematic overview of the canonical Smad-dependent transforming growth factor- β (TGF β) signalling pathway. TGF β ligands are synthesized as a large latent TGF β complex. First of all, the TGF β activation process involves the release of TGF β from the latent TGF β complex. Upon activation, TGF β dimers induce the association between TGF β type II and type I receptors (TBRII and TBR1, respectively). Type II receptors phosphorylate the type I receptors, which propagate the signal into the cell by phosphorylating the TGF β receptor-specific Smads (Smad2 and Smad3). Both of them form heteromeric complexes with the co-mediator Smad (Smad4) and translocate to the nucleus. Once in the nucleus, the R-Smad-co-Smad complex associates with the genomic Smad-binding element (SBE) in a sequence-specific manner. Generally, at the same time, other DNA-binding transcription factors bind to distinct sequences adjacent to the SBE. The nuclear proteins SKI and SNO (also known as SKIL) inhibit the transcriptional regulation by Smads. The inhibitory Smad (Smad7) inhibits the TGF β pathway through multiple mechanisms, including by mediating the degradation of the TBR1, inhibiting phosphorylation of R-Smad by TBR1 kinase or inhibiting the formation of the R-Smad-co-Smad complex. Finally, R-Smads can also modulate microRNA (miRNA) biogenesis by facilitating the processing of primary miRNA into precursor miRNA in the nucleus [171].

2.3.2 SMAD INDEPENDENT OR NON-CANONICAL PATHWAY

In addition to the canonical signalling, there are other non-canonical TGF β signalling pathways mediated by TNF receptor-associated factor 4 (TRAF4), TRAF6, TGF β -activated kinase 1, p38 mitogen-activated protein kinase, Rho, PI3K-AKT, extracellular signal-regulated kinase (Erk), JNK or nuclear factor kappa-light-chain-enhancer of activated B cells (NF- κ B). In addition, these non-canonical signals can crosstalk with the Smad pathways in a dynamic way and mutually modulate each other. Thus, cellular responses to TGF β signalling result from the dynamic combination of canonical and non-canonical signalling cascades. Moreover, both signalling pathways can also be influenced by other signalling pathways, such as the RAS, Wnt, Shh, Notch, TNF and IFN pathways (**Figure 6**) [171].

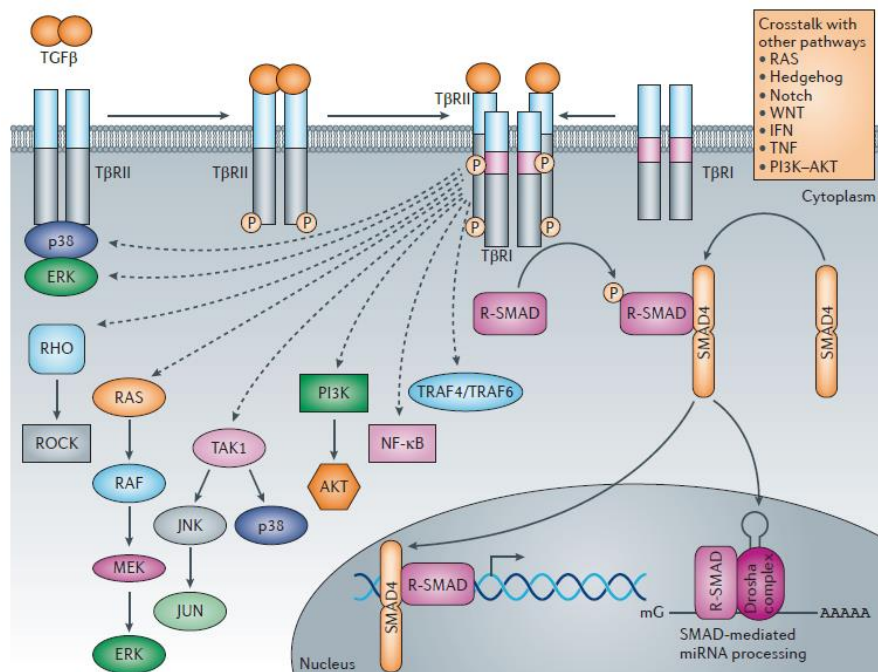


Figure 6. Schematic representation of non-canonical TGF β signalling and crosstalk with other pathways. In the non-canonical pathways, TGF β dimers induce the association between TGF β type II and type I receptors (T β RII and T β RI, respectively) and consequent activation. Then, the activated T β RI, transmits a signal through factors, such as tumour necrosis factor (TNF) receptor associated factor 4 (TRAF4) or TRAF6, RAS, TGF β -activated kinase 1 (TAK1), p38 mitogen-activated protein kinase (p38 MAPK), RHO, phosphoinositide 3-kinase (PI3K) – protein kinase B (AKT), extracellular signal-regulated kinase (ERK), Jun N-terminal kinase (JNK) or nuclear factor kappa-light-chain-enhancer of activated B cells (NF- κ B). These non-canonical signals can also crosstalk with the Smad-dependent canonical pathway. Canonical and non-canonical pathways

can both be influenced by other pathways, such as the WNT, RAS, Hedgehog, Notch, interferon (IFN), TNF, PI3K-AKT and RAS pathways [171].

In addition to these pathways, the TGF β 1 isoform regulates expression of a number of downstream transcription factors involved in EMT via both Smad-dependent and -independent pathways. For example, Snail and Slug are zinc finger proteins that function as repressors of E-cadherin transcription in cultured epithelial cells, and both can be activated by TGF β 1 via both Smad-dependent and -independent pathways in a cell type dependent fashion in cultured cells [71].

CHAPTER 3

MUCINS

MUCINS

3.1 GENERAL FEATURES

Mucosal surfaces line body cavities such as the gastrointestinal tract and lungs, protect against pathogens, and prevent dehydration. Specifically, mucus is the layer that covers, protects and lubricates these luminal surfaces. Regarding the respiratory tract, airway mucus is composed of water, ions, lung secretions, serum protein transudates, anti-microbial proteins and mucus glycoproteins (mucins) [177-179].

Mucins are classified in two groups depending if they are secreted by surface epithelial goblet cells and submucosal gland mucous and serous cells (secreted mucins) or tethered to cell membranes (transmembrane mucins (TM)). Secreted mucins are further subdivided into gel-forming and non-gel-forming mucins [180].

Mucins are encoded by *MUC* genes. To date, 21 human *MUC* genes have been identified (**Table 4**), of which 16 have been identified in the lung: ten TM mucins (MUC1, MUC4, MUC12, MUC13, MUC14, MUC15, MUC16, MUC20, MUC21, MUC22); four secreted gel-forming mucins (MUC2, MUC5AC, MUC5B, MUC19); and two secreted, non-gel-forming mucins (MUC7, MUC8) [179, 181, 182]. The most notable mucin members in the lung are MUC5AC and MUC5B, which together comprise approximately 90% of the mucin content of sputum. Nearly all the remaining 10% is made up mainly of three membrane-tethered mucins, MUC1, MUC4, and MUC16 [183].

All mucins share a characteristic feature, the presence of tandem repeat (TR) structures with high proportion of proline, threonine and serine that form the PTS domains. These domains are extensively O-glycosylated through N-acetylgalactosamine O-linkages at the threonine and serine residues [182]. The O-linked glycans constitute up to 80% of the molecular weight of the mucins, decorating the mucin protein core [180]. N-linked glycans are also often present in mucins but to a much lesser degree. The number of PTS domains encoded by a particular mucin gene can vary markedly among individuals due to variable number tandem repetition (VNTR) polymorphisms, which are associated with susceptibility to various diseases. Moreover, mucin glycosylation patterns are tissue and cell type dependent, and can be altered with cellular differentiation state or with neoplastic transformation [184].

Table 4. Classification, chromosome localization and main tissue expression of human mucins [180, 181].

| Mucin | Chromosome | Main tissue expression |
|---|------------|---|
| <i>Secreted mucins-gel-forming</i> | | |
| MUC2 | 11p15.5 | Jejunum, ileum, colon, endometrium, respiratory tract |
| MUC5AC | 11p15.5 | Respiratory tract, stomach, conjunctiva, endocervix, endometrium |
| MUC5B | 11p15.5 | Respiratory tract, submandibular glands, endocervix |
| MUC6 | 11p15.5 | Stomach, ileum, gall bladder, endocervix, endometrium |
| MUC19 | 12q12 | Sublingual gland, submandibular gland, respiratory tract, eye, middle ear epithelium |
| <i>Secreted mucins-non-gel-forming</i> | | |
| MUC7 | 4q13-q21 | Respiratory tract, sublingual and submandibular glands |
| MUC8 | 12q24.3 | Respiratory tract, uterus, endocervix, endometrium |
| MUC9 | 1p13 | Fallopian tubes |
| <i>Transmembrane mucins</i> | | |
| MUC1 | 1q21 | Breast, pancreas, duodenum, ileum, colon, trachea, bronchi, cornea, conjunctiva, fallopian tubes, uterus, endometrium, endocervix, ectocervix, vagina |
| MUC3A/B | 7q22 | Small intestine, colon, gall bladder |
| MUC4 | 3q29 | Breast, respiratory tract, small intestine, colon, conjunctiva, cornea, endocervix, ectocervix, vagina, endometrium, lungs |

| | | |
|--------------|---------|---|
| MUC12 | 7q22 | Colon, small intestine, stomach, pancreas, lung, kidney, prostate, uterus |
| MUC13 | 3q21.2 | Colon, trachea, kidney, small intestine |
| MUC14 | 4q24 | Heart, kidney, lungs |
| MUC15 | 11p14.3 | Colon, respiratory tract, small intestine, prostate |
| MUC16 | 19p13.2 | Ovary, cornea, conjunctiva, respiratory tract, endometrium |
| MUC17 | 7q22 | Stomach, duodenum, colon |
| MUC20 | 3q29 | Placenta, colon, respiratory tract, prostate, liver |
| MUC21 | 6p21 | Respiratory tract, thymus, colon |
| MUC22 | 6p21.22 | Lungs, placenta, testis |

3.2 SECRETED MUCINS

3.2.1 SECRETED GEL-FORMING MUCINS

Secreted gel-forming mucins are characterized by their high molecular weight (5–40 MDa) and size (600–900 nm), high proportion of glycosylation (50–80%) and the capacity to form viscoelastic gels [182, 185].

These mucins are characterized by lightly glycosylated carboxy and amino terminal regions rich in cysteine. The cysteine enriched region is composed of N-terminal trypsin inhibitor-like domains and C8 domains (“C8” domain has eight conserved cysteines). Other domains include N- and/or C-terminal Von Willebrand factor type D (vWD) and C domains which possess sequence similarity to Von Willebrand factor and a C terminal cysteine knot domain [182].

Secreted gel-forming mucins are able to oligomerize. This feature provides them the potential to build up dense visco-elastic mucus gel that covers many epithelia. In this way, they act as a physical barrier and protect the epithelium that lines the respiratory tract by forming a matrix where bacteria are trapped. Moreover, the gel-forming mucins give a lubricant property to the mucus [182].

As it was mentioned above, MUC5AC and MUC5B are the major secreted gel-forming airway mucins. MUC2 and MUC19 lung functions are not known.

MUC5AC, MUC5B

MUC5AC and MUC5B are believed to contribute to the barrier function and the rheology of airway mucus [179]. In normal airways, these polymeric mucins are secreted from different sites. MUC5AC is produced mainly in goblet cells in the surface epithelium, and MUC5B is produced mainly in mucous cells of the submucosal glands [185] (**Figure 7**). Moreover, it has been observed that MUC5B mucin occurs in different glycoforms, termed low- and high-charge glycoforms [185].

Based on the kind of mucin producer cell, it is speculated that MUC5AC may be an acute-response mucin that is produced as a result of insults arriving at the upper airway surfaces. However, MUC5B may be involved in the response to more chronic insults and come more into play in infection and inflammation [185]. In fact, it has been shown that MUC5B (but not MUC5AC) is required for mucociliary clearance, for controlling infections in the airways and middle ear, and for maintaining immune homeostasis in the lungs [27].

These gel-forming mucins also capture, retain and release biologically active molecules like cytokines, growth factors and trefoil factors. These association/dissociation properties may allow mucins to regulate inflammation and immune responses and to influence postinjury epithelial repair. Because mucins also bind to pathogens, these intermolecular interactions may allow mucins to serve as bridges between inflammatory mediators and microorganisms, thereby facilitating the resolution of inflammation [179].

It has been observed that MUC5AC is the main mucin in healthy airway secretions and that MUC5B predominates in cystic fibrosis and COPD [185]. Regarding to IPF, as it was mentioned in the potential risk factors section, a MUC5B gene promoter polymorphism has been associated with IPF development.

3.2.2. SECRETED NON-GEL-FORMING MUCINS

In the airways, MUC7 and MUC8 are expressed in the submucosal glands of the airway epithelium [186, 187] (**Figure 7**). They cannot oligomerize since they lack the cysteine rich domains and are thus found as monomers [182].

Although there is little information on the MUC8 glycoprotein, the MUC7 mucin has been well characterized, particularly in saliva. MUC7 is markedly smaller than the polymeric mucins, with an apparent molecular weight of between 200 and 250 kDa. The central mucin domain consists of between five and eight repeats of a 23-residue PTS domain, flanked by N-terminal (144-residue) and C-terminal (75-residue) domains. The N terminus of MUC7 contains a histatin-like domain that has antifungal activity and interacts with bacteria. Then, although MUC7 has not been shown to have a role in determining the rheological properties of the mucus gel, it is clearly an important innate defense protein [185].

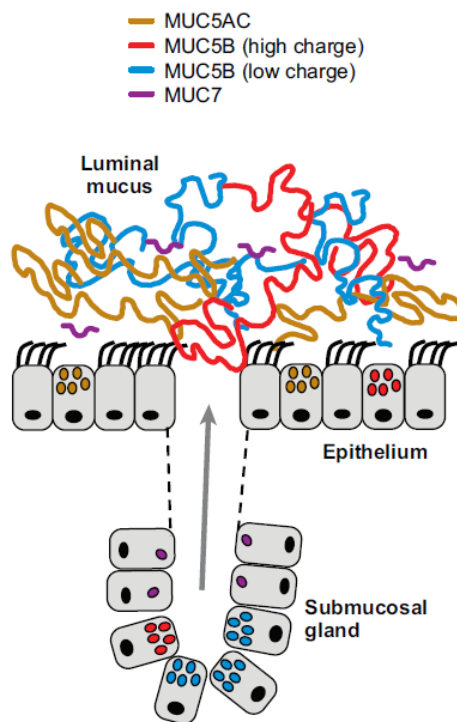


Figure 7. Major secreted mucins in the airways mucus gel and their sites of synthesis. *The secreted gel-forming mucin MUC5AC (orange) is produced mainly in epithelial goblet cells. In contrast, the secreted gel-forming mucin MUC5B (low charge, blue; high charge, red) and the secreted non-gel-forming mucin MUC7 (purple) are produced mainly in cells of the submucosal glands, MUC5B in mucous cells and MUC7 in serous cells [185].*

3.3. TRANSMEMBRANE MUCINS

TM mucins are large glycoproteins that localize to apical surfaces of epithelial cells that are in contact with relatively harsh environments [177]. Cell surface mucins are typically composed of dimers of two dissimilar subunits (α and β chain), held together by non-covalent, sodium dodecyl sulfate-labile bonds [183]. The larger subunit (α -chain) is wholly extracellular and heavily glycosylated. However, the smaller subunit (β -chain) consists of a short extracellular region, the single-pass TM domain, and the cytoplasmic tail (CT) (varies from 22 amino-acid residues in MUC4 to 80 amino acids in MUC17) (**Figure 8**) [188].

Tethered mucins have a receptor-like structure that is reminiscent of classical innate immune receptors. Then, it is likely that TM are signalling receptors that sense the external environment and activate intracellular signal transduction pathways essential for mucosal maintenance and damage repair [177].

The extracellular domain of TM mucins is mainly composed of a VNTR of PTS domain heavily O-glycosylated; sperm protein, enterokinase, and agrin (SEA) domain or epidermal growth factor (EGF)-like domain [188]. Instead of SEA domain, MUC4 contains other three domains namely nidogen-like domain (NIDO), adhesion-associated domain (AMOP) and vWD domain [182]. It has been hypothesized that mucin extracellular domains are released in response to mechanical force; interactions with microbes; alteration in pH, ionic concentration, or hydration [189] or inflammatory stimuli such as TNF α and neutrophil elastase [190].

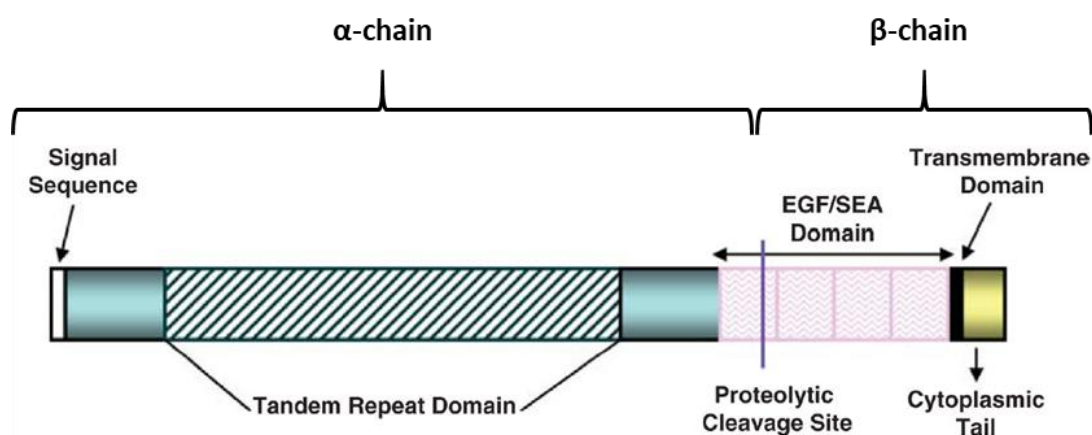


Figure 8. General structure of the transmembrane mucins. *These mucins are typically composed of two subunits (α and β chain), based on the putative proteolytic cleavage site in the EGF/SEA domain. The larger subunit (α -chain) is extracellular and predominantly composed of variable number of tandem repeats. The smaller subunit (β -chain) consists of short extracellular region (containing either sperm protein, enterokinasein, and agrin (SEA) domain or epidermal growth*

factor (EGF)-like domain), single transmembrane domain, and the cytoplasmic tail. Adapted image from Bafna S, et al.[188].

The high level of glycosylation in this extracellular domain shields the protein backbone of the extracellular domain from proteolytic attack by bacteria and host proteases and contributes to barrier formation. In addition, damage of the epithelial barrier may lead to excessive shedding of mucin extracellular domains and subsequent activation of pathways linking to cell proliferation and apoptosis. Therefore, mucins could be sensing both bacteria and damage at the epithelial interface.

TM mucins can also modulate immunological response, facilitate cell adhesion during tumour metastasis and alter the functions of proteins interacting with the mucin carbohydrate moieties [188]. Furthermore, the intracellular tails of all TM mucins contain putative phosphorylation sites, but it is emphasized that they are dissimilar in sequence and length and do not contain any conserved domains. Then, these observations suggest a high degree of functional divergence and most likely signalling specificity between different TM mucins [177].

Ten TM mucins (MUC1, MUC4, MUC12, MUC13, MUC14, MUC15, MUC16, MUC20, MUC21, MUC22) have been identified in the lung, with MUC1 (discussed in section 3.3.3 in detail), MUC4 and MUC16 being the predominant ones.

3.3.1 MUC4

MUC4, at roughly 900kDa, localizes mainly to cilia [183]. It is derived from a single gene that is posttranslationally processed into an O-glycosylated extracellular subunit of approximately 600–800 kDa and a largely N-glycosylated fragment of approximately 120 kDa.

This heterodimer is a homolog of ascites sialoglycoprotein (ASGP)-1 and ASGP-2, which form the rat sialomucin complex. The ASGP-1-like extracellular domain or MUC4 α contains an N-terminal signal sequence followed by: (a) three imperfect repeats of 126–130 residues, (b) a unique sequence, (c) the 16-residue serine- and threonine-rich VNTR (typically 145–395 repeats), and (d) a cysteine-rich domain followed by NIDO, AMOP and vWD domains and the proteolytic cleavage site. Otherwise, the ASGP-2-like or MUC4 β subunit is rich in N-glycosylation sites and contains up to three EGF-like domains, a hydrophobic transmembrane region, and a 22-amino-acid CT containing a single tyrosine residue [183].

The ASGP-2-like subunit tethers the mucin domain to the cell membrane and, via an EGF-like domain, serves as an intramembrane ligand for the receptor tyrosine kinase (ErbB) 2 [183]. Binding of MUC4 to ErbB2 may competitively inhibit the interaction of ErbB2 with its soluble ligands, and induces ErbB2 phosphorylation. In this way, MUC4 regulates cell proliferation, growth, survival and differentiation. Moreover, MUC4 can also modulate cell apoptosis, regulate cell–cell adhesion, and serve as tumour marker or target for cancer therapy [179, 183].

3.3.2 MUC16

MUC16 at >2000 kDa is the largest of all known mucins and expressed on the surface of cilia [183]. Like other mucins, the peptide backbone of MUC16 is composed of an N-terminal region and a C-terminal region.

The N-terminal subunit is a typical, heavily O-glycosylated mucin domain and the C-terminal portion consists of an extracellular portion composed of more than 60 TRs of 156 amino acids, a transmembrane region, and a 32-residue CT with several tyrosine, serine, and threonine sites for potential phosphorylation. In contrast to other tethered mucins, which have only a single SEA domain, MUC16 has 16 SEA modules. Intriguingly, only the second MUC16 SEA domain resembles those found in other mucins; therefore it may provide a site of proteolytic cleavage [183].

MUC16 has been recognized as a tumour-associated antigen which is cleaved from ovarian cancer cell surface into the blood stream. Hence CA125 (a peptide epitope of MUC16) is considered as a well-known biomarker for ovarian cancer, which is found to promote cancer cell proliferation as well as inhibits anti-cancer immune response [182]. As a large heavily glycosylated molecule, MUC16 extends from the surface of ovarian cancer cells and binds to mesothelin, a protein that is found on the surface of the mesothelial cells that line the peritoneum [188]. Although no intracellular signalling has yet been reported as a consequence of the MUC16-mesothelin association, the interaction is capable of enhancing ovarian cancer cell metastasis, suggesting that the binding of these proteins does trigger pathways involved in the regulation of cellular adhesion and motility [183]. Then, MUC16-mesothelin association could be an interesting IPF target.

3.3.3 MUC1

MUC1 is a membrane-bound O-glycoprotein with a rigid structure that extends up to 200–500 nm from the cell surface [183]. This mucin is expressed at the basal level in most epithelial cells mainly around lung microvilli. In fact, in the uninjured lung, MUC1 is primarily expressed in ATI cells. However, in patients with various types of interstitial/fibrotic lung diseases, it has been observed that MUC1 is aberrantly expressed in hyperplastic ATI cells and alveolar macrophages. In addition, MUC1 has long been viewed as a tumour-associated molecule because of its frequent overexpression and aberrant glycosylation in most carcinomas (>90% of breast carcinomas, and frequently in other types of cancer, including ovarian, lung, colon, and pancreatic carcinomas) [188].

3.3.3.1 STRUCTURE AND LOCATION

MUC1 is a large TM glycoprotein (approximately 200 kDa) that acts as a membrane receptor. The actual relative molecular mass varies in proportion to the polymorphic VNTR domain. In fact it can be more than double with full glycosylation [183]. MUC1 is translated as a single polypeptide that undergoes autoproteolysis at the conserved GSVVV motif in the SEA domain to form two subunits: the MUC1 N-terminal subunit (MUC1-N) or α -chain and the C-terminal subunit (MUC1-C) or β -chain, which anchors the mucin to the surface of the cell [191].

MUC1-N contains sites of O and N-linked glycosylation, a signal peptide, a VNTR domain with 25–125 repeats of a 20-amino acid sequence and the SEA domain. MUC1-C is short, comprising a 58 amino acid extracellular domain, a 28 amino acid TM domain, and a 72 amino acid CT. MUC1-C also contains sites of N-linked glycosylation [192] (**Figure 9**).

Once at the plasma membrane, the MUC1 extracellular domain can be shed into the lumen by proteolytic cleavage of the conserved GSVVV motif in the SEA domain [193]. Therefore, one of the functions of the SEA domain may be to protect epithelial cells against mechanical force and another function may be to release the mucin extracellular domain [177]. An alternative mechanism to release the mucin extracellular domain is proteolytic cleavage close to the plasma membrane by the action of tumour necrosis α -converting enzyme (TACE/ADAM17) and MT1-MMP or MMP14 [194, 195]. It is possible that disruption of the SEA domain or release of the extracellular domain by sheddases can be sensed by the cell and activates signalling by the CT [177] (**Figure 10**).

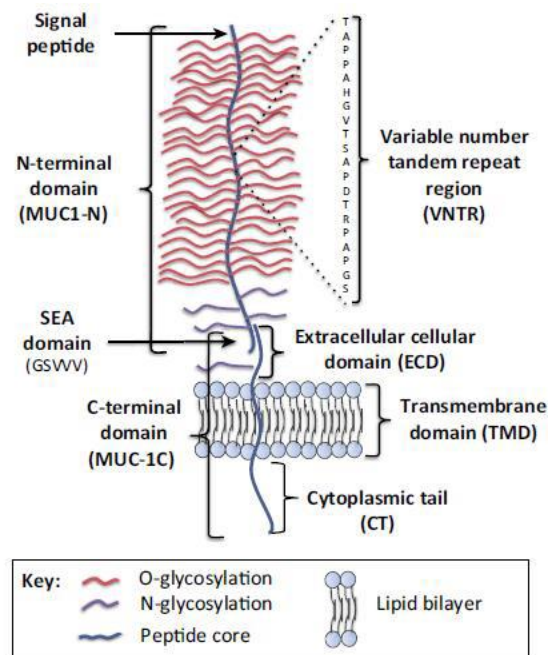


Figure 9. Schematic representation of the structure of MUC1. MUC1 comprises 2 subunits: a N-terminal subunit (MUC1-N) and a C-terminal subunit (MUC1-C). Both subunits associate around the SEA domain forming a stable heterodimeric complex. MUC1-N contains the signal peptide, variable number tandem repeat (VNTR) region, and SEA domain. The VNTR region of MUC1-N is composed of 20 amino acids that are extensively O-glycosylated (red) at the serine and threonine residues. MUC1-N and MUC1-C are sparingly N-glycosylated (violet) at asparagine residues. MUC1-C consists of the extracellular domain, transmembrane domain, and cytoplasmic tail [192].

It has been observed that in the uninjured lung, low levels of extracellular MUC1 are found in BALF. However, in patients with various types of interstitial/fibrotic lung diseases, extracellular MUC1 levels are markedly increased in both BALF and serum [196]. In fact, levels of released MUC1 protein (also known as KL-6 based on its unique extracellular epitope), are used in the diagnosis and differential diagnosis of interstitial pneumonia. Regarding IPF, several studies have reported increased serum KL-6 levels during acute exacerbation. In fact, a recent study has demonstrated that serial increases in serum KL-6 levels correlate with a rapid decline in FVC predicted, and further demonstrated that higher KL-6 levels are correlated with lower survival rates [197]. It has been also observed that isolated KL-6 can promote lung fibroblast migration, proliferation and transformation to myofibroblast, as well as, alveolar EMT and mouse lung fibrosis [198-200].

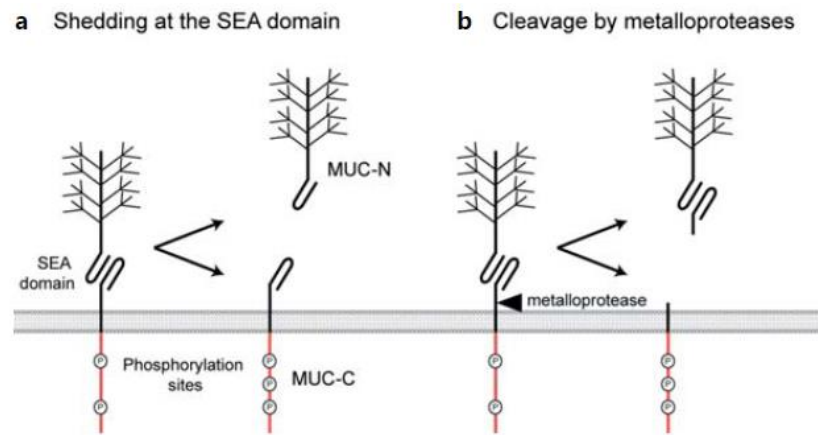


Figure 10. Shedding and cleavage of MUC1. MUC1 extracellular domains can be released from the surface. (A) Shedding of the Muc1 extracellular domain by proteolytic cleavage of the SEA domain. (B) Cleavage of the extracellular domain by metalloproteases. It remains to be established if release of the extracellular domain leads to phosphorylation and activation of the intracellular tail and the initiation of signalling pathways. Adapted image from van Putten J P M, et al.[177].

The MUC1 heterodimer is positioned at the apical border of normal epithelial cells. With loss of polarity associated with the epithelial stress response or transformation, MUC1 is repositioned over the entire cell membrane and interacts with receptor tyrosine kinases, such as ErbB1-4, and participates in their downstream signalling pathways [191]. In this regard, the MUC1-CT serves as a substrate for phosphorylation in response to activation of the epidermal growth factor receptor (EGFR), fibroblast growth factor receptor (FGFR)3, PDGFR and Met [191]. Moreover, the MUC1-C extracellular domain is glycosylated on Asn-36 and then serves as a binding site for the profibrotic galectin 3 ligand. Galectin 3 functions as a bridge to associate MUC1-C with the EGFR and potentially other cell surface receptors [201].

The MUC1-CT include a CQC sequence adjacent to the TM domain. This sequence is necessary for the formation of MUC1-C oligomers [191]. In carcinoma cells, MUC1-C accumulates in the cytoplasm as a result of release from the cell membrane and/or redirection from the ER. MUC1-C is also targeted to the nucleus by a mechanism that is dependent on its oligomerization and thereby interaction of RRR motif with importin β [191, 202]. In the nucleus, MUC1-C associates with certain transcription factors that include β -catenin/TCF4, p53, estrogen receptor- α , NF- κ B p65 and STATs [191]. These complexes in turn occupy response elements on promoters of target genes [191]. MUC1-CT also contains 18 documented and putative tyrosine

and serine/threonine potential phosphorylation sites that contribute to modulate multiple intracellular signals through interactions largely regulated by phosphorylation with various effectors linked to transformation [203]. For example, phosphorylation of the YEKV site induces binding of the MUC1-C cytoplasmic SAGNGGSSL sequence to β -catenin [204] (**Figure 11**).



Figure 11. Amino-acid sequence of the MUC1-C cytoplasmic domain. For the amino acids in large, red font, phosphorylation was demonstrated by mass spectrometry as reported by PhosphoSitePlus (<http://www.phosphosite.org/>). Known kinases are indicated. The CQC motif is necessary for MUC1-C oligomerization and the RRK motif is necessary for MUC1-C binding to importin β and targeting to the nucleus. Also highlighted is the β -catenin-binding site [177, 203].

3.3.3.2 SIGNALLING

3.3.3.2.1 Barrier function, mucosal maintenance, and interactions with mucosal pathogens

A protective role of MUC1 during bacterial invasion has been most convincingly demonstrated in the context of the bacterial pathogen *Helicobacter pylori* (*H. pylori*). This pathogen is well known for its ability to colonize the stomach and initiate precancerous processes at the site of infection. *H. pylori* directly binds to MUC1 and released MUC1 extracellular domain can act as a soluble decoy that prevents *H. pylori* attachment to epithelial cells [177].

MUC1 also plays a protective role during infection with the major bacterial foodborne pathogen *Campylobacter jejuni*. In fact, it has been observed that MUC1-knockout (KO) mice are more susceptible to gastrointestinal *C. jejuni* infection [177].

Finally, it has been observed that the pathogenic bacterium *Pseudomonas aeruginosa*, an opportunistic pathogen that colonizes the lungs of cystic fibrosis and nosocomial pneumonia patients, or the purified flagellin, serve as activators of MUC1 signalling by promoting MUC1-CT phosphorylation and consequent Erk1/2 activation. This fact may represent the initial stages of host response to infection [205]. In addition, this MUC1-CT phosphorylation plays an anti-inflammatory role explained in greater detail below.

3.3.3.2.2. Regulation of inflammatory responses

Several studies have demonstrated a direct interaction of MUC1 with different players of the NF- κ B pathway. For example, during *H. pylori* infection of the stomach mentioned above, the MUC1 intracellular tail blocks NF- κ B activation and IL-8 production in response to *H. pylori*. In mouse and human cancer cell lines, a direct interaction of MUC1 with the NF- κ B subunit p65 was shown, and this interaction has proinflammatory effects as it results in the upregulation of IL-6 and TNF α transcription [177].

MUC1 can also directly interact with TLRs and thereby modulate TLR responses. In this context, it has been described that during the late stage of *Pseudomonas aeruginosa* infection, MUC1-CT phosphorylation leads to inhibition of TLR5 signalling and downregulation of inflammation (**Figure 12**) [206]. It is known that *Pseudomonas aeruginosa* flagellin engages TLR5 to stimulate downstream signalling and innate immune responses. Because TLR5 and MUC1 are flagellin receptors and both are expressed by airway epithelial cells, it is speculated that MUC1/TLR5 interaction in airway epithelial cells prevents NF- κ B activation [177, 179].

MUC1 is also part of a feedback loop that downregulates TLR2-induced IL-8 and TNF α production after infection with nontypeable *Haemophilus influenzae* in airway epithelial cells [177].

In line with its antiinflammatory effects in epithelial cells, MUC1 dampens phagocytosis by macrophages and decreases secretion of TNF α and IFN- γ after stimulation with LPS or flagellin in dendritic cells (DCs). In addition to macrophages and DCs, MUC1 is expressed on activated T cells and may be involved in release of T cell-lymph node interactions to move to tissue locations [177].

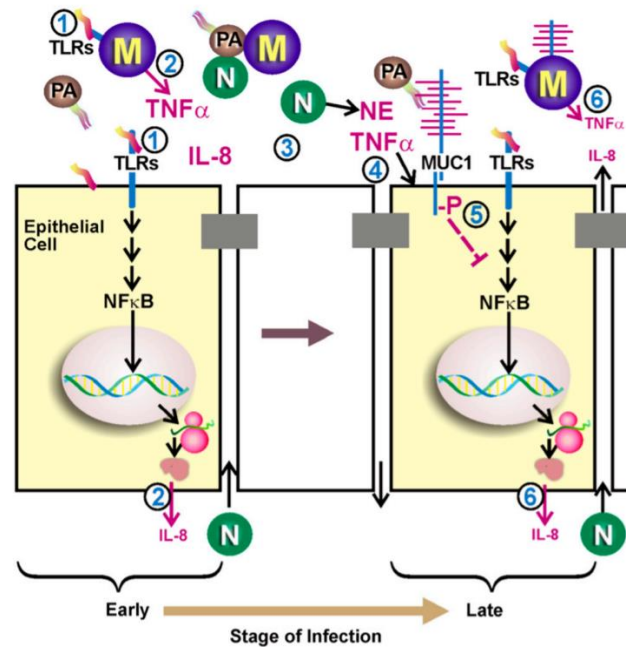


Figure 12. Antiinflammatory role of MUC1 during *Pseudomonas aeruginosa* (PA) airway infection. (1) During the early stage of infection by PA, flagellin activates toll like receptor (TLR) 5 and nuclear factor kappa-light-chain-enhancer of activated B cells (NF- κ B) on airway epithelial cells and macrophages (M). (2) Activation of NF- κ B leads to increased expression of tumour necrosis factor (TNF) α and interleukin-8 (IL-8), which are subsequently secreted. (3) IL-8 recruits neutrophils (N) across the epithelial barrier that release neutrophil elastase (NE) into the lumen of the airways. (4) NE and TNF α up-regulate MUC1 gene expression, resulting in increased expression of MUC1 mucin at the apical surface of lung epithelial cells. (5) During the late stage of infection, tyrosine phosphorylation of MUC1 cytoplasmic tail domain, induced by PA interaction with MUC1 extracellular domain, leads to inhibition of TLR5 signalling and downregulation of inflammation [206].

3.3.3.2.3. Contribution to carcinogenesis and metastasis

Overexpression of MUC1 is associated with invasive and metastatic tumours of the colon, pancreas, gall bladder, and oral epithelium. Mammary tumours of MUC1-KO mice grow slower and have a reduced ability to metastasize. In fact, increased serum levels of MUC1 tumour-associated antigens (CA15-3) correlate with an increasing tumour burden and poor prognosis in breast cancer [177].

The oncogenic effects of MUC1 are believed to occur through the interaction of its CT with various signalling molecules that can bind to several proteins implicated in the cancer regulation by affecting the proliferation, apoptosis, and transcription of various genes [188].

Regulation of cell-cell interactions by the extracellular domain

MUC1 interacts with adhesion molecules such as the endothelial intracellular adhesion molecule-1 (ICAM-1). Binding of MUC1 to ICAM-1 may assist MUC1-expressing tumour cells in the processes of invasion into the endothelium and reattachment at distant sites of metastasis [183]. MUC1-ICAM binding also results in a rapid increase in intracellular calcium in the MUC1-expressing cells and consequently it stimulates migration [177, 183].

The interaction of galectin 3 with MUC1-C extracellular domain induces polarization of MUC1 on the surface of cancer cells. This leads to exposure of smaller cell surface adhesion molecules like CD44 and E-selectin ligands, and increases interactions with endothelial ligands, leading to homotypic aggregation of cancer cells or adhesion of cancer cells to endothelial cells [177, 207]. Binding of galectin-3 to the MUC1 extracellular domain also increases MUC1 association with EGFR, which is an important regulator of epithelial cell growth and survival in normal and cancerous tissues [208]. Furthermore, binding of galectin 3 to MUC1-C activates mitogen-activated protein kinase (MAPK) and PI3K/AKT signalling pathways, leading to enhancement of cell proliferation and motility [177, 207].

The glycosylated extracellular domain of MUC1 directly disturbs E-cadherin interactions between adjacent cells leading to the loss of cell-cell interactions and inducing anchorage-independent growth and metastasis [177] (**Figure 13**).

Regulation of cell-cell interactions by the intracellular domain

MUC1-CT can directly interact with different components of the Wnt signalling pathway, including β -catenin, adenomatous polyposis coli (APC) and GSK-3 β . Regarding β -catenin, MUC1-CT affinity can be differentially altered by phosphorylation at specific sites [209]. In fact, phosphorylation by c-SRC tyrosine kinase and protein kinase C δ (PKC δ) increase interaction, while phosphorylation by GSK-3 β negatively regulates the interaction [177].

β -catenin normally forms a complex with cell-surface adhesion molecules such as E-cadherin, resulting in stable cell-cell interactions between epithelial cells (**Figure 13**). In cancer cells where polarized expression of TM mucins is lost, the MUC1-CT competes for binding to β -catenin and thus decreases cell-cell adhesions through E-cadherin [177]. This fact stimulates anchorage-independent growth *in vitro* and may facilitate metastasis of tumour cells *in vivo*

[183]. In addition, MUC1-CT is also found in the nucleus, where it modulates transcription directly. The first studies of MUC1 in transcription focused on β -catenin, which colocalizes with MUC1-CT in the nucleus [183]. This interaction initiates EMT of pancreatic cancer cells, resulting in increased invasiveness and metastasis [210].

Impact on cell proliferation

Through its CT, MUC1 binds with the ErbB family of growth factor receptor tyrosine kinases and potentiates ErbB-dependent signal transduction [188]. Through stabilizing and enhancing the ErbB signaling by MUC1-ErbB kinase interaction, MUC1 activates Erk1/2 and thereby increases cell proliferation. In addition, MUC1 may also affect Erk signalling independently of the ErbB kinases [188].

MUC1-CT - β -catenin colocalization in the nucleus regulates genes involved in cell proliferation and differentiation (**Figure 13**) [211]. In this context, it has been observed that PDGFR induce tyrosine phosphorylation of MUC1-CT, and finally increases the binding of MUC1 to β -catenin and targeting of MUC1 and β -catenin to the nucleus [212]. Src family members have been shown to bind and phosphorylate the CT of MUC1 at the YEKV motif. This, in turn, inhibits the binding of GSK3 β with MUC1-CT, which leads to better binding of MUC1-CT with β -catenin and the inhibition of GSK3 β -mediated degradation of β -catenin [188].

Finally, MUC1-CT associates with estrogen receptor α (ER α) and this interaction is stimulated by 17 β -estradiol, which exerts effects on growth, development and homeostasis in different tissues and organs. MUC1-CT binds directly to the ER α DNA binding domain and stabilizes ER α by blocking its ubiquitination and degradation [213].

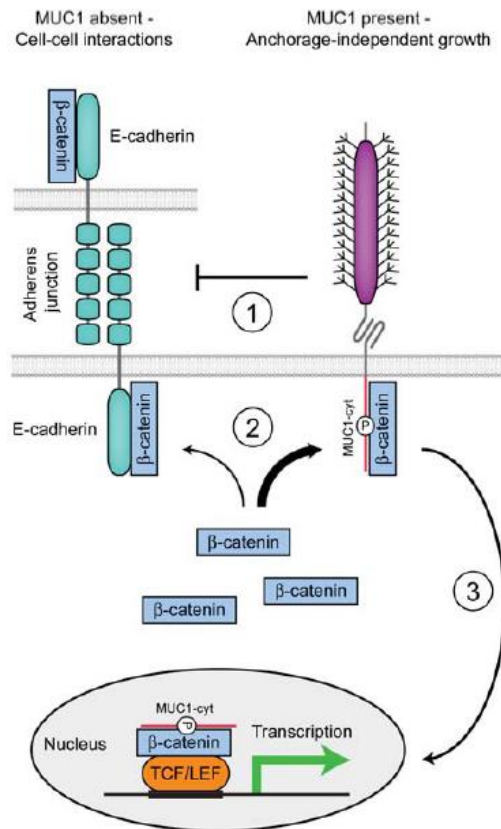


Figure 13. Regulation of cell-cell interactions, cellular proliferation and differentiation by MUC1. Overexpression and/or aberrant localization of MUC1 in cancer cells lead to the loss of cell-cell interactions and induces anchorage-independent growth. MUC1 impacts cell-cell interactions in multiple ways. (1) The glycosylated extracellular domain of MUC1 directly disturbs E-cadherin interactions between adjacent cells. (2) β -Catenin preferentially binds to the phosphorylated intracellular tail of MUC1 and thus decreases cell-cell adhesions through E-cadherin. (3) Finally, the complex β -catenin-MUC1-CT can traffic to the nucleus, bind to the Wnt signaling transcription factor TCF/LEF, and modulate the transcription of genes involved in cell proliferation and differentiation [177].

Inhibition of cancer cell death

In response to genotoxic stress, MUC1 regulates p53-responsive genes and thereby cell fate. MUC1 directly binds to the p53 regulatory domain and selectively promotes transcription of growth arrest genes and decreases transcription of apoptotic genes as a survival response to stress and thereby decreases cell death. In addition, MUC1 increases anti-apoptotic Bcl-XL and PI3K/AKT pathways to attenuate genotoxin-induced apoptosis [188].

MUC1 also activates the survival-related FOXO3a transcription factor in response to oxidative stress.

Phosphorylated MUC1-CT interacts with heat shock protein (HSP) 90 chaperone, which targets MUC1-CT to the mitochondria to attenuate intrinsic apoptotic pathway activation in response to stress; and with c-Abl, which induces c-Abl sequestring in the cytoplasm and consequently apoptotic pathway attenuation. Finally, MUC1-CT also interacts with I κ B kinase complex and induces its degradation, which help in the constitutive activation of NF- κ B and thereby blocks apoptosis and induces transformation [188].

HYPOTHESIS AND OBJECTIVES

CHAPTER 4

HYPOTHESIS

HYPOTHESIS

The proposed **hypothesis** in this work is based on the following previous findings:

- MUC1 is aberrantly expressed in ~900,000 of the 1.4 million tumours (carcinomas and certain haematological malignancies) diagnosed each year in the United States, making MUC1 overexpression one of the more common alterations in human cancers [191].
- MUC1 overexpression potentiates intracellular signalling and promotes cellular transformations like EMT, cellular proliferation, migration and metastasis [188]. Some of these cellular processes are commonly observed in IPF disease.
- MUC1 is a large glycoprotein that acts as a membrane receptor comprising 3 domains: (1) an extracellular domain, (2) a single transmembrane region, and (3) a cytoplasmic tail. The extracellular region contains the KL-6 epitope domain that in response to injury, is cleaved from the cell surface and released into the surrounding environment [196], leaving MUC1-C as a putative receptor.
- KL-6 has been found increased in serum and different biological fluids of IPF patients, and proposed as a useful biomarker to evaluate disease activity and predict the clinical outcomes in IPF [196].
- Although a broad evidence correlates KL-6 serum levels with progression and severity of IPF, nothing is known about the biological activation and cell signalling of MUC1 in IPF.
- MUC1-C engages diverse signalling pathways [191] by interactions, largely regulated by phosphorylation of the MUC1-CT, with several proteins implicated in different cellular processes such as cellular adherent junction maintenance and morphogenesis [188].
- MUC1-C extracellular domain serves as a binding site for the profibrotic galectin 3 ligand. It functions as a bridge to associate MUC1-C with different growth factor receptors [201].

- TGF β 1 is one of the main profibrotic factors in IPF and its signalling is promoted by galectin 3 binding to TGF β 1 receptor [144]. However whether TGF β 1 pathway contributes to MUC1 signalling is unknown.

Therefore, we hypothesize that **MUC1-CT bioactivation is upregulated in IPF and mediates signal transduction in collaboration with TGF β 1 and galectin 3, which may be a potential target to design future treatments for IPF.**

CHAPTER 5

OBJECTIVES

OBJECTIVES

The major objective of this project is **to assess the role of MUC1-CT bioactivation in IPF**. In order to it, the following minor objectives are proposed:

- To analyse the expression and distribution of MUC1-CT and its phosphorylated forms in human IPF tissue.
- To analyse the molecular mechanism implicated in MUC1-CT bioactivation.
- To analyse the cellular collaboration of MUC1-CT and TGF β 1 and its potential contribution to different cellular processes/transformations taking part in IPF disease.
- To analyse the role of MUC1 in IPF using a MUC1-KO mouse lung fibrosis model induced by bleomycin.

MATERIAL AND METHODS

CHAPTER 6

MATERIALS

MATERIALS

6.1. REAGENTS

| Reagent | Company | Reference |
|--|----------------------------|----------------|
| Acrylamide gel | Bio-Rad | 456-1094 |
| Amphotericin B | Lonza | H317-836E |
| Bicinchoninic acid (BCA) protein assay kit | Thermo Fisher Scientific | 23225 |
| Bleomycin | Mylan Pharmaceuticals, S.L | Mylan 15000 UI |
| Bovine serum albumin (BSA) | Sigma-Aldrich | A7906 |
| CD45 microbeads | Miltenyi Biotec | 130-045-801 |
| Cell Proliferation ELISA, BrdU kit | Roche | 11 647 229 001 |
| Chlorhydric acid (HCl) | Panreac | 131020 |
| Chloroform | Panreac | 151067 |
| Collagenase/dispase | Sigma-Aldrich | 10269638001 |
| Diethyl pyrocarbonate (DEPC) water | Applied Biosystems | AM9906 |
| Dispase II | Sigma-Aldrich | 04942078001 |
| Dnase I | AppliChem | A3778,0100 |
| DPX | Panreac | 255254 |

| | | |
|--|--------------------------|------------|
| Dual-luciferase reporter assay system | Promega | E1910 |
| Dulbecco's Modified Eagle's Medium (DMEM) | Lonza | BE12-614F |
| ECL Hyperfilm | Amersham GE Healthcare | GE28906837 |
| ECL plus | Amersham GE Healthcare | RPN2132 |
| ELISA DuoSet® mouse IL-6 | R&D systems | DY406 |
| ELISA DuoSet® mouse TGFβ1 | R&D systems | DY1679 |
| Ethanol | Panreac | 361086 |
| Ethylenediaminetetraacetic acid (EDTA) | Sigma – Aldrich | ED2SC |
| Ethylene glycol-bis(β-aminoethyl ether)-N,N,N',N'-tetraacetic acid (EGTA) | Sigma - Aldrich | E3889 |
| Fetal bovine serum (FBS) | Thermo Fisher Scientific | SH3007103 |
| Galectin 3 | Sigma-Aldrich | G5170 |
| Glycerol | Sigma-Aldrich | G5516 |
| GO-201 | Sigma-Aldrich | G7923 |
| Haematoxylin | Sigma - Aldrich | GHS322 |
| HEPES | Sigma - Aldrich | H4034 |
| Igepal CA-630 | Sigma - Aldrich | I8896 |

| | | |
|--|---------------------------|--------------|
| Immunofluorescence mounting medium (Fluoprep) | bioMérieux® | 75521 |
| Isoflurane | Baxter SL | ARREANE |
| Isopropyl alcohol | Sigma - Aldrich | I9516 |
| Ketamine | (Imalgene®) Merial | 904886 |
| Laemmli Buffer 2x | Bio-Rad | BR1610737 |
| Lipofectamine 2000 | Thermo Fisher Scientific | 11668027 |
| MACS running buffer | Miltenyi Biotec | 130-091-221 |
| Master Polymer Plus Detection System | Master diagnóstica | MAD-000237QK |
| May-Gruenwald-Giemsa stain | Sigma - Aldrich | MG1L |
| Medetomidine | (Domtor®) Esteve | 135089-1 |
| Methanol | Sharlab | ME03262500 |
| Molecular weight protein marker Amersham High-Range Rainbow | Amersham GE Healthcare | RPN756E |
| Nonidet™ P 40 | Sigma - Aldrich | 74385 |
| Opti-MEM | Thermo Fisher Scientific | 11058021 |
| Paraffin | Sigma - Aldrich | P3683 |
| Paraformaldehyde 4% | Panreac | 252931 |
| Penicillin/streptomycin | Lonza | DE17-602E |

| | | |
|---|---------------------------|-------------|
| Percoll | Amersham GE Healthcare | 17-0891-01 |
| Phenylmethylsulfonyl fluoride (PMSF) | Thermo Fisher Scientific | 36978 |
| Phosphate buffered saline (PBS) | Sigma - Aldrich | P4417 |
| Pirfenidone | Sigma- Aldrich | G5170 |
| Pronase | Sigma-Aldrich | 10165921001 |
| Protease inhibitor cocktail | Sigma - Aldrich | P8340 |
| Polyvinylidene difluoride (PVDF) membrane | Bio-Rad | 1704156 |
| Red blood cell lysis buffer | Sigma - Aldrich | 11814389001 |
| RNAlater | Thermo Fisher Scientific | AM7021 |
| Senescence cell histochemical staining Kit | Sigma-Aldrich | CS0030 |
| Sepharose 4B fast flow beads | Sigma - Aldrich | P-3296 |
| siRNA negative control | Ambion | AM4611 |
| siRNA-MUC1 | Ambion | 4392420 |
| siRNA-TβRI | Ambion | s14077 |
| siRNA-TβRII | Ambion | s14071 |
| SIS3 | Sigma- Aldrich | S0447 |

| | | |
|---|--------------------|-------------|
| Smad Binding Element (SBE) Reporter kit | BPS Bioscience | 60654 |
| Sodium chloride (NaCl) | Panreac | 141659 |
| Sodium hydroxide (NaOH) | Sigma- Aldrich | S8045 |
| TaqMan® Gene Expression Master Mix | Applied Biosystems | 4369016 |
| TaqMan® reverse transcription reagents kit | Applied Biosystems | N8080234 |
| TGFβ1 | Sigma Aldrich | T7039 |
| Trichrome stain Masson kit | Sigma - Aldrich | HT15 |
| TriPure® Isolation Reagent | Roche Diagnostics | 1667157001 |
| Tris | Panreac | 1319401211 |
| Tris-HCl | Sigma - Aldrich | 10812846001 |
| Trisodium citrate dihydrate | Sigma - Aldrich | W302600 |
| Triton X-100 | Panreac | 142314 |
| Trypan blue | Sigma-Aldrich | 93595 |
| Tween 20 | Sigma - Aldrich | P1379 |
| Xylene | Merck | 481769 |
| β-mercaptoethanol | Sigma - Aldrich | M6250 |
| 4',6-diamidino-2-phenylindole (DAPI) | Invitrogen | D1306 |

6.2. PATIENTS

Human lung tissue was obtained from Thoracic Surgery and Pathology Services of the University General Consortium Hospital of Valencia (CHGUV) (Valencia, Spain) and University and Polytechnic Hospital La Fe of Valencia (Valencia, Spain). Two types of samples have been used: A) lungs from IPF patients who were underwent surgery for organ transplantation program (n=22). B) Lung explant control samples from donors with normal lung function that were not used for transplant purposes (represents lung tissue without IPF and were used as controls), without any lung disease (n=21)) (See clinical characteristics in **Table 5**).

IPF was diagnosed according to the ATS/ERS consensus criteria, based on three major diagnostic criteria [5]:

- Exclusion of known causes of ILD.
- The presence of a UIP pattern on HRCT in patients not subjected to surgical lung biopsy.
- Specific combinations of HRCT and surgical lung biopsy UIP pattern in patients subjected to surgical lung biopsy.

All pulmonary function tests were performed within 3 months before surgery. After selection based on diagnosis criteria, all lung tissue samples used for the study were checked histologically by using the following exclusion criteria: (1) presence of tumour, (2) presence of respiratory tract infection.

The lungs taken from donor controls showed normal architecture with few intra-alveolar macrophages and edema.

The protocol was approved by the local research and independent ethics committee of the University General Consortium Hospital of Valencia (CEI CHGUV/052016) (annex 1). Informed written consent was obtained from each participant.

Table 5. Clinical characteristics of the control donor subjects and IPF patients.

| | Control donor subjects (n = 21) | IPF patients (n = 22) | P Value |
|------------------------------------|---------------------------------|-----------------------|---------|
| Age (yr), mean (SD) | 57.4 (6.7) | 60.8 (8) | NS |
| Sex (Male/Female) | 15/6 | 17/5 | |
| Smoking | | | |
| <i>Never smoked/Smokers</i> | 4/17 | 5/17 | NS |
| <i>Pack-year (range)</i> | 22 (0–30) | 22.5 (0–40) | NS |
| FEV ₁ , pred, mean (SD) | ND | 63.5 (14.5) | NS |
| FVC, % pred, mean (SD) | ND | 60.1 (12) | NS |
| DLco, % pred, mean (SD) | ND | 38 (21) | NS |
| PaO ₂ , mmHg, mean (SD) | 93.5 (4.2) | 53 (10.5) | <0.001* |
| NAC (y/n) | 0 | 16/6 | |
| Pirfenidone (y/n) | 0 | 6/16 | |
| Nintedanib (y/n) | 0 | 0 | |

% pred: % predicted; DLco: diffusion capacity of the lung for carbon monoxide; FEV₁: forced expiratory volume in 1 s; FVC: forced vital capacity; ND: not determined; Pack-year: 1 year of smoking 20 cigarettes per day; PaO₂: arterial blood oxygen tension. Data are means (SD). N-acetyl-L-cysteine (NAC)/pirfenidone/nintedanib refers to patients who received this treatment at the time of pulmonary sample. NS: not significance between groups (p>0.05). *Compared with control donors.

6.3. EXPERIMENTATION ANIMALS

Animal experimentation and handling were performed in accordance with the guidelines of the Committee of Animal Ethics and Well-being of the University of Valencia (Valencia, Spain). The protocol approved by this Committee and used in this project was entitled: “Pulmonary fibrosis bleomycin mouse model to study the role of MUC1 in IPF” and its code is: 2017/VSC/PEA/00061 (annex 2). The animal studies followed the ARRIVE (Animals in Research: Reporting In Vivo Experiments) guidelines. They consist of a checklist of 20 items describing the

minimum information that all scientific publications reporting research using animals should include [214].

Mice studies used pathogen-free male C57BL/6 of 12 weeks old (Harlan Iberica[®], Barcelona, Spain). MUC1-KO C57BL/6 mice were originally generated by Sandra Gendler (Mayo Clinic, NY, USA) and donated by the animalerie Institut de Médecine Prédictive et de Recherche Thérapeutique, (Lille Cedex, France). These MUC1-KO mice were generated using homologous recombination in mouse embryonic stem cells, as it was described in Andrew P. Spicer *et al.* [215].

Animals were in quarantine during seven days before the experiment (acclimation period). During this acclimation period and the experimental time, they were housed with free access to water and food (Harlan[®] diet Ref. 2014). All of them were randomized in cages and experimental groups. Standard conditions of the housing were:

- Relative humidity 55 ± 10 %.
- Temperature $22 \pm 3^{\circ}\text{C}$.
- 15 air cycles/ per hour.
- 12/12 h Light/Dark cycle.

CHAPTER 7

METHODS

METHODS

7.1 CELL CULTURE

7.1.1 ISOLATION AND CULTURE OF PRIMARY HUMAN ALVEOLAR TYPE II CELLS

Primary human ATII cells were obtained from distal lung parenchyma of control subjects. After pleura was separated bluntly, lung specimens were cut into 1 cm thick and 4 grams pieces and lavaged with saline. The samples were inflated with dispase II (final concentration, 2.0 U/ml) and placed in conical tubes containing dispase II, collagenase/dispase (final concentration, 1 mg/ml) and DNase I (final concentration, 0.1 mg/ml), and incubated for 120 min at 37°C with shaking. Enzymatically digested samples were minced with scissors, and filtered through nylon meshes ranging in pore size from 100 to 20 µm. The resulting cell suspension was centrifuged (300 x g, 20 min at 15°C) through a sterile Percoll gradient and the ATII cell-rich band was collected (**Figure 14**). If it was necessary, ATII cell-rich band was resuspended in red blood cell lysis buffer and spinned down. Finally, cells were resuspended in cold MACS running buffer (phosphate buffered saline (PBS) pH 7.2; 2mM ethylenediaminetetraacetic acid (EDTA); 0.5% bovine serum albumin (BSA)) and ATII cells were negatively separated using CD45 microbeads in a magnetic field (QuadroMACS™ Separator. Miltenyi Biotec). Total cells were counted to establish the final yield of freshly purified cells. Finally, ATII cells were resuspended in Dulbecco's Modified Eagle's Medium (DMEM) supplemented with 10% fetal bovine serum (FBS), 100 U/ml penicillin/streptomycin and 2,5 µg/ml amphotericin B and cultured for 48 hours to allow attachment. After media change, cells were cultured for an additional period of 3 days as maximum in a humidified atmosphere of 5% CO₂ at 37°C.

ATII cell viability was assessed with trypan blue showing greater than 95% viability. ATII purity was routinely assessed immediately after isolation by immunofluorescence analysis with pan-cytokeratin (CK) (epithelial (general structure) marker) and pro-surfactant protein C (pro-SPC) (ATII marker) (both positive) as well as α-SMA (mesenchymal marker) and CD45 (macrophages and leukocytes marker) (both negative) of cytocentrifuge preparations of ATII cells (**Table 6**). Characterization was performed at day 2 after ATII isolation by epithelial cell morphology and immunofluorescence analysis with pro-SPC + Ki67 (basal epithelial cell marker), podoplanin (ATI marker) and α-SMA + ZO-1 (epithelial (general structure) marker) (**Table 6**). ATII cells used throughout this study demonstrated 95% ± 3% purity.

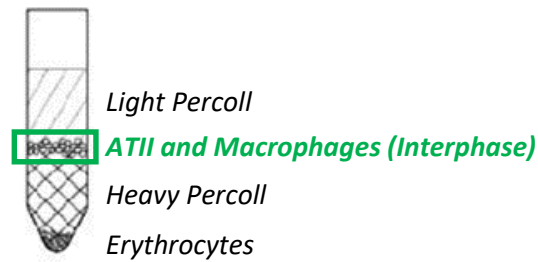


Figure 14. Percoll gradient cell separation from enzymatically digested lung pieces. *Alveolar type II (ATII) cell-rich band is highlighted.*

Table 6. Primary and secondary antibodies used in ATII purity and characterization immunofluorescence analysis.

| Epitope | Origen | Fluorochrome | Reference | Dilution | Buffer |
|------------------------------|--------|---------------------|-------------------------|----------|------------------|
| CK | Rabbit | - | Dako (Z0622) | 1:500 | BSA 0.1%/TBST |
| Pro-SPC | Rabbit | - | Millipore (AB3786) | 1:100 | BSA 0.1%/TBST |
| α -SMA | Mouse | - | Sigma- Aldrich | 1:500 | BSA 0.1%/TBST |
| CD45 | Mouse | - | BioLegend (304007) | 1:500 | BSA 0.1%/TBST |
| Ki-67 | Mouse | - | BioLegend (350503) | 1:100 | BSA 0.1%/TBST |
| ZO-1 | Rabbit | - | Invitrogen (40-2200) | 1:200 | BSA 0.1%/TBST |
| T1- α (podoplanin) | Goat | - | R&D (AF3244) | 1:100 | BSA 0.1%/TBST |
| IgG (H+L) Rabbit | Donkey | Rhodamina® 555 | Invitrogen (31660) | 1:200 | BSA 0.1%/TBST |
| IgG (H+L) Mouse | Donkey | Alexa Fluor® 488 | Invitrogen (65-6111) | 1:200 | BSA 0.1%/TBST |

| | | | | | |
|-------------------|--------|---------------------|------------------------|-------|------------------|
| IgG (H+L) Goat | Donkey | Alexa Fluor® 488 | Invitrogen (A11055) | 1:200 | BSA 0.1%/TBST |
|-------------------|--------|---------------------|------------------------|-------|------------------|

CK: cytokeratin; SPC: surfactant protein C; α -SMA: α -actin smooth muscle actin; ZO-1: zonula occludens – 1; Ig: immunoglobulin; BSA: bovine serum albumin; TBST: 0.1 % Tween 20/ Tris-buffered saline (TBS, 0.05 M Tris; 0.15 M sodium chloride, pH 7.6, at 25 °C)

7.1.2 ISOLATION AND CULTURE OF HUMAN PRIMARY LUNG FIBROBLASTS

Primary human lung fibroblasts were obtained from lung parenchyma of control subjects or macroscopically fibrotic affected areas of IPF. Lung parenchyma was cut into small pieces, treated with pronase (1 mg/ml) at 37°C for 30 min, placed in cell culture plates (**Figure 15**) and incubated in DMEM supplemented with 10% FBS, 100 U/ml penicillin/streptomycin and 2,5 μ g/ml amphotericin B. After approximately 2 weeks, fibroblasts grew from the tissue and were passaged by standard trypsinisation. Cells from passages 3–10 were used in all experiments described in the present study.



Figure 15. Human lung parenchyma explants.

7.1.3 CULTURE OF IMMORTALIZED CELL LINES

Two different immortalized cell lines from commercial origin were used in this project (Figure 16):

- **Adenocarcinomic human alveolar basal epithelial cell line (A549):** it was purchased from American Type Culture Collection (ATCC® CCL-185™; Rockville, USA) and cultured in DMEM supplemented with 10% FBS, 100 U/ml penicillin/streptomycin and 2,5 µg/ml amphotericin B at 37°C in a humidified atmosphere of 5% CO₂ in air. This cell line has been extensively used to model ATII cells.
- **Human lung fibroblast cell line (MRC5):** it was purchased from ATCC (ATCC® CCL-171™; Rockville, USA) and cultured in DMEM supplemented with 10% FBS, 100 U/ml penicillin/streptomycin and 2,5 µg/ml amphotericin B at 37°C in a humidified atmosphere of 5% CO₂ in air.

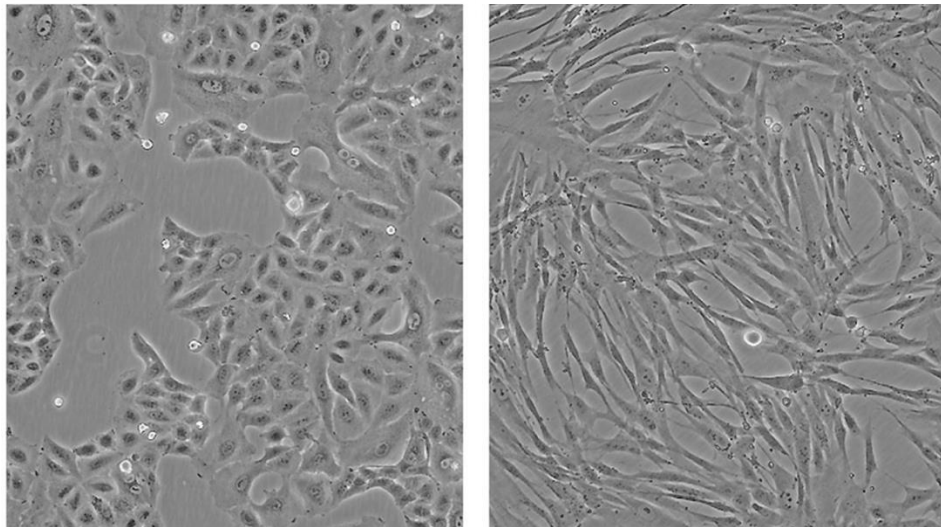


Figure 16. Morphology of immortalized cell lines A549 (left) and MRC5 (right). The pictures show high density cultures. Scale bar = 100 µm.

7.1.4 SMALL INTERFERING RNA-MEDIATED GENE SILENCING

Small interfering RNA (siRNA) is a class of double-stranded RNA molecules, 20-25 base pairs in length, which interferes with the expression of specific genes by complementary nucleotide sequence with mRNA after transcription. In this way, protein translation is prevented (**Figure 17**).

To transfer the siRNA inside the cell, liposomes able to fuse with the plasma membrane were generated (**Figure 17**). Two solutions were prepared: one solution containing the siRNA (50 μM) diluted in Opti-MEM (1:50) and one solution containing lipofectamine diluted in Opti-MEM (1:25). Both solutions were incubated separately during 5 minutes at room temperature and mixed and incubated together during 20 minutes at room temperature. The mixture was added to 70% confluent cell cultures (final concentration 50 nM siRNA and 2 $\mu\text{g}/\text{ml}$ lipofectamine) in antibiotic-free 0.1% FBS DMEM at 37°C in a humidified atmosphere of 5% CO_2 in air during 48 hours before cell stimulation (**Figure 17**).

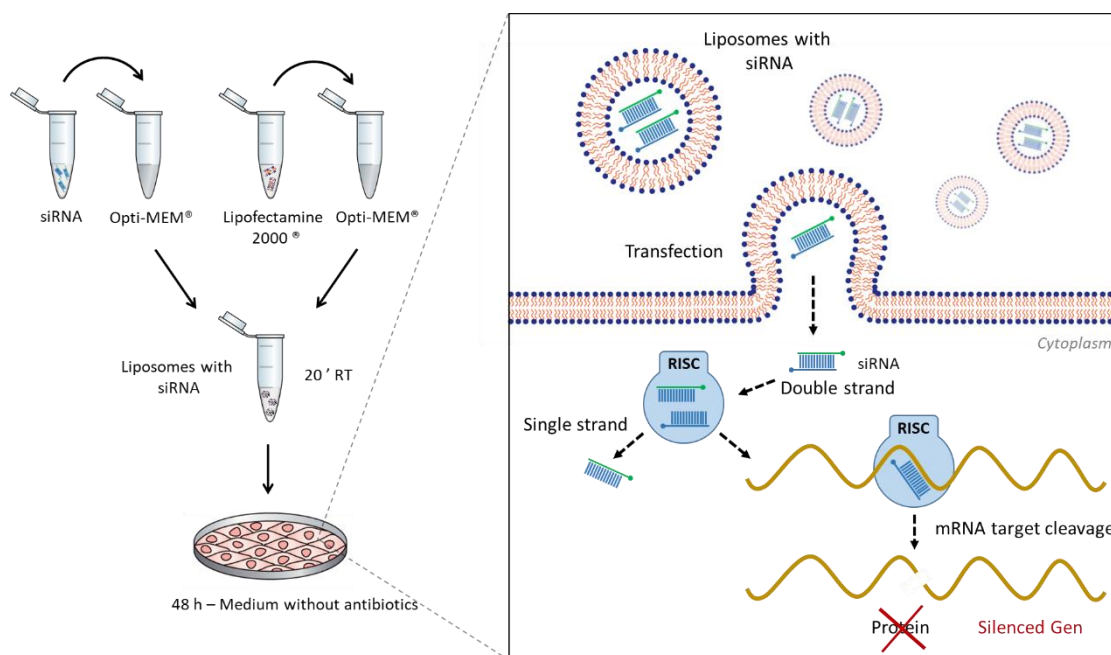


Figure 17. Small interfering RNA (siRNA) – mediated gene silencing. *Liposome/siRNA complex generation (left side): two solutions are prepared: one solution containing the siRNA (50 μM) diluted in Opti-MEM (1:50) and one solution containing Lipofectamine 2000 diluted in Opti-MEM (1:25). Both solutions are incubated separately during 5 minutes at room temperature and mixed and incubated together during 20 minutes at room temperature. The mixture is added to 70% confluent cell cultures (final concentration 50 nM siRNA and 2 $\mu\text{g}/\text{ml}$ lipofectamine) in antibiotic-*

free 0.1% FBS DMEM at 37°C in a humidified atmosphere of 5% CO₂ in air during 48 hours before cell stimulation. siRNA - mediated gene silencing (right side): liposomes fuse their membranes with the cell membrane. Once siRNA enters the cell it gets incorporated into other proteins to form the RNA-induced silencing complex (RISC). Once the siRNA is part of the RISC complex, the siRNA is unwound to form single stranded siRNA. The strand that is thermodynamically less stable is chosen to remain part of the RISC complex. Then, this strand can scan and find a complementary mRNA. Once the single stranded siRNA (part of the RISC complex) binds to its target mRNA, it induces mRNA cleavage. Consequently, mRNA is not translated into proteins.

7.1.5 IN VITRO STIMULATION

For *in vitro* studies, primary ATII cells/A549 cell line or primary lung fibroblasts/MRC5 cell line were stimulated with recombinant TGFβ₁ or galectin 3 for the indicated times and concentrations indicated for each experiment. 24 hours before stimulation, cells at 60–70% confluence were serum-deprived by incubation in 0.1% FBS DMEM.

Pirfenidone, SIS3 (an inhibitor of Smad3 phosphorylation [216]) or GO-201 (an inhibitor of MUC1-CT that blocks the formation of MUC1 oligomers in cells and attenuates targeting of MUC1 to the nucleus [217]) were added 30 min before stimulus and remained together with the stimulus until experimental evaluation. None of the drugs affected cell viability (assessed with trypan blue), showing greater than 95% viability.

7.1.6 SMAD BINDING ELEMENT ASSAY

The SBE Reporter kit was used for monitoring the activity of TGFβ/Smad signalling pathway in the cultured cells. The kit contains a transfection-ready SBE luciferase reporter vector, which is a TGFβ pathway-responsive reporter. This reporter contains a firefly luciferase gene under the control of multimerized SBE responsive element located upstream of a minimal promoter. The SBE luciferase reporter vector is premixed with constitutively expressing *Renilla* luciferase vector (internal control for transfection efficiency). The kit also includes a non-inducible firefly luciferase vector (negative control) premixed with constitutively expressing *Renilla* luciferase vector. The non-inducible luciferase vector contains a firefly luciferase gene under the control of a minimal promoter, without any additional response elements (**Figure 18**). The negative control is critical to determine pathway-specific effects and background luciferase activity.

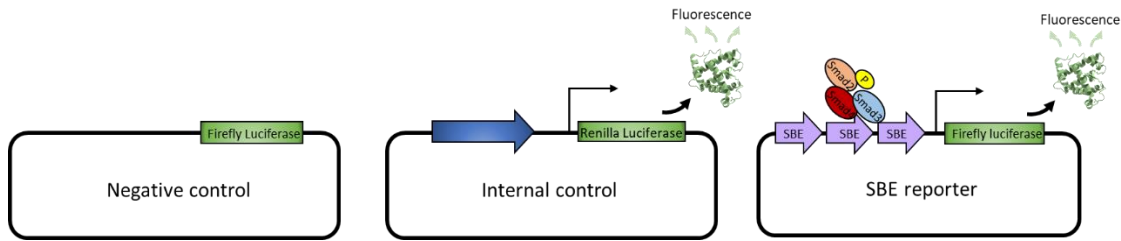


Figure 18. Smad Binding Element (SBE) Reporter kit vectors. *Negative control: non-inducible firefly luciferase vector. Internal control for transfection efficiency: constitutively expressing Renilla luciferase vector. SBE reporter: firefly luciferase gene under the control of multimerized SBE responsive element located upstream of a minimal promoter.*

This technique was used to determine the influence of *MUC1* expression on TGF β /Smad signalling pathway. In this aim, A549 cell line with *MUC1* silenced by siRNA technique (siRNA-MUC1) was used.

One day before siRNA transfection, cells were seeded in a 96-well plate at a density of 1.2×10^4 cells/well in 200 μ l of 10% FBS DMEM (antibiotic-free) so that cells were 70% confluent at the time of siRNA transfection. Plate was incubated at 37°C in a 5% CO₂ incubator. Next day, siRNA negative control or siRNA-MUC1 was transfected into cells using lipofectamine. Cells were incubated in antibiotic-free 0.1% FBS DMEM at 37°C in a 5% CO₂ incubator during 24 hours. After 24 hours of siRNA transfection, the following complexes were separately prepared:

- 60 ng of component A (SBE reporter vector + internal control vector) diluted in 22.5 μ l of Opti-MEM medium.
- 60 ng of component B (negative control vector + internal control vector) diluted in 22.5 μ l of Opti-MEM medium.
- 0.35 μ l of lipofectamine diluted in 22.5 μ l of Opti-MEM medium.

Complexes were separately incubated for 5 minutes at room temperature. Following it, diluted DNA (component A or component B) was combined with diluted lipofectamine and the mixture was incubated for 25 minutes at room temperature. 45 μ l of complexes were added to each well containing cells and antibiotic-free 0.1% FBS DMEM (55 μ l). Cells were incubated at 37°C in a 5% CO₂ incubator during 24 hours. After 24 hours, medium was changed to 0.1% FBS fresh DMEM and TGF β 1 was added to stimulate cells. After 18 hours of stimulation, luciferase activity was evaluated by dual-luciferase reporter assay system following manufacturer's protocol. Briefly, after the experiment, cells were lysed with Passive Lysis Buffer 1X during 15

minutes, shaking and room temperature. Lysed cells were mixed with reconstituted Luciferase Assay Reagent II in a 96-well white flat bottom plate. Immediately, the luminescence was measured by a microplate spectrophotometer Victor 1420 Multilabel Counter (Perkin Elmer). Reaction was stopped by Stop & Glo Reagent addition and *Renilla* luminescence was measured. To obtain the normalized firefly luciferase activity of the SBE reporter, firefly luciferase background signal (negative control) was subtracted, and the ratio of firefly luciferase luminescence from the SBE reporter vector to *Renilla* luminescence from the *Renilla* luciferase vector (internal control) was represented.

7.1.7 PROLIFERATION ASSAY

Fibroblast proliferation was measured by colorimetric immunoassay based on bromodeoxyuridine (BrdU) incorporation during DNA synthesis. In this aim, a cell proliferation enzyme-linked immunosorbent assay (ELISA) BrdU kit was used according to the manufacturer's protocol. Briefly, siRNA-MUC1 fibroblasts seeded in a 96-well plate were incubated with pirfenidone/GO-201 during 30 min followed by TGF β 1 + 10% FBS stimulation for 24 hours. After stimulation, BrdU was added to the cells and the cells were reincubated during 24 hours. During this time, the pyrimidine analogue BrdU is incorporated in place of thymidine into the DNA of proliferating cells. Following it, cells were fixed and DNA denatured by adding FixDenat from the kit, cells were incubated with anti-BrdU antibody conjugated with horseradish peroxidase (HRP) and finally tetramethylbenzidine (TMB) was used as reaction substrate. 490 nm absorbance was quantified using a microplate spectrophotometer Victor 1420 Multilabel Counter (Perkin Elmer). Proliferation data refer to the absorbance values of BrdU-labeled cellular DNA content per well.

7.1.8 CELL SENEESCENCE

siRNA-MUC1 primary human lung fibroblasts/ siRNA-MUC1 primary A166 cells were treated with pirfenidone during 30 minutes and stimulated with TGF β 1 during 48h. After that, it was used the senescence cell histochemical staining kit following manufacturer's instructions. Briefly, this kit is a preliminary screening tool for senescent behaviour based on a histochemical staining for β -galactosidase activity at pH 6. Under these conditions, β -galactosidase activity is easily detectable in senescent cells, but undetectable in quiescent, immortal, or tumour cells. First of all, cells were washed with PBS, provided by the kit, and fixed with the fixation buffer provided by the kit (20% formaldehyde; 2% glutaraldehyde; 70.4 mM Na₂HPO₄; 14.7 mM

KH₂PO₄; 1.37 M NaCl, and 26.8 mM KCl) for 6–7 minutes at room temperature. Following it, cells were stained with the staining mixture provided by the kit and incubated at 37 °C without CO₂ overnight. Finally, cells were observed under a microscope Leica DM6000B to count the blue-stained cells and the total number of cells in each field. Results were expressed as % senescent cells (β-galactosidase blue positive cells)/total number of cells in each field.

7.1.9 CELL IMMUNOFLUORESCENCE

After the corresponding *in vitro* experiments, primary ATII cells and primary fibroblasts were fixed with methanol during 5 minutes at -20°C. After that, cells were permeabilized with 0.1 % Triton X-100/PBS during 8 minutes and blocked (3% BSA/PBS) during 1 hour. Following it, cells were incubated with the primary antibodies (**Table 7**) overnight at 4°C, followed by PBS washing steps and FITC or rhodamine conjugated anti-mouse/rabbit/goat immunoglobuline (IgG antibodies (**Table 7**) incubation during two hours at 4°C. After washing steps with PBS, 2µg/ml 4', 6-Diamidino-2-Phenylindole, Dihydrochloride (DAPI) was used to mark nuclei during 3 minutes. Finally, cell preparations were mounted with immunofluorescence mounting medium.

Colocalization of MUC1-CT/phospho (p)-Smad2/3 and MUC1-CT/active (act)-β-catenin was performed using a confocal spectral Leica TCS SP2 microscope with x 1000 magnification and 3 x zoom. Red (HeNe 543 nm), green (HeNe 488 nm), and blue (Ar 351 nm, 364 nm) lasers were used. Colocalization studies were performed using the Leica confocal software v2.61. The cell images with colocalized points of the two laser canals were transformed into a white colour in the cell image.

Table 7. Primary and secondary antibodies used in cell immunofluorescence analysis

| Epitope | Origen | Fluorocrome | Reference | Dilution | Buffer |
|--|--------|---------------------------------|---|----------|------------------|
| MUC1-CT | Rabbit | - | Novus biologicals (NBP1-60046) | 1:100 | BSA 0.1%/TBST |
| p-Smad2/3 | Goat | - | Santa Cruz Biotechnology (sc-11769) | 1:100 | BSA 0.1%/TBST |
| Non-phospho active - β -catenin (Ser33/37/Thr41) | Mouse | - | Cell signaling technology (8814S) | 1:100 | BSA 0.1%/TBST |
| IgG (H+L) Rabbit | Goat | Rhodamina [®] 555 | Invitrogen (A27039) | 1:200 | BSA 0.1%/TBST |
| IgG (H+L) Mouse | Goat | Alexa Fluor [®] 488 | Invitrogen (A11001) | 1:200 | BSA 0.1%/TBST |
| IgG (H+L) Goat | Rabbit | Alexa Fluor [®] 488 | Invitrogen (A11078) | 1:200 | BSA 0.1%/TBST |

MUC1-CT: MUC1 cytoplasmic tail; p-Smad3: phospho-Smad3; Ig: immunoglobulin; BSA: bovine serum albumin; TBST: 0.1 % Tween 20/ Tris-buffered saline (TBS, 0.05 M Tris; 0.15 M sodium chloride, pH 7.6, at 25 °C)

7.2 FIBROSIS ANIMAL MODEL

7.2.1 PROTOCOL

Fibrosis animal model was generated by IT single instillation of a 1.5 U/kg dose of bleomycin in Wild type (WT) C57BL/6 mice and MUC1-KO C57BL/6 mice. This protocol effectively replicates several of the specific pathogenic molecular changes associated with IPF, and may be the best used as a model for patients with active disease [170]. It has been observed that this dose of bleomycin reproducibly generated pulmonary fibrosis in previous experiments [218, 219].

The aim of this protocol was to compare the difference between WT C57BL/6 mice and MUC1-KO C57BL/6 mice in pulmonary fibrosis progression. Several techniques have been used to achieve it: micro-CT–SPECT-positron emission tomography (PET) analysis, histology, cytokines quantification and analysis of gene and protein expression.

The account for experimental groups was estimated in a number of 10 mice (n=10) in each group: (i) saline serum (control) WT animals; (ii) saline serum (control) MUC1-KO animals (iii) bleomycin WT animals; (iv) bleomycin MUC1-KO animals.

Mice were anaesthetized with inhalatory 5% isoflurane (**Figure 19**) (Harvard Apparatus Anesthetic Vaporizers) and then a 1.5 U/kg single dose of bleomycin (dissolved in a total of 20 µL of sterile saline) was administered via the endotracheal route using a 23G tracheal cannula. Sham treated mice received the identical volume of IT saline instead of bleomycin. This procedure fixed experimentation day 1. At day 7, micro-CT-PET images were acquired to assess lung metabolic status and 24 hours before the end of the procedure (day 13) micro-CT-SPECT scans were acquired to assess the extension of fibrosis and pulmonary vascular perfusion. Finally, at the end of the treatment period (day 14), mice were sacrificed by a lethal injection of sodium pentobarbital followed by exsanguination. BALF, hearth and lungs from each mouse were collected (see workflow in **Figure 20**).

Lung function was measured as the baseline enhanced respiratory pause (Penh) at the beginning (day 0) and end (day 14) of the procedure. Along the procedure, the number of deaths was written down and survival percentage from each group was represented by Kaplan-Meier plot.

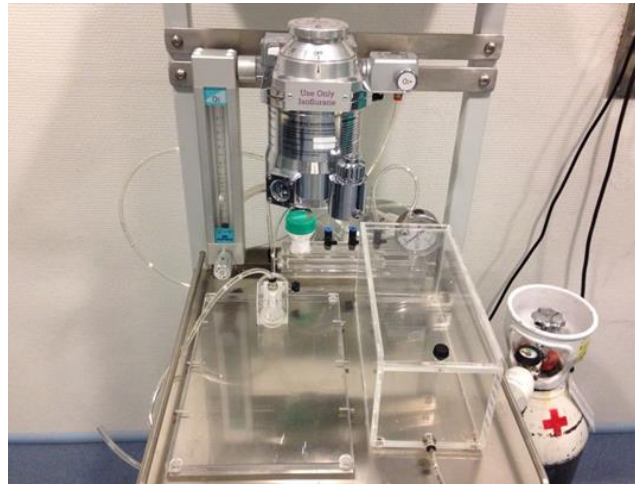


Figure 19. Isoflurane anaesthesia vaporizer and anaesthesia induction chamber.

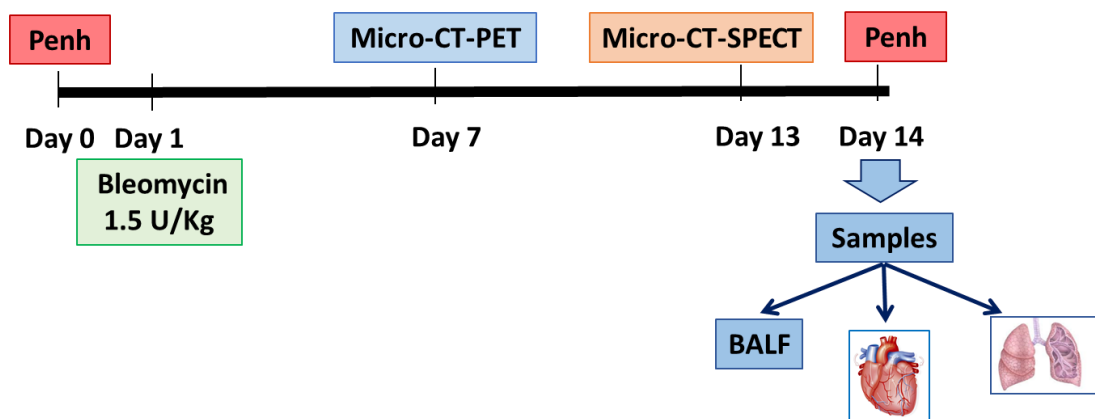


Figure 20. Bleomycin-induced pulmonary fibrosis mouse model workflow. Lung function was measured as the baseline enhanced respiratory pause (Penh) at the beginning (day 0) and end (day 14) of the procedure. At day 7, micro-computed tomography (CT)-positron emission tomography (PET) images were acquired and 24 hours before the end of the procedure (day 13) micro-CT-single-photon emission CT (SPECT) images were acquired. At day 14, mice were sacrificed by a lethal injection of sodium pentobarbital followed by exsanguination and BALF, heart and lungs from each mouse were collected.

7.2.2 LUNG FUNCTION

Lung function was measured as the baseline Penh in unrestrained conscious mice using whole-body plethysmography (**Figure 21**) (Buxco Small Animal Whole Body Plethysmography, Harvard apparatus, Minnesota, USA). Mice were placed in the chamber and allowed to equilibrate for approximately 30 minutes. Penh was calculated by the formula: $\text{Penh} = (\text{Te}/\text{Rt}-1) \times (\text{PEF}/\text{PIF})$, where Te is expiratory time (seconds); Rt is relaxation time (seconds), defined as the time of “volume” decay to 35% of the total expiratory pressure signal (area under the box pressure signal at expiration); PEF is peak expiratory flow (ml/second); and PIF is peak inspiratory flow (ml/second), according to the manufacturer’s instructions. Penh reflects changes in the waveform of the box pressure signal during both inspiration and expiration, and combines these changes with the timing comparison of early and late expiration during the animal’s spontaneous breathing. Penh was measured for 10 minutes for each experiment and mean value is shown.



Figure 21. Buxco Small Animal Whole Body Plethysmography apparatus.

7.2.3 MOLECULAR IMAGE

7.2.3.1 MICRO-CT-PET ANALYSIS

Lung metabolic status was evaluated using micro-PET-CT system (micro-CT-PET Albira II Imaging System (Oncovision®, Spain)) at day 7. Animals were anesthetized with intraperitoneal mixture of ketamine (70 mg/kg) and medetomidine (0.25 mg/kg). After 10 min of stabilization animals were injected intraperitoneally with 300 μ Ci fludeoxyglucose ^{18}F (^{18}F -FDG). After 30 min, the animals were introduced into the micro-CT-PET-SPECT system (Albira, Oncovision™,

Valencia, Spain) (**Figure 22**) in supine position in a cradle made of plexiglas to acquire micro-CT and PET images. Acquisitions of both PET and CT were made with an offset of 10 mm in length to visualize the lung region. Acquisition by CT (Carestream Molecular Imaging, Woodbridge, CT) was performed with good acquisition quality, high dose (400 μ A) and high voltage (45Kv) with the Step & Shoot acquisition mode and Filtered Back Projection reconstruction algorithm. In the PET mode, the studies were programmed with a field of vision (Field Of View (FOV)) of 80 mm, an acquisition time of 90 seconds per projection during 15 min. The images were reconstructed using the OSEM Cross algorithm with a number of iterations of 3 using the standard reconstruction parameters of the Albira Suite 5.0 Reconstructor software. The images were analysed and quantified using the PMOD analysis software version 3.2 (PMOD Technologies LTD, Zurich, Switzerland). Once acquired, the PET/CT images were reconstructed and merged. Volumes of interest (VOI) of the lung region were determined for the CT images. The VOI was analysed for each subject for their different days of acquisition. For PET images, the VOI obtained in the CT image of each subject was taken as a template and it was extrapolated to the PET image and subsequently quantified (**Figure 23**). The quantification of images provided the number of accounts acquired per pixel unit. This value was relativized by the dose injected (corrected for the radioactive decay of ^{18}F) and by subject weight, resulting in the standard uptake value (SUV).



Figure 22. Multimodal micro-CT/PET/SPECT equipment Albira II®

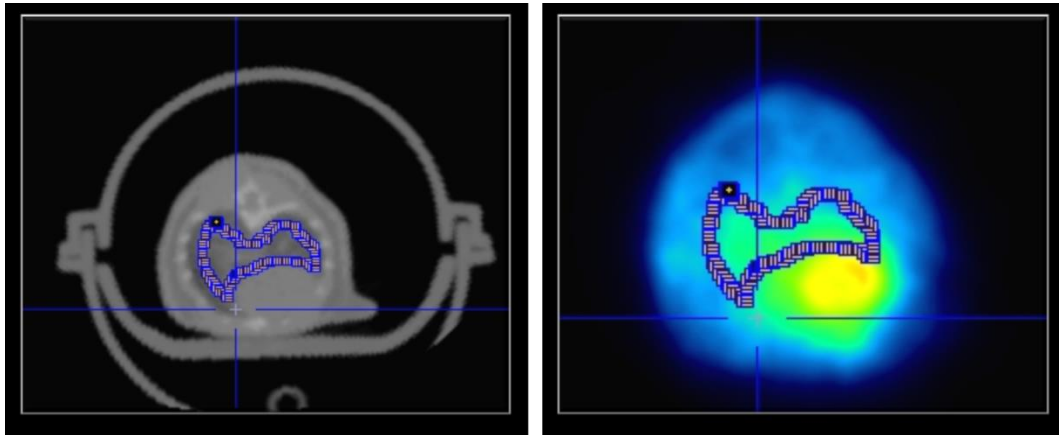


Figure 23. Volume of interest (VOI) from CT and PET images. VOI used to quantify in CT image (left) extrapolated to PET image (right).

7.2.3.2 MICRO-CT-SPECT ANALYSIS

Mice were also anesthetized with intraperitoneal mixture of ketamine (70 mg/kg) and medetomidine (0.25 mg/kg). After stabilization, the animals were introduced into the micro-CT-PET-SPECT and capture of micro-CT images were acquired at day 13. The time of each capture was 30 min (until 300000 counts). Lung images were taken as follow: planar scintigraphy in anterior, posterior, left and right lateral, and left and right posterior oblique views. X-ray captures were acquired through Step & Shoot modality using 400 μ A of current intensity, 45 kV of voltage and 0.5mm attenuation filter. The images were reconstructed with filtered back projection algorithm using the Albira Suite 5.0 software (OncoVision, Valencia, Spain). The combination of acquisition and reconstruction result in a final whole image matrix of 255*255*255 mm with a pixel size of 0.25*0.25*0.25 mm. 252 image sections corresponding to the whole lung images were acquired in each capture and analysed with the PMOD™ software selecting a whole 3D VOI. Densitometry analysis of the extension of fibrosis was quantified using micro-CT images as Hounsfield Units (HU). The mean of HU units per pixel was calculated.

To evaluate the pulmonary vascular perfusion, mice were injected with a suspension of albumin macroaggregated Tc^{99m} (MAA-Tc^{99m}) (Molipharma, Valencia Spain; 0.5–1 mCi; particle diameter 5-90 μ m) via the tail vein. Perfusion imaging entailed a SPECT scan. For each experimental group of animals, micro-CT-SPECT scans were acquired at day 13. All scans were performed with gamma cameras with large field-of-view detectors, equipped with low energy general purpose collimators. Quantification was performed by analysing the number of counts in the same VOI applied to every image (counts per pixel unit) corrected for the radioactive decay of Tc^{99m}.

7.2.4 SAMPLE COLLECTION

24 hours after the last dose of MAA-Tc^{99m}, mice were sacrificed. First of all, BALF was obtained by tracheotomy to assess inflammatory cells in the lung and to analyse cytokine expression. And secondly, after opening the thoracic cavity, trachea, lungs and heart were removed *en bloc*. Left lung was processed for histological studies and right lung was processed for biochemical or molecular biology studies. Specifically, the whole left lung was kept in paraformaldehyde at room temperature and the right lung was minced and kept with RNAlater (for gene expression analysis) or dry (for protein expression analysis) at -80°C. The right ventricular (RV) wall of the heart was dissected free and weighed along with the left ventricle wall plus septum (LV + S), and the resulting weights were reported as RV/(LV + S) ratio to provide an index of right ventricular hypertrophy.

7.2.5 BRONCHOALVEOLAR LAVAGE FLUID

BALF was recovered following three consecutive washes of the lung with 0.6 ml aliquots of sterile PBS flushed through a 24G tracheal cannula. Cell suspensions were concentrated by low speed centrifugation (150 x g, 5 min) and cells resuspended in PBS to determine total cell counts and differential cell counts. After the counting, the remaining cells were stored in dry at -80°C to analyse IL-6 and TGFβ1 expression by RT-PCR. Supernatants were stored at -80°C to analyse IL-6 and TGFβ1 expression by ELISA.

7.2.5.1 TOTAL AND DIFFERENTIAL CELL COUNT

Total cell counts were made in a haemocytometer, in which cell viability was assessed by trypan blue staining.

Differential cell counts were determined from cytocentrifuge preparations from 100µl of BALF centrifuged at 300 x g during 10 minutes in a Cytospin™ 4 Cytocentrifuge (Thermo Fisher Scientific). Cytocentrifuge preparations were stained with May-Gruenwald-Giemsa stain and 300 cells were counted differentially into the different groups of leukocytes. Cytospin preparations were observed at Leica DM6000B microscope.

7.2.5.2 ENZYME – LINKED IMMUNOSORBENT ASSAY

IL-6 and active TGFβ1 cytokines were measured in mice BALF using commercially available ELISA DuoSet® mouse IL-6 and TGFβ1 according to the manufacturer's protocol. To measure latent complexes of TGFβ1, activation was accomplished by acid treatment. Therefore,

0.1 ml of BALF was treated with 0.1 ml of 1 mM HCl, incubated for 10 min, and then neutralised with 0.1 ml of 1.2 M NaOH/0.5 M HEPES.

Briefly, both ELISA kits use the variant “sandwich” ELISA (**Figure 24**) in which the antigens are quantified between two layers of antibodies (i.e. capture (immobilized on the plate) and detection antibody). The antigen to be measured must contain at least two antigenic epitope capable of binding to antibody, since at least two antibodies act in the sandwich. Detection antibodies are coupled to a substrate-modifying enzyme (HRP). Then, substrate (TMB) is converted by this enzyme to elicit a chromogenic signal proportional to the binding capture antibody-sample. Absorbance at 450 nm was measured using a spectrophotometer Victor 1420 Multilabel Counter (Perkin Elmer). Results were extrapolated from the standard curve.

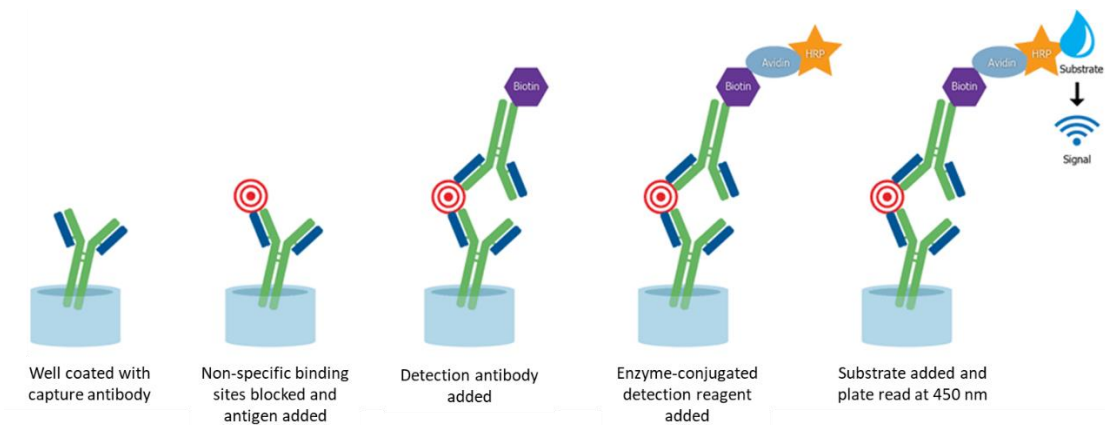


Figure 24. Sandwich ELISA schematic protocol

7.3 HISTOLOGY

7.3.1 TISSUE FIXATION AND DEHYDRATION

Human and mouse lung tissues were fixed with paraformaldehyde 4% during at least 48h. Following it, samples were dehydrated (**Table 8**) and embedding into paraffin blocks using the EC350-1 Myr Paraffin Embedder (Leica Geosystems). Finally, paraffin blocks were cut in 5 μ m thickness sections using a microtome HM 340 E (Leica Geosystems).

Table 8. Lung tissue fixation and dehydration protocol

| Treatment | Time | Number of repeats |
|---------------------|------------|-------------------|
| Paraformaldehyde 4% | 48 hours | x1 |
| Ethanol 70% | 60 minutes | x1 |
| Ethanol 95% | 60 minutes | x2 |
| Ethanol 100% | 60 minutes | x3 |
| Xylene | 60 minutes | x2 |
| Paraffin | 24 hours | x1 |

7.3.2 IMMUNOHISTOCHEMICAL ANALYSIS

For immunohistochemical analysis of human and mouse lungs, tissue sections were first of all deparaffinized and hydrated (**Table 9**). After that, to avoid peroxidase endogenous activity, lung sections were incubated in 3% distilled water/methanol during 20 minutes and washed with 0.1 % Tween 20 / Tris-buffered saline (0.05 M Tris; 0.15 M sodium chloride, pH 7.6, at 25 °C) (TBST). A heat-induced antigen retrieval was performed using 0.01M sodium citrate buffer (10mM sodium citrate dihydrate, 0.1% Nonidet™ P 40, pH=6, 100°C, 20 minutes). Cell membranes were permeabilized using 0.1% Triton X 100/PBS during 10 minutes, and non-specific binding sites in the tissue sample were blocked with 5% FBS/PBS during 1 hour after

washing with TBST buffer. Following it, lung sections were incubated with primary antibodies (**Table 10**) overnight at 4°C. After washing with TBST, a Master Polymer Plus HRP from the Master Polymer Plus Detection System kit was used for immunohistochemistry during 30 minutes. The substrate used, after washing with TBST, was 3'-Diaminobenzidine (DAB) during few seconds. Finally, sections were stained with haematoxylin during 15 seconds and dehydrated (**Table 11**) for mounting with DPX. The non-immune IgG isotype control was used as negative control and gave negative for all samples. Samples were observed at the microscope Nikon Eclipse TE200 and a representative picture from each condition is shown.

Table 9. Deparaffination and hydration protocol for immunohistochemical analysis

| Treatment | Time | Number of repeats |
|-----------------|------|-------------------|
| Oven 60°C | 15' | - |
| Xylene | 10' | x2 |
| Ethanol 100% | 10' | x3 |
| Ethanol 95% | 10' | x2 |
| Ethanol 80% | 3' | x1 |
| Distilled water | 5' | x1 |

Table 10. Primary antibodies used in immunohistochemical analysis

| Epitope | Reference | Dilution | Buffer |
|---------------|------------------------------------|----------|---------------|
| MUC1-CT | Novus biologicals (NBP1-60046) | 1:100 | BSA 0.1%/TBST |
| MUC5B | Abcam (ab77995) | 1:100 | BSA 0.1%/TBST |
| TGFβ1 | Cell Signaling (3709S) | 1:100 | BSA 0.1%/TBST |
| MUC1-P/T-1224 | Abgent (AP3728a) | 1:100 | BSA 0.1%/TBST |
| MUC1-P/Y-1229 | Abcam (ab79226) | 1:100 | BSA 0.1%/TBST |
| NOX4 | Novus biologicals (NB110-58849) | 1:100 | BSA 0.1%/TBST |

MUC1-CT: MUC1 cytoplasmic tail; TGFβ1: transforming growth factor β1; MUC1-P/T-1224: MUC1 phosphorylated form at Thr 1224; MUC1-P/Y-1229: MUC1 phosphorylated form at Tyr 1229; NOX4: NADPH oxidase 4; BSA: bovine serum albumin; TBST: 0.1 % Tween 20/ Tris-buffered saline (TBS, 0.05 M Tris; 0.15 M sodium chloride, pH 7.6, at 25 °C).

Table 11. Dehydration protocol for immunohistochemical analysis

| Treatment | Time | Number of repeats |
|--------------|------|-------------------|
| Ethanol 90% | 5' | x2 |
| Ethanol 100% | 5' | x2 |
| Xylene | 10' | x2 |

7.3.3 MASSON'S TRICHROME STAINING

Mouse lung tissue sections were stained with Masson's trichrome staining kit to detect collagen deposition and for assessment of the fibrotic injury and pulmonary artery remodeling. Briefly, lung tissue sections were deparaffinized and hydrated (**Table 9**). Following it, samples were re-fixed in preheated Bouin's Solution (this solution improve Masson's trichrome staining quality) at 56°C for 15 minutes. After that, two staining solutions were used: Weigert's iron haematoxylin working solution (nuclei staining - black) and Biebrich scarlet-acid fuchsin solution (cytoplasm and muscle staining - red). After that, a differentiation step using phosphomolybdic/phosphotungstic acid solution was performed and collagen was demonstrated by blue staining with Aniline blue solution. Rinsing in acetic acid after staining rendered the shades of colour more delicate and transparent. Finally, lung sections were dehydrated (**Table 11**) for mounting with DPX.

Severity of lung fibrosis was scored on a scale from 0 (normal lung) to 8 (total fibrotic obliteration of fields) according to Ashcroft score (**Table 12**). Samples were observed at the microscope Nikon Eclipse TE200 and 10 representative images from each condition were scored. One representative image from each condition is shown.

Table 12. Criteria for grading lung fibrosis [220].

| Grade of fibrosis | Histological features |
|-------------------|--|
| 0 | Normal lung |
| 1 | Minimal fibrous thickening of alveolar or bronchiolar walls |
| 2 – 3 | Moderate thickening of walls without obvious damage to lung architecture |
| 4-5 | Increased fibrosis with definite damage to lung structure and formation of fibrous bands or small fibrous masses |
| 6-7 | Severe distortion of structure and large fibrous areas; "honeycomb lung" is placed in this category |
| 8 | Total fibrous obliteration of the field |

7.3.4 COIMMUNOFLUORESCENCE ANALYSIS

Human and mouse lung sections were first of all deparaffinized and hydrated (**Table 9**). Following it, antigen retrieval, cell membrane permeabilization and blocking were performed (see section 7.3.2). Primary antibodies were incubated during 1 hour at 37°C and after washing with TBST, FITC or rhodamine conjugated anti-mouse/rabbit/goat IgG antibodies were used as secondary antibodies and incubated during 1 hour at 37°C (see primary and secondary antibodies used in section 7.1.9). After TBST washing again, DAPI (2µg/ml) was used to mark nuclei during 3 minutes. Finally, lung sections were mounted with immunofluorescence mounting medium.

Colocalization of MUC1-CT/ p-Smad2/3 and MUC1-CT/ act-β-catenin was performed in the same way than in cell immunofluorescence analysis (see section 7.1.9). However, the tissue images with colocalized points of the two laser canals were transformed into an orange color.

7.4 GENE EXPRESSION ANALYSIS

7.4.1 RNA EXTRACTION AND QUANTIFICATION

Total RNA was isolated using TriPure® Isolation Reagent. Briefly, samples were first of all minced using the TissueLyser II (Qiagen®) system (tissue) or vortex (cells) in the presence of the TriPure® Isolation Reagent. Following it, chloroform was added to separate after centrifugation two different phases (an aqueous phase containing RNA and an organic phase containing DNA and proteins). After that, RNA was precipitated using isopropyl alcohol on ice followed by centrifugation. Finally, RNA was washed with 75% ethanol and centrifugation steps and it was resuspended in 20 µl diethyl pyrocarbonate (DEPC) water at 60°C during 5 minutes.

RNA quantification (ng/µl) and purity (260nm absorbance (A_{260})/280 nm absorbance (A_{280})) was determined by the spectrophotometer NanoDrop 2000C (ThermoFisher Scientific). The integrity of the extracted RNA was confirmed with Bioanalyzer (Agilent) following manufacturer's instructions.

RNA was kept at -80°C until its use.

7.4.2 REVERSE TRANSCRIPTION REACTION

Reverse transcription was performed in 300 ng of total RNA with a TaqMan® reverse transcription reagents kit according to the manufacturer's instructions (RT reaction setup – **Table 13**). This reaction in which RNA was retrotranscribed to cDNA was performed in the 9800 Fast Thermal Cycler (Applied Biosystems).

Reaction steps were:

- 10 minutes at 25°C: primer hybridation to RNA.
- 30 minutes at 37°C: optimal temperature for retrotranscriptase enzyme.
- 5 minutes at 95°C: denaturation RNA-cDNA hybrid.

cDNA was kept at -20°C until its use.

Table 13. Reverse transcription reaction setup

| Component | Volume (μl) |
|------------------------------|-------------|
| DEPC – treated water | To 20 μl |
| 10X RT Buffer | 2 |
| 25 mM MgCl ₂ | 1.4 |
| 10 mM dNTP mix (2.5 mM each) | 4 |
| RNase Inhibitor (20 U / μl) | 1 |
| MultiScribe™ RT (50 U / μl) | 1 |
| 50 μM Random hexamers | 1 |
| Template RNA | Varies |

7.4.3 REAL TIME PCR

PCR is used to exponentially amplify a single copy or a few copies of a specific segment of DNA to generate thousands to millions of copies of a particular DNA sequence. The variant Real time (RT)-PCR monitors the amplification of a targeted DNA molecule during the PCR, i.e. in real-time, and not at its end. RT-PCR was performed in the 7900HT Fast Real-Time PCR System (Applied Biosystems) using Taqman® Gene Expression Master Mix (RT-PCR reaction setup – **Table 14**). cDNA (10 ng) was amplified with specific Taqman primers and probes predesigned by Applied Biosystems (**Table 15**).

Table 14. RT-PCR reaction setup

| Component | Volume (μl) |
|------------------------------------|-------------|
| cDNA | 2 |
| Taqman® Gene Expression Master Mix | 2.5 |
| Taqman primer | 0.25 |
| DEPC water | 0.25 |

Before the RT-PCR cyclic process, an initial denaturation step (2 minutes at 50°C and 10 minutes at 95°C) was performed. Following it, the following cycle process was repeated 40 times:

- 15 seconds at 95°C (denaturation step).
- 1 minute at 60°C (primer annealing and extension step).

Expression of the target gene was expressed as the fold increase or decrease relative to the expression of β -actin as an endogenous control. The mean value of the replicates for each sample (standard deviation ≤ 1) was calculated and expressed as the cycle threshold (Ct) (**Figure 25**). The level of gene expression was then calculated as the difference (Δ Ct) between the Ct value of the target gene and the Ct value of β -actin. The fold changes in the target gene mRNA levels were designated $2^{-\Delta Ct}$.

Table 15. Taqman primers used in the RT-PCR

| Gene | Gene symbol | Reference |
|-----------------------|---------------|----------------|
| Muc1 human | MUC1 | Hs00159357_m1 |
| α -SMA human | ACTA1 | Hs00559403_m1 |
| Collagen type I human | COL1A1 | Hs00164004_m1 |
| Snail human | SNAI1 | Hs00195591_m1 |
| Slug human | SNAI2 | Hs00161904_m1 |
| E-Cadherin human | CDH1 | Hs01023894_m1, |
| Vimentin human | VIM | Hs00958111_m1 |
| p21 human | PAK3 | Hs01040810_m1 |
| p16 human | CDKN2A | Hs00923894_m1 |
| β -actin human | ACTB | Hs01060665_m1 |
| IL-6 mouse | Il6 | Mm00446190_m1 |
| TGF β 1 mouse | Tgf β 1 | Mm01178820_m1 |
| Collagen type I mouse | Col1a1 | Mm00801666_g1 |
| CTGF mouse | Ctgf | Mm01192933_g1 |
| IL-13 mouse | Il13 | Mm00434204_m1 |
| Muc1 mouse | Muc1 | Mm00449604_m1 |
| β -actin mouse | Actb | Mm02619580_g1 |

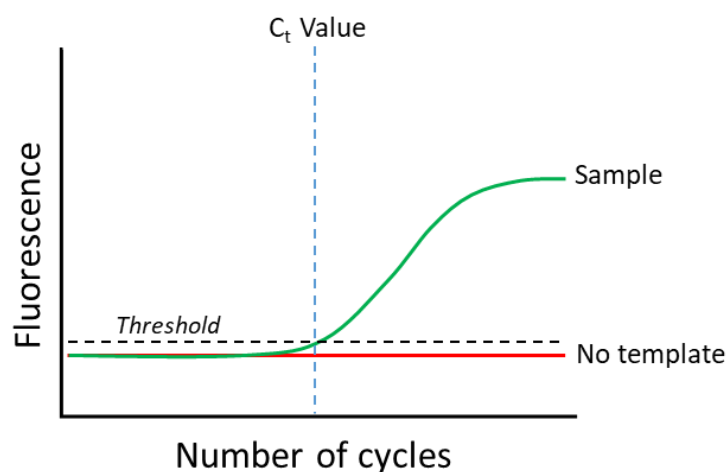


Figure 25. Cycle threshold (Ct) value on a real-time PCR amplification curve. *PCR instrument will collect fluorescence data during each cycle. This will appear as a straight line starting from the zero cycle point. The threshold level will be just above this, but at the point where the samples start moving into exponential phase of PCR amplification. Computer software RQ Manager, calculates this exact point (Ct).*

7.5 PROTEIN EXPRESSION ANALYSIS

7.5.1 WESTERN BLOTTING ANALYSIS

Western blotting analysis was used to detect protein expression changes in human and mouse lung tissues, and in primary ATII/A549 cells and primary lung fibroblast/MRC5 cells. Previously -80°C dry stored lung tissue was homogenized with the TissueLyser II system (Qiagen®) in the presence of 500 µl of a lysis buffer comprising a complete protease inhibitor cocktail, phenylmethylsulfonyl fluoride (PMSF), and Buffer C (0.02M HEPES; 0.001 M EDTA; 0.001M ethylene glycol-bis(β-aminoethyl ether)-N,N,N',N'-tetraacetic acid (EGTA); 0.4M NaCl and 21.1% glycerol). Cells were scraped and homogenized from a confluent 25-cm² flask in the presence of 500 µl of the same lysis buffer. In both cases, a thermal shock lysis procedure was performed (three thermal shock cycles (liquid nitrogen – 37°C)). After that, 1% Nonidet™ P 40 was added during 15 minutes on ice and shaking. Finally, supernatant from centrifugation (1000 x g, 20 minutes, 4°C) was collected and protein level was quantified using the Bicinchoninic acid protein assay (BCA) kit according to the manufacturer's instructions. Briefly, the principle of this method is that proteins can reduce Cu⁺² to Cu⁺¹ in an alkaline solution (the biuret reaction) and result in a purple colour formation by bicinchoninic acid.

Sodium dodecyl sulfate (SDS) polyacrylamide gel electrophoresis was used to separate the proteins according to their molecular weight. Before sample loading, proteins were denatured with 2X Laemmli buffer containing β -mercaptoethanol (1:1) during 10 minutes at 95°C. Briefly, 15 μ g of proteins (denatured) along with a high-range rainbow molecular weight protein marker were loaded onto an 4 – 20% acrylamide resolving gel and run through the gel by application of 100 V for 1 h (**Figure 26**). Proteins were transferred from the gel to a 0.2 μ m polyvinylidene difluoride (PVDF) membrane using a semi-dry blotting method. The membrane was blocked with 5% BSA or milk in 0.1% Tween 20/PBS (PBST) or TBST during 2 hours and incubated with primary antibodies (**Table 16**) overnight at 4°C. After that, the membrane was incubated with the corresponding HRP-conjugated secondary antibody during 1 hour. The enhanced chemiluminescence method of protein detection using enhanced chemiluminescence reagents (ECL Plus) was used to detect labeled proteins in an Amersham ECL Hyperfilm. Densitometry of films was performed using the Image J 1.42q software (available at <http://rsb.info.nih.gov/ij/>, USA). Results of target protein expression were expressed as the ratio of the densitometry from the β -actin endogenous controls.

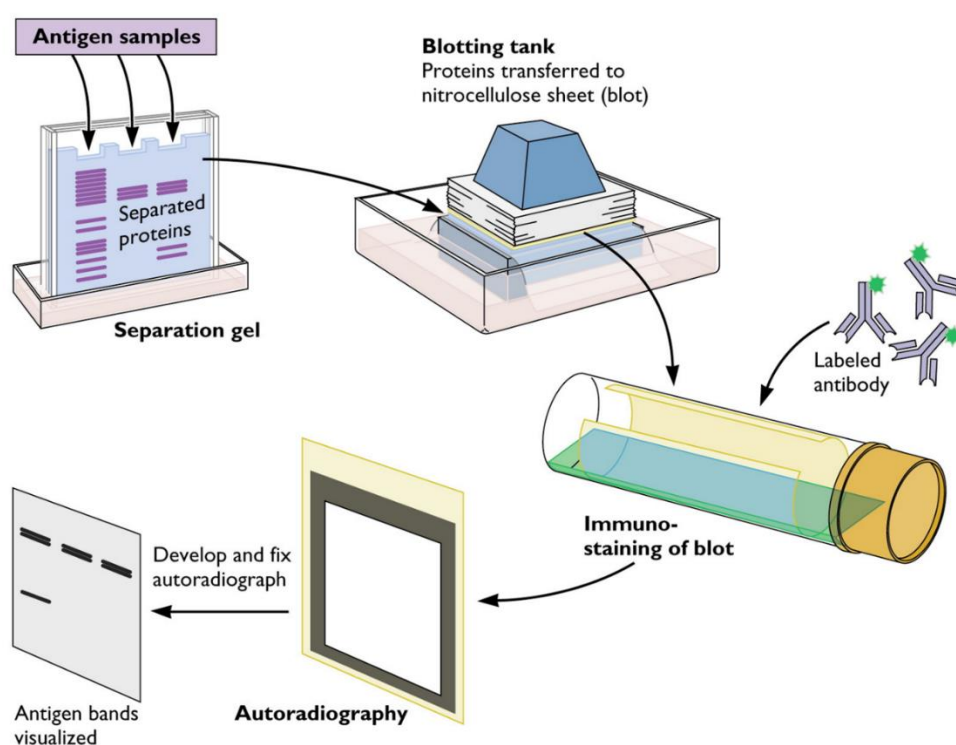


Figure 26. Western Blotting schematic protocol

Table 16. Primary and secondary antibodies used in Western Blotting

| Epitope | Reference | Dilution | Buffer |
|-----------------|---|----------|--------------|
| MUC1-CT | Novus biologicals (NBP1-60046) | 1:500 | Milk 5%/PBST |
| TGFβ1 | Cell Signalling (3709S) | 1:1000 | Milk 5%/PBST |
| MUC1-P/T-1224 | Abgent (AP3728a) | 1:500 | BSA 5%/TBST |
| MUC1-P/Y-1229 | Abcam (ab79226) | 1:500 | BSA 5%/TBST |
| α-SMA | Sigma-Aldrich (A5228) | 1:1000 | Milk 5%/PBST |
| Collagen type I | Calbiochem (234167) | 1:1000 | Milk 5%/PBST |
| p-Smad3 | Millipore (PS1023) | 1:1000 | BSA 5%/TBST |
| Smad3 | Calbiochem (566414) | 1:1000 | Milk 5%/PBST |
| E-Cadherin | ECM BioScience (CM1681) | 1:1000 | Milk 5%/PBST |
| CTGF | Santa Cruz Biotechnology (SC-34772) | 1:1000 | Milk 5%/PBST |
| p21 | Novus Biologicals (NB100-1941) | 1:1000 | Milk 5%/PBST |
| p-Erk1/2 | Sigma-Aldrich (M-9692) | 1:1000 | BSA 5%/TBST |
| Erk1/2 | Cell Signaling (4695) | 1:1000 | Milk 5%/PBST |

| | | | |
|--|--|--------|--------------|
| Non-phospho (active) β -catenin (Ser33/37/Thr41) | Cell Signaling (8814S) | 1:500 | Milk 5%/PBST |
| IL-6 | Novus Biologicals (NBP1-77894) | 1:500 | Milk 5%/PBST |
| IL-13 | Santa Cruz Biotechnology (sc-393365) | 1:500 | Milk 5%/PBST |
| β -actin | Sigma-Aldrich (A1978) | 1:1000 | Milk 5%/PBST |
| HRP - IgG (H+L) Rabbit | Thermo Fisher Scientific (SA1-100) | 1:5000 | Milk 5%/PBST |
| HRP - IgG (H+L) Mouse | Thermo Fisher Scientific (SA1-200) | 1:5000 | Milk 5%/PBST |

MUC1-CT: MUC1 cytoplasmic tail; TGF β 1: transforming growth factor β 1; MUC1-P/T-1224: MUC1 phosphorylated form at Thr 1224; MUC1-P/Y-1229: MUC1 phosphorylated form at Tyr 1229; α -SMA: α -smooth muscle actin; p-Smad3: phospho-Smad3; CTGF: connective tissue growth factor; p-Erk1/2: phospho- extracellular signal-regulated kinase 1/2; IL-6: interleukin-6; IL-13: interleukin-13; HRP: Horseradish peroxidase; IgG: immunoglobulin G; BSA: bovine serum albumin; PBST: 0.1 % Tween 20/ Phosphate-buffered saline (PBS); TBST: 0.1 % Tween 20/ Tris-buffered saline (TBS, 0.05 M Tris; 0.15 M sodium chloride, pH 7.6, at 25 °C).

7.5.2 IMMUNOPRECIPITATION

Equal amounts of protein (200 μ g) from total protein extracts were incubated with 2 μ g of anti-p-Smad3, anti-act- β -catenin or anti-MUC1-CT antibodies and the IgG isotype control at 4°C during 1 hour. The immune complexes were precipitated with protein G on Sepharose 4B fast flow beads overnight at 4°C (**Figure 27**). After washing three times with NET buffer (20 mM Tris-HCl at pH 8.0, 100 mM NaCl, 1mM EDTA and 0.1% Igepal CA-630) to eliminate non-immunoprecipitated proteins, the bound materials were eluted from the immunoprecipitates in reducing 2X Laemmli buffer containing β -mercaptoethanol, at 100°C for 10 min. Immunoprecipitated protein complexes were assayed by western blotting and probed using anti-p-Smad3, anti-act- β -catenin or anti-MUC1-CT antibodies, as appropriate.

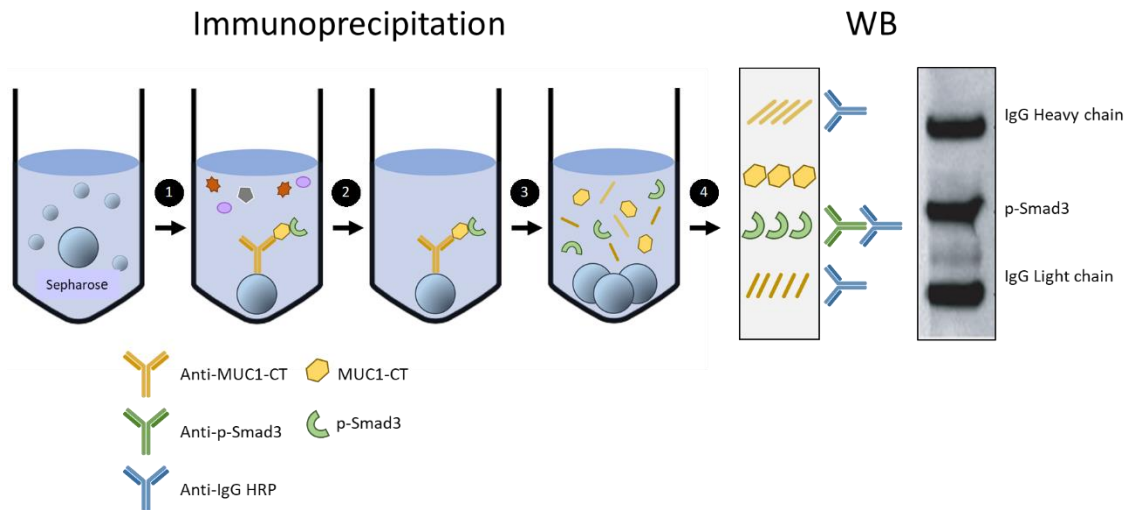


Figure 27. MUC1-cytoplasmic tail (CT) – phospho (p)-Smad3 complex immunoprecipitation schematic protocol. (1) Anti-MUC1-CT immune complexes (Anti-MUC1-CT + MUC1-CT + p-Smad3) precipitation with protein G on Sepharose 4B fast flow beads. (2) Washing steps to eliminate non-immunoprecipitated proteins. (3) Elution of the immunoprecipitated materials (anti-MUC1-CT heavy chain, anti-MUC1-CT light chain, MUC1-CT, p-Smad3) from the protein G sepharose beads. (4) Western Blotting using anti-p-Smad3 and the corresponding horseradish peroxidase secondary antibody (Anti-IgG HRP).

7.6 STATISTICAL ANALYSIS

Statistical analysis of results was carried out by parametric (animal and cellular studies) or non-parametric (human tissue studies) analysis as appropriate. $P < 0.05$ was considered statistically significant. Non-parametric tests were used to compare results from human samples of control subjects and IPF patients. In this case, data were displayed as mean \pm SD and between-group differences were analyzed by the Mann Whitney test. Results from animal and cellular *in vitro* mechanistic cell experiments were expressed as mean \pm SE of n experiments. In this case, statistical analysis was carried out by parametric analysis and multiple comparisons were analysed by one-way or two-way analysis of variance (ANOVA) followed by Bonferroni post hoc test.

RESULTS

CHAPTER 8

MUC1-CT EXPRESSION AND ACTIVATION IN IPF PATIENTS

MUC1-CT EXPRESSION AND ACTIVATION IN IPF PATIENTS

8.1 MUC1-CT EXPRESSION IS INCREASED AND ACTIVATED IN THE LUNG OF IPF PATIENTS

Both, control and IPF patients used in this study were prospectively recruited from the thoracic surgery of the University General Consortium Hospital and University and Polytechnic Hospital La Fe (Valencia, Spain) between 2014 and 2017. The clinical data of the patients are shown in **Table 5**. As it was expected, considering the older age and smoking as IPF potential risk factors, mean age of IPF patients was 60.8 and ~ 77% of IPF patients were smokers. In addition, % predicted FVC and % predicted DL_{CO} were low in spite of ~ 72% and ~ 27% of patients under NAC and pirfenidone treatments respectively.

MUC1-CT mRNA transcript level was measured in homogenized lung tissue from both human groups, and it was higher in that of IPF patients than in that of controls ($P = 0.0007$; **Figure 28A**). In the same way, for MUC1-CT protein expression, it was also higher in IPF patients than in control subjects ($P < 0.0001$; **Figure 28B**). The highly conserved CT in the C-terminal subunit of MUC1 modulates multiple intracellular signals through interactions largely regulated by phosphorylation of tyrosines, serines and threonines. In this context, protein expression of MUC1-CT phosphorylated forms at Thr⁴¹ (1224) (MUC1-P/T-1224) and Tyr⁴⁶ (1229) (MUC1-P/Y-1229) was also measured. Then, it was observed that these active MUC1-CT forms were upregulated in IPF lung tissue. However, the levels were almost undetectable in control lung tissue ($P < 0.0001$ and $P = 0.0012$ respectively; **Figure 28B**). Finally, regarding immunohistochemistry studies, control lung sections showed weak MUC1-CT expression that was localized mainly to ATII cells (**Figure 29**, blue arrows). By contrast, in IPF lung tissue, MUC1-CT was elevated in hyperplastic ATII cells (**Figure 29**, red arrows) and fibroblasts (**Figure 29**, black arrows). Phosphorylated MUC1-CT at Thr⁴¹ (1224) and Tyr⁴⁶ (1229) residues was not detected in healthy lung tissue, and showed similar pattern of distribution than MUC1-CT, including cytoplasmic and nuclei localization in fibrotic areas of the lung.

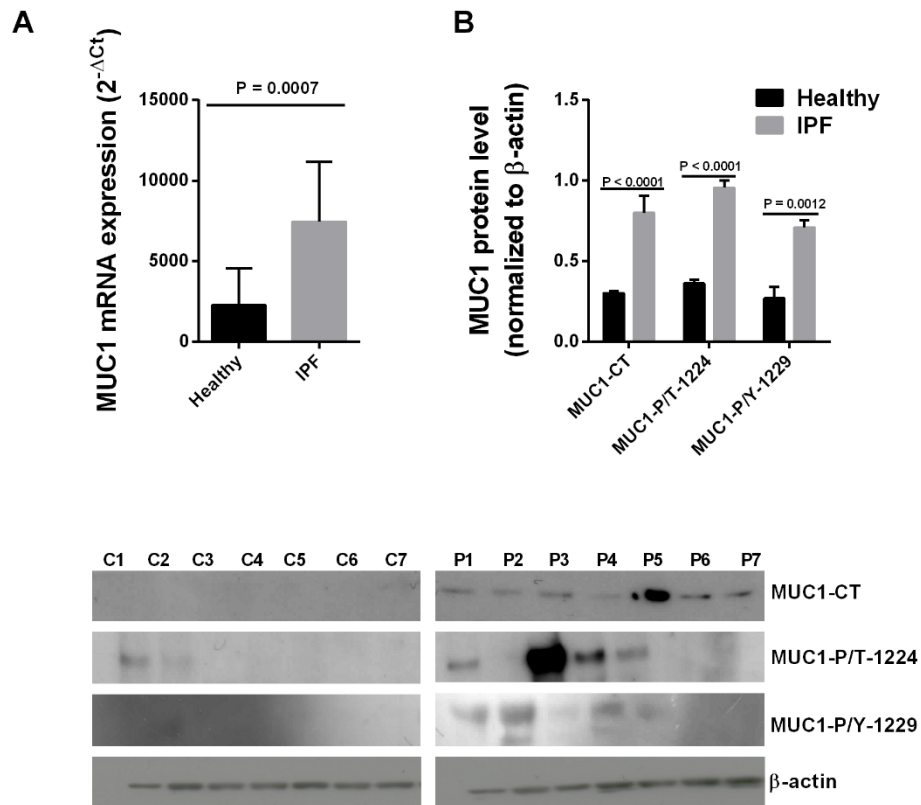


Figure 28. MUC1-cytoplasmic tail (MUC1-CT) and its phosphorylated forms MUC1-P/T-1224 and MUC1-P/Y-1229 are over-expressed in lung tissue from idiopathic pulmonary fibrosis (IPF) patients. Lung tissue from healthy controls ($n = 21$) and IPF patients ($n = 22$) was obtained. (A) Gene mRNA expression of MUC1 was analysed by real-time PCR. (B) Protein expression of MUC1-CT, MUC1-P/T-1224 and MUC1-P/Y-1229 were analysed by western blot. Data are expressed as the ratio to β -actin protein. Data are presented as mean \pm SD. Exact p values were obtained using the Mann–Whitney test.

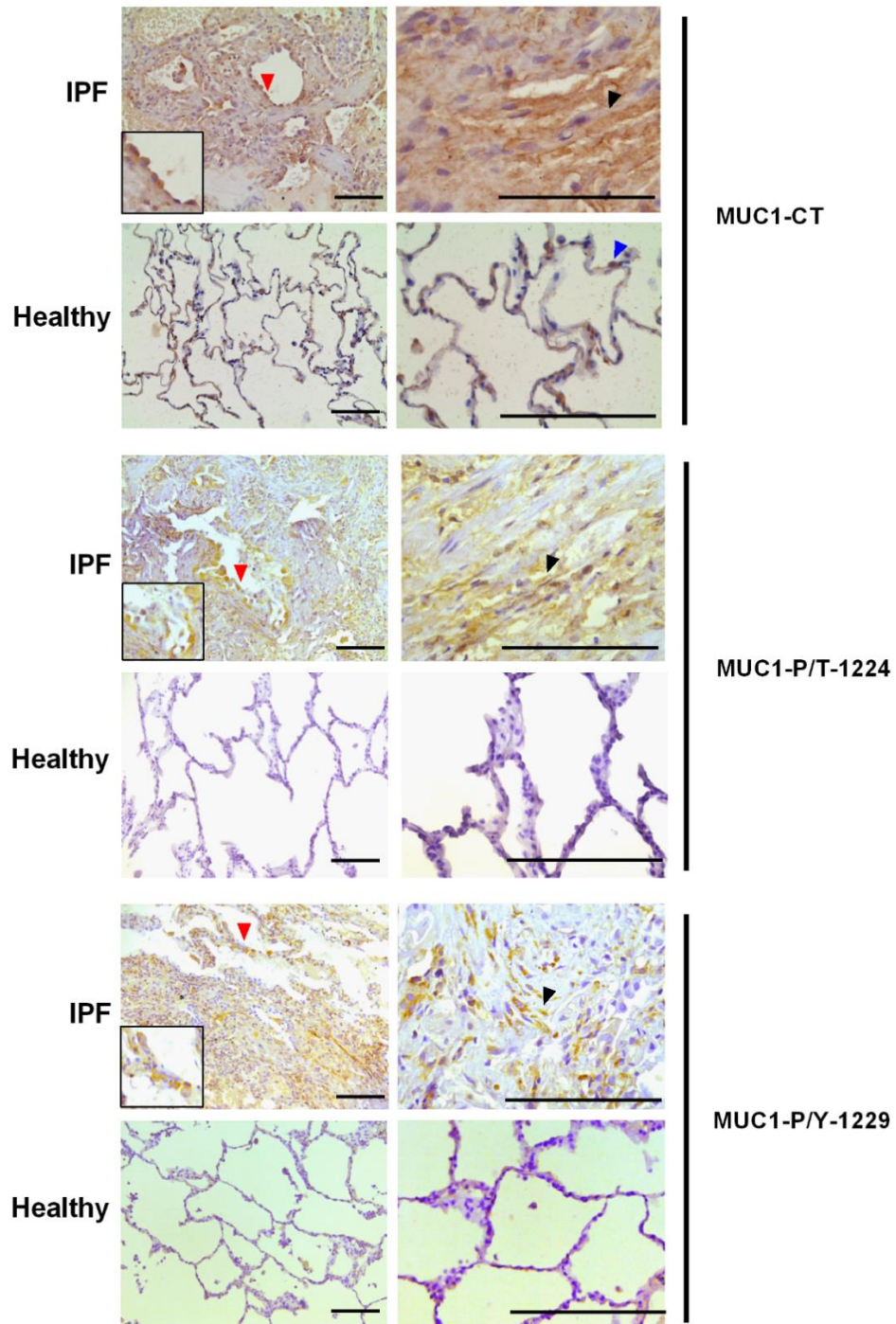


Figure 29. MUC1-cytoplasmic tail (MUC1-CT) and its phosphorylated forms MUC1-P/T-1224 and MUC1-P/Y-1229 are over-expressed and mainly localised to the hyperplastic alveolar type II (ATII) cells and fibroblasts in lung tissue from idiopathic pulmonary fibrosis (IPF) patients. Lung tissue sections from healthy controls and IPF patients were obtained. Immunohistochemistry of MUC1-CT, MUC1-P/T-1224 and MUC1-P/Y-1229. Scale bar: 100 μ m. Red arrows indicate hyperplastic ATII cells. Black arrows indicate lung fibroblasts. Blue arrows indicate normal ATII cells.

8.2 TGF β 1 PHOSPHORYLATES MUC1-CT

To elucidate the molecular agent responsible for MUC1-CT phosphorylation/bioactivation, primary human ATII cells, the A549 cell line, primary human lung fibroblasts and the MRC5 cell line were stimulated with TGF β 1, principal IPF profibrotic factor, during 40 minutes. After that, it was observed that TGF β 1 significantly increased the MUC1-CT phosphorylation at the Thr⁴¹ (1224) and Tyr⁴⁶ (1229) amino acid positions, which was inhibited by the anti-fibrotic pirfenidone (**Figures 30 and 31**). However, variations in MUC1-CT expression were almost undetectable due to the short time of TGF β 1 stimulation.

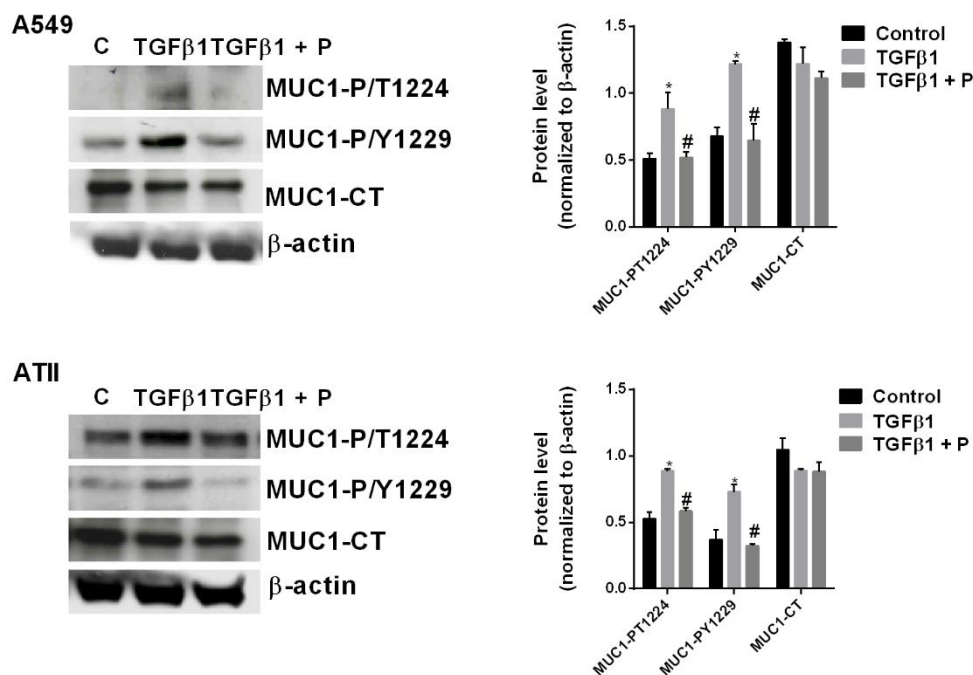


Figure 30. Transforming growth factor β 1 (TGF β 1) phosphorylates MUC1-cytoplasmic tail (MUC1-CT) at the 1224 threonine (MUC1-P/T1224) and 1229 tyrosine (MUC1-P/Y1229) amino acid positions in human alveolar type II (ATII) cells. Human primary ATII cells were isolated from the lungs of control subjects. A549 and primary ATII cells were stimulated for 40 minutes with 5 ng/ml TGF β 1 in the presence or absence of pirfenidone (P) 200 μ M. Data are expressed as the ratio to β -actin protein. The results are expressed as mean \pm SE of $n = 3$ independent experiments per condition. One-way ANOVA (for A549 cells) or two-way ANOVA (for primary ATII cells) followed by post-hoc bonferroni tests. * $P < 0.05$ vs. control; # $P < 0.05$ vs. TGF β 1.

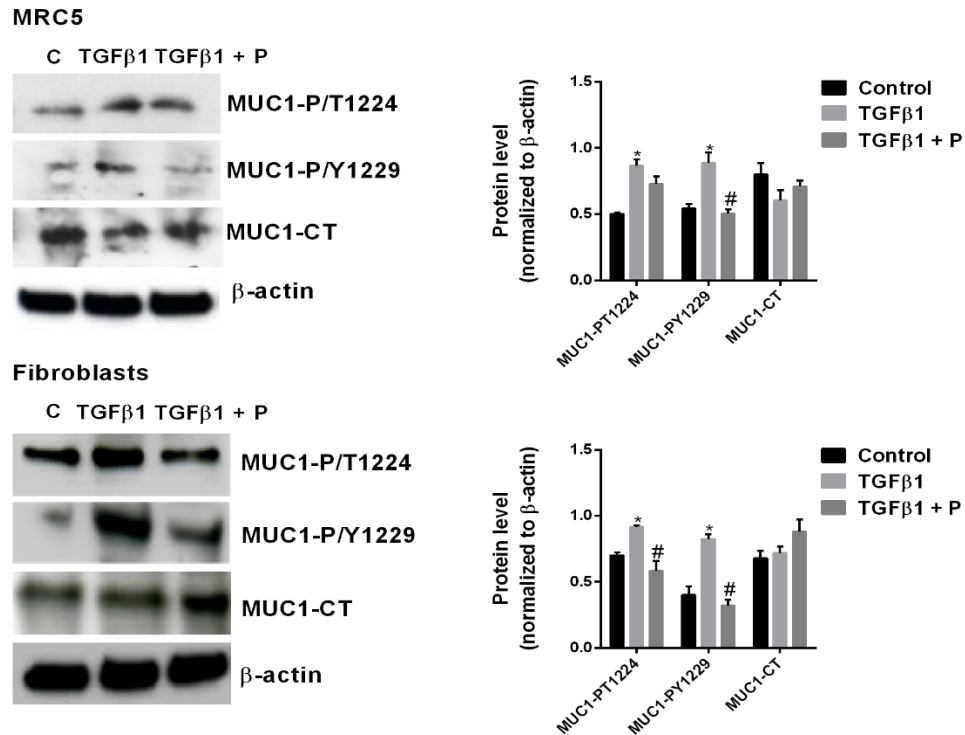


Figure 31. Transforming growth factor β1 (TGFβ1) phosphorylates MUC1-cytoplasmic tail (MUC1-CT) at the 1224 threonine (MUC1-P/T1224) and 1229 tyrosine (MUC1-P/Y1229) amino acid positions in lung fibroblasts. Human primary lung fibroblasts were isolated from the lungs of control subjects. MRC5 and primary lung fibroblasts were stimulated for 40 minutes with 5 ng/ml TGFβ1 in the presence or absence of pirfenidone (P) 200 μM. Data are expressed as the ratio to β-actin protein. The results are expressed as mean ± SE of $n = 3$ independent experiments per condition. One-way ANOVA (for MRC5 cells) or two-way ANOVA (for primary lung fibroblasts) followed by post-hoc bonferroni tests. * $P < 0.05$ vs. control; # $P < 0.05$ vs. TGFβ1.

CHAPTER 9

TGF β 1 AND MUC1-CT CROSSTALK IN IPF

TGF β 1 AND MUC1-CT CROSSTALK IN IPF

9.1 TGF β 1 COLLABORATES WITH MUC1-CT TO INDUCE ALVEOLAR TYPE II EPITHELIAL TO MESENCHYMAL AND FIBROBLAST TO MYOFIBROBLAST TRANSITIONS

In this work, EMT and FMT processes were simulated with TGF β 1 stimulation of primary human ATII, A549, primary lung fibroblasts and MRC5 cells. In this way, TGF β 1 promoted the ATII to mesenchymal transition and FMT increasing the protein and gene expression of the mesenchymal markers α -SMA and collagen type I in primary ATII cells and fibroblasts. However, pirfenidone had antifibrotic effect because it inhibited both types of mesenchymal transitions (**Figure 32**). In the same way, TGF β 1 also increased the protein and gene expression of the mesenchymal markers α -SMA, collagen type I, Slug and Snail in A549 and MRC5 cell lines. Furthermore, TGF β 1 decreased the expression of the epithelial marker E-cadherin in A549 cell line. Pirfenidone had also antifibrotic effect in these cells (**Figures 33** and **34**). Similarly, TGF β 1 stimulation of A549 and MRC5 cell lines also increased the canonical Smad3 phosphorylation pathway as well as the non-canonical Erk1/2 phosphorylation and the active- β -catenin pathway, all of them inhibited by pirfenidone (**Figures 33A** and **34A**). However, in A549 and MRC5 cells selectively transfected with siRNA-MUC1, TGF β 1 wasn't able to induce ATII-mesenchymal and fibroblast-mesenchymal transitions as well as β -catenin activation. By contrast, Smad3 and Erk1/2 phosphorylation pathways were elevated by TGF β 1 stimulation in spite of MUC1 silencing (**Figures 33** and **34**). MUC1 silencing was confirmed by RT-PCR (**Figure 33B** and **34B**).

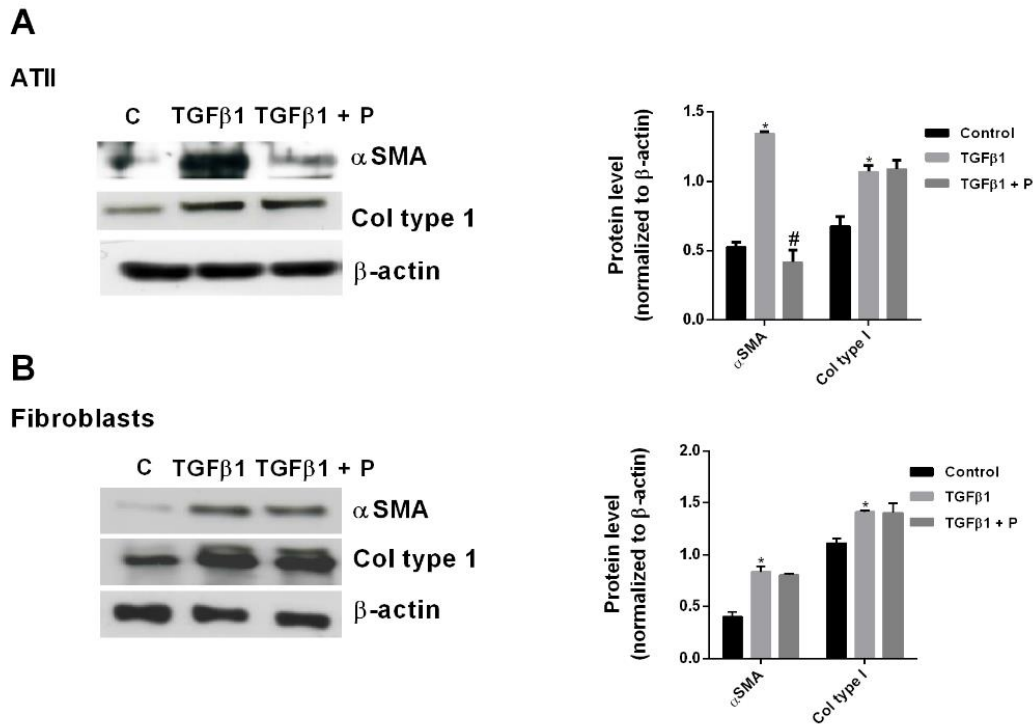


Figure 32. Transforming growth factor β 1 (TGF β 1) induces alveolar type II (ATII) to mesenchymal transition and fibroblast to myofibroblast transition. Primary ATII cells and lung fibroblasts were isolated from the lungs of control subjects. (A) ATII cells and (B) lung fibroblasts were stimulated 72h with TGF β 1 5 ng/ml in the presence or absence of pirfenidone (p) 200 μ M and the expression of mesenchymal α -smooth muscle actin (α -SMA) and collagen type I (Col type I) markers was measured using western blot and quantified by densitometry. Data are expressed as the ratio to β -actin protein. The results are expressed as mean \pm SE of $n = 3$ independent experiments per condition. Two-way ANOVA followed by post-hoc bonferroni tests. * $P < 0.05$ vs. control; # $P < 0.05$ vs. TGF β 1.

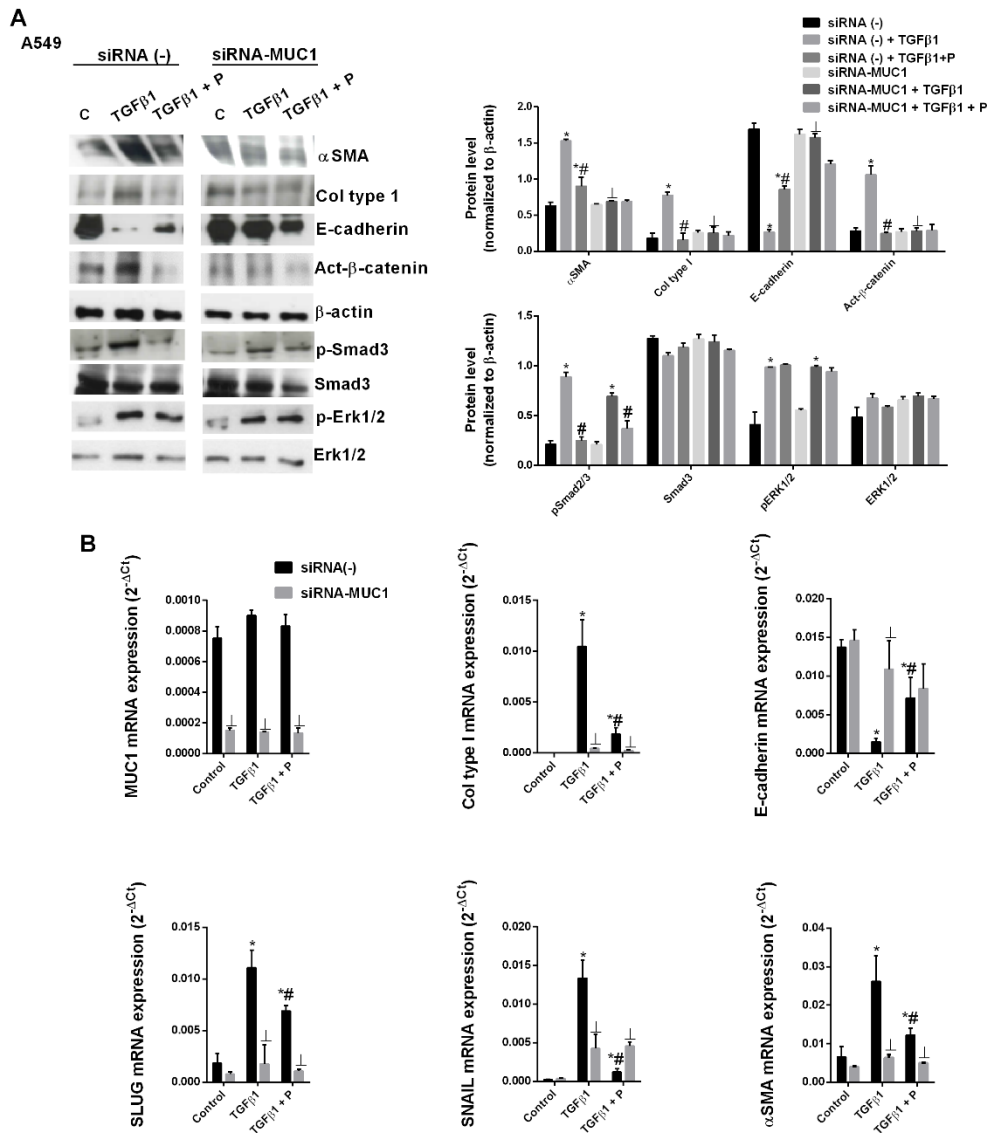


Figure 33. Transforming growth factor β 1 (TGF β 1) and MUC1 collaborate to induce alveolar type II (ATII) to mesenchymal transition. A549 cell line was transfected with control siRNA (-) or siRNA-MUC1 and stimulated for 48 h with TGF β 1 5 ng/ml in the presence or absence of pirfenidone (P) 200 μ M. Total protein and RNA from cell lysates were analyzed by (A) western blot and quantified by densitometry and by (B) Real time (RT)-PCR. α -smooth muscle actin (α -SMA), collagen type I (Col type I), E-cadherin, active (act)- β -catenin, phospho (p)-Smad3, Smad3, phospho (p)-extracellular signal-regulated kinase (Erk1/2) and Erk1/2 were measured using (A) western blot. MUC1, col type I, α -SMA, SLUG, SNAIL and E-cadherin were measured using (B) RT-PCR. Data are expressed as the ratio to β -actin for protein levels and $2^{-\Delta Ct}$ for mRNA levels. The results are expressed as mean \pm SE of $n = 3$ independent experiments per condition. One-way ANOVA followed by post-hoc bonferroni tests. * $P < 0.05$ vs. siRNA (-) control/siRNA-MUC1 control; # $P < 0.05$ vs. siRNA (-) TGF β 1/siRNA-MUC1 TGF β 1; $\perp P < 0.05$ vs. siRNA (-).

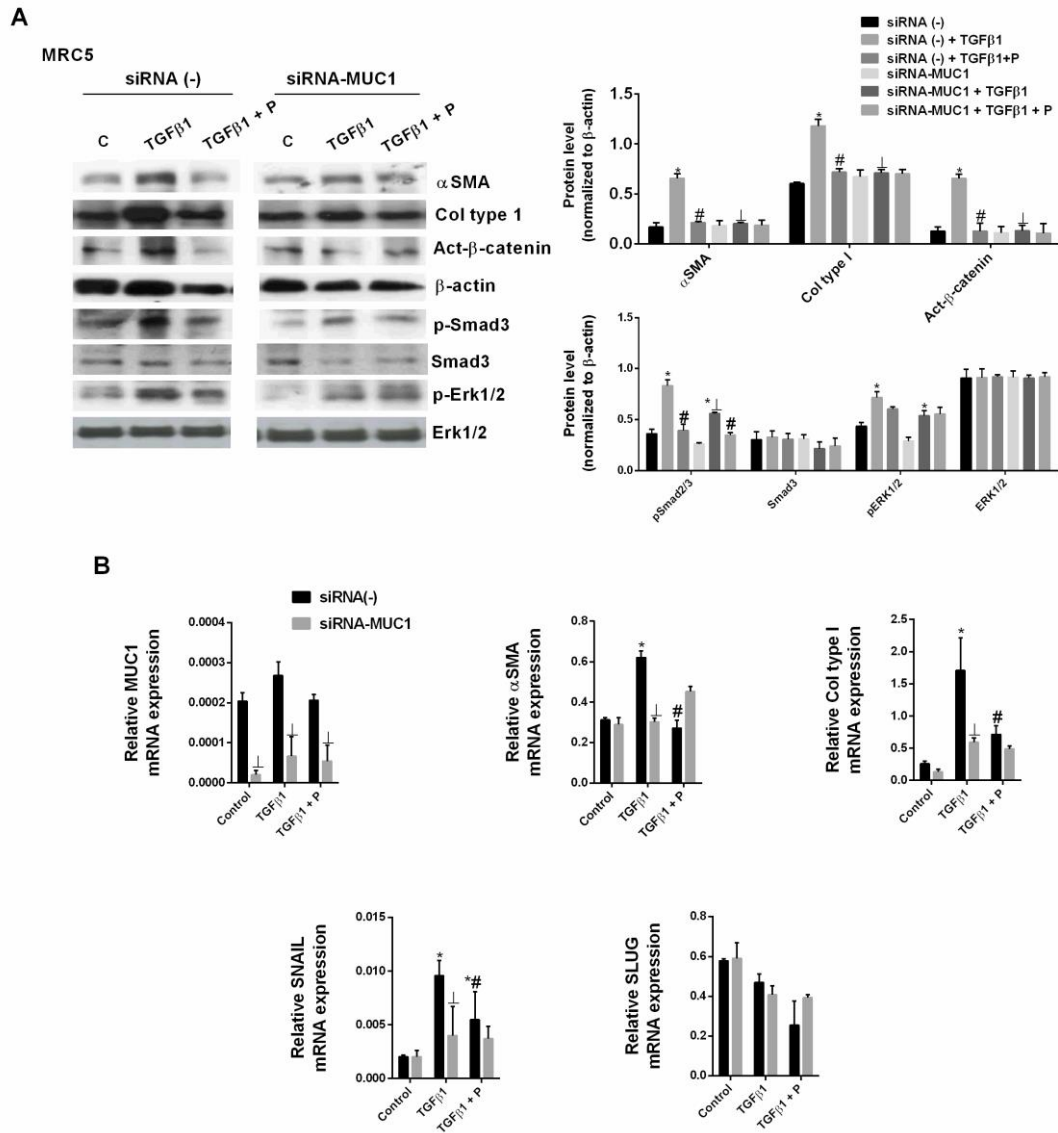


Figure 34. Transforming growth factor $\beta 1$ (TGF $\beta 1$) and MUC1 collaborate to induce fibroblast to myofibroblast transition. MRC5 cell line was transfected with control siRNA (-) or siRNA-MUC1 and stimulated for 48 h with TGF $\beta 1$ 5 ng/ml in the presence or absence of pirfenidone (P) 200 μ M. Total protein and RNA from cell lysates were analysed by (A) western blot and quantified by densitometry and by (B) Real time (RT) - PCR. (A) α - smooth muscle actin (α -SMA), collagen type I (Col type I), E-cadherin, active (act)- β -catenin, phospho (p)-Smad3, Smad3, phospho (p)-extracellular signal-regulated kinase (Erk1/2) and Erk1/2 were measured using (A) western blot. (B) MUC1, collagen type I, α -SMA, SLUG and SNAIL were measured using RT-PCR. Data are expressed as the ratio to β -actin protein and $2^{-\Delta Ct}$ for mRNA levels. The results are expressed as mean \pm SE of $n = 3$ independent experiments per condition. One-way ANOVA followed by post-hoc bonferroni tests. * $P < 0.05$ vs. siRNA (-)/siRNA-MUC1 control; # $P < 0.05$ vs. siRNA (-) TGF $\beta 1$ /siRNA-MUC1 TGF $\beta 1$; $\perp P < 0.05$ vs. siRNA (-).

9.2 TGF β 1 PATHWAY ACTIVATION PROMOTES A P-SMAD3/MUC1-CT/ACT- β -CATENIN NUCLEAR PROTEIN COMPLEX FORMATION AND SMAD BINDING ELEMENT ACTIVATION

To elucidate in detail the TGF β 1 and MUC1-CT collaboration to induce EMT and FMT, immunoprecipitation and immunofluorescence analysis of MUC1-CT with p-Smad3 were carried out. Likewise, as β -catenin has been shown to induce the transcription of IPF related genes in response to TGF β 1 and colocalizes with MUC1-CT in the nucleus to regulate genes involved in cell proliferation and differentiation, it also took part in these analysis.

First of all, it was observed that in primary human ATII cells and lung fibroblasts, TGF β 1 stimulus promoted the formation of protein complexes including p-Smad3/MUC1-CT and act- β -catenin/MUC1-CT as showed the immunoprecipitations (**Figure 35**) and confocal microscope images co-localization (**Figures 36 and 37**). More in detail, these co-localization images showed a nuclear co-localization of these complexes after TGF β 1 stimulation. However, it is highlighted that pirfenidone was able to inhibit the protein complexes formation in these conditions (**Figures 35 - 37**).

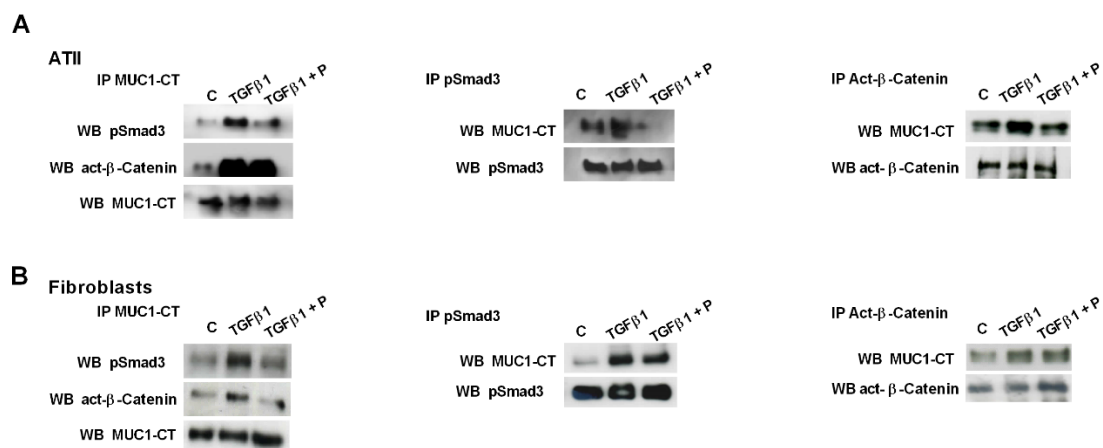


Figure 35. MUC1-cytoplasmic tail (MUC1-CT) co-immunoprecipitates with phospho (p)-Smad3 and active (act)- β -catenin in primary human alveolar epithelial type II (ATII) cells and lung fibroblasts stimulated with transforming growth factor β 1 (TGF β 1). Primary ATII cells and lung fibroblasts were isolated from the lungs of control subjects. (A) ATII cells and (B) fibroblasts were stimulated with TGF β 1 5 ng/ml for 1h in the presence or absence of pirfenidone (P) 200 μ M. Total protein was extracted and immunoprecipitated with MUC1-CT, p-Smad3 or act- β -catenin. Different western blots were proved against act- β -catenin, p-Smad3 and MUC1-CT, as appropriate.

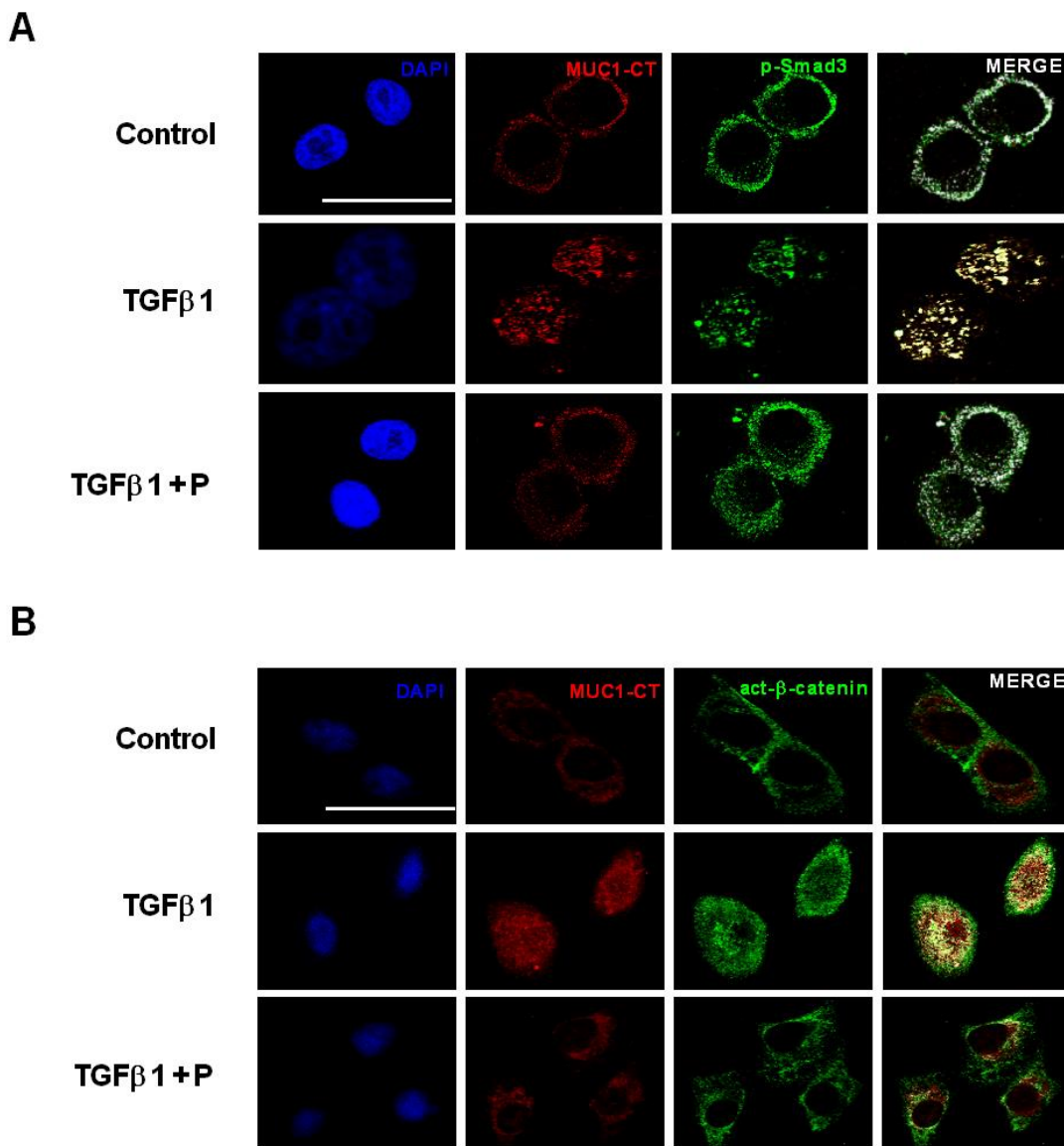


Figure 36. MUC1 - cytoplasmic tail (MUC1-CT) co-localizes with phospho (p)-Smad3 and active (act)-β-catenin in the nucleus of alveolar epithelial type II (AII) cells stimulated with transforming growth factor β1 (TGFβ1). Primary AII cells were isolated from the lungs of control subjects. AII cells were stimulated with TGFβ1 5 ng/ml for 1h in the presence or absence of pirfenidone (P) 200 μM. Co-localization was analysed using a confocal spectral microscope (Leica TCS SP2) that generated a bidimensional cytofluorogram that selected common localized points of both antibodies (white color). Scale bars: 10 μm. Confocal immunofluorescence microscope images showed the nuclear translocation and co-localization of MUC1-CT/p-Smad3 (A) and MUC1-CT/act-β-catenin (B), which was inhibited by pirfenidone.

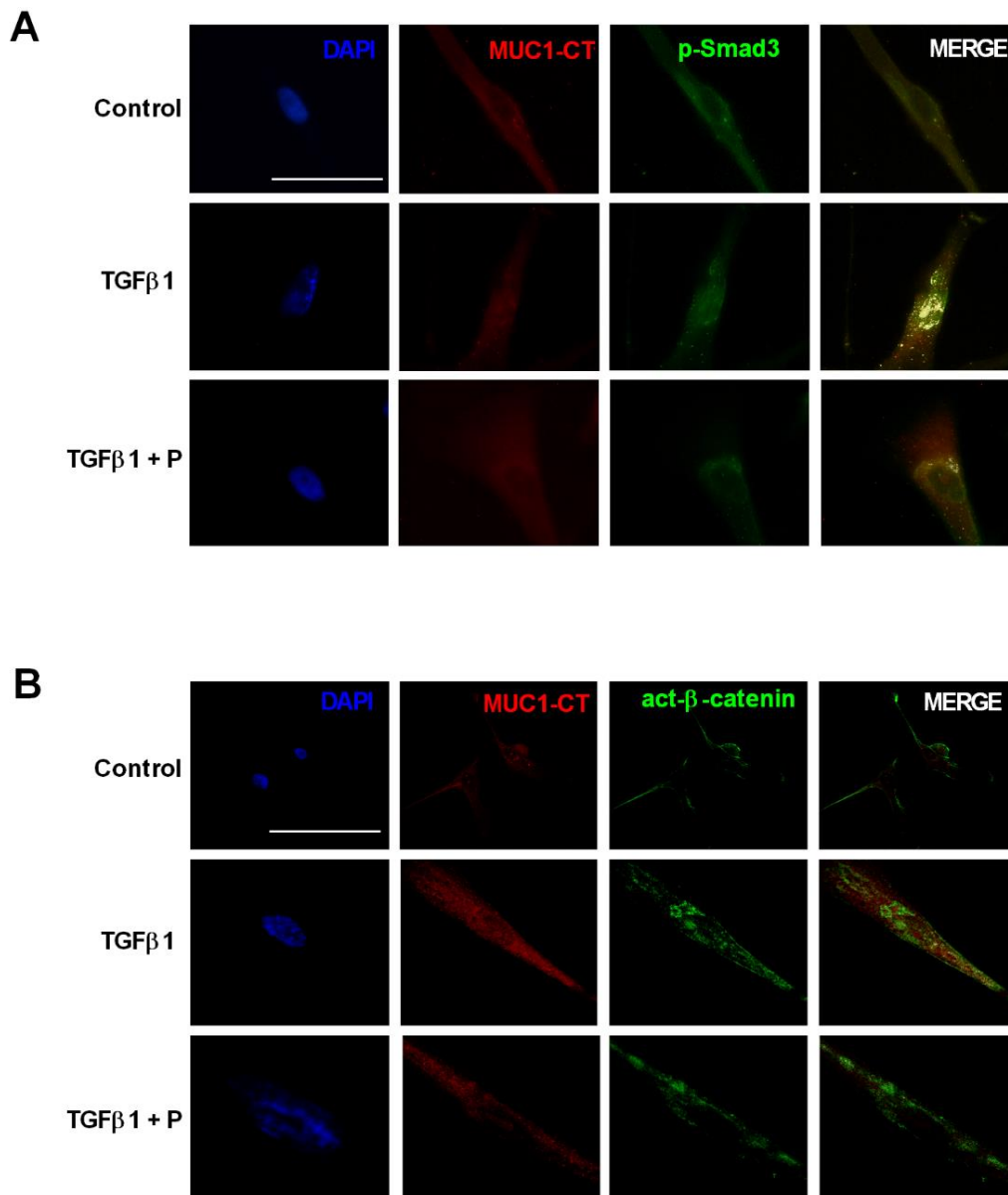
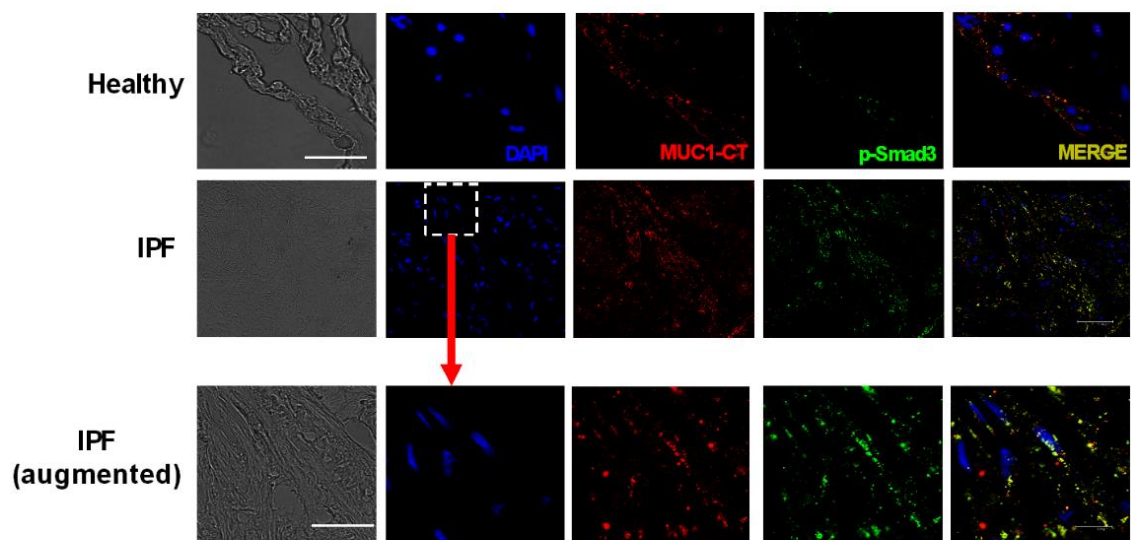


Figure 37. MUC1 - cytoplasmic tail (MUC1-CT) co-localizes with phospho (p)-Smad3 and active (act)-β-catenin in the nucleus of lung fibroblasts stimulated with transforming growth factor β1 (TGFβ1). Primary lung fibroblasts from idiopathic pulmonary fibrosis (IPF) patients were stimulated with TGFβ1 5 ng/ml for 1h in the presence or absence of pirfenidone (P) 200 μM. Co-localization was analysed using a confocal spectral microscope (Leica TCS SP2) that generated a bidimensional cytofluorogram that selected common localized points of both antibodies (white color). Scale bars: 10 μm. Con-focal immunofluorescence microscope images showed the nuclear translocation and co-localization of MUC1-CT/p-Smad3 and MUC1-CT/act-β-catenin, which was inhibited by pirfenidone.

Secondly, co-immunofluorescence studies were also performed in healthy and IPF human lung tissue. It was observed that MUC1-CT and act- β -catenin were localized on the cell membrane of ATII cells in lung sections of healthy patients whilst p-Smad3 was absent, as indicated fluorescence images (**Figure 38**). However, the expression of MUC1-CT and p-Smad3 was increased and co-localized in cell cytoplasm and nucleus of lung fibrotic areas of IPF patients. Similar pattern of distribution was also observed for MUC1-CT and act- β -catenin co-localization in lung sections of IPF patients (**Figure 38**).

A



B

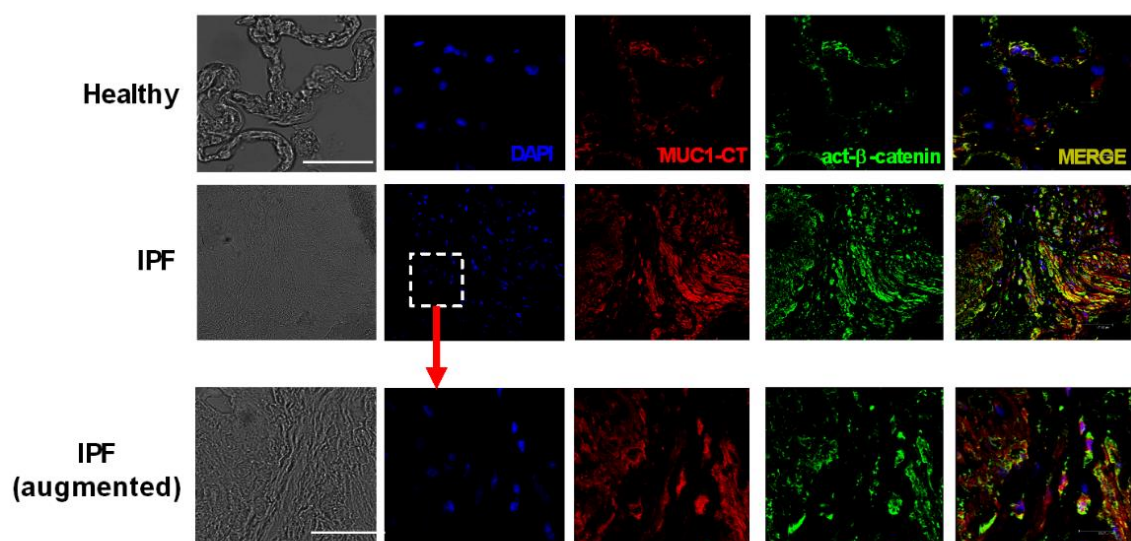


Figure 38. MUC1- cytoplasmic tail (MUC1-CT) co-localizes with phospho (p)-Smad3 and active (act)- β -catenin in lung tissue from idiopathic pulmonary fibrosis (IPF) patients. Confocal immunofluorescence microscope co-localization images of lung sections from healthy and IPF patients probed against MUC1-CT/p-Smad3 and MUC1-CT/act- β -catenin combinations. Co-localization was analysed using a confocal spectral microscope (Leica TCS SP2) that generated a bidimensional cytofluorogram representing common localized points of both antibodies (orange colour). Scale bars: 10 μ m. Confocal immunofluorescence microscope images showed the cytoplasmic and nuclear co-localization of MUC1-CT/p-Smad3 (A) and MUC1-CT/act- β -catenin (B) in IPF patients.

Finally, A549 cells transiently transfected with siRNA-MUC1 were stimulated with TGF β 1 and the SBE activation was evaluated. As it was expected, TGF β 1 stimulation of A549 cells induced the Smad-dependent canonical pathway activation and consequently the SBE activation. However, this activation was inhibited by pirfenidone and prevented in cells transiently transfected with siRNA-MUC1 (**Figure 39**).

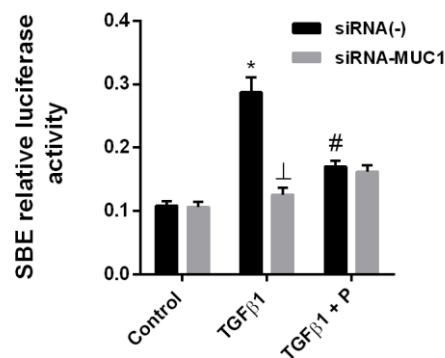


Figure 39. MUC1 enhances the Smad binding element (SBE) activation induced by transforming growth factor β 1 (TGF β 1). A549 transiently transfected with siRNA-MUC1 were stimulated with 10 ng/ml of TGF β 1 during 18 hours. TGF β 1 induced the SBE activation that was prevented in siRNA-MUC1 transiently transfected cells and inhibited by pirfenidone (P). Results are expressed as mean \pm SE of $n = 3$ independent experiments run in triplicate. One-way ANOVA was followed by the post hoc Bonferroni test. * $P < 0.05$ vs. control; # $P < 0.05$ vs. TGF β 1; $\perp P < 0.05$ vs. siRNA(-) + TGF β 1.

9.3 MUC1-CT AND β -CATENIN ACTIVATION ARE DEPENDENT OF SMAD3 PHOSPHORYLATION

Primary ATII and A549 cells, as well as, primary lung and MRC5 fibroblasts were incubated with the inhibitor of Smad3 phosphorylation SIS3. It significantly reduced the TGF β 1-induced MUC1-CT phosphorylation at Thr⁴¹ (1224) and Tyr⁴⁶ (1229) residues, suggesting a role of Smad3 activation (phosphorylation) on MUC1-CT phosphorylation, that is to say, co-phosphorylation events as events downstream of Smad3 phosphorylation (**Figure 40** and **41**). As expected, SIS3 also inhibited the Smad3 phosphorylation and the increase of active- β -catenin expression induced by TGF β 1 action (**Figure 40** and **41**). Variations in MUC1-CT expression were almost undetectable due to the short time of TGF β 1 stimulation.

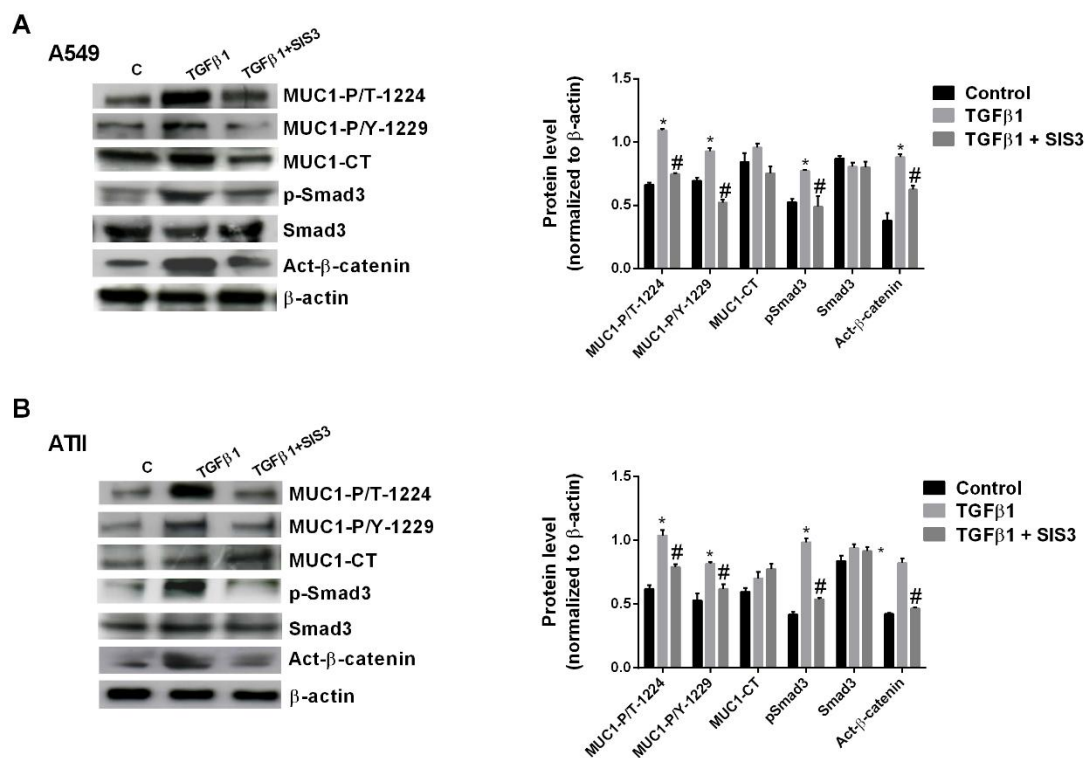


Figure 40. Phosphorylation of Smad3 activates MUC1-cytoplasmic tail (MUC1-CT) and β -catenin in alveolar type II epithelial cells (ATII). ATII cells were isolated from the lungs of control subjects. Cells were incubated for 1 h with SIS3 (3 μ M), and then stimulated with transforming growth factor β 1 (TGF β 1) 5 ng/ml for 40 minutes. Protein expression of MUC1-CT, MUC1-P/T-1224, MUC1-P/Y-1229, phospho (p)-Smad3, Smad3 and active (act)- β -catenin were analysed with the internal control β -actin by western blot and quantified by densitometry. Results are expressed as mean \pm SE of $n = 3$ independent experiments. Two-way ANOVA was followed by the post hoc bonferroni test. * $P < 0.05$ vs. control; # $P < 0.05$ vs. TGF β 1.

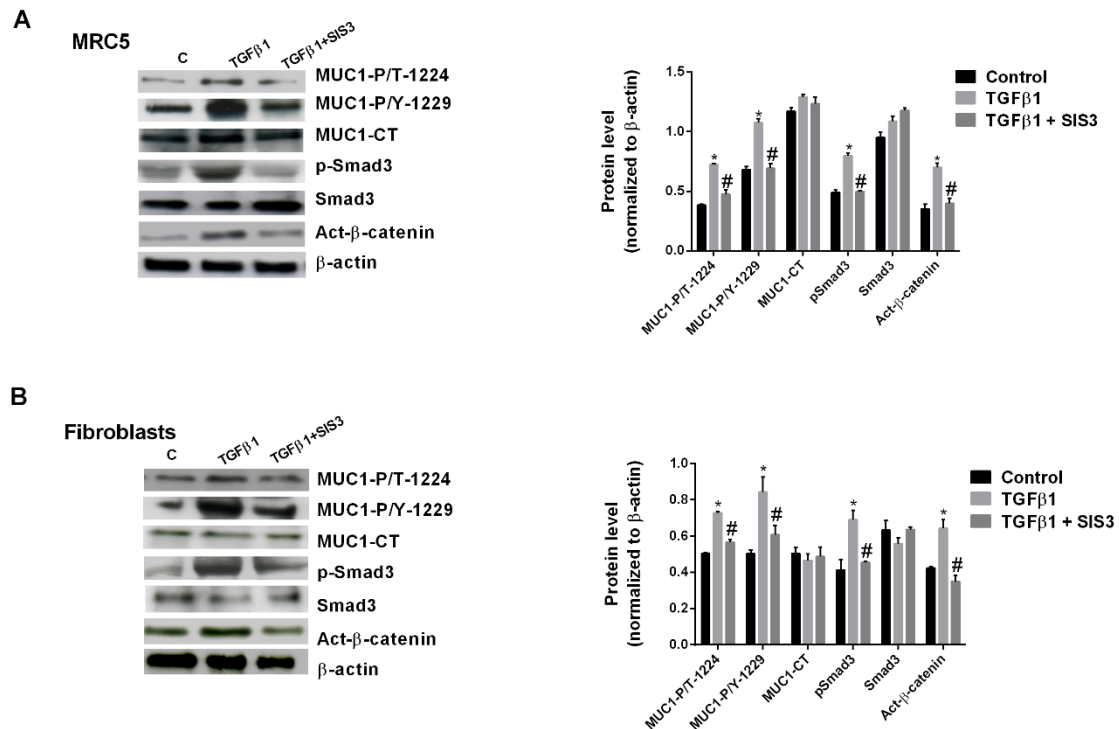


Figure 41. Phosphorylation of Smad3 activates MUC1-cytoplasmic tail (MUC1-CT) and β-catenin in lung fibroblasts. Lung fibroblasts were isolated from the lungs of IPF patients. Cells were incubated for 1 h with SIS3 (3 μM), and then stimulated with transforming growth factor β1 (TGFβ1) 5 ng/ml for 40 minutes. Protein expression of MUC1-CT, MUC1-P/T-1224, MUC1-P/Y-1229, phospho (p)-Smad3, Smad3 and active (act)-β-catenin were analysed with the internal control β-actin by western blot and quantified by densitometry. Results are expressed as mean ± SE of n = 3 independent experiments. Two-way ANOVA was followed by the post hoc bonferroni test. *P < 0.05 vs. control; #P < 0.05 vs. TGFβ1.

9.4 MUC1 MEDIATES CELL SENESCENCE AND PROLIFERATION INDUCED BY TGFβ1 IN ATII CELLS AND LUNG FIBROBLASTS

Cellular senescence and proliferation are two key processes in IPF disease. TGFβ1 seems to promote cell senescence in ATII cells and lung fibroblasts, as well as, to induce cell proliferation in lung fibroblasts. These actions depend on the cell phenotype and cell culture conditions [221-223]. In this work, we observed a critical point of IPF primary lung fibroblast phenotype change after *in vitro* TGFβ1 stimulation. Firstly, TGFβ1 increased cell proliferation during 48h (**Figure 42A**). However, at this point, lung fibroblasts increased β-galactosidase activity thus probably changing the active proliferative to senescent fibroblast phenotype. Both

phenotypes were inhibited by pirfenidone and attenuated in siRNA-MUC1 transfected cells (Figure 42A-C). In other experiments, we observed that TGF β 1 stimulation during 72 hours increased the β -galactosidase activity in ATII cells that was inhibited by pirfenidone and attenuated in siRNA-MUC1 transfected cells (Figure 43). Therefore, it was highlighted the importance of TGF β 1 and MUC1 collaboration in the induction of two key IPF cellular processes.

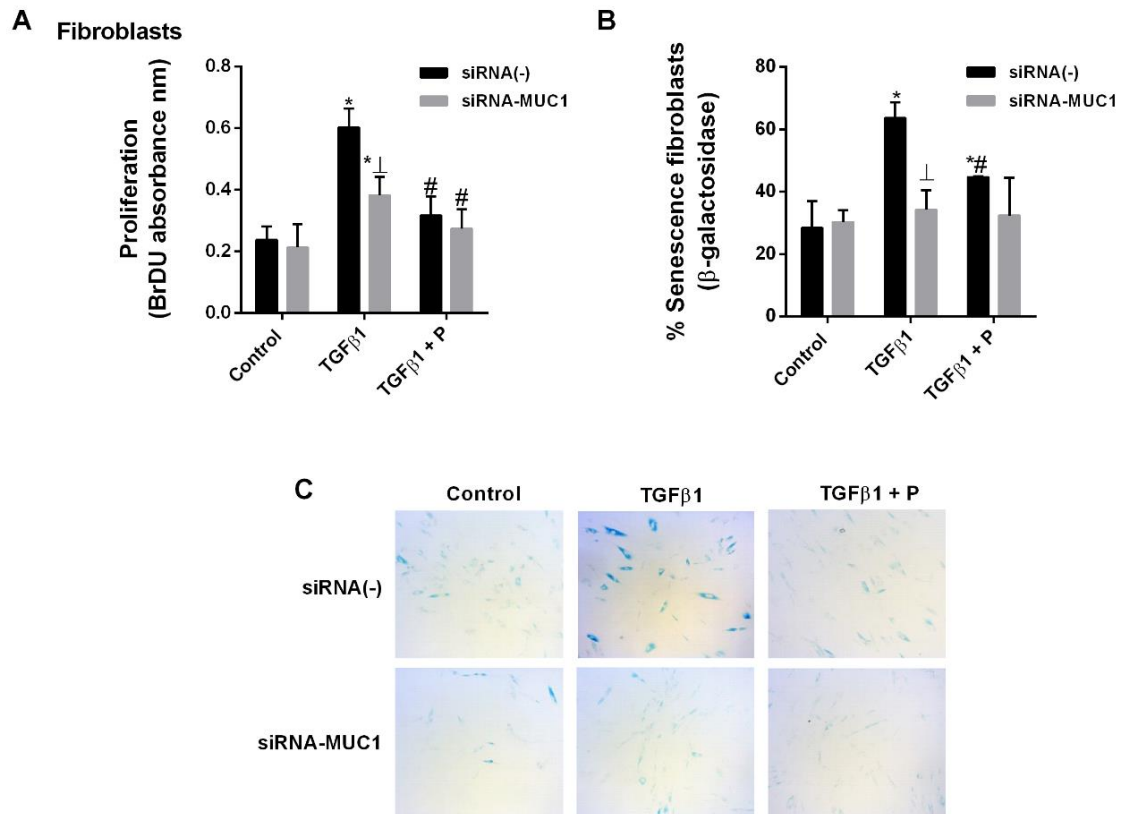


Figure 42. MUC1 mediates transforming growth factor β 1 (TGF β 1) - induced lung fibroblast proliferation and senescence. Lung fibroblasts were isolated from the lungs of IPF patients. (A) Fibroblast proliferation during 48 h was evaluated by the Bromodeoxyuridine (BrdU) assay. Pirfenidone (P) (200 μ M) was added 30 min before 10% foetal bovine serum (FBS) + 10 ng/ml TGF β 1 incubation during 24h in siRNA-MUC1 or siRNA(-) primary human lung fibroblasts. (C) siRNA-MUC1 or siRNA(-) primary human lung fibroblasts were stained, after 72h of 10ng/ml TGF β 1 stimulation, for senescence-associated β -galactosidase activity and microscopic (magnification of 40 \times) images were taken. (B) Percentage of cells expressing β -galactosidase (blue-stained cells) from the total number of siRNA-MUC1 or siRNA(-) primary human lung fibroblasts. Results are expressed as mean \pm SE of n = 3 independent experiments. Two-way ANOVA was followed by the post hoc Bonferroni test. *P < 0.05 vs. siRNA (-)/siRNA-MUC1 control; #P < 0.05 vs. siRNA (-)/siRNA-MUC1 + TGF β 1; \perp P < 0.05 vs. siRNA(-) + TGF β 1.

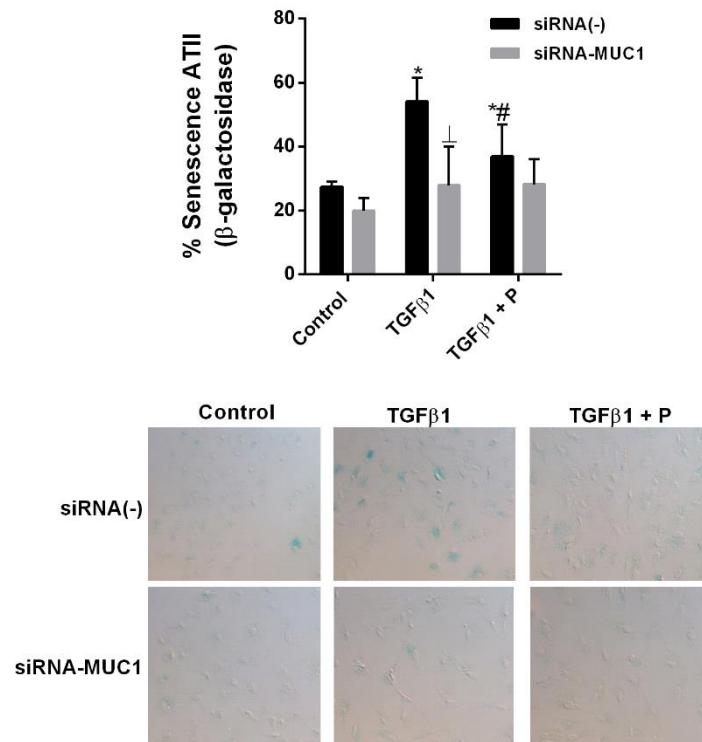


Figure 43. MUC1 mediates transforming growth factor β 1 (TGF β 1) - induced senescence of epithelial alveolar type II (ATII) cells. ATII cells were isolated from the lungs of control subjects. siRNA-MUC1 or siRNA(-) primary human ATII cells were stained, after 72h of 10ng/ml TGF β 1 stimulation, for senescence-associated β -galactosidase activity and microscopic (magnification of 40 \times) images were taken. Percentage of cells expressing β -galactosidase (blue-stained cells) from the total number of siRNA-MUC1 or siRNA(-) primary human ATII cells was represented. Results are expressed as mean \pm SE of $n = 3$ independent experiments. Two-way ANOVA was followed by the post hoc Bonferroni test. * $P < 0.05$ vs. siRNA (-)/siRNA-MUC1 control; # $P < 0.05$ vs. siRNA (-)/siRNA-MUC1 + TGF β 1; $\perp P < 0.05$ vs. siRNA(-) + TGF β 1.

9.5 GALECTIN 3 ACTIVATES MUC1-CT VIA DEPENDENT AND INDEPENDENTLY OF THE TGF RECEPTORS

Galectin 3 is a recognized pro-fibrotic factor in IPF [144] and has been proved that activates MUC1 downstream signals [207]. Furthermore, galectin 3 binds TGF receptors promoting signalling to Smads and activating β -catenin to form concomitant nuclear accumulation of Smads and β -catenin leading to transcription of mesenchymal genes [144]. In the present work, to elucidate if there is any relationship between MUC1-CT phosphorylation and galectin 3 action in our IPF *in vitro* model, and if this relationship is dependent or

independent of the TGF β 1 pathway promotion by galectin 3, A549 cell line was transiently transfected to silence TGF β 1 receptor (T β RI and T β RII) and stimulated with TGF β 1 and/or galectin 3.

Firstly, it was observed that in siRNA(-) control cells, as it was expected, TGF β 1 stimulation increased the Smad3 phosphorylation, the active- β -catenin, and the MUC1-CT phosphorylations at Thr⁴¹ (1224) and Tyr⁴⁶ (1229) residues. These TGF β 1 actions were significantly potentiated by the addition of galectin 3 (**Figure 44**). However, galectin 3 stimulus in absence of TGF β 1, also increased p-Smad3, MUC1-CT P/T 1224 and P/Y 1229 and the active- β -catenin with similar effect than TGF β 1 stimulus. By contrast, in cells transiently transfected with siRNA-T β RI/II, as it was expected, the effects of TGF β 1 were suppressed. The galectin 3 or the combination of TGF β 1 + galectin 3 stimulus in siRNA-T β RI/II cells did not modify the Smad3 phosphorylation, but increased in a similar range the expression of the active- β -catenin and MUC1-CT P/T 1224 and P/Y 1229 phosphorylations. Nevertheless, in all the cases, protein levels after TGF β 1 + galectin 3 stimulation were higher in non siRNA-T β RI/II transfected cells than in siRNA-T β RI/II transfected cells because of the dual effect of TGF β 1 and galectin 3 (**Figure 44**). All these findings suggest that galectin 3 can stimulate MUC1-CT *via* dependent and independently of the activation of TGF β receptors in an IPF ATII cell model.

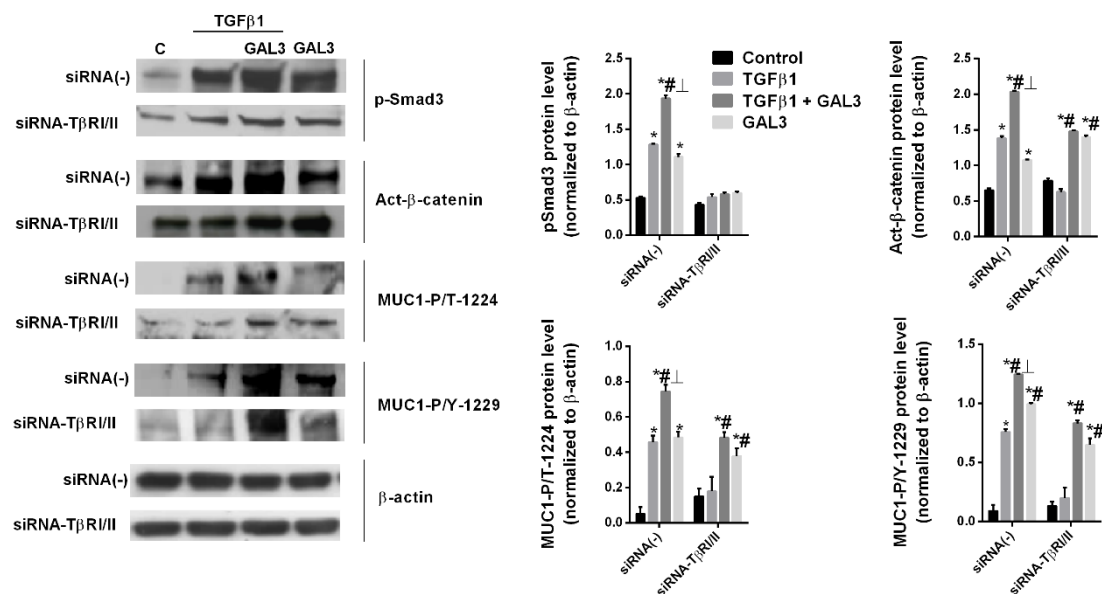


Figure 44. Galectin 3 activates MUC1-cytoplasmic tail (CT) via dependent and independently of transforming growth factor β 1 (TGF β 1) pathway. A549 cells were transfected with siRNA(-) or siRNA-T β RI/II, and then incubated for 1 h with 5 μ g/ml galectin 3 and/or 10 ng/ml TGF β 1. Protein expression of p-Smad3, active(act)- β -catenin, MUC1-P/T-1224 and MUC1-P/Y-1229 was analysed with the internal control β -actin by western blot and quantified by densitometry.

Results are expressed as mean \pm SE of $n = 3$ independent experiments. One-way ANOVA was followed by the post hoc Bonferroni test. * $P < 0.05$ vs. control; # $P < 0.05$ vs. TGF β 1; $\perp P < 0.05$ vs. siRNA-T β RI/II.

9.6 MUC1-CT CQC MOTIF INHIBITION REDUCES TGF1-INDUCED MUC1-CT NUCLEAR TRANSLOCATION, ALVEOLAR TYPE II TO MESENCHYMAL TRANSITION, FIBROBLAST TO MYOFIBROBLAST TRANSITION, ALVEOLAR TYPE II AND FIBROBLAST SENEESCENCE AND FIBROBLAST PROLIFERATION

In the same way than transient silencing of MUC1, GO-201, an inhibitor of the CQC motif of MUC1-CT that blocks the formation of MUC1-C oligomers in cells and attenuates targeting of MUC1-C to the nucleus, inhibited the effect of TGF β 1 on the increase of the expression of the mesenchymal markers α -SMA and vimentin, as well as the decrease of E-cadherin expression in ATII cells (**Figure 45A – 45C**). Cell senescence p21 and p16 markers were also elevated after TGF β 1 stimulation and inhibited by GO-201 in ATII cells (**Figures 46A and 46B**). In lung fibroblasts from IPF patients, TGF β 1 - increased gene expression of the myofibroblast marker collagen type I (**Figure 45D**), as well as, the senescence markers p21 and p16 (**Figure 46C and 46D**) were also inhibited by GO-201. Moreover, GO-201 also inhibited fibroblast proliferation induced by TGF β 1 after 48h of stimulation (**Figure 46E**). Therefore, these findings confirm the essential role of MUC1-CT nuclear translocation in the development of IPF cellular processes.

Figure 47 shows MUC1-CT nuclear localization in the cell line A549, used as ATII cell model in this work, after 1h of TGF β 1 stimulation. It is also shown the effective inhibition of this nuclear translocation by GO-201 action.

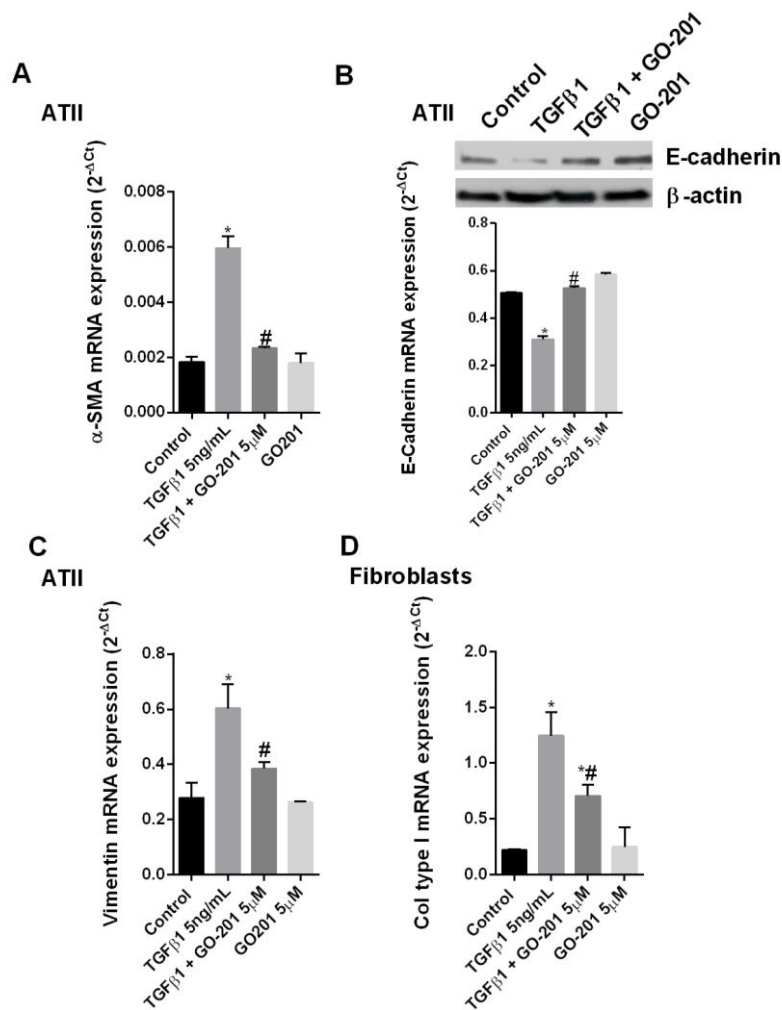


Figure 45. Inhibition of MUC1-C nuclear translocation suppressed alveolar type II (ATII) to mesenchymal and fibroblast to myfibroblast transitions. Human ATII primary cells were isolated from the lungs of control subjects, and primary human lung fibroblasts were isolated from the lungs of idiopathic pulmonary fibrosis (IPF) patients. Human ATII primary cells (A,B,C) and primary human lung fibroblasts (D) were stimulated for 48 h with TGF β 1 5 ng/mL in the presence or absence of GO-201 5 μ M. Total protein and RNA from cell lysates were analyzed by Real time (RT) PCR and western blot. (A) Mesenchymal α -smooth muscle actin (α -SMA), (C) collagen type I (Col type I) and (D) vimentin were measured using RT-PCR and (B) epithelial E-cadherin was measured using western blot and quantified by densitometry. Data are expressed as the ratio to β -actin protein. Results are expressed as mean \pm SE of $n = 3$ independent experiments. Two-way ANOVA was followed by the post hoc Bonferroni test. * $P < 0.05$ vs. control; # $P < 0.05$ vs. TGF β 1.

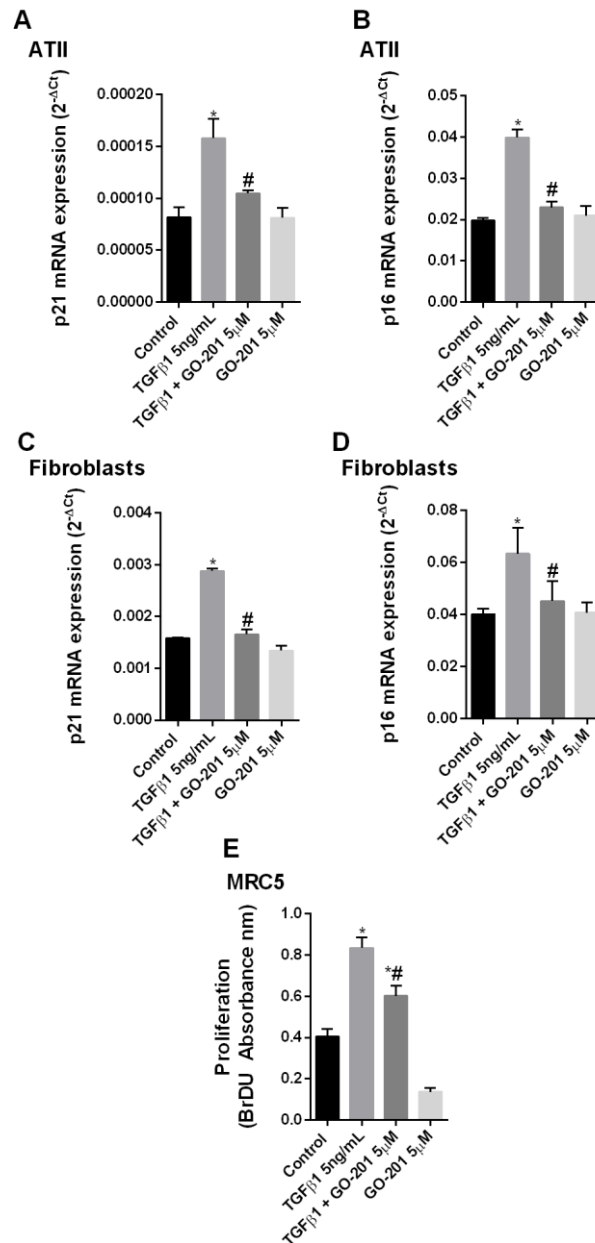


Figure 46. Inhibition of MUC1-C nuclear translocation suppressed alveolar type II (ATII) senescence and fibroblast proliferation and senescence. Human ATII primary cells were isolated from the lungs of control subjects, and primary human lung fibroblasts were isolated from the lungs of idiopathic pulmonary fibrosis (IPF) patients. Human ATII primary cells (A, B) and primary human lung fibroblasts (C, D) were stimulated for 72 h with TGF β 1 5 ng/mL in the presence or absence of GO-201 5 μ M. Senescence p21 (A, C) and p16 (B, D) markers were measured using Real time PCR. (E) MRC5 proliferation during 48 h was evaluated by the BrdU assay. 5 μ M GO-201 was added 30 min before 10% foetal bovine serum and 2 ng/ml TGF β 1 stimulation during 24 h. Results are expressed as mean \pm SE of $n = 3$ independent experiments. Two-way ANOVA was followed by the post hoc Bonferroni test. * $P < 0.05$ vs. control; # $P < 0.05$ vs. TGF β 1.

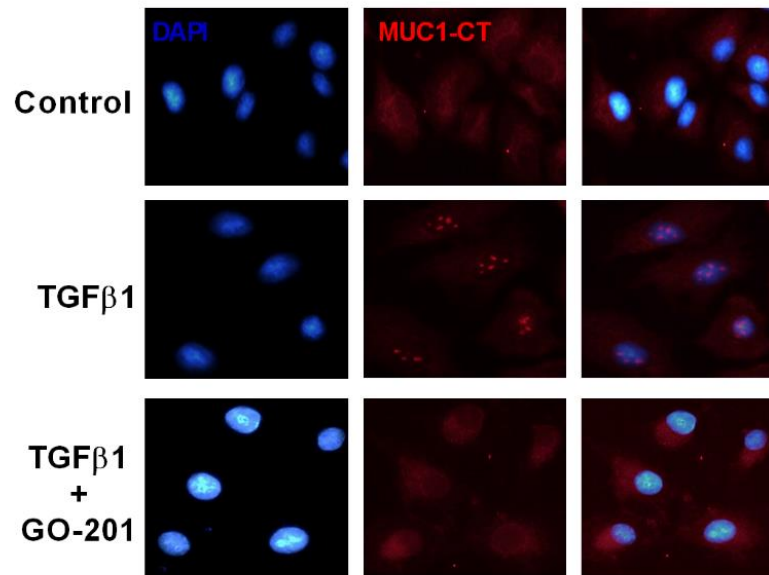


Figure 47. GO-201 blocks MUC1-cytoplasmic tail (MUC1-CT) nuclear translocation induced by transforming growth factor β 1 (TGF β 1) in an alveolar type II (AII) cell model. A549 cells were fixed, permeabilized, and used for MUC1-CT (red) immunostaining after stimulation for 1 h with TGF β 1 5 ng/ml in the presence or absence of 5 μ M GO-201. DAPI, blue nuclei. Scale bars: 10 μ m.

CHAPTER 10

MUC1-KO MOUSE MODEL OF BLEOMYCIN - INDUCED PULMONARY FIBROSIS

MUC1-KO MOUSE MODEL OF BLEOMYCIN-INDUCED PULMONARY FIBROSIS

10.1 SURVIVAL AND LUNG FUNCTION ARE IMPROVED IN A MUC1-KO BLEOMYCIN-INDUCED PULMONARY FIBROSIS MOUSE MODEL

Pulmonary fibrosis was induced by 1.5U/kg of IT bleomycin administration in WT C57BL/6 mice and MUC1-KO C57BL/6 mice. As consequence of the pulmonary fibrosis induced, WT C57BL/6 mice mortality was increased by ~60% after 14 days of experimental procedure. However, mortality was reduced in MUC1-KO mice to ~30%. As it was expected, both control groups had 100% survival (**Figure 48A**).

Lung function was assessed by the difference in Penh value measured by whole-body plethysmography at day 0 and day 14. WT bleomycin treated animals showed an impaired respiratory function, represented by the increase of Penh values after 14 days of experimental procedure. By contrast, this increase was significantly lower in the MUC1-KO bleomycin group (**Figure 48B**).

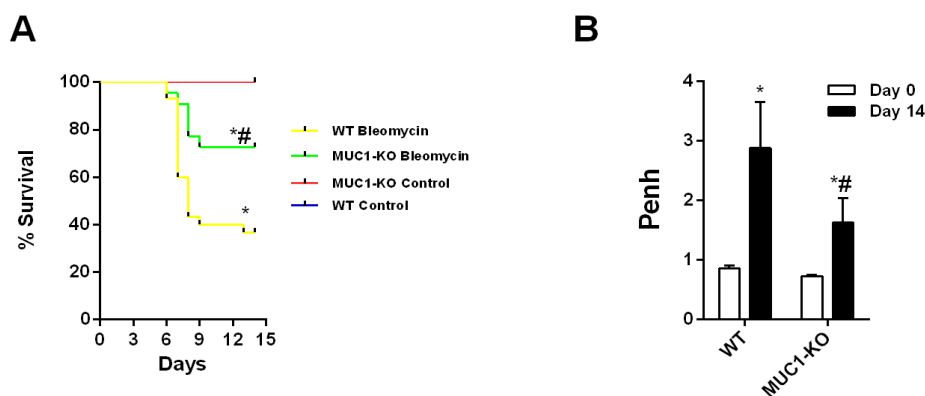


Figure 48. Survival and lung function are improved in a MUC1-Knockout (KO) bleomycin-induced pulmonary fibrosis mouse model. Wild type (WT) C57BL/6 mice and MUC1-KO C57BL/6 mice received a single intratracheal dose of bleomycin (1.5 U/kg) on day 1 ($n = 10$). (A) Kaplan-Meier survival analysis from each group for 14 days. * $P < 0.05$ vs. WT/ MUC1-KO control; # $P < 0.05$ vs. WT Bleomycin. (B) Pulmonary functions were evaluated by the difference in enhanced respiratory pause (Penh) value at day 0 and day 14 after bleomycin administration. Whole-body plethysmography was employed and Penh was used as a non-invasive index of airway dysfunction. * $P < 0.05$ vs. day 0; # $P < 0.05$ vs. WT day 14. The results are expressed as mean \pm SE. One-way ANOVA was followed by the post hoc Bonferroni test.

10.2 LUNG FIBROSIS IS INHIBITED IN A MUC1-KO BLEOMYCIN-INDUCED PULMONARY FIBROSIS MOUSE MODEL

Lung fibrotic tissue was evaluated by Masson's trichrome histochemistry using ashcroft score analysis (**Figure 49A**) and micro-CT analysis (**Figure 49B**) using Hounsfield units. WT bleomycin treated mice showed higher ashcroft score value, that is to say, higher collagen deposition (blue staining) and lesser air spaces (higher micro-CT hounsfield units) than MUC1-KO mice. Therefore, these results reflect a reduction of the lung fibrotic extension as consequence of MUC1-KO.

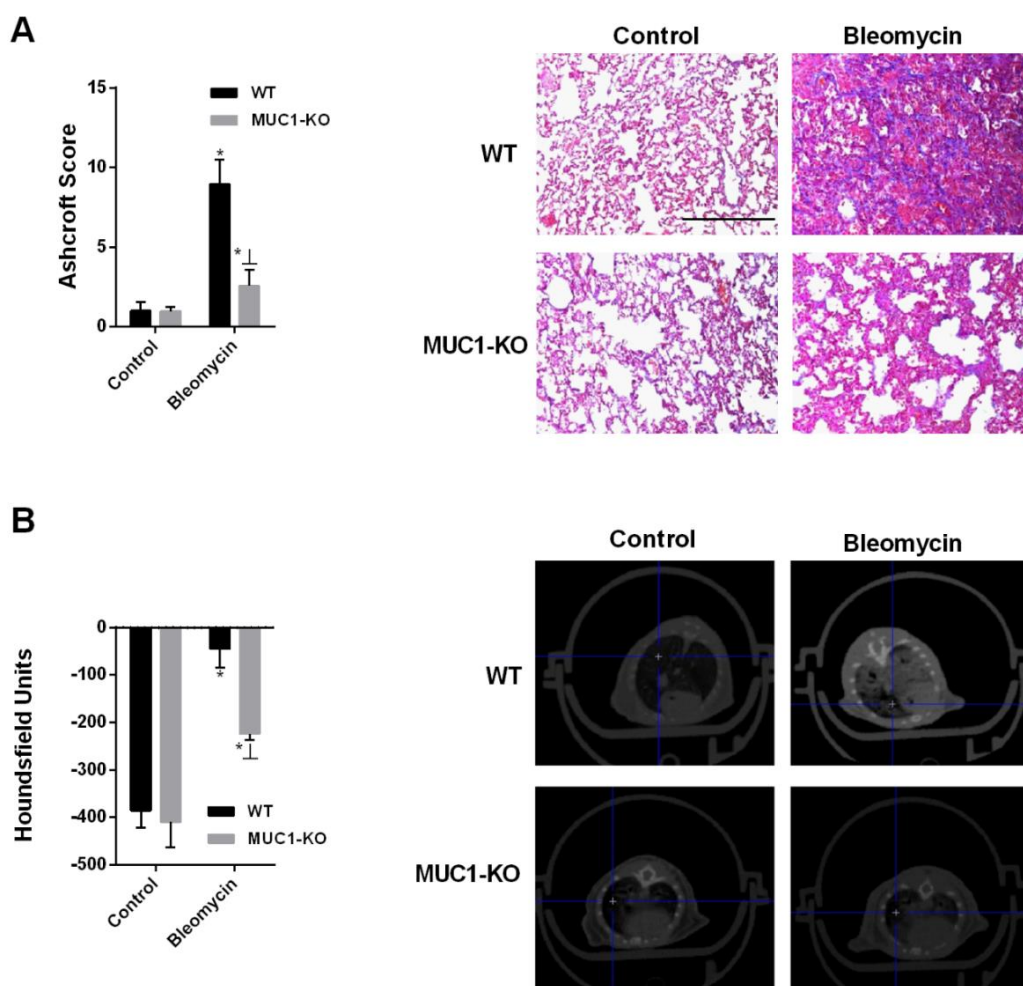


Figure 49. Lung fibrosis is inhibited in a MUC1-Knockout (KO) bleomycin-induced pulmonary fibrosis mouse model. Wild type (WT) C57BL/6 mice and MUC1-KO C57BL/6 mice received a single intratracheal dose of bleomycin (1.5 U/kg) on day 1 (n= 10). (A) Masson's trichrome (right panels, scale bar: 100 μ m) of WT control, WT Bleomycin, MUC1-KO Control and MUC1-KO

*Bleomycin tissue. Fibrosis Ashcroft scores were assessed as described in the Methods section. One-way ANOVA was followed by the post hoc Bonferroni test. *P < 0.05 vs. WT/MUC1-KO control; LP < 0.05 vs. WT. (B) Micro-computed tomography (CT) images were acquired on day 14 (right panels) and quantified as Hounsfield units. The results are expressed as mean \pm SE. One-way ANOVA was followed by the post hoc Bonferroni test. *P < 0.05 vs. WT/MUC1-KO control; LP < 0.05 vs. WT.*

10.3 PULMONARY ARTERY REMODELLING AND LUNG METABOLIC ACTIVITY ARE ATTENUATED IN A MUC1-KO BLEOMYCIN-INDUCED PULMONARY FIBROSIS MOUSE MODEL

Secondary to the lung fibrosis developed by IT bleomycin administration, pulmonary artery remodelling is developed. This remodelling increases right ventricle hypertrophy and consequently develops PH [224]. In this work, pulmonary artery remodelling was evaluated at endpoint by the ratio RV/(LV+S) and the consequent pulmonary perfusion was evaluated the day before by micro-SPECT-MAA-Tc^{99m} radiation signal. RV/(LV+S) ratio value was higher in bleomycin treated groups than in control groups, but this ratio was higher in WT mice than in MUC1 – KO mice. Therefore, MUC1 – KO mice had reduced the right ventricle hypertrophy caused by bleomycin IT administration (**Figure 50A**). Micro-SPECT-MAA-Tc^{99m} radiation signal was significantly higher in MUC1 – KO bleomycin treated group than in WT bleomycin treated group (**Figure 50B** and **Figure 50C**), that is to say, MUC1 – KO mice had improved pulmonary circulation and perfusion.

High lung metabolic activity is also a characteristic feature of fibrotic tissue. In this work, the metabolic activity was evaluated by SUV measures corresponding to ¹⁸F - FDG uptake by the lung. SUV measures were approximately 1 in the control groups. However, fibrotic tissue, as it can be observed in PET images, had an increased glyceic metabolism, so higher ¹⁸F – FDG uptake and SUV measures were registered. It should be highlighted that this increased glyceic metabolism after IT bleomycin administration is significantly higher in the WT bleomycin treated group than in the MUC1 – KO bleomycin treated group (**Figure 51**).

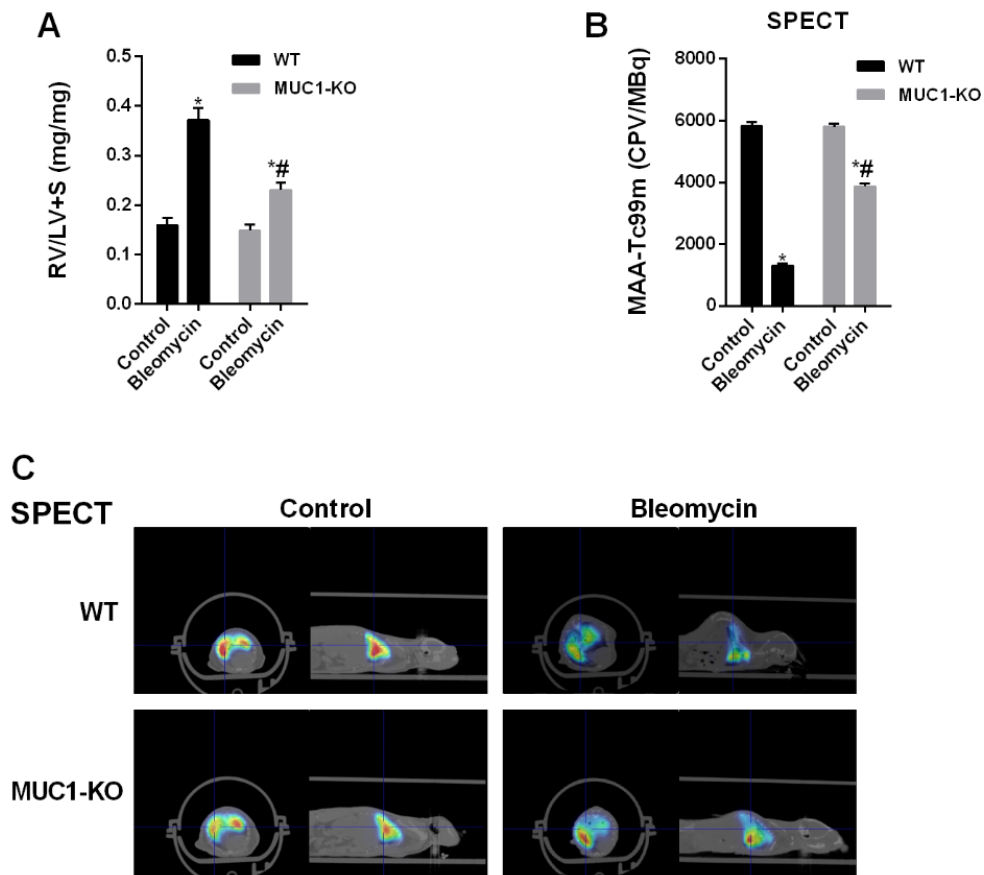


Figure 50. Right ventricular hypertrophy is inhibited and pulmonary perfusion is improved in a MUC1-Knockout (KO) bleomycin-induced pulmonary fibrosis mouse model. *Wild type (WT) C57BL/6 mice and MUC1-KO C57BL/6 mice received a single intratracheal dose of bleomycin (1.5 U/kg) on day 1 (n= 10). (A) Right ventricular hypertrophy (expressed as right ventricle (RV)/(left ventricle (LV) + septum (S)) ratio) at day 14. (B, C) Perfusion was measured at day 13 by the injection of macro-aggregates of albumin marked with technetium metastable (MAA-Tc^{99m}) and analysed as micro-single-photon emission computed tomography (SPECT). The results are expressed as mean \pm SE. One-way ANOVA was followed by the post hoc Bonferroni test. *P < 0.05 vs. control; #P < 0.05 vs. WT.*

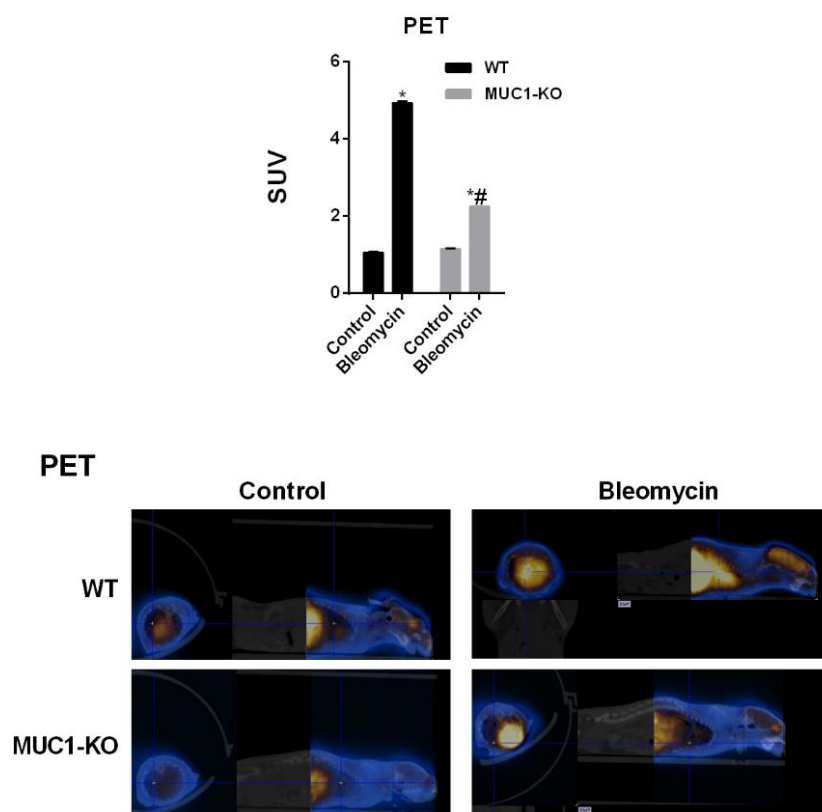


Figure 51. Lung metabolic activity is reduced in a MUC1-Knockout (KO) bleomycin-induced pulmonary fibrosis mouse model. Lung metabolism was measured at day 7 by the injection of ^{18}F -fluorodeoxyglucose and analysed by micro-positron emission tomography (PET) and the corresponding Standard Uptake Value (SUV). The results are expressed as mean \pm SE. One-way ANOVA was followed by the post hoc Bonferroni test. * $P < 0.05$ vs. control; # $P < 0.05$ vs. WT.

10.4 TISSUE REMODELLING IS INHIBITED IN A MUC1-KO BLEOMYCIN-INDUCED PULMONARY FIBROSIS MOUSE MODEL

To determine the bleomycin – induced inflammatory response, BALF from every mouse was obtained at the end of the experimental procedure. Through the BALF, all the cells and biological components in airway spaces are obtained so, BALF reflects the inflammatory cell infiltration in the lung. In the **Figure 52A**, it is shown that the number of BALF inflammatory cells was increased due to IT bleomycin administration, which produced higher amount of BALF inflammatory cells in WT mice than in MUC1-KO mice. Unlike the control groups, bleomycin groups had a BALF inflammatory cell profile made up of neutrophils and lymphocytes in addition to alveolar macrophages, the only cell type in the BALF from control groups (**Figure 52B**). It

reflects an inflammatory response induced by bleomycin and in the same way than in **Figure 52A**, BALF cell number after bleomycin administration was higher in WT mice than in MUC1 – KO mice (**Figure 52B**).

From the BALF supernatant and mRNA from BALF inflammatory cells, the levels of TGF β 1 and IL-6 cytokines were quantified by ELISA (**Figure 52C** and **52D**) and RT-PCR (**Figure 52E** and **52F**) respectively. As it was mentioned above, TGF β 1 is the main profibrotic factor and IL-6 has been shown to induce, in collaboration with IL-13, EMT and FMT processes [225]. Moreover, high levels of IL-6 characterize early-on IPF-acute exacerbations and an increase in the levels of IL-6 associates with worse outcome in all patients [226]. These BALF supernatant levels, as well, as the gene mRNA expression, were higher in WT bleomycin treated mice than in MUC1-KO bleomycin treated mice (**Figures 52C - 52F**). WT and MUC1-KO control mice showed similar TGF β 1/ IL-6 levels.

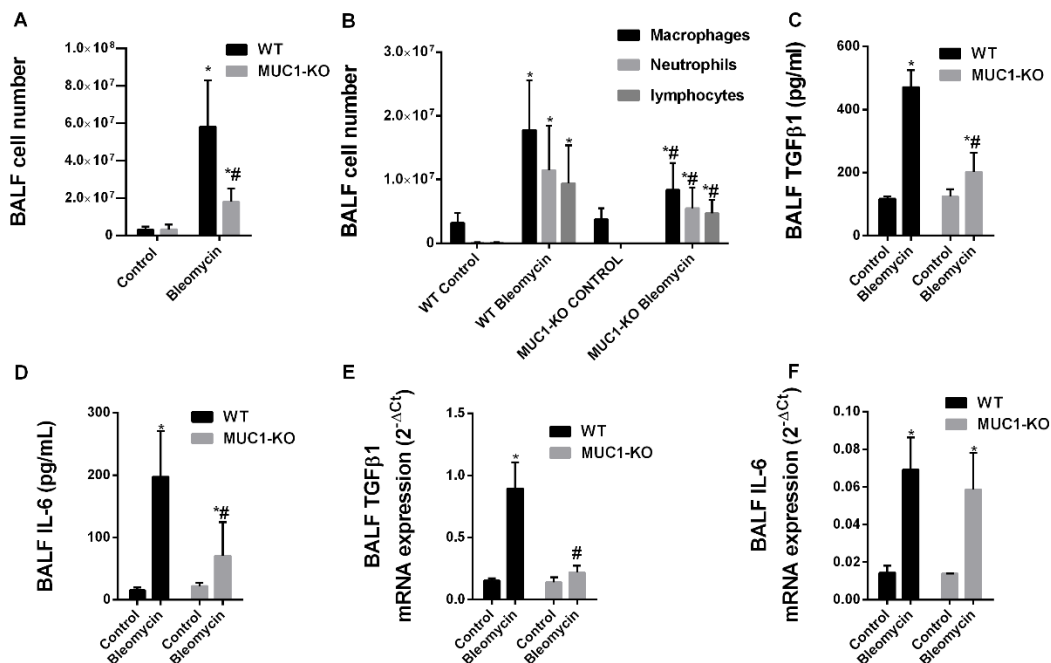


Figure 52. Bronchoalveolar lavage fluid (BALF) inflammatory cells extravasation is inhibited in a MUC1-Knockout (KO) bleomycin-induced pulmonary fibrosis mouse model. *Wild type (WT) C57BL/6 mice and MUC1 KO C57BL/6 mice received a single intratracheal dose of bleomycin (1.5 U/kg) on day 1 (n= 10). (A, B) Total BALF inflammatory cells and (C-F) interleukin-6 (IL-6) and transforming growth factor β 1 (TGF β 1) content were measured at day 14 after bleomycin administration, by ELISA (C,D) and Real time-PCR (E,F). The results are expressed as mean \pm SE. One-way ANOVA was followed by the post hoc Bonferroni test. * $P < 0.05$ vs. control; # $P < 0.05$ vs. WT.*

From the lung tissue, MUC1-KO was checked by RT-PCR and western blot (**Figure 53F** and **Figure 54**). mRNA gene and protein expression of recognized fibrotic markers and mediators such as collagen type I, TGF β 1, CTGF, IL-6 and IL-13 were also measured by RT-PCR and western blot. Bleomycin induced the expression of all of them in lung tissue from WT mice, whilst MUC1-KO animals maintained a minimal elevation (**Figure 53A-51E** and **Figure 54**). The expression of MUC1-CT (**Figure 53F** and **Figure 54**) and its phosphorylated forms at Thr⁴¹ (1224) and Tyr⁴⁶ (1229) amino acid positions (**Figure 54**) was increased in lung tissue from WT mice after bleomycin administration. Furthermore, the activation of downstream signals of TGF β 1 such as Smad3 and Erk1/2 phosphorylation, as well as, the activation of β -catenin, were increased in WT bleomycin treated mice whilst MUC1-KO bleomycin treated mice showed similar levels than untreated mice (**Figure 54**). The expression of the senescence marker p21 was also increased in WT bleomycin treated mice but not in MUC1-KO bleomycin mice (**Figure 54**).

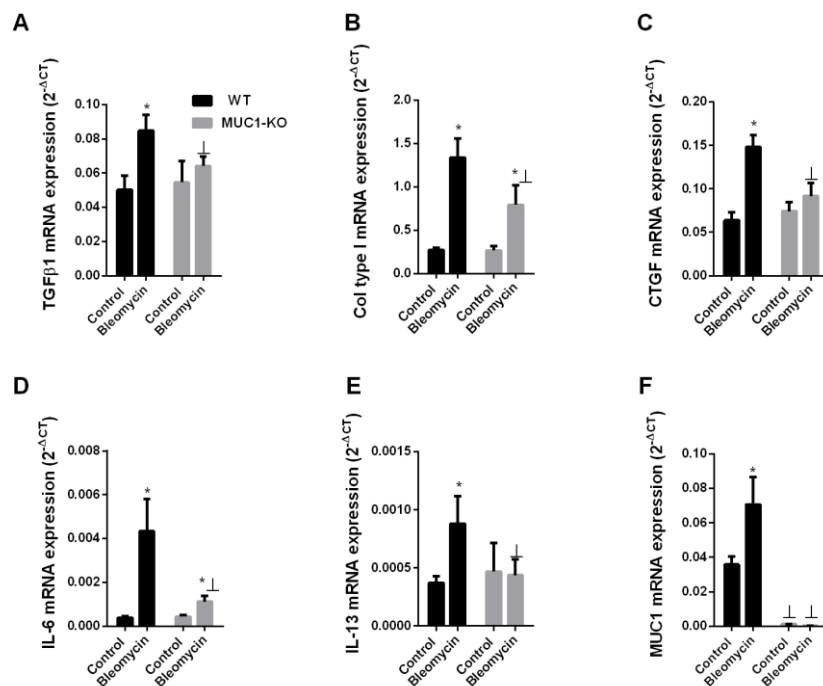


Figure 53. mRNA gene expression of lung fibrosis molecular markers is inhibited in a MUC1-Knockout (KO) bleomycin-induced pulmonary fibrosis mouse model. Wild type (WT) C57BL/6 mice and MUC1-KO C57BL/6 mice received a single intratracheal dose of bleomycin (1.5 U/kg) on day 1 ($n = 10$). (A) Transforming growth factor β 1 (TGF β 1), (B) collagen type I (Col type I), (C) connective tissue growth factor (CTGF), (D) interleukin-6 (IL-6), (E) interleukin-13 (IL-13) and (F) MUC1 expression were analyzed by Real time-PCR in lung tissue. The results are expressed as mean \pm SE. One-way ANOVA was followed by the post hoc Bonferroni test. * $P < 0.05$ vs. control; LP < 0.05 vs. WT.

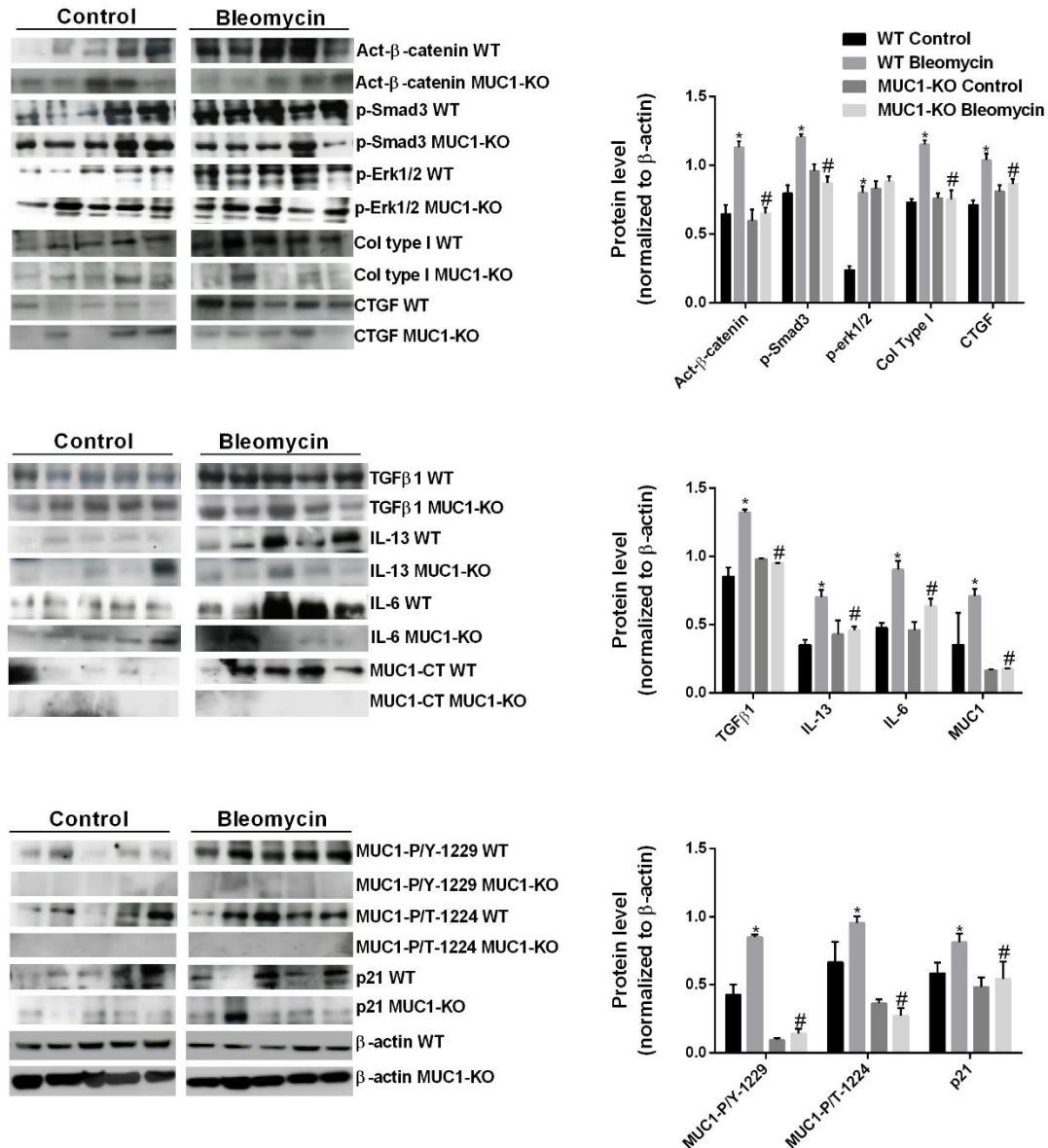
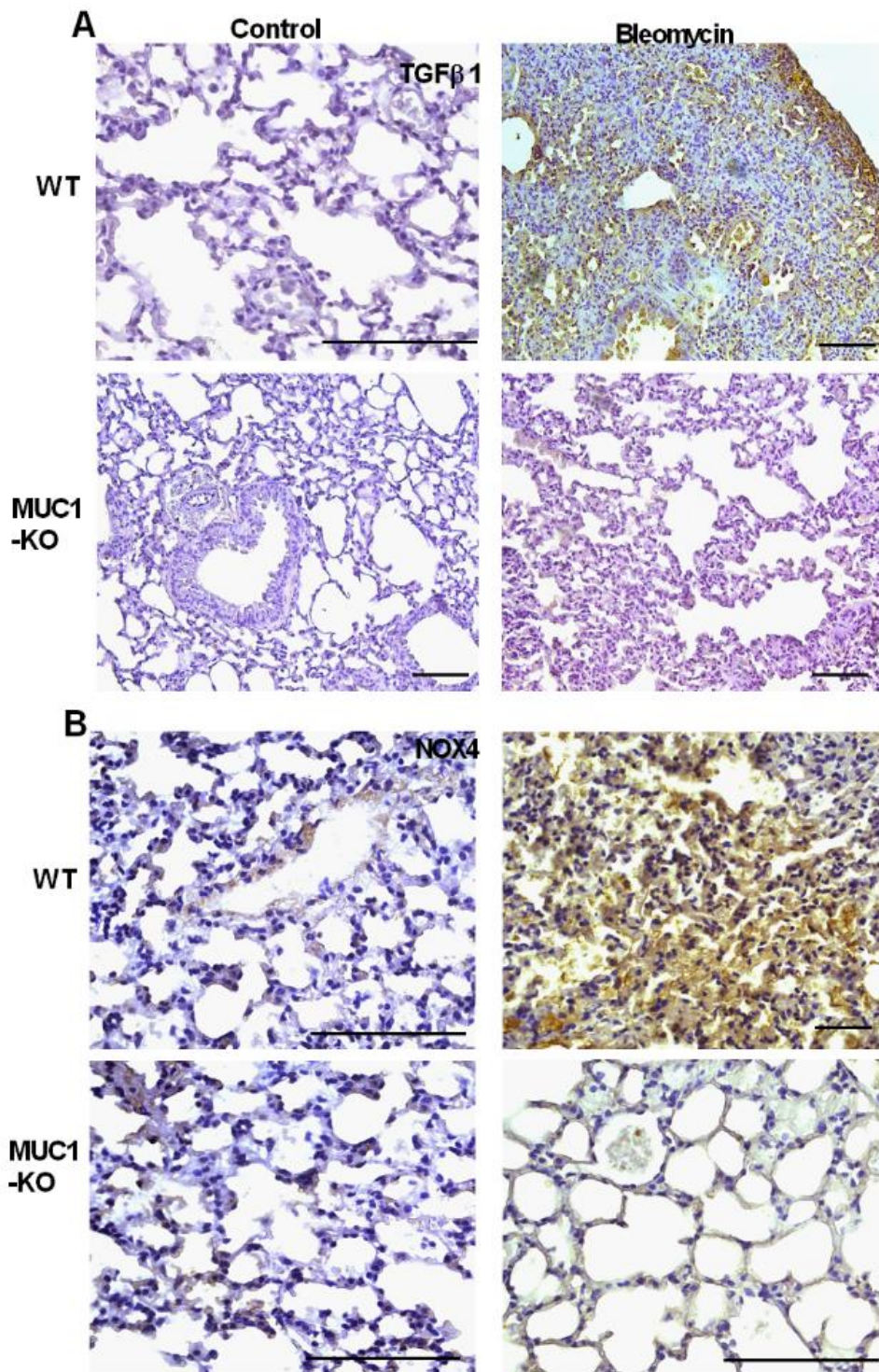


Figure 54. Protein expression of lung fibrosis molecular markers was inhibited in a MUC1-Knockout (KO) bleomycin-induced pulmonary fibrosis mouse model. Wild type (WT) C57BL/6 mice and MUC1-KO C57BL/6 mice received a single intratracheal dose of bleomycin (1.5 U/kg) on day 1 (n = 10). Total protein was analyzed by western blot in lung tissue and quantified by densitometry. Active (act)-β-catenin, phospho (p)-Smad3, phospho (p)- extracellular signal-regulated kinase (Erk)1/2, collagen type I (Col type I), connective tissue growth factor (CTGF), transforming growth factor (TGFβ1), interleukin-13 (IL-13), interleukin-6 (IL-6), MUC1-cytoplasmic tail (MUC1-CT), MUC1-P/Y-1229, MUC1-P/T-1224 and p21 were measured using western blot. Data are expressed as the ratio to β-actin protein. The results are expressed as mean ± SE. One-way ANOVA was followed by the post hoc Bonferroni test. *P < 0.05 vs. control; #P < 0.05 vs. WT.

From the lung tissue, it was also assessed the protein expression and localization of TGF β 1, NADPH oxidase 4 (NOX4), MUC1-CT and MUC5B by immunohistochemistry analysis. TGF β 1 showed again an elevated expression in WT mice exposed to bleomycin but not in MUC1-KO mice. This expression was mainly located in pleural epithelial cells, ATII cells and fibroblasts. NOX4, which has been proposed as one of the main producers of reactive oxygen species (ROS) in IPF [227], was also increased in lung tissue from WT mice after bleomycin administration but not in MUC1-KO mice . Furthermore, MUC5B expression, which has been shown to be altered in IPF patients [28], was also increased in WT bleomycin treated mice but not in MUC1-KO, and distributed in altered lung honeycomb lesions as observed for MUC1-CT overexpression. For all of these markers, expression in control groups was almost undetectable, as well as, MUC1-CT expression in MUC1-KO mice (**Figure 55**). Regarding to general histopathological features, all WT bleomycin images show fibrotic zones, composed mainly of dense collagen, alternated with areas of honeycomb pattern, frequently lined by bronchiolar epithelium with hyperplasia of ATII cells. By contrast, fibrotic zones are almost absent in MUC1-KO bleomycin images (**Figure 55**).



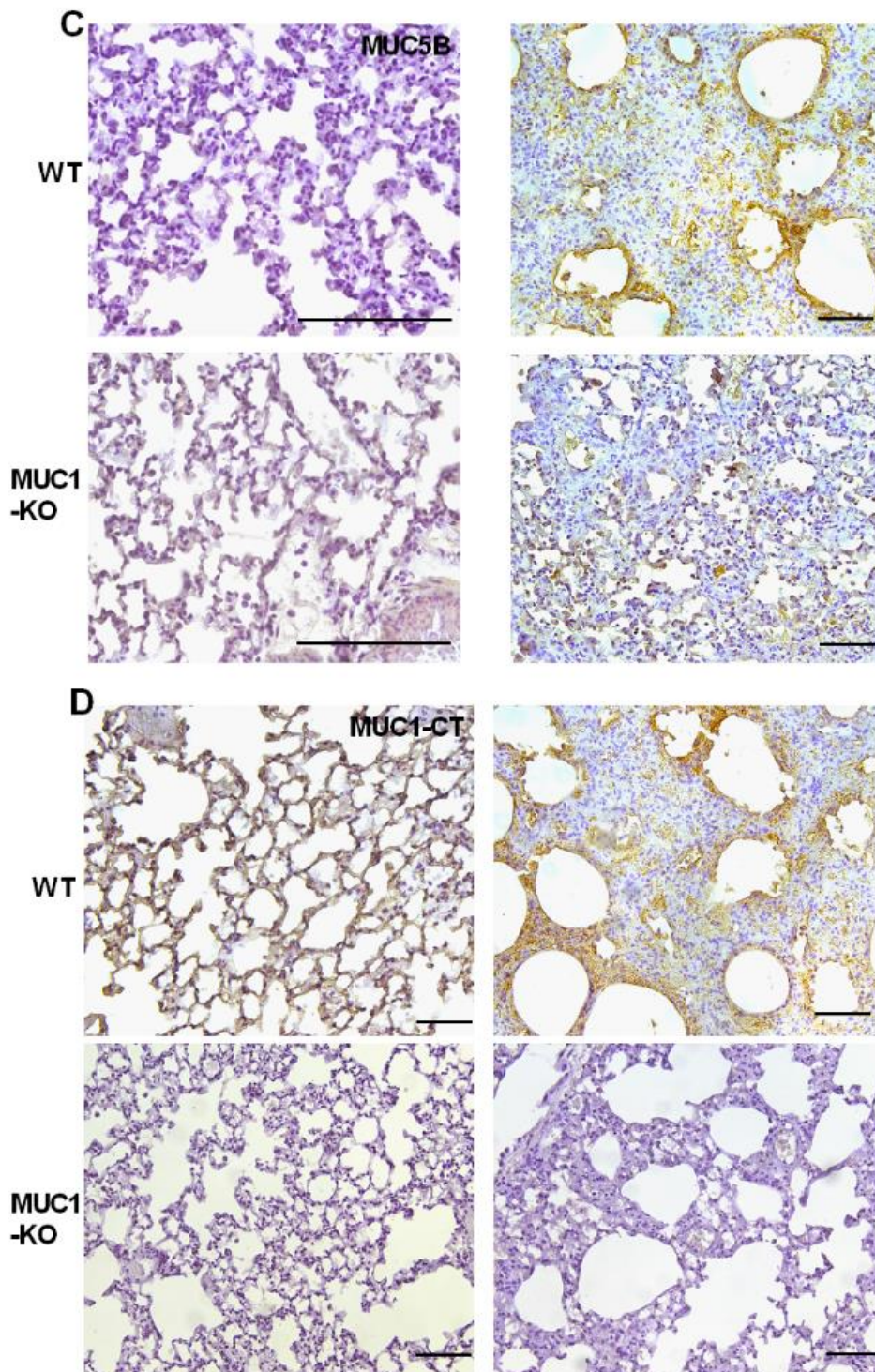
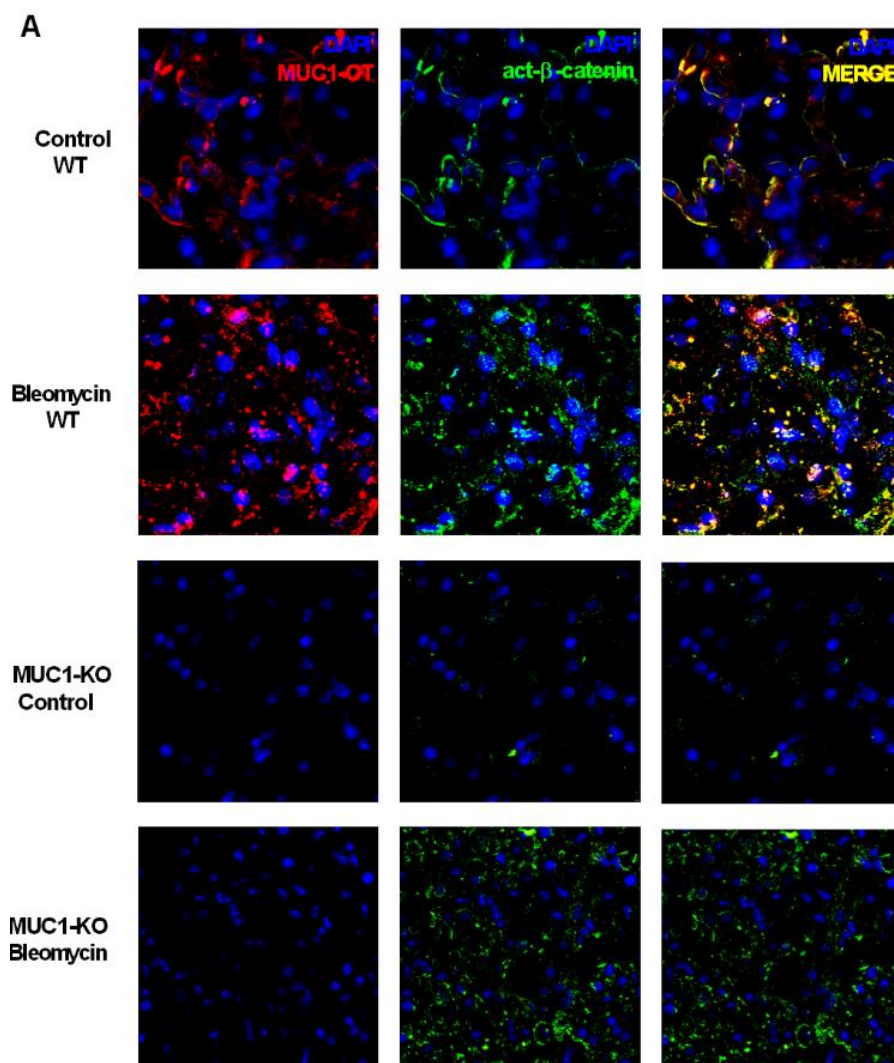


Figure 55. Immunohistochemical analysis of fibrotic markers in MUC1-Knockout (KO) and Wild type (WT) mice treated with bleomycin. WT C57BL/6 mice and MUC1-KO C57BL/6 mice received a single intratracheal dose of bleomycin (1.5 U/kg) on day 1 ($n = 10$). Representative images of lung tissue from WT control, WT Bleomycin, MUC1-KO Control and MUC1-KO-bleomycin tissue subjected to immunohistochemistry for transforming growth factor $\beta 1$ (TGF $\beta 1$), NADPH oxidase 4 (NOX4), MUC5B and MUC1-cytoplasmic tail (CT). Scale bar = 100 μm .

10.5 P-SMAD3/MUC1-CT/ACT- β -CATENIN NUCLEAR PROTEIN COMPLEX IS PROMOTED IN A BLEOMYCIN – INDUCED PULMONARY FIBROSIS MOUSE MODEL

MUC1-CT co-localization with p-Smad3 and act- β -catenin was also studied by confocal microscope immunofluorescence images of bleomycin – induced pulmonary fibrosis mice lung sections. In the same way than in lung tissue from IPF patients, mouse lung tissue sections showed co-localized cytoplasmic and nuclear distribution of the complexes act- β -catenin/MUC1-CT and p-Smad3/MUC1-CT in fibrotic areas of WT bleomycin treated mice. However, control WT mice showed MUC1-CT/act- β -catenin co-localization in the plasmatic membrane of AII cells, but to a lesser degree (**Figure 56**), and p-Smad3 was absent in control WT mice, as indicated fluorescence images. These patterns of co-localization were not observed in MUC1-KO mice due to MUC1 absence.



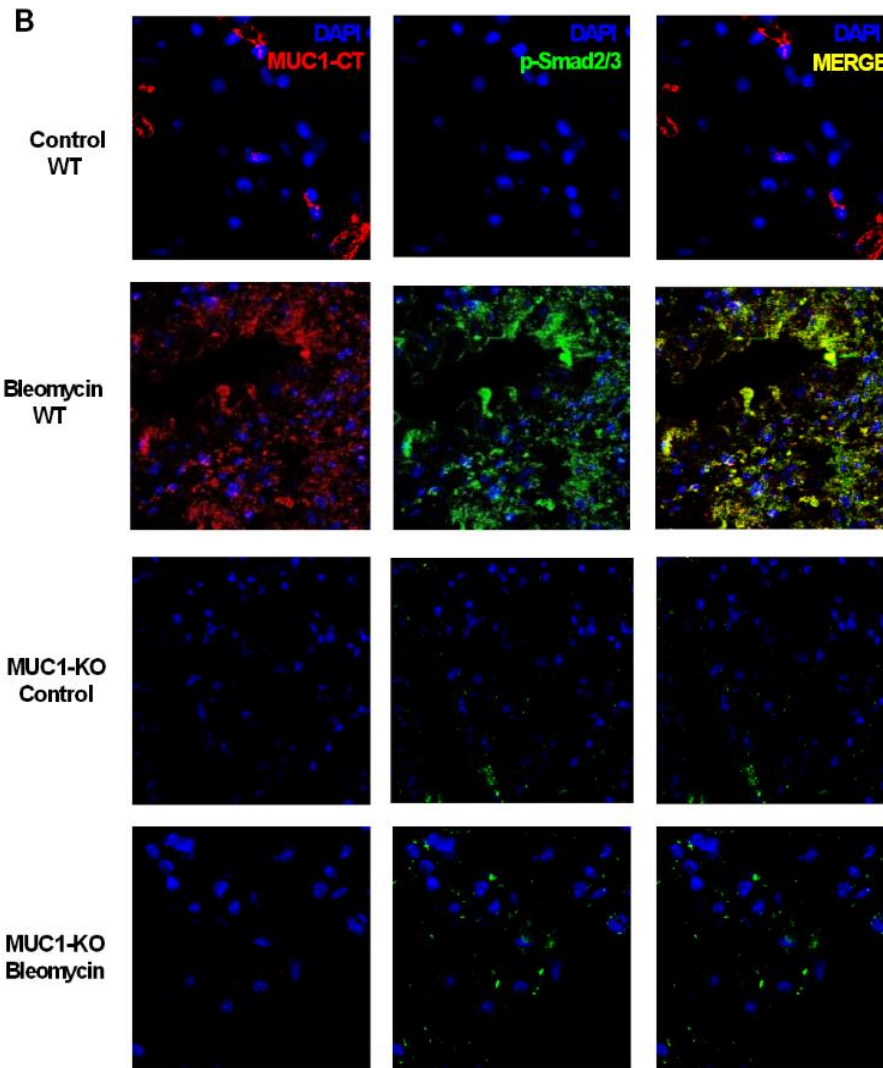


Figure 56. MUC1-cytoplasmic tail (MUC1-CT) nuclear translocation and co-localization with phospho (p)-Smad3 and active (act)- β -catenin is induced by bleomycin. Wild type (WT) C57BL/6 mice and MUC1 Knockout (MUC1-KO) C57BL/6 mice received a single intratracheal dose of bleomycin (1.5 U/kg) on day 1 ($n=10$). Representative images of lung tissue from WT control, WT bleomycin, MUC1-KO Control and MUC1-KO bleomycin tissue fixed, permeabilized, and used for (A) MUC1-CT and act- β -catenin immunostaining and (B) MUC1-CT and p-Smad3 immunostaining. Co-localization was analyzed using a confocal spectral microscope (Leica TCS SP2) that generated a merge of both antibodies (yellow color). DAPI, blue nuclei. Scale bars: 10 μ m.

DISCUSSION AND CONCLUSIONS

CHAPTER 11

DISCUSSION

DISCUSSION

KL6/MUC1 soluble extracellular domain has been found increased in serum and different biological fluids of IPF patients, and proposed as a useful biomarker to evaluate disease activity and predict the clinical outcomes in IPF [196]. However, to our knowledge there is no evidence of the intracellular bioactivation of MUC1 cytoplasmic domain and its role in IPF, which may be of potential value to understand and design new strategies to treat IPF. In the present work we analysed the MUC1 intracellular bioactivation as an important mediator of IPF. MUC1-CT and its phosphorylated forms at Thr⁴¹ (1224) and Tyr⁴⁶ (1229) in the cytoplasmic domain are overexpressed in IPF lung tissue. Cell transformations such as the ATII to mesenchymal transition and fibroblast to myofibroblast transition induced by TGF β 1 are mediated in part by the MUC1-CT bioactivation. TGF β 1 stimulus phosphorylates Smad3 that promotes the phosphorylation of MUC1-CT at Thr⁴¹ and Tyr⁴⁶, thus increasing the activation of β -catenin to induce the nuclear translocation of the transcription factor complex phospho-Smad3/MUC1-CT/ β -catenin. This complex increases the activation of smad binding element (SBE) DNA sequence to promote pro-fibrotic gene expression, proliferation or cell senescence in lung fibroblasts and ATII cells. The pro-fibrotic mediator galectin 3 serves as a bridge to associate MUC1-CT with the T β RI/II, thus mediating indirect MUC1-CT activation, but also mediates T β RI/II independent MUC1-CT activation indicating that MUC1-CT can be activated by non-canonical and canonical pathways. The mouse model of bleomycin-induced lung fibrosis reproduces what happens in lung tissue and cells from IPF patients, and MUC1-KO mice show protective effects against lung fibrosis.

In summary, the results provided in this work show novel evidence on the intracellular bioactivation of MUC1-CT in IPF, which could be of potential value to understand IPF pathogenesis, as well as, to develop future treatments of IPF.

11.1 MUC1-CT EXPRESSION, LOCATION AND BIOACTIVATION IN IPF

The expression of MUC1 has been studied previously in human lung tissue of different ILDs, where it was found an increased gene mRNA and KL-6/MUC1 protein expression compared with healthy controls [196, 228]. In addition, distribution of KL-6/MUC1 was found restricted to ATII cell surface of healthy and IPF patients [196].

MUC1 is a large glycoprotein that acts as a membrane receptor comprising the KL-6/MUC1-N and MUC1-C subunits, which form a stable non-covalent complex. However, under

lung fibrotic conditions, the elevated levels of metalloproteases mediate MUC1 proteolytic cleavage close to the plasma membrane, thus releasing extracellular KL-6 domain that can be detected in many IPF biological fluids. Soluble KL-6/MUC1 has activity on lung fibroblasts, promoting cell proliferation, migration and myofibroblast transition [198, 199], and antibodies against KL-6 attenuate bleomycin-induced lung fibrosis [200]. However, some contradictory findings are also found in the literature, since silica-induced lung fibrosis in MUC1-KO mice increased lung fibrosis rather than decrease [229].

MUC1-C acts as a putative receptor that engages diverse signalling pathways linked to cell transformation [191]. In particular, the highly conserved CT in the MUC1-C subunit is the responsible for these multiple intracellular signals modulations through interactions largely regulated by phosphorylation with several proteins implicated in proliferation, apoptosis, and transcription of various genes [188]. Secreted KL-6/MUC1 serves as biomarker in IPF. However, currently, there is no evidence on the expression, location and function of the signalling independent molecule MUC1-CT in IPF.

In this work, lung tissue from 21 healthy subjects and 22 IPF patients was obtained and MUC1-CT expression, as well as, the expression of two MUC1-CT phosphorylated forms (MUC1-P/T-1224 and MUC1-P/Y-1229) was analysed in both groups. It was observed that MUC1-CT was overexpressed in lung tissue from IPF patients, and located mostly in hyperplastic AII cells and fibroblasts of fibrotic areas, in which it was mainly distributed in cell cytoplasm and nucleus. MUC1-P/T-1224 and MUC1-P/Y-1229 were detected only in IPF lung tissue, with a similar pattern of distribution than non-phosphorylated MUC1-CT, which represents a different role of previously studied KL6/MUC1. In addition, this pattern of distribution reflects that the intracellular signals modulated by these MUC1-CT phosphorylations take part in IPF patients but not in healthy subjects. In the same way, Thr⁴¹ (1224) and Tyr⁴⁶ (1229) MUC1-CT phosphorylations, as well as, MUC1-CT, were overexpressed in the lung tissue of WT bleomycin-induced pulmonary fibrosis mouse model.

MUC1-CT consists of 72 amino acids with 13 documented tyrosine and serine/threonine phosphorylation sites [191]. The rationale for the research's focus upon these particular MUC1-CT phosphorylation sites is based on the fact that Thr⁴¹ (1224) phosphorylation at the TDR amino acid site by PKC δ and Tyr⁴⁶ (1229) phosphorylation at the YEKV amino acid site by c-SRC tyrosine kinase, induces binding of the MUC1-CT SAGNGGSSLS sequence to β -catenin, promoting the activation of Wnt target genes [204] and CTGF [230], both of them associated with IPF [3, 84]. Therefore, loss of MUC1 decreases levels of total and act- β -catenin. Furthermore, Thr⁴¹(1224) and Tyr⁴⁶(1229) phosphorylation promotes nuclear translocation of MUC1-CT/ β -catenin

complex to activate dependent gene expression involved in cell proliferation and differentiation [183]. Finally, it has been observed that phosphorylation of MUC1-CT occurs in response to the activation of several cell-surface growth factor receptors involved in cellular processes related to IPF, including FGFR-3, PDGFR β , and ErbB family members, which modulate their signal transduction [202]. For instance, it has been observed that invasiveness of pancreatic adenocarcinoma cells is determined by PDGFR β - induced MUC1-CT tyrosine phosphorylation and consequent nuclear localization of the MUC1-CT - β -catenin complex, influencing WNT signalling and the transcription of cyclin D1, as well as, EMT [177, 210]. Therefore, all these findings support the hypothesized role of MUC1-CT signalling in IPF.

11.2 TGF β 1 AND MUC1-CT CROSSTALK IN THE IPF CONTEXT

TGF β 1 is one of the most key growth factors involved in the pathogenesis of IPF disease [231]. It is well established that TGF β 1 promotes differentiation of fibroblasts into activated myofibroblasts, enhances collagen synthesis, and reduces collagen degradation by downregulation of proteases and upregulation of protease inhibitors [174]. Previously, it has been observed that several growth factors can activate MUC1-CT [192]. However, it is still unknown if TGF β 1 can activate it.

TGF β 1 signalling is propagated by at least two independent routes: the Smad-dependent canonical pathway and the Smad-independent or non-canonical pathway. In this work, it was observed that TGF β 1 was able to phosphorylate Thr⁴¹ (1224) and Tyr⁴⁶ (1229) MUC1-CT residues in A11 and lung fibroblasts. However, treatment of these cells with the Smad3 phosphorylation inhibitor, SIS3, blocked the TGF β 1-induced MUC1-CT phosphorylations. However, these cells were also transiently transfected by the use of siRNA-MUC1, and it didn't inhibit Smad3 phosphorylation, which indicates that Smad3 phosphorylation is required to phosphorylate MUC1-CT. TGF β 1 was also able to increase the active form of β -catenin that was inhibited by both, SIS3 and siRNA-MUC1 treatments, thus suggesting that Thr⁴¹ (1224) and Tyr⁴⁶ (1229) MUC1-CT phosphorylations by p-Smad3 action are needed to increase act- β -catenin in A11 cells and lung fibroblasts from IPF patients (**Figure 57**). This increase of act- β -catenin by MUC1-CT phosphorylation has been mentioned above. It has been shown to contribute to carcinogenesis and metastasis by MUC1-CT competition with E-cadherin for binding to act- β -catenin and by nuclear localization of the MUC1-CT - β -catenin complex, influencing profibrotic processes [177, 210].

Immunoprecipitation and immunofluorescence analysis in ATII cells and lung fibroblasts revealed that MUC1-CT forms protein complexes with p-Smad3 and act- β -catenin in response to TGF β 1 and that this stimulus promotes the nuclear translocation of these complexes. It is known that phosphorylated Smad2 and Smad3, together with the common mediator Smad4, translocate to the nucleus in response to TGF β 1 pathway activation and preferentially associate with the SBE DNA sequence to induce the expression of profibrotic molecules such as collagen, CTGF and α -SMA [171, 176]. In this work, siRNA-MUC1 transiently transfected ATII cells didn't activate SBE DNA sequence in response to TGF β 1 stimulus. Therefore, it is hypothesized that the phospho-Smad3/MUC1-CT/ β -catenin complex is required to activate SBE DNA sequence to promote pro-fibrotic gene expression. Nuclear co-localization of this complex was also observed in lung tissue sections of IPF patients and in an animal model of bleomycin-induced lung fibrosis, thus reproducing the *in vitro* observations. The Thr⁴¹ (1224) and Tyr⁴⁶ (1229) MUC1-CT phosphorylations, phospho-Smad3 and active- β -catenin were also increased in the lung tissue of WT bleomycin animal model together with the increase of fibrotic mediators such as TGF β 1, CTGF, NOX4, MUC5B, collagen type I, IL-13 and IL-6. Furthermore, lung function was impaired and lung tissue remodelling, inflammation and mortality were induced in WT bleomycin animal model. However, all of these findings were attenuated in MUC1-KO bleomycin mice, which suggest a role for MUC1-CT controlling fibrogenesis.

Lung cells in IPF are undergoing different transformations [232]. The most recognized cell transformations in IPF are ATII to mesenchymal transition and FMT, which contribute to the increased amount of lung myofibroblasts. They are a cell phenotype with shared characteristics between smooth muscle cells and fibroblasts, which allow to contract and migrate, as well as, to release ECM to invade lung tissue. Therefore, EMT could be observed by down-regulation of the epithelial marker E-cadherin and up-regulation of cytoskeletal markers such as α -SMA and vimentin, ECM markers such as collagen type I, and transcription factors such as Snail and Slug. FMT is also characterized by up-regulation of these markers. TGF β 1 is the best characterized and the most potent cellular transformer of fibroblasts and ATII cells, and multiple pathways can modulate its function [171]. In this work, both, ATII cells and fibroblasts transiently transfected with siRNA-MUC1 were not transformed to myofibroblasts after TGF β 1 stimulation, thus showing novel evidence of the connection of TGF β 1 canonical pathway and MUC1-CT bioactivation to induce ATII to mesenchymal transition and FMT. Previous findings in cancer cells showed that MUC1-C can induce EMT and cellular invasion by a ZEB1-mediated mechanism, as well as, mediating Wnt/ β -catenin activation and Snail expression [233, 234]. In this work, MUC1-

CT bioactivation by TGF β 1 mediated the activation of β -catenin, as well as, the expression of Snail in ATII and lung fibroblasts.

In addition to cell transformations, senescence of ATII cells and fibroblasts are key pathologic processes in IPF. The metabolic active, hypersecretory and apoptotic resistant senescence phenotype of ATII cells and lung fibroblasts is abundant in lungs from IPF patients and contributes to the release of a number of fibrotic growth factors such as TGF β 1, CTGF or IL-13 between others [235]. Also, the fibroblast proliferative phenotype coexists with the senescent phenotype, which indicates the complex interrelation of lung cells in IPF. In this work we observed that TGF β 1 increased first fibroblast proliferation followed by cell senescence as previously outlined [221, 223]. However, the inhibition of MUC1 expression using siRNA-MUC1 blocked the ATII and fibroblast cell senescence, as well as, lung fibroblast proliferation induced by TGF β 1. Similar results were observed in the MUC1-KO model where p21 senescence marker was more reduced in the bleomycin group than in the bleomycin WT group. The senescent phenotype could be explained by the interaction and activation mentioned above of β -catenin by MUC1-CT, since previous studies have proposed the Wnt/ β -catenin as a driver of cell senescence in IPF [236]. Furthermore, SBE activation by p-Smad3 pathway also increases the expression of senescence p21 and p16 markers [237]. Therefore, MUC1-CT connects with TGF β 1 canonical (Smad3) and non-canonical (β -catenin) pathways to mediate cell senescence. In this work, MUC1 also controlled lung fibroblast proliferation induced by TGF β 1, but not *via* Erk1/2 pathway as occurs in cancer cells [207]. In fact, Erk1/2 phosphorylation induced by TGF β 1 action was not altered as consequence of siRNA-MUC1 treatment. Therefore, MUC1 action in cell proliferation was possibly enhancing SBE transcription expression of cyclin kinases [238].

11.3 PHARMACOLOGICAL APPROACHES

To date, no pharmacologic therapies have definitively been shown to meaningfully improve IPF survival. Nevertheless, there are currently two approved medications for the treatment of IPF (pirfenidone and nintedanib), and a potential interest in the developing of new IPF treatments is being developed since a long time ago.

Transiently in response to stress and constitutively in carcinoma cells, MUC1-C is targeted to the nucleus [239]. Then, to confirm that the effects of MUC1-CT on the ATII to mesenchymal transition and FMT, as well as, ATII and fibroblast senescence and fibroblast proliferation, were dependent on MUC1-CT nuclear translocation, the peptide GO-201 was used in this work. MUC1-C nuclear translocation is mediated by a CQC motif in the MUC1-CT, which

contributes to the formation of MUC1-C oligomers and thereby RRK MUC1-CT motif interaction with importin β , necessary for this targeting [191, 192]. The GO-201 peptide, synthesized by Raina *et al.* [217], is derived from the N-terminal region of MUC1-CT that contains the CQC motif, binds to MUC1-CT, blocks formation of MUC1-C oligomers and attenuates targeting of MUC1-CT to the nucleus inducing death of human breast cancer cells *in vitro* and in tumour models. In this work, we showed that the MUC1-CT CQC motif inhibitor GO-201 inhibited the TGF β 1-induced MUC1-CT nuclear translocation, the TGF β 1-induced ATII to mesenchymal transition, FMT, ATII and fibroblast senescence and lung fibroblast proliferation (**Figure 57**), thus demonstrating the role of MUC1-CT and its nuclear translocation on IPF cellular processes.

Therefore, these results suggest that MUC1-CT CQC motif blockade can be a potential IPF druggable approach to inhibit MUC1-CT nuclear localization and its transcriptional function. In this context, currently, a phase I/II trial of another MUC1-CT CQC motif inhibitor (GO-203) in patients with relapsed or refractory acute myeloid leukemia is currently recruiting patients (ClinicalTrials.gov Identifier: NCT02204085).

Galectin 3 is a promising target for fibrotic diseases, including IPF [1]. In fact, it has been observed an increased expression of galectin 3 in the BALF and serum from patients with stable IPF compared with nonspecific interstitial pneumonitis and controls [144]. Previous findings have shown that galectin 3 binds to T β R causing cell surface retention and promoting signalling to Smads and AKT/ β -catenin, thus leading to cell transformations and lung fibrosis [144]. On the other hand, a phase I/II clinical trial to assess the safety, tolerability, pharmacokinetics and pharmacodynamics of TD139 (galectin 3 inhibitor) in IPF patients has been successful. Furthermore, previous findings have shown that this inhibitor significantly inhibits *in vitro* the TGF β 1-dependent Smad2 phosphorylation in human lung fibroblasts [240] and blocks the TGF β 1-induced β -catenin activation *in vitro* and *in vivo*, attenuating the late-stage progression of lung fibrosis after bleomycin [144, 240]. In this work, in addition to confirm previous observations, we extended them and demonstrated that in an IPF ATII cell model, galectin 3 reinforces TGF β 1 activation of Smad3 and MUC1-CT Thr⁴¹ (1224) and Tyr⁴⁶ (1229) phosphorylations, thus increasing the amount of act- β -catenin. Furthermore, galectin 3 also triggered MUC1-CT and β -catenin activation independently of T β R (**Figure 57**). These results indicate that MUC1-CT can be activated by galectin 3 indirectly *via* p-Smad3 mediated signalling, and directly *via* galectin 3 binding as recently outlined [207]. In IPF, the increased metalloproteases mediate MUC1 proteolytic cleavage close to the plasma membrane, thus releasing MUC1-N/KL-6. The remaining MUC1-C terminal includes a 58-amino acid extracellular domain that is glycosylated on Asn-36 and then serves as a binding site for the galectin 3 ligand.

It is the basis of potential bridge between MUC1 and different growth factor receptors [201], which may be represented by T β R as we showed in this work. β -catenin activation *via* galectin 3 binding and Tcf reporter activation has been shown in cancer cell lines [241]. Then, this direct activation might be also suggested in IPF. Nevertheless, it has been observed that galectin-3/MUC1 binding can trigger the recruitment of β -catenin to MUC1-CT and consequent β -catenin activation [242]. The phosphorylated sites of MUC1-CT after galectin-3/MUC1 binding have not been elucidated yet, but it has been speculated that galectin 3-triggered signalling leads to phosphorylation of the Tyr⁴⁶ (1229) residue of MUC1-CT and consequent β -catenin recruitment [207].

To be functional, galectin-3 oligomerization through association of the galectin-3 N-terminal domain is necessary. In this regard, MUC1 seems to be one of the most preferable ligand glycoproteins for oligomerizing galectin-3, because O-glycans, which are the binding sites of galectins, may be expressed repeatedly on the tandem repeats of the MUC1 core protein. Furthermore, it is an extremely high molecular glycoprotein and easily accessible to galectin-3 because of its rod-like structure, which is longer (200–500 nm) than typical cell surface adhesion molecules (~30 nm) [207]. Otherwise, because homooligomerization of MUC1-C plays a crucial role in MUC1-mediated signal transduction, clustering of MUC1 through the binding of galectin-3 to MUC1 may assist oligomerization of MUC1-C [207].

Then, all these findings about the relationship between MUC1 and the two profibrotic factors galectin-3 and TGF β 1, as well as, other growth factors such as FGF and PDGF, highlight even more the potential pharmacologic targeting of MUC1-CT bioactivation in IPF.

Regarding to IPF approved treatments, nintedanib mechanism of action is well characterized, but the target of pirfenidone is not well understood [1]. Previous findings have reported that pirfenidone has a number of anti-inflammatory and antifibrotic effects, including inhibition of collagen synthesis, down-regulation of TGF β 1 effects and signalling, and reduction in fibroblast proliferation and fibrosis in bleomycin-induced animal models [115, 243]. Furthermore, interestingly, it has been observed that IPF patients with concomitant lung cancer who received perioperative pirfenidone treatment had a decrease in the serum KL-6 levels compared to the controls [244]. In this work, we analysed the pirfenidone mechanism of action in several experiments and we provided a potential mechanism that explain, almost in part, pirfenidone antifibrotic effects. Specifically, it was observed that pirfenidone inhibited the TGF β 1-induced Smad3 phosphorylation and MUC1-CT Thr⁴¹ (1224) and Tyr⁴⁶ (1229) phosphorylations, thus reducing the amount of active- β -catenin and the nuclear translocation of the phospho-Smad3/MUC1-CT/ β -catenin complex. Therefore, pirfenidone inhibited the

TGF β 1-induced ATII to mesenchymal transition and FMT and the TGF β 1-induced senescence and proliferation (**Figure 57**).

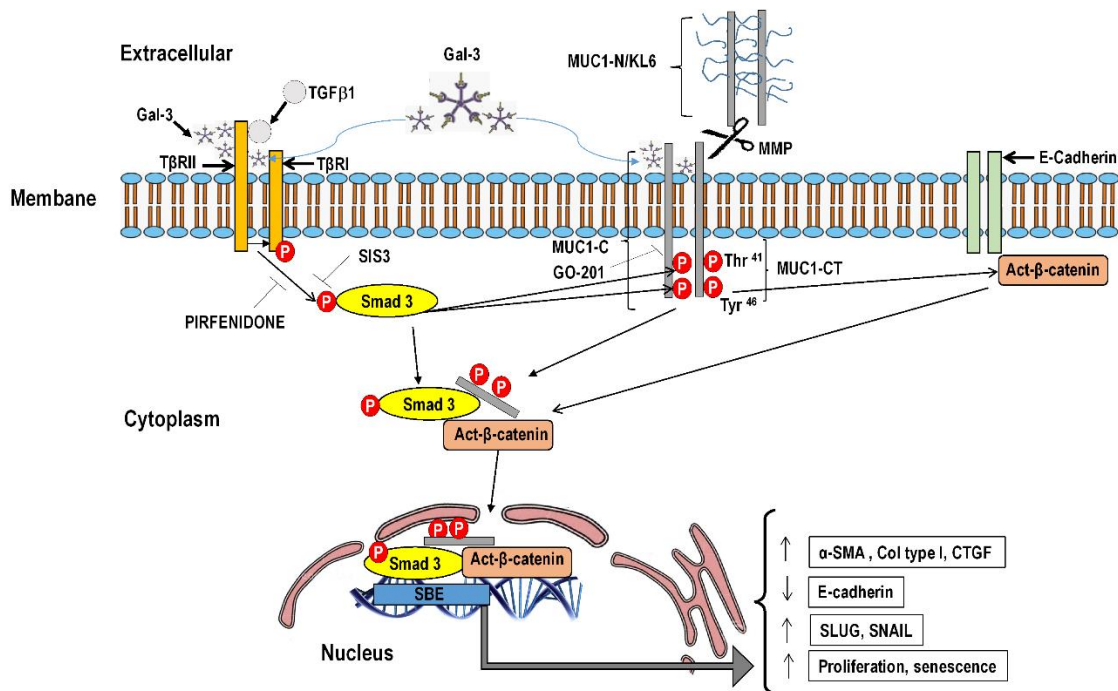


Figure 57. Schematic showing novel evidence on the bioactivation of MUC1-CT in Idiopathic pulmonary fibrosis (IPF). Under lung fibrotic conditions, the elevated levels of metalloproteases mediate proteolytic cleavage of MUC1 close to the plasma membrane, thus releasing extracellular KL6/MUC1-N domain and leaving the MUC1-C domain anchored to the plasmatic membrane. MUC1 cytoplasmic tail (MUC1-CT), as well as, MUC1-CT phosphorylated forms at Thr⁴¹ (1224) and Tyr⁴⁶ (1229) residues, have been observed overexpressed in IPF lung tissue and these phosphorylations are induced *in vitro* by transforming growth factor β 1 (TGF β 1). TGF β 1 binds to its receptors (T β R1/II) leading to recruitment and phosphorylation of Smad3. Phosphorylated Smad3 (p-Smad3) promotes the phosphorylation of MUC1-CT at Thr⁴¹ (1224) and Tyr⁴⁶ (1229) residues, thus increasing the active form of β -catenin (act- β -catenin), which is initially bind to E-cadherin. MUC1-CT competes with E-cadherin for binding to act- β -catenin and p-Smad3/MUC1-CT/act- β -catenin complexes are formed in the cytoplasm. These complexes migrate into the nucleus, activating Smad binding element (SBE) DNA sequence to promote alveolar type II (ATII) to mesenchymal transition, fibroblast to mesenchymal transition (FMT), fibroblast proliferation or ATII/fibroblast senescence. Galectin 3 (Gal-3) pentamers bind to T β R1/II and reinforce TGF β 1 activation of Smad3 and MUC1-CT Thr⁴¹ (1224) and Tyr⁴⁶ (1229) phosphorylations, thus increasing the amount of act- β -catenin. Furthermore, Gal-3 binds to

MUC1-C, which could serve as a bridge to associate MUC1-C with TβRI/II. Otherwise it can also activate directly MUC1-CT Thr⁴¹ (1224) and Tyr⁴⁶ (1229) phosphorylations. The inhibition of p-Smad3 using SIS3 or pirfenidone is supposed to block the TGFβ1-induced Thr⁴¹ (1224) and Tyr⁴⁶ (1229) MUC1-CT phosphorylations, thus reducing the amount of act-β-catenin and the nuclear translocation of p-Smad3/MUC1-CT/act-β-catenin. The MUC1-CT nuclear translocation is at the same time mediated by a mechanism that is dependent on MUC1-C oligomerization. In this regard, the MUC1-CT CQC motif inhibitor GO-201 abrogates MUC1-C oligomerization, TGFβ1-induced MUC1-CT nuclear translocation and MUC1-CT transcriptional function.

CHAPTER 12

CONCLUSIONS

CONCLUSIONS

- MUC1-CT is overexpressed, phosphorylated in MUC1-CT Thr⁴¹ and Tyr⁴⁶ residues and located in the cell nucleus of hyperplastic ATII cells and fibroblasts from IPF fibrotic areas.
- MUC1-CT participates in the ATII to mesenchymal and fibroblast to myofibroblast transitions, ATII and lung fibroblast senescence and lung fibroblast proliferation induced by TGFβ1 *in vitro*.
- TGFβ1 increases the phosphorylation of Smad3 that bioactivates MUC1 through the phosphorylations of MUC1-CT Thr⁴¹ and Tyr⁴⁶ residues, thus mediating β-catenin activation.
- Bioactivated MUC1-CT forms protein complexes with p-Smad3 and act-β-catenin, which migrate into the nucleus of ATII and fibroblasts to promote SBE DNA activation and to increase profibrotic gene transcripton
- Bleomycin-induced lung fibrosis is attenuated in MUC1-KO mice. In the same way, pulmonary artery remodelling and pulmonary hypertension development are also inhibited in MUC1-KO mice.
- MUC1-CT-induced lung fibrotic processes are dependent of TGFβ1 pathway and independent of TGFβ1 pathway through galectin 3 action.
- Pirfenidone's mechanism of action is explained, almost in part, by inhibition of TGFβ1-induced Smad3 phosphorylation and consequent inhibition of MUC1-CT Thr⁴¹ (1224) and Tyr⁴⁶ (1229) phosphorylations, thus reducing the act-β-catenin and the nuclear translocation of p-Smad3/MUC1-CT/act-β-catenin.

BIBLIOGRAPHY

BIBLIOGRAPHY

- [1] Lederer DJ, Martinez FJ. Idiopathic Pulmonary Fibrosis. *N Engl J Med*, 2018; 378: 1811-1823.
- [2] American Thoracic S, European Respiratory S. American Thoracic Society/European Respiratory Society International Multidisciplinary Consensus Classification of the Idiopathic Interstitial Pneumonias. This joint statement of the American Thoracic Society (ATS), and the European Respiratory Society (ERS) was adopted by the ATS board of directors, June 2001 and by the ERS Executive Committee, June 2001. *Am J Respir Crit Care Med*, 2002; 165: 277-304.
- [3] Martinez FJ, Collard HR, Pardo A, Raghu G, Richeldi L, Selman M, Swigris JJ, Taniguchi H, Wells AU. Idiopathic pulmonary fibrosis. *Nat Rev Dis Primers*, 2017; 3: 17074.
- [4] Travis WD, Costabel U, Hansell DM, King TE, Jr., Lynch DA, Nicholson AG, Ryerson CJ, Ryu JH, Selman M, Wells AU, Behr J, Bouros D, Brown KK, Colby TV, Collard HR, Cordeiro CR, Cottin V, Crestani B, Drent M, Dudden RF, Egan J, Flaherty K, Hogaboam C, Inoue Y, Johkoh T, Kim DS, Kitaichi M, Loyd J, Martinez FJ, Myers J, Protzko S, Raghu G, Richeldi L, Sverzellati N, Swigris J, Valeyre D, Pneumonias AEColl. An official American Thoracic Society/European Respiratory Society statement: Update of the international multidisciplinary classification of the idiopathic interstitial pneumonias. *Am J Respir Crit Care Med*, 2013; 188: 733-48.
- [5] Raghu G, Collard HR, Egan JJ, Martinez FJ, Behr J, Brown KK, Colby TV, Cordier JF, Flaherty KR, Lasky JA, Lynch DA, Ryu JH, Swigris JJ, Wells AU, Ancochea J, Bouros D, Carvalho C, Costabel U, Ebina M, Hansell DM, Johkoh T, Kim DS, King TE, Jr., Kondoh Y, Myers J, Muller NL, Nicholson AG, Richeldi L, Selman M, Dudden RF, Griss BS, Protzko SL, Schunemann HJ, Fibrosis AEJACoIP. An official ATS/ERS/JRS/ALAT statement: idiopathic pulmonary fibrosis: evidence-based guidelines for diagnosis and management. *Am J Respir Crit Care Med*, 2011; 183: 788-824.
- [6] Ley B, Collard HR, King TE, Jr. Clinical course and prediction of survival in idiopathic pulmonary fibrosis. *Am J Respir Crit Care Med*, 2011; 183: 431-40.
- [7] Hutchinson J, Fogarty A, Hubbard R, McKeever T. Global incidence and mortality of idiopathic pulmonary fibrosis: a systematic review. *Eur Respir J*, 2015; 46: 795-806.

- [8] Diamantopoulos A, Wright E, Vlahopoulou K, Cornic L, Schoof N, Maher TM. The Burden of Illness of Idiopathic Pulmonary Fibrosis: A Comprehensive Evidence Review. *Pharmacoeconomics*, 2018; 36: 779-807.
- [9] Kreuter M, Ehlers-Tenenbaum S, Palmowski K, Bruhwylter J, Oltmanns U, Muley T, Heussel CP, Warth A, Kolb M, Herth FJ. Impact of Comorbidities on Mortality in Patients with Idiopathic Pulmonary Fibrosis. *PLoS One*, 2016; 11: e0151425.
- [10] Raghu G, Amatto VC, Behr J, Stowasser S. Comorbidities in idiopathic pulmonary fibrosis patients: a systematic literature review. *Eur Respir J*, 2015; 46: 1113-30.
- [11] Sack C, Vedal S, Sheppard L, Raghu G, Barr RG, Podolanczuk A, Doney B, Hoffman EA, Gassett A, Hinckley-Stukovsky K, Williams K, Kawut S, Lederer DJ, Kaufman JD. Air pollution and subclinical interstitial lung disease: the Multi-Ethnic Study of Atherosclerosis (MESA) air-lung study. *Eur Respir J*, 2017; 50.
- [12] Tang YW, Johnson JE, Browning PJ, Cruz-Gervis RA, Davis A, Graham BS, Brigham KL, Oates JA, Jr., Loyd JE, Stecenko AA. Herpesvirus DNA is consistently detected in lungs of patients with idiopathic pulmonary fibrosis. *J Clin Microbiol*, 2003; 41: 2633-40.
- [13] Tobin RW, Pope CE, 2nd, Pellegrini CA, Emond MJ, Sillery J, Raghu G. Increased prevalence of gastroesophageal reflux in patients with idiopathic pulmonary fibrosis. *Am J Respir Crit Care Med*, 1998; 158: 1804-8.
- [14] Appel JZ, 3rd, Lee SM, Hartwig MG, Li B, Hsieh CC, Cantu E, 3rd, Yoon Y, Lin SS, Parker W, Davis RD. Characterization of the innate immune response to chronic aspiration in a novel rodent model. *Respir Res*, 2007; 8: 87.
- [15] Downing TE, Sporn TA, Bollinger RR, Davis RD, Parker W, Lin SS. Pulmonary histopathology in an experimental model of chronic aspiration is independent of acidity. *Exp Biol Med (Maywood)*, 2008; 233: 1202-12.
- [16] Raghu G, Yang ST, Spada C, Hayes J, Pellegrini CA. Sole treatment of acid gastroesophageal reflux in idiopathic pulmonary fibrosis: a case series. *Chest*, 2006; 129: 794-800.
- [17] Lee JS, Ryu JH, Elicker BM, Lydell CP, Jones KD, Wolters PJ, King TE, Jr., Collard HR. Gastroesophageal reflux therapy is associated with longer survival in patients with idiopathic pulmonary fibrosis. *Am J Respir Crit Care Med*, 2011; 184: 1390-4.
- [18] Kim JS, Podolanczuk AJ, Borker P, Kawut SM, Raghu G, Kaufman JD, Stukovsky KDH, Hoffman EA, Barr RG, Gottlieb DJ, Redline SS, Lederer DJ. Obstructive Sleep Apnea and Subclinical Interstitial Lung Disease in the Multi-Ethnic Study of Atherosclerosis (MESA). *Ann Am Thorac Soc*, 2017; 14: 1786-1795.
-

-
- [19] Mora AL, Rojas M, Pardo A, Selman M. Emerging therapies for idiopathic pulmonary fibrosis, a progressive age-related disease. *Nat Rev Drug Discov*, 2017; 16: 810.
- [20] Richeldi L, Collard HR, Jones MG. Idiopathic pulmonary fibrosis. *Lancet*, 2017; 389: 1941-1952.
- [21] Stuart BD, Choi J, Zaidi S, Xing C, Holohan B, Chen R, Choi M, Dharwadkar P, Torres F, Girod CE, Weissler J, Fitzgerald J, Kershaw C, Klesney-Tait J, Mageto Y, Shay JW, Ji W, Bilguvar K, Mane S, Lifton RP, Garcia CK. Exome sequencing links mutations in PARN and RTEL1 with familial pulmonary fibrosis and telomere shortening. *Nat Genet*, 2015; 47: 512-7.
- [22] Kropski JA, Mitchell DB, Markin C, Polosukhin VV, Choi L, Johnson JE, Lawson WE, Phillips JA, 3rd, Cogan JD, Blackwell TS, Loyd JE. A novel dyskerin (DKC1) mutation is associated with familial interstitial pneumonia. *Chest*, 2014; 146: e1-e7.
- [23] Alder JK, Stanley SE, Wagner CL, Hamilton M, Hanumanthu VS, Armanios M. Exome sequencing identifies mutant TINF2 in a family with pulmonary fibrosis. *Chest*, 2015; 147: 1361-1368.
- [24] Stanley SE, Gable DL, Wagner CL, Carlile TM, Hanumanthu VS, Podlevsky JD, Khalil SE, DeZern AE, Rojas-Duran MF, Applegate CD, Alder JK, Parry EM, Gilbert WV, Armanios M. Loss-of-function mutations in the RNA biogenesis factor NAF1 predispose to pulmonary fibrosis-emphysema. *Sci Transl Med*, 2016; 8: 351ra107.
- [25] Fahy JV, Dickey BF. Airway mucus function and dysfunction. *N Engl J Med*, 2010; 363: 2233-47.
- [26] Young HW, Williams OW, Chandra D, Bellinghausen LK, Perez G, Suarez A, Tuvim MJ, Roy MG, Alexander SN, Moghaddam SJ, Adachi R, Blackburn MR, Dickey BF, Evans CM. Central role of Muc5ac expression in mucous metaplasia and its regulation by conserved 5' elements. *Am J Respir Cell Mol Biol*, 2007; 37: 273-90.
- [27] Roy MG, Livraghi-Butrico A, Fletcher AA, McElwee MM, Evans SE, Boerner RM, Alexander SN, Bellinghausen LK, Song AS, Petrova YM, Tuvim MJ, Adachi R, Romo I, Bordt AS, Bowden MG, Sisson JH, Woodruff PG, Thornton DJ, Rousseau K, De la Garza MM, Moghaddam SJ, Karmouty-Quintana H, Blackburn MR, Drouin SM, Davis CW, Terrell KA, Grubb BR, O'Neal WK, Flores SC, Cota-Gomez A, Lozupone CA, Donnelly JM, Watson AM, Hennessy CE, Keith RC, Yang IV, Barthel L, Henson PM, Janssen WJ, Schwartz DA, Boucher RC, Dickey BF, Evans CM. Muc5b is required for airway defence. *Nature*, 2014; 505: 412-6.
-

- [28] Seibold MA, Wise AL, Speer MC, Steele MP, Brown KK, Loyd JE, Fingerlin TE, Zhang W, Gudmundsson G, Groshong SD, Evans CM, Garantziotis S, Adler KB, Dickey BF, du Bois RM, Yang IV, Herron A, Kervitsky D, Talbert JL, Markin C, Park J, Crews AL, Slifer SH, Auerbach S, Roy MG, Lin J, Hennessy CE, Schwarz MI, Schwartz DA. A common MUC5B promoter polymorphism and pulmonary fibrosis. *N Engl J Med*, 2011; 364: 1503-12.
- [29] Allen RJ, Porte J, Braybrooke R, Flores C, Fingerlin TE, Oldham JM, Guillen-Guio B, Ma SF, Okamoto T, John AE, Obeidat M, Yang IV, Henry A, Hubbard RB, Navaratnam V, Saini G, Thompson N, Booth HL, Hart SP, Hill MR, Hirani N, Maher TM, McAnulty RJ, Millar AB, Molyneaux PL, Parfrey H, Rassi DM, Whyte MKB, Fahy WA, Marshall RP, Oballa E, Bosse Y, Nickle DC, Sin DD, Timens W, Shrine N, Sayers I, Hall IP, Noth I, Schwartz DA, Tobin MD, Wain LV, Jenkins RG. Genetic variants associated with susceptibility to idiopathic pulmonary fibrosis in people of European ancestry: a genome-wide association study. *Lancet Respir Med*, 2017; 5: 869-880.
- [30] Levy D, Neuhausen SL, Hunt SC, Kimura M, Hwang SJ, Chen W, Bis JC, Fitzpatrick AL, Smith E, Johnson AD, Gardner JP, Srinivasan SR, Schork N, Rotter JI, Herbig U, Psaty BM, Sastry M, Murray SS, Vasan RS, Province MA, Glazer NL, Lu X, Cao X, Kronmal R, Mangino M, Soranzo N, Spector TD, Berenson GS, Aviv A. Genome-wide association identifies OBFC1 as a locus involved in human leukocyte telomere biology. *Proc Natl Acad Sci U S A*, 2010; 107: 9293-8.
- [31] Mangino M, Hwang SJ, Spector TD, Hunt SC, Kimura M, Fitzpatrick AL, Christiansen L, Petersen I, Elbers CC, Harris T, Chen W, Srinivasan SR, Kark JD, Benetos A, El Shamieh S, Visvikis-Siest S, Christensen K, Berenson GS, Valdes AM, Vinuela A, Garcia M, Arnett DK, Broeckel U, Province MA, Pankow JS, Kammerer C, Liu Y, Nalls M, Tishkoff S, Thomas F, Ziv E, Psaty BM, Bis JC, Rotter JI, Taylor KD, Smith E, Schork NJ, Levy D, Aviv A. Genome-wide meta-analysis points to CTC1 and ZNF676 as genes regulating telomere homeostasis in humans. *Hum Mol Genet*, 2012; 21: 5385-94.
- [32] Petrovski S, Todd JL, Durheim MT, Wang Q, Chien JW, Kelly FL, Frankel C, Mebane CM, Ren Z, Bridgers J, Urban TJ, Malone CD, Finlen Copeland A, Brinkley C, Allen AS, O'Riordan T, McHutchison JG, Palmer SM, Goldstein DB. An Exome Sequencing Study to Assess the Role of Rare Genetic Variation in Pulmonary Fibrosis. *Am J Respir Crit Care Med*, 2017; 196: 82-93.
- [33] Fingerlin TE, Murphy E, Zhang W, Peljto AL, Brown KK, Steele MP, Loyd JE, Cosgrove GP, Lynch D, Groshong S, Collard HR, Wolters PJ, Bradford WZ, Kossen K, Seiwert SD, du Bois RM, Garcia CK, Devine MS, Gudmundsson G, Isaksson HJ, Kaminski N, Zhang Y, Gibson
-

-
- KF, Lancaster LH, Cogan JD, Mason WR, Maher TM, Molyneaux PL, Wells AU, Moffatt MF, Selman M, Pardo A, Kim DS, Crapo JD, Make BJ, Regan EA, Walek DS, Daniel JJ, Kamatani Y, Zelenika D, Smith K, McKean D, Pedersen BS, Talbert J, Kidd RN, Markin CR, Beckman KB, Lathrop M, Schwarz MI, Schwartz DA. Genome-wide association study identifies multiple susceptibility loci for pulmonary fibrosis. *Nat Genet*, 2013; 45: 613-20.
- [34] Rabinovich EI, Kapetanaki MG, Steinfeld I, Gibson KF, Pandit KV, Yu G, Yakhini Z, Kaminski N. Global methylation patterns in idiopathic pulmonary fibrosis. *PLoS One*, 2012; 7: e33770.
- [35] Sanders YY, Ambalavanan N, Halloran B, Zhang X, Liu H, Crossman DK, Bray M, Zhang K, Thannickal VJ, Hagoood JS. Altered DNA methylation profile in idiopathic pulmonary fibrosis. *Am J Respir Crit Care Med*, 2012; 186: 525-35.
- [36] Wilborn J, Crofford LJ, Burdick MD, Kunkel SL, Strieter RM, Peters-Golden M. Cultured lung fibroblasts isolated from patients with idiopathic pulmonary fibrosis have a diminished capacity to synthesize prostaglandin E2 and to express cyclooxygenase-2. *J Clin Invest*, 1995; 95: 1861-8.
- [37] Crystal RG, Fulmer JD, Roberts WC, Moss ML, Line BR, Reynolds HY. Idiopathic pulmonary fibrosis. Clinical, histologic, radiographic, physiologic, scintigraphic, cytologic, and biochemical aspects. *Ann Intern Med*, 1976; 85: 769-88.
- [38] Keogh BA, Crystal RG. Alveolitis: the key to the interstitial lung disorders. *Thorax*, 1982; 37: 1-10.
- [39] Wolters PJ, Collard HR, Jones KD. Pathogenesis of idiopathic pulmonary fibrosis. *Annu Rev Pathol*, 2014; 9: 157-79.
- [40] Basset F, Ferrans VJ, Soler P, Takemura T, Fukuda Y, Crystal RG. Intraluminal fibrosis in interstitial lung disorders. *Am J Pathol*, 1986; 122: 443-61.
- [41] Corrin B, Dewar A, Rodriguez-Roisin R, Turner-Warwick M. Fine structural changes in cryptogenic fibrosing alveolitis and asbestosis. *J Pathol*, 1985; 147: 107-19.
- [42] Kuhn C, 3rd, Boldt J, King TE, Jr., Crouch E, Vartio T, McDonald JA. An immunohistochemical study of architectural remodeling and connective tissue synthesis in pulmonary fibrosis. *Am Rev Respir Dis*, 1989; 140: 1693-703.
- [43] McDonald JA. Idiopathic pulmonary fibrosis. A paradigm for lung injury and repair. *Chest*, 1991; 99: 87S-93S.
- [44] Strieter RM. Pathogenesis and natural history of usual interstitial pneumonia: the whole story or the last chapter of a long novel. *Chest*, 2005; 128: 526S-532S.
-

- [45] Strieter RM, Mehrad B. New mechanisms of pulmonary fibrosis. *Chest*, 2009; 136: 1364-70.
- [46] Wallace WA, Fitch PM, Simpson AJ, Howie SE. Inflammation-associated remodelling and fibrosis in the lung - a process and an end point. *Int J Exp Pathol*, 2007; 88: 103-10.
- [47] Kliment CR, Oury TD. Oxidative stress, extracellular matrix targets, and idiopathic pulmonary fibrosis. *Free Radic Biol Med*, 2010; 49: 707-17.
- [48] Sisson TH, Mendez M, Choi K, Subbotina N, Courey A, Cunningham A, Dave A, Engelhardt JF, Liu X, White ES, Thannickal VJ, Moore BB, Christensen PJ, Simon RH. Targeted injury of type II alveolar epithelial cells induces pulmonary fibrosis. *Am J Respir Crit Care Med*, 2010; 181: 254-63.
- [49] Selman M, Pardo A. Revealing the pathogenic and aging-related mechanisms of the enigmatic idiopathic pulmonary fibrosis. an integral model. *Am J Respir Crit Care Med*, 2014; 189: 1161-72.
- [50] Horowitz JC, Thannickal VJ. Epithelial-mesenchymal interactions in pulmonary fibrosis. *Semin Respir Crit Care Med*, 2006; 27: 600-12.
- [51] Cosgrove GP, Brown KK, Schiemann WP, Serls AE, Parr JE, Geraci MW, Schwarz MI, Cool CD, Worthen GS. Pigment epithelium-derived factor in idiopathic pulmonary fibrosis: a role in aberrant angiogenesis. *Am J Respir Crit Care Med*, 2004; 170: 242-51.
- [52] Kotani I, Sato A, Hayakawa H, Urano T, Takada Y, Takada A. Increased procoagulant and antifibrinolytic activities in the lungs with idiopathic pulmonary fibrosis. *Thromb Res*, 1995; 77: 493-504.
- [53] Scotton CJ, Chambers RC. Molecular targets in pulmonary fibrosis: the myofibroblast in focus. *Chest*, 2007; 132: 1311-21.
- [54] Singh SR, Hall IP. Airway myofibroblasts and their relationship with airway myocytes and fibroblasts. *Proc Am Thorac Soc*, 2008; 5: 127-32.
- [55] Li Y, Jiang D, Liang J, Meltzer EB, Gray A, Miura R, Wogensen L, Yamaguchi Y, Noble PW. Severe lung fibrosis requires an invasive fibroblast phenotype regulated by hyaluronan and CD44. *J Exp Med*, 2011; 208: 1459-71.
- [56] White ES, Thannickal VJ, Carskadon SL, Dickie EG, Livant DL, Markwart S, Toews GB, Arenberg DA. Integrin alpha4beta1 regulates migration across basement membranes by lung fibroblasts: a role for phosphatase and tensin homologue deleted on chromosome 10. *Am J Respir Crit Care Med*, 2003; 168: 436-42.
- [57] Klingberg F, Hinz B, White ES. The myofibroblast matrix: implications for tissue repair and fibrosis. *J Pathol*, 2013; 229: 298-309.
-

-
- [58] Thannickal VJ, Toews GB, White ES, Lynch JP, 3rd, Martinez FJ. Mechanisms of pulmonary fibrosis. *Annu Rev Med*, 2004; 55: 395-417.
- [59] Evans JN, Kelley J, Krill J, Low RB, Adler KB. The myofibroblast in pulmonary fibrosis. *Chest*, 1983; 83: 97S-98S.
- [60] Kasai H, Allen JT, Mason RM, Kamimura T, Zhang Z. TGF-beta1 induces human alveolar epithelial to mesenchymal cell transition (EMT). *Respir Res*, 2005; 6: 56.
- [61] Yao HW, Xie QM, Chen JQ, Deng YM, Tang HF. TGF-beta1 induces alveolar epithelial to mesenchymal transition in vitro. *Life Sci*, 2004; 76: 29-37.
- [62] Mehrad B, Strieter RM. Fibrocytes and the pathogenesis of diffuse parenchymal lung disease. *Fibrogenesis Tissue Repair*, 2012; 5 Suppl 1: S22.
- [63] Almudever P, Milara J, De Diego A, Serrano-Mollar A, Xaubet A, Perez-Vizcaino F, Cogolludo A, Cortijo J. Role of tetrahydrobiopterin in pulmonary vascular remodelling associated with pulmonary fibrosis. *Thorax*, 2013; 68: 938-48.
- [64] Nataraj D, Ernst A, Kalluri R. Idiopathic pulmonary fibrosis is associated with endothelial to mesenchymal transition. *Am J Respir Cell Mol Biol*, 2010; 43: 129-30.
- [65] Fernandez IE, Eickelberg O. New cellular and molecular mechanisms of lung injury and fibrosis in idiopathic pulmonary fibrosis. *Lancet*, 2012; 380: 680-8.
- [66] Hung C, Linn G, Chow YH, Kobayashi A, Mittelsteadt K, Altemeier WA, Gharib SA, Schnapp LM, Duffield JS. Role of lung pericytes and resident fibroblasts in the pathogenesis of pulmonary fibrosis. *Am J Respir Crit Care Med*, 2013; 188: 820-30.
- [67] Zolak JS, Jagirdar R, Surolia R, Karki S, Oliva O, Hock T, Guroji P, Ding Q, Liu RM, Bolisetty S, Agarwal A, Thannickal VJ, Antony VB. Pleural mesothelial cell differentiation and invasion in fibrogenic lung injury. *Am J Pathol*, 2013; 182: 1239-47.
- [68] Nasreen N, Mohammed KA, Mubarak KK, Baz MA, Akindipe OA, Fernandez-Bussy S, Antony VB. Pleural mesothelial cell transformation into myofibroblasts and haptotactic migration in response to TGF-beta1 in vitro. *Am J Physiol Lung Cell Mol Physiol*, 2009; 297: L115-24.
- [69] Mubarak KK, Montes-Worboys A, Regev D, Nasreen N, Mohammed KA, Faruqi I, Hensel E, Baz MA, Akindipe OA, Fernandez-Bussy S, Nathan SD, Antony VB. Parenchymal trafficking of pleural mesothelial cells in idiopathic pulmonary fibrosis. *Eur Respir J*, 2012; 39: 133-40.
- [70] Willis BC, Liebler JM, Luby-Phelps K, Nicholson AG, Crandall ED, du Bois RM, Borok Z. Induction of epithelial-mesenchymal transition in alveolar epithelial cells by
-

- transforming growth factor-beta1: potential role in idiopathic pulmonary fibrosis. *Am J Pathol*, 2005; 166: 1321-32.
- [71] Willis BC, Borok Z. TGF-beta-induced EMT: mechanisms and implications for fibrotic lung disease. *Am J Physiol Lung Cell Mol Physiol*, 2007; 293: L525-34.
- [72] Mehrad B, Strieter RM. Fibrocytes and the pathogenesis of diffuse parenchymal lung disease. *Fibrogenesis Tissue Repair*, 2012; 5: S22.
- [73] Epperly MW, Guo H, Gretton JE, Greenberger JS. Bone marrow origin of myofibroblasts in irradiation pulmonary fibrosis. *Am J Respir Cell Mol Biol*, 2003; 29: 213-24.
- [74] Hashimoto N, Jin H, Liu T, Chensue SW, Phan SH. Bone marrow-derived progenitor cells in pulmonary fibrosis. *J Clin Invest*, 2004; 113: 243-52.
- [75] Metz CN. Fibrocytes: a unique cell population implicated in wound healing. *Cell Mol Life Sci*, 2003; 60: 1342-50.
- [76] Phillips RJ, Burdick MD, Hong K, Lutz MA, Murray LA, Xue YY, Belperio JA, Keane MP, Strieter RM. Circulating fibrocytes traffic to the lungs in response to CXCL12 and mediate fibrosis. *J Clin Invest*, 2004; 114: 438-46.
- [77] Schmidt M, Sun G, Stacey MA, Mori L, Mattoli S. Identification of circulating fibrocytes as precursors of bronchial myofibroblasts in asthma. *J Immunol*, 2003; 171: 380-9.
- [78] Piera-Velazquez S, Li Z, Jimenez SA. Role of endothelial-mesenchymal transition (EndoMT) in the pathogenesis of fibrotic disorders. *Am J Pathol*, 2011; 179: 1074-80.
- [79] Que J, Wilm B, Hasegawa H, Wang F, Bader D, Hogan BL. Mesothelium contributes to vascular smooth muscle and mesenchyme during lung development. *Proc Natl Acad Sci U S A*, 2008; 105: 16626-30.
- [80] Armulik A, Genove G, Betsholtz C. Pericytes: developmental, physiological, and pathological perspectives, problems, and promises. *Dev Cell*, 2011; 21: 193-215.
- [81] Bergers G, Song S. The role of pericytes in blood-vessel formation and maintenance. *Neuro Oncol*, 2005; 7: 452-64.
- [82] Schrimpf C, Xin C, Campanholle G, Gill SE, Stallcup W, Lin SL, Davis GE, Gharib SA, Humphreys BD, Duffield JS. Pericyte TIMP3 and ADAMTS1 modulate vascular stability after kidney injury. *J Am Soc Nephrol*, 2012; 23: 868-83.
- [83] Konigshoff M, Balsara N, Pfaff EM, Kramer M, Chrobak I, Seeger W, Eickelberg O. Functional Wnt signaling is increased in idiopathic pulmonary fibrosis. *PLoS One*, 2008; 3: e2142.
- [84] Konigshoff M, Kramer M, Balsara N, Wilhelm J, Amarie OV, Jahn A, Rose F, Fink L, Seeger W, Schaefer L, Gunther A, Eickelberg O. WNT1-inducible signaling protein-1 mediates
-

-
- pulmonary fibrosis in mice and is upregulated in humans with idiopathic pulmonary fibrosis. *J Clin Invest*, 2009; 119: 772-87.
- [85] Vuga LJ, Ben-Yehudah A, Kovkarova-Naumovski E, Oriss T, Gibson KF, Feghali-Bostwick C, Kaminski N. WNT5A is a regulator of fibroblast proliferation and resistance to apoptosis. *Am J Respir Cell Mol Biol*, 2009; 41: 583-9.
- [86] Chilosi M, Poletti V, Zamo A, Lestani M, Montagna L, Piccoli P, Pedron S, Bertaso M, Scarpa A, Murer B, Cancellieri A, Maestro R, Semenzato G, Doglioni C. Aberrant Wnt/beta-catenin pathway activation in idiopathic pulmonary fibrosis. *Am J Pathol*, 2003; 162: 1495-502.
- [87] Chakraborty S, Chopra P, Ambi SV, Dastidar SG, Ray A. Emerging therapeutic interventions for idiopathic pulmonary fibrosis. *Expert Opin Investig Drugs*, 2014; 23: 893-910.
- [88] Coon DR, Roberts DJ, Loscertales M, Kradin R. Differential epithelial expression of SHH and FOXF1 in usual and nonspecific interstitial pneumonia. *Exp Mol Pathol*, 2006; 80: 119-23.
- [89] Stewart GA, Hoyne GF, Ahmad SA, Jarman E, Wallace WA, Harrison DJ, Haslett C, Lamb JR, Howie SE. Expression of the developmental Sonic hedgehog (Shh) signalling pathway is up-regulated in chronic lung fibrosis and the Shh receptor patched 1 is present in circulating T lymphocytes. *J Pathol*, 2003; 199: 488-95.
- [90] Schafer MJ, White TA, Iijima K, Haak AJ, Ligresti G, Atkinson EJ, Oberg AL, Birch J, Salmonowicz H, Zhu Y, Mazula DL, Brooks RW, Fuhrmann-Stroissnigg H, Pirtskhalava T, Prakash YS, Tchkonja T, Robbins PD, Aubry MC, Passos JF, Kirkland JL, Tschumperlin DJ, Kita H, LeBrasseur NK. Cellular senescence mediates fibrotic pulmonary disease. *Nat Commun*, 2017; 8: 14532.
- [91] Waters DW, Blokland KEC, Pathinayake PS, Burgess JK, Mutsaers SE, Prele CM, Schuliga M, Grainge CL, Knight DA. Fibroblast senescence in the pathology of idiopathic pulmonary fibrosis. *Am J Physiol Lung Cell Mol Physiol*, 2018.
- [92] Lehmann M, Korfei M, Mutze K, Klee S, Skronska-Wasek W, Alsafadi HN, Ota C, Costa R, Schiller HB, Lindner M, Wagner DE, Gunther A, Konigshoff M. Senolytic drugs target alveolar epithelial cell function and attenuate experimental lung fibrosis ex vivo. *Eur Respir J*, 2017; 50.
- [93] Raghu G, Rochweg B, Zhang Y, Garcia CA, Azuma A, Behr J, Brozek JL, Collard HR, Cunningham W, Homma S, Johkoh T, Martinez FJ, Myers J, Protzko SL, Richeldi L, Rind D, Selman M, Theodore A, Wells AU, Hoogsteden H, Schunemann HJ, American Thoracic
-

- S, European Respiratory s, Japanese Respiratory S, Latin American Thoracic A. An Official ATS/ERS/JRS/ALAT Clinical Practice Guideline: Treatment of Idiopathic Pulmonary Fibrosis. An Update of the 2011 Clinical Practice Guideline. *Am J Respir Crit Care Med*, 2015; 192: e3-19.
- [94] Demedts M, Behr J, Buhl R, Costabel U, Dekhuijzen R, Jansen HM, MacNee W, Thomeer M, Wallaert B, Laurent F, Nicholson AG, Verbeken EK, Verschakelen J, Flower CD, Capron F, Petruzzelli S, De Vuyst P, van den Bosch JM, Rodriguez-Becerra E, Corvasce G, Lankhorst I, Sardina M, Montanari M, Group IS. High-dose acetylcysteine in idiopathic pulmonary fibrosis. *N Engl J Med*, 2005; 353: 2229-42.
- [95] Idiopathic Pulmonary Fibrosis Clinical Research N, Raghu G, Anstrom KJ, King TE, Jr., Lasky JA, Martinez FJ. Prednisone, azathioprine, and N-acetylcysteine for pulmonary fibrosis. *N Engl J Med*, 2012; 366: 1968-77.
- [96] Idiopathic Pulmonary Fibrosis Clinical Research N, Martinez FJ, de Andrade JA, Anstrom KJ, King TE, Jr., Raghu G. Randomized trial of acetylcysteine in idiopathic pulmonary fibrosis. *N Engl J Med*, 2014; 370: 2093-101.
- [97] Oldham JM, Ma SF, Martinez FJ, Anstrom KJ, Raghu G, Schwartz DA, Valenzi E, Witt L, Lee C, Vij R, Huang Y, Strek ME, Noth I, Investigators IP. TOLLIP, MUC5B, and the Response to N-Acetylcysteine among Individuals with Idiopathic Pulmonary Fibrosis. *Am J Respir Crit Care Med*, 2015; 192: 1475-82.
- [98] King TE, Jr., Albera C, Bradford WZ, Costabel U, Hormel P, Lancaster L, Noble PW, Sahn SA, Szwarcberg J, Thomeer M, Valeyre D, du Bois RM, Group IS. Effect of interferon gamma-1b on survival in patients with idiopathic pulmonary fibrosis (INSPIRE): a multicentre, randomised, placebo-controlled trial. *Lancet*, 2009; 374: 222-8.
- [99] King TE, Jr., Brown KK, Raghu G, du Bois RM, Lynch DA, Martinez F, Valeyre D, Leconte I, Morganti A, Roux S, Behr J. BUILD-3: a randomized, controlled trial of bosentan in idiopathic pulmonary fibrosis. *Am J Respir Crit Care Med*, 2011; 184: 92-9.
- [100] Raghu G, Behr J, Brown KK, Egan JJ, Kawut SM, Flaherty KR, Martinez FJ, Nathan SD, Wells AU, Collard HR, Costabel U, Richeldi L, de Andrade J, Khalil N, Morrison LD, Lederer DJ, Shao L, Li X, Pedersen PS, Montgomery AB, Chien JW, O'Riordan TG, Investigators* A-I. Treatment of idiopathic pulmonary fibrosis with ambrisentan: a parallel, randomized trial. *Ann Intern Med*, 2013; 158: 641-9.
- [101] Raghu G, Million-Rousseau R, Morganti A, Perchenet L, Behr J, Group MS. Macitentan for the treatment of idiopathic pulmonary fibrosis: the randomised controlled MUSIC trial. *Eur Respir J*, 2013; 42: 1622-32.
-

-
- [102] Antoniou KM, Wells AU. Acute exacerbations of idiopathic pulmonary fibrosis. *Respiration*, 2013; 86: 265-74.
- [103] Raghu G, Brown KK, Costabel U, Cottin V, du Bois RM, Lasky JA, Thomeer M, Utz JP, Khandker RK, McDermott L, Fatenejad S. Treatment of idiopathic pulmonary fibrosis with etanercept: an exploratory, placebo-controlled trial. *Am J Respir Crit Care Med*, 2008; 178: 948-55.
- [104] Malouf MA, Hopkins P, Snell G, Glanville AR, Everolimus in IPFSI. An investigator-driven study of everolimus in surgical lung biopsy confirmed idiopathic pulmonary fibrosis. *Respirology*, 2011; 16: 776-83.
- [105] Daniels CE, Lasky JA, Limper AH, Mieras K, Gabor E, Schroeder DR, Imatinib IPFSI. Imatinib treatment for idiopathic pulmonary fibrosis: Randomized placebo-controlled trial results. *Am J Respir Crit Care Med*, 2010; 181: 604-10.
- [106] Gunther A, Mosavi P, Ruppert C, Heinemann S, Temmesfeld B, Velcovsky HG, Morr H, Grimminger F, Walmrath D, Seeger W. Enhanced tissue factor pathway activity and fibrin turnover in the alveolar compartment of patients with interstitial lung disease. *Thromb Haemost*, 2000; 83: 853-60.
- [107] Noth I, Anstrom KJ, Calvert SB, de Andrade J, Flaherty KR, Glazer C, Kaner RJ, Olman MA, Idiopathic Pulmonary Fibrosis Clinical Research N. A placebo-controlled randomized trial of warfarin in idiopathic pulmonary fibrosis. *Am J Respir Crit Care Med*, 2012; 186: 88-95.
- [108] Idiopathic Pulmonary Fibrosis Clinical Research N, Zisman DA, Schwarz M, Anstrom KJ, Collard HR, Flaherty KR, Hunninghake GW. A controlled trial of sildenafil in advanced idiopathic pulmonary fibrosis. *N Engl J Med*, 2010; 363: 620-8.
- [109] Han MK, Bach DS, Hagan PG, Yow E, Flaherty KR, Toews GB, Anstrom KJ, Martinez FJ, Investigators IP. Sildenafil preserves exercise capacity in patients with idiopathic pulmonary fibrosis and right-sided ventricular dysfunction. *Chest*, 2013; 143: 1699-708.
- [110] Mitani Y, Sato K, Muramoto Y, Karakawa T, Kitamado M, Iwanaga T, Nabeshima T, Maruyama K, Nakagawa K, Ishida K, Sasamoto K. Superoxide scavenging activity of pirfenidone-iron complex. *Biochem Biophys Res Commun*, 2008; 372: 19-23.
- [111] Salazar-Montes A, Ruiz-Corro L, Lopez-Reyes A, Castrejon-Gomez E, Armendariz-Borunda J. Potent antioxidant role of pirfenidone in experimental cirrhosis. *Eur J Pharmacol*, 2008; 595: 69-77.
- [112] Behr J, Bendstrup E, Crestani B, Gunther A, Olschewski H, Skold CM, Wells A, Wuyts W, Koschel D, Kreuter M, Wallaert B, Lin CY, Beck J, Albera C. Safety and tolerability of
-

- acetylcysteine and pirfenidone combination therapy in idiopathic pulmonary fibrosis: a randomised, double-blind, placebo-controlled, phase 2 trial. *Lancet Respir Med*, 2016; 4: 445-53.
- [113] Hisatomi K, Mukae H, Sakamoto N, Ishimatsu Y, Kakugawa T, Hara S, Fujita H, Nakamichi S, Oku H, Urata Y, Kubota H, Nagata K, Kohno S. Pirfenidone inhibits TGF-beta1-induced over-expression of collagen type I and heat shock protein 47 in A549 cells. *BMC Pulm Med*, 2012; 12: 24.
- [114] Lin X, Yu M, Wu K, Yuan H, Zhong H. Effects of pirfenidone on proliferation, migration, and collagen contraction of human Tenon's fibroblasts in vitro. *Invest Ophthalmol Vis Sci*, 2009; 50: 3763-70.
- [115] Oku H, Shimizu T, Kawabata T, Nagira M, Hikita I, Ueyama A, Matsushima S, Torii M, Arimura A. Antifibrotic action of pirfenidone and prednisolone: different effects on pulmonary cytokines and growth factors in bleomycin-induced murine pulmonary fibrosis. *Eur J Pharmacol*, 2008; 590: 400-8.
- [116] Choi K, Lee K, Ryu SW, Im M, Kook KH, Choi C. Pirfenidone inhibits transforming growth factor-beta1-induced fibrogenesis by blocking nuclear translocation of Smads in human retinal pigment epithelial cell line ARPE-19. *Mol Vis*, 2012; 18: 1010-20.
- [117] Xiao H, Zhang GF, Liao XP, Li XJ, Zhang J, Lin H, Chen Z, Zhang X. Anti-fibrotic effects of pirfenidone by interference with the hedgehog signalling pathway in patients with systemic sclerosis-associated interstitial lung disease. *Int J Rheum Dis*, 2018; 21: 477-486.
- [118] Azuma A, Nukiwa T, Tsuboi E, Suga M, Abe S, Nakata K, Taguchi Y, Nagai S, Itoh H, Ohi M, Sato A, Kudoh S. Double-blind, placebo-controlled trial of pirfenidone in patients with idiopathic pulmonary fibrosis. *Am J Respir Crit Care Med*, 2005; 171: 1040-7.
- [119] Taniguchi H, Ebina M, Kondoh Y, Ogura T, Azuma A, Suga M, Taguchi Y, Takahashi H, Nakata K, Sato A, Takeuchi M, Raghu G, Kudoh S, Nukiwa T, Pirfenidone Clinical Study Group in J. Pirfenidone in idiopathic pulmonary fibrosis. *Eur Respir J*, 2010; 35: 821-9.
- [120] Noble PW, Albera C, Bradford WZ, Costabel U, Glassberg MK, Kardatzke D, King TE, Jr., Lancaster L, Sahn SA, Szwarcberg J, Valeyre D, du Bois RM, Group CS. Pirfenidone in patients with idiopathic pulmonary fibrosis (CAPACITY): two randomised trials. *Lancet*, 2011; 377: 1760-9.
- [121] King TE, Jr., Bradford WZ, Castro-Bernardini S, Fagan EA, Glaspole I, Glassberg MK, Gorina E, Hopkins PM, Kardatzke D, Lancaster L, Lederer DJ, Nathan SD, Pereira CA, Sahn
-

-
- SA, Sussman R, Swigris JJ, Noble PW, Group AS. A phase 3 trial of pirfenidone in patients with idiopathic pulmonary fibrosis. *N Engl J Med*, 2014; 370: 2083-92.
- [122] Margaritopoulos GA, Trachalaki A, Wells AU, Vasarmidi E, Bibaki E, Papastratigakis G, Detorakis S, Tzanakis N, Antoniou KM. Pirfenidone improves survival in IPF: results from a real-life study. *BMC Pulm Med*, 2018; 18: 177.
- [123] Chaudhary NI, Roth GJ, Hilberg F, Muller-Quernheim J, Prasse A, Zissel G, Schnapp A, Park JE. Inhibition of PDGF, VEGF and FGF signalling attenuates fibrosis. *Eur Respir J*, 2007; 29: 976-85.
- [124] Richeldi L, Costabel U, Selman M, Kim DS, Hansell DM, Nicholson AG, Brown KK, Flaherty KR, Noble PW, Raghu G, Brun M, Gupta A, Juhel N, Kluglich M, du Bois RM. Efficacy of a tyrosine kinase inhibitor in idiopathic pulmonary fibrosis. *N Engl J Med*, 2011; 365: 1079-87.
- [125] Efficacy and Safety of Nintedanib in Idiopathic Pulmonary Fibrosis. *N Engl J Med*, 2015; 373: 782.
- [126] Kolb M, Richeldi L, Behr J, Maher TM, Tang W, Stowasser S, Hallmann C, du Bois RM. Nintedanib in patients with idiopathic pulmonary fibrosis and preserved lung volume. *Thorax*, 2017; 72: 340-346.
- [127] Peters-Golden M, Bailie M, Marshall T, Wilke C, Phan SH, Toews GB, Moore BB. Protection from pulmonary fibrosis in leukotriene-deficient mice. *Am J Respir Crit Care Med*, 2002; 165: 229-35.
- [128] Wilborn J, Bailie M, Coffey M, Burdick M, Strieter R, Peters-Golden M. Constitutive activation of 5-lipoxygenase in the lungs of patients with idiopathic pulmonary fibrosis. *J Clin Invest*, 1996; 97: 1827-36.
- [129] Swigris JJ, Ogura T, Scholand M, Glaspole I, Maher TM, Kardatzke D, Kaminski J, Castro M, Owen R, Neighbors M, Belloni P. The RIFF Study (Cohort A): A Phase II, Randomized, Double-Blind, Placebo-Controlled Trial of Lebrikizumab as Monotherapy in Patients with Idiopathic Pulmonary Fibrosis.
- [130] Maher TM, Kondon Y, Corte TJ, Glassberg MK, Costabel U, Lancaster LH, Kardatzke D, Kaminski J, Howard M, Olso J, Neighbors M, Owen R, Belloni P. The RIFF Study (Cohort B): A Phase II, Randomized, Double-Blind, Placebo-Controlled Trial of Lebrikizumab in Combination with Pirfenidone in Patients with Idiopathic Pulmonary Fibrosis.
- [131] Raghu G, Martinez FJ, Brown KK, Costabel U, Cottin V, Wells AU, Lancaster L, Gibson KF, Haddad T, Agarwal P, Mack M, Dasgupta B, Nnane IP, Flavin SK, Barnathan ES. CC-
-

- chemokine ligand 2 inhibition in idiopathic pulmonary fibrosis: a phase 2 trial of carlumab. *Eur Respir J*, 2015; 46: 1740-50.
- [132] Rice LM, Padilla CM, McLaughlin SR, Mathes A, Ziemek J, Goummih S, Nakerakanti S, York M, Farina G, Whitfield ML, Spiera RF, Christmann RB, Gordon JK, Weinberg J, Simms RW, Lafyatis R. Fresolimumab treatment decreases biomarkers and improves clinical symptoms in systemic sclerosis patients. *J Clin Invest*, 2015; 125: 2795-807.
- [133] Maden CH, Fairman D, Chalker M, Costa MJ, Fahy WA, Garman N, Lukey PT, Mant T, Parry S, Simpson JK, Slack RJ, Kendrick S, Marshall RP. Safety, tolerability and pharmacokinetics of GSK3008348, a novel integrin alphavbeta6 inhibitor, in healthy participants. *Eur J Clin Pharmacol*, 2018; 74: 701-709.
- [134] Gorina E, Goldin J, Hyun KG, Zhong M, Sekayan T, Yu P, Kouchakji E. Lung Fibrosis Measured by Quantitative High Resolution Computed Tomography (qHRCT) in Idiopathic Pulmonary Fibrosis (IPF) Patients Treated with Pamrevlumab (FG-3019). *Am J Respir Crit Care Med*, 2018; 197: A7688.
- [135] Marshall RP, Gohlke P, Chambers RC, Howell DC, Bottoms SE, Unger T, McAnulty RJ, Laurent GJ. Angiotensin II and the fibroproliferative response to acute lung injury. *Am J Physiol Lung Cell Mol Physiol*, 2004; 286: L156-64.
- [136] Wang R, Zagariya A, Ibarra-Sunga O, Gidea C, Ang E, Deshmukh S, Chaudhary G, Baraboutis J, Filippatos G, Uhal BD. Angiotensin II induces apoptosis in human and rat alveolar epithelial cells. *Am J Physiol*, 1999; 276: L885-9.
- [137] Wang R, Zagariya A, Ang E, Ibarra-Sunga O, Uhal BD. Fas-induced apoptosis of alveolar epithelial cells requires ANG II generation and receptor interaction. *Am J Physiol*, 1999; 277: L1245-50.
- [138] Marshall RP, McAnulty RJ, Laurent GJ. Angiotensin II is mitogenic for human lung fibroblasts via activation of the type 1 receptor. *Am J Respir Crit Care Med*, 2000; 161: 1999-2004.
- [139] Couluris M, Kinder BW, Xu P, Gross-King M, Krischer J, Panos RJ. Treatment of idiopathic pulmonary fibrosis with losartan: a pilot project. *Lung*, 2012; 190: 523-7.
- [140] Funke M, Zhao Z, Xu Y, Chun J, Tager AM. The lysophosphatidic acid receptor LPA1 promotes epithelial cell apoptosis after lung injury. *Am J Respir Cell Mol Biol*, 2012; 46: 355-64.
- [141] Palmer SM, Snyder L, Todd JL, Soule B, Christian R, Anstrom K, Luo Y, Gagnon R, Rosen G. Randomized, Double-Blind, Placebo-Controlled, Phase 2 Trial of BMS-986020, a
-

-
- Lysophosphatidic Acid Receptor Antagonist for the Treatment of Idiopathic Pulmonary Fibrosis. *Chest*, 2018; 154: 1061-1069.
- [142] Brewer GJ, Dick R, Ullenbruch MR, Jin H, Phan SH. Inhibition of key cytokines by tetrathiomolybdate in the bleomycin model of pulmonary fibrosis. *J Inorg Biochem*, 2004; 98: 2160-7.
- [143] Burdick MD, Murray LA, Keane MP, Xue YY, Zisman DA, Belperio JA, Strieter RM. CXCL11 attenuates bleomycin-induced pulmonary fibrosis via inhibition of vascular remodeling. *Am J Respir Crit Care Med*, 2005; 171: 261-8.
- [144] Mackinnon AC, Gibbons MA, Farnworth SL, Leffler H, Nilsson UJ, Delaine T, Simpson AJ, Forbes SJ, Hirani N, Gauldie J, Sethi T. Regulation of transforming growth factor-beta1-driven lung fibrosis by galectin-3. *Am J Respir Crit Care Med*, 2012; 185: 537-46.
- [145] Hirani N, Mackinnon A, Nicol L, Walker J, Ford P, Schambye H, Pederson A, Nilsson U, Leffler H, Thomas T, Francombe D, Simpson J, Gibbons M, Maher TM. TD139, A Novel Inhaled Galectin-3 Inhibitor for the Treatment of Idiopathic Pulmonary Fibrosis (IPF). Results from the First in (IPF) Patients Study. *Am J Respir Crit Care Med*, 2017; 195: A7560.
- [146] Lawrence J, Nho R. The Role of the Mammalian Target of Rapamycin (mTOR) in Pulmonary Fibrosis. *Int J Mol Sci*, 2018; 19.
- [147] Maher TM, Bareille P, Costa MJ, Fahy WA, Harrison SA, Holman BF, Lukey P, Man Y, Saunders P, Simpson JK, Toshner R, Woodcock HV, Yang S, Marshall RP. A Randomised, Placebo-Controlled, Double-Blind, Repeat Dose Escalation Study with Omipalisib (GSK2126458) in Patients with Idiopathic Pulmonary Fibrosis (IPF). *Am J Respir Crit Care Med*, 2017; 195: A7010.
- [148] Wilkes DS, Chew T, Flaherty KR, Frye S, Gibson KF, Kaminski N, Klemsz MJ, Lange W, Noth I, Rothhaar K. Oral immunotherapy with type V collagen in idiopathic pulmonary fibrosis. *Eur Respir J*, 2015; 45: 1393-402.
- [149] Castano AP, Lin SL, Surowy T, Nowlin BT, Turlapati SA, Patel T, Singh A, Li S, Lupper ML, Jr., Duffield JS. Serum amyloid P inhibits fibrosis through Fc gamma R-dependent monocyte-macrophage regulation in vivo. *Sci Transl Med*, 2009; 1: 5ra13.
- [150] Pilling D, Roife D, Wang M, Ronkainen SD, Crawford JR, Travis EL, Gomer RH. Reduction of bleomycin-induced pulmonary fibrosis by serum amyloid P. *J Immunol*, 2007; 179: 4035-44.
- [151] Raghu G, van den Blink B, Hamblin MJ, Brown AW, Golden JA, Ho LA, Wijsenbeek MS, Vasakova M, Pesci A, Antin-Ozerkis DE, Meyer KC, Kreuter M, Santin-Janin H, Mulder GJ,
-

- Bartholmai B, Gupta R, Richeldi L. Effect of Recombinant Human Pentraxin 2 vs Placebo on Change in Forced Vital Capacity in Patients With Idiopathic Pulmonary Fibrosis: A Randomized Clinical Trial. *JAMA*, 2018; 319: 2299-2307.
- [152] Crestani B, Chapron J, Wallaert B, Bergot E, Delaval P, Israel-Biet D, Lacronique J, Monnet I, Reynaud-Gaubert M, Tazi A, Lebtahi R, Debray MP, Brauner M, Dehoux M, Dornic Q, Aubier M, Mentre F, Duval X. Octreotide treatment of idiopathic pulmonary fibrosis: a proof-of-concept study. *Eur Respir J*, 2012; 39: 772-5.
- [153] Knipe RS, Tager AM, Liao JK. The Rho kinases: critical mediators of multiple profibrotic processes and rational targets for new therapies for pulmonary fibrosis. *Pharmacol Rev*, 2015; 67: 103-17.
- [154] Averill F, Albertson TE, Baratz DM, Chaudhary S, Mobin S, O'Brien T, Scholand MB, Whelan TPM, Poyurovsky M, Schueller O, Ryan J, Gibson KF. A Phase 2 Trial of KD025 to Assess Efficacy, Safety and Tolerability in Patients with Idiopathic Pulmonary Fibrosis.
- [155] Ninou I, Magkrioti C, Aidinis V. Autotaxin in Pathophysiology and Pulmonary Fibrosis. *Front Med (Lausanne)*, 2018; 5: 180.
- [156] Maher TM, van der Aar EM, Van de Steen O, Allamassey L, Desrivot J, Dupont S, Fagard L, Ford P, Fieuw A, Wuyts W. Safety, tolerability, pharmacokinetics, and pharmacodynamics of GLPG1690, a novel autotaxin inhibitor, to treat idiopathic pulmonary fibrosis (FLORA): a phase 2a randomised placebo-controlled trial. *Lancet Respir Med*, 2018; 6: 627-635.
- [157] Axell-House DB, Yu V, Zhang Z, Burdick MD, Strieter RM, Mehrad B. Fibrocytes in Pulmonary Fibrosis: Double-Blind Placebo-Controlled Crossover Pilot Study of Sirolimus in Idiopathic Pulmonary Fibrosis. *Am J Respir Crit Care Med*, 2018; 197: A4353.
- [158] Li Y, Chung S, Li Z, Overstreet JM, Gagnon L, Grouix B, Leduc M, Laurin P, Zhang MZ, Harris RC. Fatty acid receptor modulator PBI-4050 inhibits kidney fibrosis and improves glycemic control. *JCI Insight*, 2018; 3.
- [159] Khalil N, Manganas H, Ryerson CJ, Shapera S, Cantin AM, Hernandez P, Turcotte EE, Parker JM, Moran JE, Albert GR, Sawtell R, Hagerimana A, Laurin P, Gagnon L, Cesari F, Kolb M. Phase 2 clinical trial of PBI-4050 in patients with idiopathic pulmonary fibrosis. *Eur Respir J*, 2018.
- [160] Fitzgerald DB, Moloney F, Twomey M, O'Connell JO, Cronin O, Harty L, Harney S, Henry MT. Efficacy and Safety of Rituximab in Connective Tissue Disease related Interstitial Lung Disease. *Sarcoidosis Vasc Diffuse Lung Dis*, 2015; 32: 215-21.
-

-
- [161] van der Velden JL, Ye Y, Nolin JD, Hoffman SM, Chapman DG, Lahue KG, Abdalla S, Chen P, Liu Y, Bennett B, Khalil N, Sutherland D, Smith W, Horan G, Assaf M, Horowitz Z, Chopra R, Stevens RM, Palmisano M, Janssen-Heininger YM, Schafer PH. JNK inhibition reduces lung remodeling and pulmonary fibrotic systemic markers. *Clin Transl Med*, 2016; 5: 36.
- [162] Varone F, Sgalla G, Iovene B, Bruni T, Richeldi L. Nintedanib for the treatment of idiopathic pulmonary fibrosis. *Expert Opin Pharmacother*, 2018; 19: 167-175.
- [163] Vancheri C, Kreuter M, Richeldi L, Ryerson CJ, Valeyre D, Grutters JC, Wiebe S, Stansen W, Quaresima M, Stowasser S, Wuyts WA, Investigators IT. Nintedanib with Add-on Pirfenidone in Idiopathic Pulmonary Fibrosis. Results of the INJOURNEY Trial. *Am J Respir Crit Care Med*, 2018; 197: 356-363.
- [164] Horton MR, Santopietro V, Mathew L, Horton KM, Polito AJ, Liu MC, Danoff SK, Lechtzin N. Thalidomide for the treatment of cough in idiopathic pulmonary fibrosis: a randomized trial. *Ann Intern Med*, 2012; 157: 398-406.
- [165] Yung GL, Kriett JM, Jamieson SW, Johnson FW, Newhart J, Kinninger K, Channick RN. Outpatient inhaled nitric oxide in a patient with idiopathic pulmonary fibrosis: a bridge to lung transplantation. *J Heart Lung Transplant*, 2001; 20: 1224-7.
- [166] Dutta P, Funston W, Mossop H, Ryan V, Jones R, Forbes R, Sen S, Pearson J, Griffin SM, Smith JA, Ward C, Forrest IA, Simpson AJ. Randomised, double-blind, placebo-controlled pilot trial of omeprazole in idiopathic pulmonary fibrosis. *Thorax*, 2019.
- [167] Jenkins RG, Moore BB, Chambers RC, Eickelberg O, Konigshoff M, Kolb M, Laurent GJ, Nanthakumar CB, Olman MA, Pardo A, Selman M, Sheppard D, Sime PJ, Tager AM, Tatler AL, Thannickal VJ, White ES, Cell ATSAoR, Molecular B. An Official American Thoracic Society Workshop Report: Use of Animal Models for the Preclinical Assessment of Potential Therapies for Pulmonary Fibrosis. *Am J Respir Cell Mol Biol*, 2017; 56: 667-679.
- [168] Degryse AL, Lawson WE. Progress toward improving animal models for idiopathic pulmonary fibrosis. *Am J Med Sci*, 2011; 341: 444-9.
- [169] Tashiro J, Rubio GA, Limper AH, Williams K, Elliot SJ, Ninou I, Aidinis V, Tzouvelekis A, Glassberg MK. Exploring Animal Models That Resemble Idiopathic Pulmonary Fibrosis. *Front Med (Lausanne)*, 2017; 4: 118.
- [170] Peng R, Sridhar S, Tyagi G, Phillips JE, Garrido R, Harris P, Burns L, Renteria L, Woods J, Chen L, Allard J, Ravindran P, Bitter H, Liang Z, Hogaboam CM, Kitson C, Budd DC, Fine JS, Bauer CM, Stevenson CS. Bleomycin induces molecular changes directly relevant to idiopathic pulmonary fibrosis: a model for "active" disease. *PLoS One*, 2013; 8: e59348.
-

- [171] Akhurst RJ, Hata A. Targeting the TGFbeta signalling pathway in disease. *Nat Rev Drug Discov*, 2012; 11: 790-811.
- [172] Puthawala K, Hadjiangelis N, Jacoby SC, Bayongan E, Zhao Z, Yang Z, Devitt ML, Horan GS, Weinreb PH, Lukashev ME, Violette SM, Grant KS, Colarossi C, Formenti SC, Munger JS. Inhibition of integrin alpha(v)beta6, an activator of latent transforming growth factor-beta, prevents radiation-induced lung fibrosis. *Am J Respir Crit Care Med*, 2008; 177: 82-90.
- [173] Munger JS, Huang X, Kawakatsu H, Griffiths MJ, Dalton SL, Wu J, Pittet JF, Kaminski N, Garat C, Matthay MA, Rifkin DB, Sheppard D. The integrin alpha v beta 6 binds and activates latent TGF beta 1: a mechanism for regulating pulmonary inflammation and fibrosis. *Cell*, 1999; 96: 319-28.
- [174] Kelly M, Kolb M, Bonniaud P, Gauldie J. Re-evaluation of fibrogenic cytokines in lung fibrosis. *Curr Pharm Des*, 2003; 9: 39-49.
- [175] O'Riordan TG, Smith V, Raghu G. Development of novel agents for idiopathic pulmonary fibrosis: progress in target selection and clinical trial design. *Chest*, 2015; 148: 1083-92.
- [176] Shi Y, Massague J. Mechanisms of TGF-beta signaling from cell membrane to the nucleus. *Cell*, 2003; 113: 685-700.
- [177] van Putten JPM, Strijbis K. Transmembrane Mucins: Signaling Receptors at the Intersection of Inflammation and Cancer. *J Innate Immun*, 2017; 9: 281-299.
- [178] Martinez-Anton A, Debolos C, Garrido M, Roca-Ferrer J, Barranco C, Alobid I, Xaubet A, Picado C, Mullol J. Mucin genes have different expression patterns in healthy and diseased upper airway mucosa. *Clin Exp Allergy*, 2006; 36: 448-57.
- [179] Lillehoj EP, Kato K, Lu W, Kim KC. Cellular and molecular biology of airway mucins. *Int Rev Cell Mol Biol*, 2013; 303: 139-202.
- [180] Ma J, Rubin BK, Voynow JA. Mucins, Mucus, and Goblet Cells. *Chest*, 2018; 154: 169-176.
- [181] Corfield AP. Mucins: a biologically relevant glycan barrier in mucosal protection. *Biochim Biophys Acta*, 2015; 1850: 236-52.
- [182] Dhanisha SS, Guruvayoorappan C, Drishya S, Abeesh P. Mucins: Structural diversity, biosynthesis, its role in pathogenesis and as possible therapeutic targets. *Crit Rev Oncol Hematol*, 2018; 122: 98-122.
- [183] Hatrup CL, Gendler SJ. Structure and function of the cell surface (tethered) mucins. *Annu Rev Physiol*, 2008; 70: 431-57.
-

-
- [184] Carraway KL, 3rd, Funes M, Workman HC, Sweeney C. Contribution of membrane mucins to tumor progression through modulation of cellular growth signaling pathways. *Curr Top Dev Biol*, 2007; 78: 1-22.
- [185] Thornton DJ, Rousseau K, McGuckin MA. Structure and function of the polymeric mucins in airways mucus. *Annu Rev Physiol*, 2008; 70: 459-86.
- [186] Biesbrock AR, Bobek LA, Levine MJ. MUC7 gene expression and genetic polymorphism. *Glycoconj J*, 1997; 14: 415-22.
- [187] Shankar V, Pichan P, Eddy RL, Jr., Tonk V, Nowak N, Sait SN, Shows TB, Schultz RE, Gotway G, Elkins RC, Gilmore MS, Sachdev GP. Chromosomal localization of a human mucin gene (MUC8) and cloning of the cDNA corresponding to the carboxy terminus. *Am J Respir Cell Mol Biol*, 1997; 16: 232-41.
- [188] Bafna S, Kaur S, Batra SK. Membrane-bound mucins: the mechanistic basis for alterations in the growth and survival of cancer cells. *Oncogene*, 2010; 29: 2893-904.
- [189] Hollingsworth MA, Swanson BJ. Mucins in cancer: protection and control of the cell surface. *Nat Rev Cancer*, 2004; 4: 45-60.
- [190] Blalock TD, Spurr-Michaud SJ, Tisdale AS, Gipson IK. Release of membrane-associated mucins from ocular surface epithelia. *Invest Ophthalmol Vis Sci*, 2008; 49: 1864-71.
- [191] Kufe DW. Mucins in cancer: function, prognosis and therapy. *Nat Rev Cancer*, 2009; 9: 874-85.
- [192] Nath S, Mukherjee P. MUC1: a multifaceted oncoprotein with a key role in cancer progression. *Trends Mol Med*, 2014; 20: 332-42.
- [193] Palmai-Pallag T, Khodabukus N, Kinarsky L, Leir SH, Sherman S, Hollingsworth MA, Harris A. The role of the SEA (sea urchin sperm protein, enterokinase and agrin) module in cleavage of membrane-tethered mucins. *FEBS J*, 2005; 272: 2901-11.
- [194] Thathiah A, Blobel CP, Carson DD. Tumor necrosis factor-alpha converting enzyme/ADAM 17 mediates MUC1 shedding. *J Biol Chem*, 2003; 278: 3386-94.
- [195] Thathiah A, Carson DD. MT1-MMP mediates MUC1 shedding independent of TACE/ADAM17. *Biochem J*, 2004; 382: 363-73.
- [196] Ishikawa N, Hattori N, Yokoyama A, Kohno N. Utility of KL-6/MUC1 in the clinical management of interstitial lung diseases. *Respir Investig*, 2012; 50: 3-13.
- [197] Wakamatsu K, Nagata N, Kumazoe H, Oda K, Ishimoto H, Yoshimi M, Takata S, Hamada M, Koreeda Y, Takakura K, Ishizu M, Hara M, Ise S, Izumi M, Akasaki T, Maki S, Kawabata M, Mukae H, Kawasaki M. Prognostic value of serial serum KL-6 measurements in patients with idiopathic pulmonary fibrosis. *Respir Investig*, 2017; 55: 16-23.
-

- [198] Ohshimo S, Yokoyama A, Hattori N, Ishikawa N, Hirasawa Y, Kohno N. KL-6, a human MUC1 mucin, promotes proliferation and survival of lung fibroblasts. *Biochem Biophys Res Commun*, 2005; 338: 1845-52.
- [199] Xu L, Yan DR, Zhu SL, Gu J, Bian W, Rong ZH, Shen C. KL-6 regulated the expression of HGF, collagen and myofibroblast differentiation. *Eur Rev Med Pharmacol Sci*, 2013; 17: 3073-7.
- [200] Xu L, Yang D, Zhu S, Gu J, Ding F, Bian W, Rong Z, Shen C. Bleomycin-induced pulmonary fibrosis is attenuated by an antibody against KL-6. *Exp Lung Res*, 2013; 39: 241-8.
- [201] Ramasamy S, Duraisamy S, Barbashov S, Kawano T, Kharbanda S, Kufe D. The MUC1 and galectin-3 oncoproteins function in a microRNA-dependent regulatory loop. *Mol Cell*, 2007; 27: 992-1004.
- [202] Carson DD. The cytoplasmic tail of MUC1: a very busy place. *Sci Signal*, 2008; 1: pe35.
- [203] Kufe D. Oncogenic function of the MUC1 receptor subunit in gene regulation. *Oncogene*, 2010; 29: 5663-6.
- [204] Huang L, Chen D, Liu D, Yin L, Kharbanda S, Kufe D. MUC1 oncoprotein blocks glycogen synthase kinase 3 β -mediated phosphorylation and degradation of beta-catenin. *Cancer Res*, 2005; 65: 10413-22.
- [205] Lillehoj EP, Kim H, Chun EY, Kim KC. *Pseudomonas aeruginosa* stimulates phosphorylation of the airway epithelial membrane glycoprotein Muc1 and activates MAP kinase. *Am J Physiol Lung Cell Mol Physiol*, 2004; 287: L809-15.
- [206] Kim KC, Lillehoj EP. MUC1 mucin: a peacemaker in the lung. *Am J Respir Cell Mol Biol*, 2008; 39: 644-7.
- [207] Mori Y, Akita K, Yashiro M, Sawada T, Hirakawa K, Murata T, Nakada H. Binding of Galectin-3, a beta-Galactoside-binding Lectin, to MUC1 Protein Enhances Phosphorylation of Extracellular Signal-regulated Kinase 1/2 (ERK1/2) and Akt, Promoting Tumor Cell Malignancy. *J Biol Chem*, 2015; 290: 26125-40.
- [208] Piyush T, Chacko AR, Sindrewicz P, Hilkens J, Rhodes JM, Yu LG. Interaction of galectin-3 with MUC1 on cell surface promotes EGFR dimerization and activation in human epithelial cancer cells. *Cell Death Differ*, 2017; 24: 1937-1947.
- [209] Singh PK, Hollingsworth MA. Cell surface-associated mucins in signal transduction. *Trends Cell Biol*, 2006; 16: 467-76.
- [210] Roy LD, Sahraei M, Subramani DB, Besmer D, Nath S, Tinder TL, Bajaj E, Shanmugam K, Lee YY, Hwang SI, Gendler SJ, Mukherjee P. MUC1 enhances invasiveness of pancreatic
-

- cancer cells by inducing epithelial to mesenchymal transition. *Oncogene*, 2011; 30: 1449-59.
- [211] Wen Y, Caffrey TC, Wheelock MJ, Johnson KR, Hollingsworth MA. Nuclear association of the cytoplasmic tail of MUC1 and beta-catenin. *J Biol Chem*, 2003; 278: 38029-39.
- [212] Singh PK, Wen Y, Swanson BJ, Shanmugam K, Kazlauskas A, Cerny RL, Gendler SJ, Hollingsworth MA. Platelet-derived growth factor receptor beta-mediated phosphorylation of MUC1 enhances invasiveness in pancreatic adenocarcinoma cells. *Cancer Res*, 2007; 67: 5201-10.
- [213] Wei X, Xu H, Kufe D. MUC1 oncoprotein stabilizes and activates estrogen receptor alpha. *Mol Cell*, 2006; 21: 295-305.
- [214] Kilkenny C, Browne WJ, Cuthill IC, Emerson M, Altman DG. Improving bioscience research reporting: the ARRIVE guidelines for reporting animal research. *PLoS Biol*, 2010; 8: e1000412.
- [215] Spicer AP, Rowse GJ, Lidner TK, Gendler SJ. Delayed mammary tumor progression in Muc-1 null mice. *J Biol Chem*, 1995; 270: 30093-101.
- [216] Jinnin M, Ihn H, Tamaki K. Characterization of SIS3, a novel specific inhibitor of Smad3, and its effect on transforming growth factor-beta1-induced extracellular matrix expression. *Mol Pharmacol*, 2006; 69: 597-607.
- [217] Raina D, Ahmad R, Joshi MD, Yin L, Wu Z, Kawano T, Vasir B, Avigan D, Kharbanda S, Kufe D. Direct targeting of the mucin 1 oncoprotein blocks survival and tumorigenicity of human breast carcinoma cells. *Cancer Res*, 2009; 69: 5133-41.
- [218] Ji X, Wu B, Fan J, Han R, Luo C, Wang T, Yang J, Han L, Zhu B, Wei D, Chen J, Ni C. The Anti-fibrotic Effects and Mechanisms of MicroRNA-486-5p in Pulmonary Fibrosis. *Sci Rep*, 2015; 5: 14131.
- [219] Withana NP, Ma X, McGuire HM, Verdoes M, van der Linden WA, Ofori LO, Zhang R, Li H, Sanman LE, Wei K, Yao S, Wu P, Li F, Huang H, Xu Z, Wolters PJ, Rosen GD, Collard HR, Zhu Z, Cheng Z, Bogyo M. Non-invasive Imaging of Idiopathic Pulmonary Fibrosis Using Cathepsin Protease Probes. *Sci Rep*, 2016; 6: 19755.
- [220] Ashcroft T, Simpson JM, Timbrell V. Simple method of estimating severity of pulmonary fibrosis on a numerical scale. *J Clin Pathol*, 1988; 41: 467-70.
- [221] Alvarez D, Cardenes N, Sellares J, Bueno M, Corey C, Hanumanthu VS, Peng Y, D'Cunha H, Sembrat J, Nouraie M, Shanker S, Caufield C, Shiva S, Armanios M, Mora AL, Rojas M. IPF lung fibroblasts have a senescent phenotype. *Am J Physiol Lung Cell Mol Physiol*, 2017; 313: L1164-L1173.

- [222] Minagawa S, Araya J, Numata T, Nojiri S, Hara H, Yumino Y, Kawaishi M, Odaka M, Morikawa T, Nishimura SL, Nakayama K, Kuwano K. Accelerated epithelial cell senescence in IPF and the inhibitory role of SIRT6 in TGF-beta-induced senescence of human bronchial epithelial cells. *Am J Physiol Lung Cell Mol Physiol*, 2011; 300: L391-401.
- [223] Penke LR, Speth JM, Dommeti VL, White ES, Bergin IL, Peters-Golden M. FOXM1 is a critical driver of lung fibroblast activation and fibrogenesis. *J Clin Invest*, 2018; 128: 2389-2405.
- [224] Milara J, Ballester B, Morell A, Ortiz JL, Escriva J, Fernandez E, Perez-Vizcaino F, Cogolludo A, Pastor E, Artigues E, Morcillo E, Cortijo J. JAK2 mediates lung fibrosis, pulmonary vascular remodelling and hypertension in idiopathic pulmonary fibrosis: an experimental study. *Thorax*, 2018; 73: 519-529.
- [225] Milara J, Hernandez G, Ballester B, Morell A, Roger I, Montero P, Escriva J, Lloris JM, Molina-Molina M, Morcillo E, Cortijo J. The JAK2 pathway is activated in idiopathic pulmonary fibrosis. *Respir Res*, 2018; 19: 24.
- [226] Papiris SA, Tomos IP, Karakatsani A, Spathis A, Korbila I, Analitis A, Kolilekas L, Kagouridis K, Loukides S, Karakitsos P, Manali ED. High levels of IL-6 and IL-8 characterize early-on idiopathic pulmonary fibrosis acute exacerbations. *Cytokine*, 2018; 102: 168-172.
- [227] Hecker L, Vittal R, Jones T, Jagirdar R, Luckhardt TR, Horowitz JC, Pennathur S, Martinez FJ, Thannickal VJ. NADPH oxidase-4 mediates myofibroblast activation and fibrogenic responses to lung injury. *Nat Med*, 2009; 15: 1077-81.
- [228] Horimasu Y, Ishikawa N, Taniwaki M, Yamaguchi K, Hamai K, Iwamoto H, Ohshimo S, Hamada H, Hattori N, Okada M, Arihiro K, Ohtsuki Y, Kohno N. Gene expression profiling of idiopathic interstitial pneumonias (IIPs): identification of potential diagnostic markers and therapeutic targets. *BMC Med Genet*, 2017; 18: 88.
- [229] Kato K, Zemskova MA, Hanss AD, Kim MM, Summer R, Kim KC. Muc1 deficiency exacerbates pulmonary fibrosis in a mouse model of silicosis. *Biochem Biophys Res Commun*, 2017; 493: 1230-1235.
- [230] Behrens ME, Grandgenett PM, Bailey JM, Singh PK, Yi CH, Yu F, Hollingsworth MA. The reactive tumor microenvironment: MUC1 signaling directly reprograms transcription of CTGF. *Oncogene*, 2010; 29: 5667-77.
- [231] Ask K, Bonniaud P, Maass K, Eickelberg O, Margetts PJ, Warburton D, Groffen J, Gauldie J, Kolb M. Progressive pulmonary fibrosis is mediated by TGF-beta isoform 1 but not TGF-beta3. *Int J Biochem Cell Biol*, 2008; 40: 484-95.
-

-
- [232] Bagnato G, Harari S. Cellular interactions in the pathogenesis of interstitial lung diseases. *Eur Respir Rev*, 2015; 24: 102-14.
- [233] Gnemmi V, Bouillez A, Gaudelot K, Hemon B, Ringot B, Pottier N, Glowacki F, Villers A, Vindrieux D, Cauffiez C, Van Seuning I, Bernard D, Leroy X, Aubert S, Perrais M. MUC1 drives epithelial-mesenchymal transition in renal carcinoma through Wnt/beta-catenin pathway and interaction with SNAIL promoter. *Cancer Lett*, 2014; 346: 225-36.
- [234] Rajabi H, Alam M, Takahashi H, Kharbanda A, Guha M, Ahmad R, Kufe D. MUC1-C oncoprotein activates the ZEB1/miR-200c regulatory loop and epithelial-mesenchymal transition. *Oncogene*, 2014; 33: 1680-9.
- [235] Waters DW, Blokland KEC, Pathinayake PS, Burgess JK, Mutsaers SE, Prele CM, Schuliga M, Grainge CL, Knight DA. Fibroblast senescence in the pathology of idiopathic pulmonary fibrosis. *Am J Physiol Lung Cell Mol Physiol*, 2018; 315: L162-L172.
- [236] Lehmann M, Baarsma HA, Konigshoff M. WNT Signaling in Lung Aging and Disease. *Ann Am Thorac Soc*, 2016; 13: S411-S416.
- [237] Carlson ME, Hsu M, Conboy IM. Imbalance between pSmad3 and Notch induces CDK inhibitors in old muscle stem cells. *Nature*, 2008; 454: 528-32.
- [238] Zhu X, Ozturk F, Liu C, Oakley GG, Nawshad A. Transforming growth factor-beta activates c-Myc to promote palatal growth. *J Cell Biochem*, 2012; 113: 3069-85.
- [239] Kufe DW. Functional targeting of the MUC1 oncogene in human cancers. *Cancer Biol Ther*, 2009; 8: 1197-203.
- [240] Parmar N, Tatler A, Ford P, Jenkins G. S76 Role of galectin-3 in the development of idiopathic pulmonary fibrosis. *Thorax*, 2017; 72: A48-A48.
- [241] Shimura T, Takenaka Y, Tsutsumi S, Hogan V, Kikuchi A, Raz A. Galectin-3, a novel binding partner of beta-catenin. *Cancer Res*, 2004; 64: 6363-7.
- [242] Tanida S, Mori Y, Ishida A, Akita K, Nakada H. Galectin-3 binds to MUC1-N-terminal domain and triggers recruitment of beta-catenin in MUC1-expressing mouse 3T3 cells. *Biochim Biophys Acta*, 2014; 1840: 1790-7.
- [243] Iyer SN, Gurujeyalakshmi G, Giri SN. Effects of pirfenidone on procollagen gene expression at the transcriptional level in bleomycin hamster model of lung fibrosis. *J Pharmacol Exp Ther*, 1999; 289: 211-8.
- [244] Iwata T, Yoshida S, Nagato K, Nakajima T, Suzuki H, Tagawa T, Mizobuchi T, Ota S, Nakatani Y, Yoshino I. Experience with perioperative pirfenidone for lung cancer surgery in patients with idiopathic pulmonary fibrosis. *Surg Today*, 2015; 45: 1263-70.
-

ABBREVIATIONS INDEX

ABBREVIATIONS INDEX

| | |
|---------------------------------------|--|
| Act-β-catenin | Active- β -catenin |
| AEC | Alveolar epithelial cell |
| AMOP domain | Adhesion-associated domain |
| ATII cell | Alveolar type II cell |
| ATS | American Thoracic Society |
| α-SMA | α -smooth muscle actin |
| BALF | Bronchoalveolar lavage fluid |
| BSA | Bovine serum albumin |
| BrdU | Bromodeoxyuridine |
| BM | Basement membrane |
| CCL2 | C-C motif chemokine ligand 2 |
| COPD | Chronic obstructive pulmonary disease |
| CT | Computed tomography |
| CTGF | Connective tissue growth factor |
| DAPI | 4',6-diamidino-2-phenylindole |
| DL_{co} | Diffusing capacity for carbon monoxide |
| DMEM | Dulbecco's Modified Eagle's Medium |
| DPLD | Diffuse parenchymal lung disease |
| ECM | Extracellular matrix |
| EDTA | Ethylenediaminetetraacetic acid |
| EGFR | Epidermal growth factor |
| EMT | Epithelial-mesenchymal transition |
| EndMT | Endothelial-mesenchymal transition |
| ER | Endoplasmic reticulum |

| | |
|---------------------------|---|
| ErbB receptor | Erythroblastosis oncogene B receptor |
| Erk1/2 | Extracellular signal-regulated kinase 1/2 |
| ELISA | Enzyme-linked immunosorbent assay |
| ERS | European Respiratory Society |
| ET-1 | Endothelin-1 |
| ¹⁸F-FDG | Fludeoxyglucose ¹⁸ F |
| FDA | Food and Drug Administration |
| FGF | Fibroblast growth factor |
| FGFR | Fibroblast growth factor receptor |
| FIP | Familial interstitial pneumonia |
| FMT | Fibroblast-mesenchymal transition |
| FVC | Forced vital capacity |
| GER | Gastroesophageal reflux |
| GSK-3β | Glycogen synthase kinase-3β |
| HRCT | High resolution computed tomography |
| HRP | Horseradish peroxidase |
| IFN | Interferon |
| Ig | Immunoglobulin |
| IL | Interleukin |
| ILD | Interstitial lung disease |
| IIP | Idiopathic interstitial pneumonia |
| IPF | Idiopathic pulmonary fibrosis |
| IT administration | Intratracheal administration |
| JNK | Jun N-Terminal Kinase |
| KO | Knockout |

| | |
|-----------------------------|--|
| LPA | Lysophosphatidic acid |
| LV+S | Left ventricle + septum |
| MAA-Tc^{99m} | Albumin macroaggregated marked with technetium metastable |
| miRNA | microRNA |
| MMP | Matrix metalloproteinase |
| mTOR | Mammalian Target of Rapamycin |
| MUC1 | Mucin 1 |
| MUC1-C | MUC1 C-terminal subunit |
| MUC1-N | MUC1 N-terminal subunit |
| MUC1-P/T-1224 | MUC1 phosphorylated form at Thr ¹²²⁴ |
| MUC1-P/Y-1229 | MUC1 phosphorylated form at Tyr ¹²²⁹ |
| MUC5B | Mucin 5B |
| NAC | N-acetyl L-cystein |
| NIDO domain | Nidogen-like domain |
| NF-κB | Nuclear factor kappa-light-chain-enhancer of activated B cells |
| NO | Nitric oxide |
| NOX 4 | NADPH oxidase 4 |
| PARN | Poly (A)-specific Ribonuclease Deadenylation Nuclease |
| PBS | Phosphate buffered saline |
| PCR | Polimerase chain reaction |
| PDE | Phosphodiesterase |
| PDGF | Platelet derived growth factor |
| PDGFR | Platelet derived growth factor receptor |
| PH | Pulmonary hypertension |
| PI3K | Phosphoinositide 3-kinase |

| | |
|-------------------------------|---|
| PKCδ | Protein kinase C δ |
| PMC | Pleural mesothelial cell |
| P-Smad3 | Phospho-Smad3 |
| PTS domains | Tandem repeat structures with high proportion of proline, threonine and serine residues |
| Penh | Enhanced respiratory pause |
| PET | Positron emission tomography |
| ROS | Reactive oxygen species |
| RTEL1 | Regulator of Telomere Elongation Helicase 1 |
| RT-PCR | Real time-PCR |
| RV | Right ventricle |
| SBE | Smad binding element |
| Shh | Sonic hedgehog |
| siRNA | Small interfering RNA |
| SPECT | Single-photon emission computed tomography |
| SUV | Standard uptake value |
| TBS | Tris-buffered saline |
| TBST | 0.1% Tween 20/TBS |
| TβRI | TGF β 1 receptor type I |
| TβRII | TGF β 1 receptor type II |
| TGFβ | Transforming growth factor β |
| TLR | Toll like receptor |
| TM mucin | Transmembrane mucin |
| TMB | Tetramethylbenzidine |
| TNFα | Tumour necrosis factor α |
| TR | Tandem repeat |

| | |
|-------------------|-------------------------------------|
| TOLLIP | Toll-interacting protein |
| UIP | Usual interstitial pneumonia |
| VEGF | Vascular endothelial growth factor |
| VNTR | Variable number tandem repeat |
| VOI | Volume of interest |
| vWD domain | Von Willebrand factor type D domain |
| WT | Wild type |
| ZO-1 | Zonula occludens-1 |
| 5-LO | 5-lipoxygenase |
| 6MWD | 6-minute walk distance |

ANNEXES

ANNEX 1

ETHICS COMMITTEE APPROVAL AND WRITTEN INFORMED CONSENT MODEL FROM PATIENTS

APROBACIÓN PROYECTOS DE INVESTIGACIÓN

- ANEXO 11 -

Este CEIm tras evaluar en su reunión de 26 de Octubre de 2017 el Proyecto de Investigación:

| | | | |
|---------|--|-----------------|----------|
| Título: | Estudio de las mucinas ancladas a membrana como diana farmacológica en la fibrosis pulmonar idiopática y en la hipertensión pulmonar asociada: análisis preclínico y traslacional. | | |
| I.P.: | Javier Milara Páya | Servicio/Unidad | Farmacia |

Acuerda respecto a esta documentación:

Que se cumplen los requisitos éticos y metodológicos y la Hoja de Información al Paciente y Consentimiento Informado presentado reúnen las condiciones exigidas por este CEIC, por tanto se decide su APROBACIÓN.

COMPOSICIÓN DEL CEIm

Presidente: Dra. Elena Rubio Gomis (Unidad de Farmacología Clínica)

Vocales:

- Dr. Francisco Antón Garcia (Att primaria)
- Dra. Pilar Blasco Segura (Servicio de Farmacia)
- Dr. Ernesto Bataller Alonso (Director Económico del CHGUV)
- Dña. Pepa Balaguer Cusi (Miembro independiente de la organización asistencial)
- Dr. Enrique Ortega Gonzalez (Gerente Chguv)
- Dra. Dolores Ocete Mochón (Servicio de Microbiología)
- Dr. Miguel Garcia del Toro (Unidad de Infecciosos)
- D. Fráncico Javier Gracia Pérez (Servicio de Reanimación)
- Dr. Julio Cortijo Gimeno (Unidad de Docencia e Investigación)
- Dña. María Teresa Jareño (Unidad de Reanimación Cardiaca)
- D. Alejandro Moner González (Gerencia CHGUV – Asesoría Jurídica)
- Dr. Alberto Berenguer Jofresa (Servicio de Cardiología)
- Dra. Ana Blasco Cordellat (Servicio de Oncología)
- Dr. Antonio Martorell Aragonés (Unidad de Alergología)

Consorcio Hospital General Universitario de Valencia

Comité Ético de Investigación Clínica

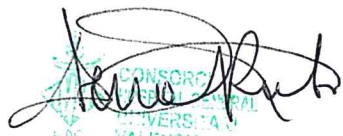
- Dr. Aurelio Quesada Dorador (Servicio de Cardiología)
- Dra. M^a José Safont Aguilera (Servicio de Oncología)
- Dr. Javier Milara Payá (Servicio de Farmacia)
- Dra. Goitzane Marcaida Benito (Servicio de Análisis Clínicos)
- Dr. Pedro Polo Martín (Servicio de Pediatría- Atención Primaria)
- Dña. Carmen Sarmiento Cabañes (Miembro independiente de la organización asistencial)
- Dr. Enrique Zapater Latorre (Servicio de Otorrino)

Secretario: Dr. Elias Ruiz Rojo (Farmacéutico Att Primaria)

El CEIm del Consorcio Hospital General Universitario de Valencia, cumple con las normas de BPC (CPMP/ICH/135/95) tanto en su composición como en sus procedimientos y con la legislación vigente que regula su funcionamiento, y que la composición del CEIm es la indicada en el anexo I, teniendo en cuenta que en el caso de que algún miembro participe en el ensayo o declare algún conflicto de interés no habrá participado en la evaluación ni en el dictamen de la solicitud de autorización del ensayo clínico

Lo que comunico a efectos oportunos:

Valencia a 31 de octubre de 2017

| |
|---|
| Fdo. Dra. Elena Rubio Gomis (Presidenta CEIC CHGUV) |
|  |

CONSORCIO
HOSPITAL GENERAL
UNIVERSITARI
H.G.C. VALÈNCIA
COMITÉ ÈTIC DE
INVESTIGACIÓ CLÍNICA

ANNEX 2

ETHICS COMMITTEE APPROVAL FOR EXPERIMENTATION ANIMAL PROCEDURE

AUTORIZACION PROCEDIMIENTO 2017/VSC/PEA/00061

Vista la solicitud realizada en fecha **24/03/17** con nº reg. entrada **14257** por D/D^a. **Pilar Campins Falcó**, Vicerrectora de Investigación y Política Científica, centro usuario **ES462500001003**, para realizar el procedimiento:

“Inducción de fibrosis pulmonar por bleomicina en ratón para el estudio del papel del gen muc 1 en dicha patología”

Teniendo en cuenta la documentación aportada, según se indica en el artículo 33, punto 5 y 6, y puesto que dicho procedimiento se halla sujeto a autorización en virtud de lo dispuesto en el artículo 31 del Real Decreto 53/2013, de 1 de febrero,

Vista la propuesta del jefe del servicio de Producción y Sanidad Animal.

AUTORIZO:

la realización de dicho procedimiento al que se le asigna el código: **2017/VSC/PEA/00061** tipo **2**, de acuerdo con las características descritas en la propia documentación para el número de animales, especie y periodo de tiempo solicitado. Todo ello sin menoscabo de las autorizaciones pertinentes, por otras Administraciones y entidades, y llevándose a cabo en las siguientes condiciones:

Usuario: **Universitat de Valencia**

Responsable del proyecto: **Julio Cortijo Gimeno**

Establecimiento: **Animalario Facultad de Medicina – Campus Blasco Ibañez**

Necesidad de evaluación retrospectiva:

Condiciones específicas:

Observaciones:

Valencia a, fecha de la firma electrónica

El director general de Agricultura, Ganadería y Pesca

Firmado por Rogelio Llanes Ribas el
03/05/2017 11:57:40

GENERALITAT
VALENCIANA